1993

Brainstem Control Of Three-dimensional Eye Movements

J Douglas Crawford

BRAINSTEM CONTROL OF THREE-DIMENSIONAL EYE MOVEMENTS

by

J. Douglas Crawford

Department of Physiology

Submitted in partial fulfilment

of the requirements for the degree of

Doctor of Philosophy

Faculty of Graduate Studies

The University of Western Ontario

London, Ontario

January 1993

ISBN 0-315-81289-3

ABSTRACT

This thesis examines the neural mechanisms that generate torsional and vertical eye movements, and how they handle the kinematics of three-dimensional rotations. Three-dimensional eye rotations were recorded in alert monkeys, and the midbrain was studied using single unit recording, electrical microstimulation, and pharmacological inactivation.

The direction of VOR slow phases was usually opposite to that of head rotation, as required for optimal visual stabilization. However, direction errors sometimes occurred because of low gain about a head-fixed torsional axis. This axis was orthogonal to Listing's plane of saccadic eye positions, which suggests that saccades and the VOR share the same coordinate system. As predicted by the laws of rotational kinematics, even slow phase axes with zero torsional components produced torsional violations of Listing's law. This proves that mechanics of the plant are not responsible for Listing's law. Furthermore, the final positions were held. This signifies that the eye velocity signal is multiplied by position feedback before entering the oculomotor integrator. Finally, these violations of Listing's law were corrected by VOR quick phases.

Microstimulation and inactivation of the rostral interstitial nucleus of the medial longitudinal fasciculus (riMLF) demonstrated two right riMLF burst neuron populations that generate clockwise-upward-rightward and clockwise-downward-leftward rotations respectively, and two left riMLF populations for counterclockwise-upward-leftward and counterclockwise-downward-rightward rotations. The torsional axes of eye rotation evoked by riMLF stimulation were orthogonal to Listing's plane, whereas axes that remained after riMLF inactivation aligned with Listing's plane. This suggests that the neural coordinates of motor systems reflect their behavioral constraints.

The neural integrator, which generates the eye position signal, is central to

oculomotor control. Post-saccadic drift during inactivation of the midbrain interstitial nucleus of Cajal (INC) showed that this nucleus is the integrator for vertical and torsional eye positions. Stimulation showed that the right INC controls clockwise rotations and the left INC controls counterclockwise rotations. Simulations of the drift suggested that the INC distributes integration over parallel independent neural compartments. This makes the integrator more computationally robust, and suggests a similar role for the modular connectivity observed throughout the brain.

This thesis is dedicated to my parents,

John C. Crawford and Signe M. Crawford,

for their kindness and generous support.

ACKNOWLEDGEMENTS

It is difficult find a few brief words to thank Tutis Vilis. I know that only the very few people who have experienced a strong and good mentor figure could understand my feelings in this regard. To a large extent, this work reflects his vision of science, a vision that I will carry in me throughout my career. Thank you Tutis, for your support and guidance, and for teaching me to shoot pucks in the net without giving up figure skating. I hope that my future accomplishments will give you reason to feel proud of the career that you have set in motion.

Doug Tweed has occupied a unique role in my graduate studies. Initially he was like a second supervisor to me, and now a much-prized associate. To a large extent this thesis builds on Doug's own, and on his personal instruction. I can admit now that some years ago I decided to set Doug Tweed as my standard for intellectual achievement.

Two other figures influenced my academic life. Stan Caveney fanned the flames of my interest in science for years before giving me my first experience in serious research (would I be here without you?). Second, Jon Hore has inspired me personally and instructed me in the many subtle aspects of the game, particularly in all forms of communicating science.

I owe a great debt to Mel Goodale, Dick Weick, David Cooke, and Stan Leung, for going above and beyond the call of duty in reading long-winded manuscripts and writing too-kind letters of reference. Thanks Werner Cadera for your surgeon's humour and magic fingers. Thanks to Garth Santor for frequently making everything right in the computer world again, and Leopold Van Cleef, the great electronics wizard / man behind the scenes. Also I am pleased to thank Sheila Nicol and Sherry Watts for dealing with the animals, filling in the gaps, and being forced to listen to my personal problems. Finally, hats off to the assorted characters, Brian, Rick, et al., who made lab life bearable.

My special thanks and love are reserved for Maria and Bruno, for making my life complete, and my parents who have supported me in all ways throughout my education.

A Medical Research Council of Canada studentship has supported me during this project.

TABLE OF CONTENTS

LIST OF FIGURES

LIST OF APPENDICES

parallel distributed properties of their model remained untested (Robinson 1989).

1.3 PHYSICAL PROPERTIES OF 3-D ROTATIONS

The previous discussion has been confined to eye movements in one-dimension, but in real life the eyes rotate in three-dimensions. Before examining the brain mechanisms for such movements, it is necessary to understand the basic issues that arise when one considers three-dimensional rotations.

1.3.1 *Coordinate systems and reference frames.*

In order to describe the location or orientation of some object, we need a coordinate system. Lets start with a familiar example. Consider an airborne plane that is currently 2 km north and 1 km west of this location (my office at U.W.O) at an elevation of 3 km (to simplify matters let's assume that the earth is flat). In order to interpret this, we must have understood concepts that capture all of the general principles of coordinate systems. First, we used an origin, my office. Second, we have what are called, in the parlance of linear algebra, basis vectors (Nicholson 1986). These can be visualized as lines going from the origin to three points positioned at one km north, one km west, and one km straight up from my office (south, east, and down can be considered the negatives of these three). These basis vectors incorporate both the notions of direction, and a relativistic unit of magnitude (the km). The number of distance units that we specified along each direction are called the components (i.e. components of the vector going from my office to the plane). Finally, we implicitly assumed the reference frame to be the earth, which means that the orientation of the basis vectors is always the same with respect to the earth.

In the above example we considered translational position, but in the oculomotor system we are interested in angular positions of the eye. Again, at least three

are very high, up to ~1000°/s in monkeys, their durations are short compared to the period of visual latency (Carpenter 1988). For these reasons, saccades are thought to be driven by an open-loop, machine-like system (Becker et al. 1981; Robinson 1975). Normally a latency of about 200 ms is required to initiate a saccade in response to a visual stimulus, but this latency may be cut in half if the subject is "primed" for an anticipated movement (Ross and Ross 1980).

The second major function of the oculomotor system, image stabilization, is mainly subserved by the vestibuloocular reflex (VOR). The VOR gets its name from the fact that it is an automatic movement of the eyes in response to stimulation of the vestibular organs (Baker et al. 1984; Collewijn et al. 1985; Robinson 1975; Simpson and Graf 1985; Skavenski et al. 1979). This behaviour is so fundamental for vision that it appears to have preceded the development of a focusing apparatus in the evolution of the eye (Land and Fernald 1992). Whenever one's head moves with respect to the visual scene, the VOR produces compensatory eye movements to maintain the point of fixation, and in general minimize slip of the visual image across the retina. When the object of interest is close to the eye, geometry requires that the eyes also rotate to compensate for their own relative translational motion (Snyder and King 1992a; Viirre et al. 1986). Consequently, the VOR is simplest when the fixation point is far away. Here, stabilization will be achieved if the eyes rotate with the same speed that the head rotates in, but in the opposite direction. In this case the one-dimensional gain of the reflex (eye movement / head movement) is 1.0, or more correctly -1.0 to indicate that the eye and head movements are in opposite directions. For such a response it is clearly the semicircular canals, which sense head rotation, that provide the input signal for the reflex.

Even in one dimension and looking far away the VOR is not really so simple as described above. The gain of the VOR in the dark is significantly less than one, but

In addition to the intrinsic importance of the oculomotor system, its simplicity, and the specific issues of visuomotor coordination that arise, there is yet another reason why physiologists elect to study this system. It probable that the brain utilizes a fundamental and common set of principles wherever possible for all types of movement. By studying eye movements, we may gain insight into more complex systems, particularly with regards to kinematic control. The present thesis exploits this axiom to examine several general issues in motor control, including 1. the problem of maintaining postures and matching them to the intervening movements, 2. kinematic redundancy (often called the "overcompleteness" or "degrees of freedom" problem), 3. choices of neural coordinate systems, 4. parallel distributed processing and modularity in neural tissue, and 5. representation of the physical laws of the external world in the central nervous system. For most of these issues, examination of the oculomotor system only becomes fruitful when eye rotations are studied in three dimensions.

1.2 SACCADES AND THE VESTIBULOOCULAR REFLEX IN ONE DIMENSION

Although the present thesis is concerned with the three-dimensional aspects of eye movements, many of the major oculomotor issues arose historically from experiments and theories that utilized a one-dimensional perspective. This section summarizes some findings regarding horizontal eye rotations that are a necessary background for a three-dimensional analysis of conjugate eye movement systems.

1.2.1 *Behaviour of eye movements in one dimension.*

The oculomotor system has two main functions. The first, acquiring visual targets, is realized by saccades. Saccades are the rapid, goal-directed eye movements that we make several times a second during waking life. In general, there is a fixed relationship between saccade amplitude and angular velocity (Robinson 1964). Since these velocities

1.2.2 *The oculomotor plant and motoneurons*

The oculomotor plant consists of the eye, the orbital tissues, and the extraocular muscles. Rotation of the eye occurs about a point in the orbit which is approximately fixed, and the inertial load of the eye itself is negligible (Helmholtz 1925). Thus, muscular torques are necessary mainly to do work against passive forces in the tissues surrounding the eye, including the muscles themselves (Robinson 1970, 1975). In the case of horizontal movements, these torques are produced by tension changes in the two horizontal recti of each eye.

Specific net torques are required to move and hold the eye, requiring specific patterns of motoneuron input. These patterns were demonstrated by D. A. Robinson and co-workers in the early 1970's (Robinson 1975). For example, if one records action potentials from a motoneuron innervating the agonist muscle for a movement, say a saccade, one finds a stereotyped pattern. A highly idealized illustration of this pattern is shown in Figure 1, based on single-unit recordings in the alert monkey (Robinson 1970; Robinson and Keller 1972; Skavenski and Robinson 1973). During the fixation preceding the movement, action potentials occur at a tonic steady frequency. Just before and during the saccade, there is a phasic burst of high-frequency action potentials (Fig. 1 B). Then, at the final point of fixation there is again a steady action potential rate, but one that is higher than the original rate. These tonic inputs after saccades and phasic inputs during saccades have been called the step and pulse, respectively (Fig. 1 C).

Why are a neural pulse and step required? The answer lies in mechanics of the plant (Robinson 1970). First, the muscles and other orbital tissues are viscous. Since this produces a resisting force proportional to eye speed, the eye muscles must be contracted in proportion to the desired speed for a movement. Hence, a speed-related pulse of input is required. Second, the same tissues are elastic. Thus they produce a restoring force at eccentric eye positions, pulling the eye towards some resting point. To counteract this

visuo-oculomotor responses, i.e. smooth pursuit and/or the optokinetic reflex, appear to supplement the VOR in the light (Barr et al. 1976; Ferman et al. 1987b; Skavenski et al. 1979). At the opposite extreme, the VOR can be cancelled by visual fixation on a target that moves with the head (Leigh et al. 1989). Furthermore, gain and phase are frequency dependent, although they are stable and near ideal during head rotations above 0.1 Hz (Yasui and Young 1984). Alsc important in maintaining gain near one is the subjects intention to stabilize gaze, even towards an imagined target in the dark (Barr et al. 1976). Thus, the optimal "vestibuloocular reflex" in the light is neither completely vestibular in origin, or purely reflexive.

Finally, the gain of the VOR has remarkable adaptive capability (Gonshor and Melvill Jones 1976; Miles and Fuller 1974; Schultheis and Robinson 1981; Snyder and King 1988). For example, gain can be dramatically increased or reduced by exposure to any motion of the visual image across the retina that would suggest such adjustments are necessary, whether this motion is in fact due to VOR error or due to some experimental manipulation. Thus, in some respects, to study kinematics of the normal VOR is to examine how well this reflex is adapted to fit the requirements of its task.

How does the VOR interact with saccades? During large head rotations, an unassisted VOR would quickly become useless as the eyes would jam against the limit of their range. To prevent this, some resetting movement is required. This is accomplished by rapid eye movements called "quick phases" of the VOR, to distinguish them from the stabilizing "slow phase " VOR movements discussed above (Chun and Robinson 1978; Ron et al. 1972). Quick phases have both reflexive and voluntary characteristics. On one hand, rhythmic neural commands for quick phases may occur in the absence of consciousness, and even without eyes (McIntyre 1939). On the other hand, the reader can readily confirm his / her ability to voluntarily look towards various targets during head rotation.

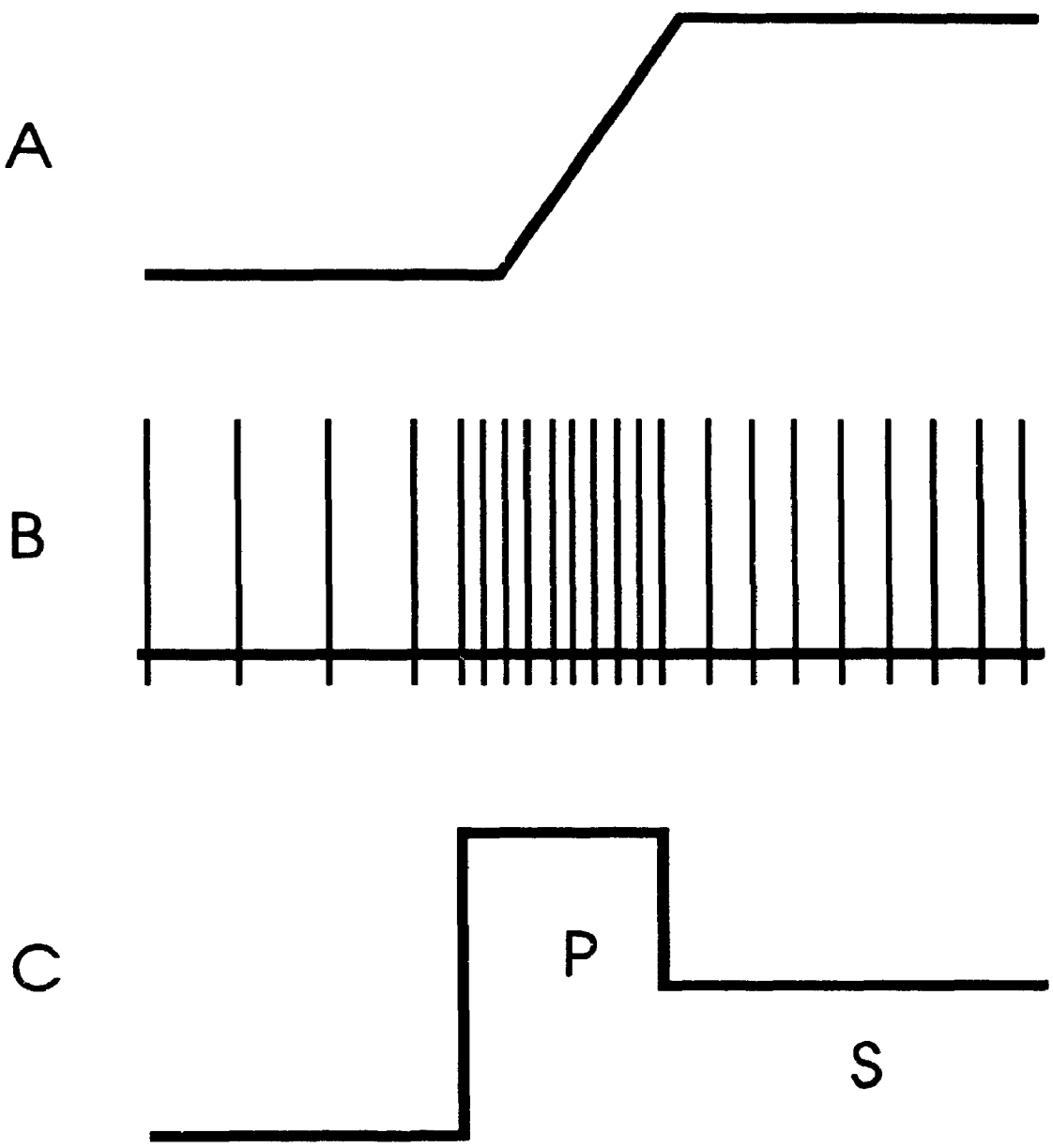

FIGURE 1. Agonist motoneuron activity during an eye movement. *A*: Eye position plotted as a function of time. *B*: Typical pattern of action potentials during this time. *C*: Action potential frequency, revealing pulse (P) and step (S) components.

force, the position-related step input to the motoneurons is required.

Single unit recordings in monkeys and other animals have shown a remarkably linear relationship between both the motoneuron pulse and the first derivative of eye position with respect to time (equivalent to both speed and velocity in 1-D), and between the step and eye position. Motoneuron firing rate can be characterized as follows:

$$m = kH + rH \qquad (1)$$

Where m is action potential frequency, k is an elasticity constant, r is a viscosity constant, H is horizontal eye position, and $\dot{H}$ is the first derivative of the latter (Robinson 1975). If we consider a pair of motoneurons innervating opposing horizontal recti, both with straight-ahead threshold positions and the same r and k, then positive values of m can be interpreted as activity in one neuron, and negative as activity in the other. Equation 1 implies that with the eye still, there is a fixed ratio between motoneuron firing rate, net muscular torque, and eye position. Moreover, Equation 1 is essentially correct for a neuron during all types of eye movement (Robinson 1975; Robinson and Keller 1972; Skavenski and Robinson 1973). This simple but surprisingly realistic one-dimensional model of the plant is utilized in simulations later in this thesis. The next question that arises is, what is the origin of the pulse and step?

1.2.3 *Pulse generation*

If action potentials are recorded from neurons that synapse directly on the ocular motoneurons, in many cases the activity profile resembles the pulse, whereas the step is functionally absent (Fernandez and Goldberg 1971a, 1971b; Luschei and Fuchs 1972). There are several classes of these premotor pulse generators, each of which is active only for a certain type of eye movement. Here we will only examine relationships between

1-D eye movement and firing patterns of the pulse generators for saccades and VOR slow phases (anatomical locations and coordinate systems will be considered later).

Single unit recordings in the monkey made by Luschei and Fuchs (1972) and later others (Büttner et al. 1977; Hepp et al. 1988; King and Fuchs 1979; Moschovakis et al. 1991a, 1991b; Strassman et al. 1986a, 1986b; Van Gisbergen et al. 1981) have shown that the brainstem possesses a class of oculomotor units called (short lead) burst neurons. Burst neurons are named for their intense periods of high-frequency action potentials, beginning 8-12 milliseconds before rapid eye movements (either saccades or quick phases) in their preferred direction. Burst neuron activity correlates well with saccade metrics, e.g. total number of spikes with saccade amplitude, peak firing rate (below a saturation non-linearity) with peak saccade speed, and burst duration with saccade duration. Given the direct projections from identified burst neurons to motoneurons (Strassman et al. 1986a, 1986b; Moschovakis et al. 1991a, 1991b) and the similarity in the saccadic pulse component between the two, it is logical to conclude that burst neurons are the source of this pulse. This is corroborated by the finding that pharmacological inactivation of regions that possess these neurons creates a severe oculomotor deficit that is specific to rapid eye movements (Cohen et al. 1968), without affecting position holding (Henn et al. 1984).

In the case of VOR slow phases, there is already an appropriate angular velocity-related signal in the primary vestibular afferents (Fernandez and Goldberg 1971a, 1971b). Such signals are adequate to produce the pulse for a simple VOR during head rotations while looking far away, with the proper gain elements and reversal of sign. In fact, there can be as little as one intervening neuron between the latter afferents and ocular motoneurons. This pathway is called the direct path of the VOR (Robinson 1975).

Recalling that horizontal eye movement is the result of net torque between two opposing muscles, is important to consider the analogue of pulse input to the antagonist

for a given movement. In addition to burst neurons that excite the agonist motoneurons, there are inhibitory burst neurons which produce a pause in activity of the antagonist motoneurons (Strassman et al. 1986a, 1986b). This is called " push-pull organization". Push-pull connections are even more important for the VOR. Since the vestibular afferents have high resting discharge rates even in the absence of head movement (Fernandez and Goldberg 1971a), push-pull is necessary to cancel these inputs by the motoneuron level. In any case, the net output of all pulse generators is zero when the eye is stable with respect to the head. Thus, they cannot provide the step that maintains eye position.

1.2.4 *The oculomotor integrator*

What generates the position-related step signal observed in ocular motoneurons? This has been a fundamental question in oculomotor control for decades. Clearly, e.g. in the VOR, the original neural command is purely phasic (Fernandez and Goldberg 1971a, 1971b). Such inputs to motoneurons would move the eye while the head is moving, but after the head stops the eye would drift towards some resting position. This drift would have an exponential rate with a time constant equal to r / k. For David A. Robinson, the solution to this problem was clear. To get a position-related signal (the motoneuron step) from a velocity-related signal (i.e. in canal afferents and other pulse generators), a process equivalent to mathematical integration is required (Robinson 1968; Skavenski and Robinson 1973). However, the motoneurons themselves do not integrate their inputs. Thus, Robinson proposed that in addition to the direct pathway for velocity-related inputs to ocular motoneurons, there is an indirect pathway. The latter pathway would contain a specific neural structure that converts this signal into a position-related signal, the so-called oculomotor integrator (Robinson 1968, 1975, 1989). Thus, we have the simple model for 1-D eye movement illustrated in Figure 2.

The appeal and importance of the oculomotor neural integrator concept are threefold. First, it elegantly explains position holding during all types of conjugate eye movement. Second, the positional drift that results from damage to such an integrator would account for the commonly observed clinical disorder called gaze-evoked nystagmus (Leigh and Zee 1991). Finally, it provides a general hypothesis to explain conversion of phasic neural commands into tonic signals throughout the brain.

The ensuing search for the neural integrator amassed favourable evidence. Stimulation of the PPRF (Fig. 3) induced constant-velocity horizontal eye movements that held their final position when stimulation stopped (Cohen and Komatsuzaki 1972). This suggested that the PPRF either was the integrator, or was upstream from the integrator. Later experiments confirmed the latter to be the case (Henn et al. 1984). Furthermore, lesions of the cerebellum gave rise to eye position drift consistent with imperfect integration (Carpenter 1972, Robinson 1974). This search culminated in the discovery of a small area in the nucleus prepositus hypoglossi and medial vestibular nucleus (Fig. 3) that is essential for maintenance of horizontal position of both eyes, i.e. the integrator for horizontal eye position (Cannon and Robinson 1987; Cheron and Godaux 1987).

The key observation following injection of neurotoxins into the prepositus hypoglossi region was exponential drift of horizontal eye position towards a central resting or "null" position, without abolishing eye movements (Fig. 2 C). Furthermore, the horizontal position-related step signal appeared to be absent during all types of conjugate eye movement. Thus, the existence and location of the horizontal integrator were confirmed, as was the theoretical prediction that a single integrator is shared amongst all conjugate eye movement systems (Robinson 1975). Currently, most investigators believe that oculomotor integration is achieved by a distributed network with connections throughout the brainstem, including the vestibular nuclei (King et al. 1981; Fukushima 1987). Therefore, instead of saying that the nucleus prepositus hypoglossi is *the* horizontal

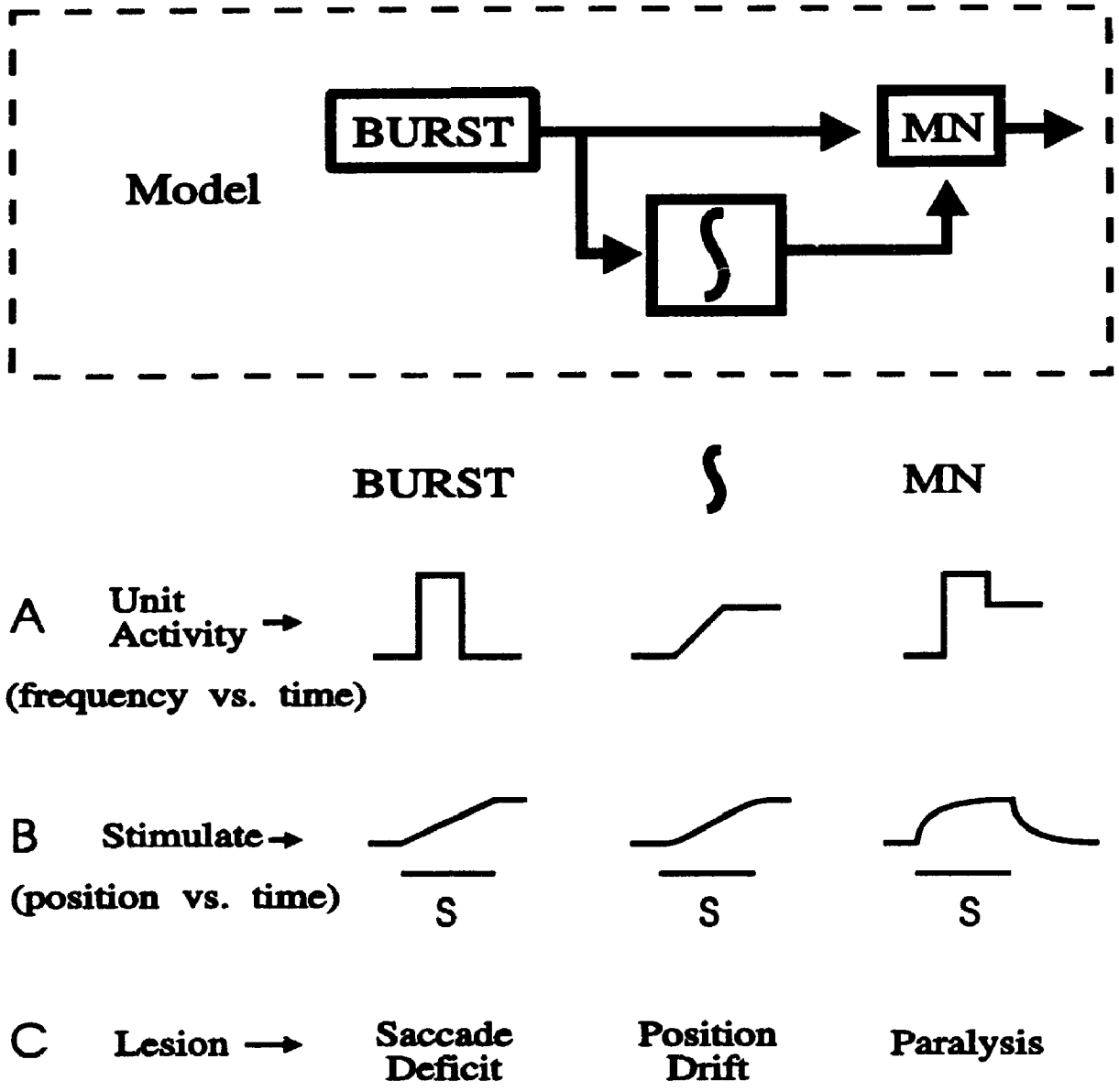

FIGURE 2. One-dimensional model of the brainstem saccade generator. The burst generator (BURST) has input directly to the motoneurons (MN) and indirectly through the neural integrator (∫). Lower 3 rows show predicted experimental results from these three structures using three techniques: (A) pattern of action potentials observed during a saccade in the agonist direction, (B) eye movement vs. time during electrical microstimulation (S), and (C) movement deficit during a selective lesion.

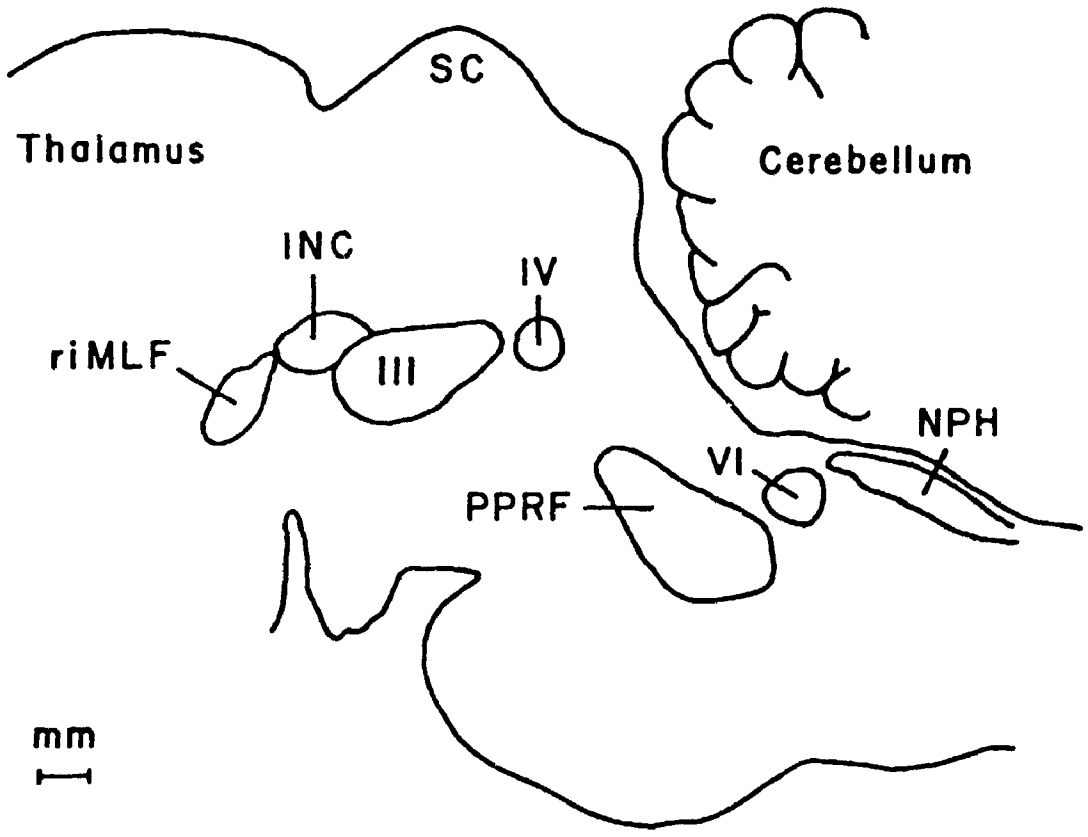

FIGURE 3. Anatomy of brainstem structures involved in producing eye movements. A parasagittal view from the monkey is shown. Cranial nerve nuclei supply motoneurons to the extraocular muscles. III: ipsilateral medial rectus, inferior rectus, and inferior oblique, and contralateral superior rectus. IV: contralateral superior oblique. VI: ipsilateral lateral rectus. The paramedian pontine reticular formation (PPRF) and rostral interstitial nucleus of the medial longitudinal fasciculus (riMLF) possess burst neurons for horizontal and vertical saccades, respectively. The integrator for horizontal eye position appears to be centred in the nucleus prepositus hypoglossi (NPH) region.

integrator, it may be more accurate to say that this nucleus comprises a critical component of the integrator.

1.2.5 *Hypothetical integrator mechanisms*

The concept of neural integration has inspired a number of theoretical examinations (Cannon et al 1983; Cannon and Robinson 1985; Galiana and Outerbridge 1984; Kamath and Keller 1976; Robinson 1989; Rosen 1972; Tweed and Vilis 1987). Any such integrator must change its output in response to phasic inputs, and then maintain that activity, essentially by using a positive feedback loop. An early model of oculomotor integrator neurons utilized parallel units with discrete on or off states (Rosen 1972), but subsequent experiments clearly showed that action potential frequencies in neurons of putative integrator sites are linearly related to eye position (King et al. 1981; Tomlinson and Robinson 1984). Another model of the integrator utilized more realistic units arranged in parallel, but the output of these neurons was lumped together to form a single positive feedback loop for integration (Kamath and Keller 1976).

Cannon et al. (1983) pointed out that integration in any model based on a single positive feedback loop is very sensitive to minute errors in feedback gain. Damage to such an integrator would produce a simple position-dependent exponential drift of the eye towards a unique "null" position, with a time constant that is inversely proportional to the amount of damage (Robinson 1989). For example, reduction of excitatory feedback gain by only 0.4% would decrease the time constant of integrator leak from a normal value of 20-25 seconds to 1.2 seconds, i.e. the position signal would decrease by 63% in this time. Such an arrangement is clearly not robust, when the potential for biological noise and neural damage is considered.

To address these problems, Cannon et al. (1983) proposed a model whose basic circuit was a pair of neurons with inputs that changed in opposite directions during

movement. The need for "negative" firing frequencies was overcome by modulating integrator neuron activity up or down from a baseline firing rate. These neuron pairs had mutually inhibitory lateral connections, so that each excited itself through disinhibition. If the two neurons in each pair were located on opposite sides of the brain, then this would give a scheme with bilateral push-pull inputs and a commissural feedback loop, similar to the suggestion of Galiana and co-workers (Galiana and Outerbridge 1984). Lateral inhibition solved one particular problem: these neurons only integrated push-pull movement commands and not background inputs.

To solve the problem of robustness, the number of parallel neuron units was increased. This in itself does not give robustness, i.e. a network of neurons that are equally inter-dependent will still respond to a given percentage of damage like a single leaky integrator. Rather, robustness was achieved by organizing the pattern of lateral inhibitory connections so that connections were dense between neighbouring units, but sparse between distant units. Taken to a conceptual extreme, this would result in a number of parallel and independent integrator "modules". Simulated damage to many neurons in a local portion of the network would disrupt integration in local modules without affecting modules in other regions. Simulation of this situation predicted a post-saccadic drift that was initially rapid, but then stabilized, essentially holding within a second at a slightly less eccentric position maintained by the undamaged integrator circuits (Cannon et al 1983). The remaining circuits were still able to maintain most of the eye position signal, and could eventually be recalibrated to compensate for the damage. Furthermore, this integrator circuit was relatively immune from random computational errors. For its net output to leak like that of a single leaky integrator, all of its circuits would have to be equally affected. Thus, this model had structural parallel distributed properties that had important functional implications. Although Cannon and Robinson (1987) later investigated the pontine oculomotor integrator experimentally, the

parallel distributed properties of their model remained untested (Robinson 1989).

1.3 PHYSICAL PROPERTIES OF 3-D ROTATIONS

The previous discussion has been confined to eye movements in one-dimension, but in real life the eyes rotate in three-dimensions. Before examining the brain mechanisms for such movements, it is necessary to understand the basic issues that arise when one considers three-dimensional rotations.

1.3.1 *Coordinate systems and reference frames.*

In order to describe the location or orientation of some object, we need a coordinate system. Lets start with a familiar example. Consider an airborne plane that is currently 2 km north and 1 km west of this location (my office at U.W.O) at an elevation of 3 km (to simplify matters let's assume that the earth is flat). In order to interpret this, we must have understood concepts that capture all of the general principles of coordinate systems. First, we used an origin, my office. Second, we have what are called, in the parlance of linear algebra, basis vectors (Nicholson 1986). These can be visualized as lines going from the origin to three points positioned at one km north, one km west, and one km straight up from my office (south, east, and down can be considered the negatives of these three). These basis vectors incorporate both the notions of direction, and a relativistic unit of magnitude (the km). The number of distance units that we specified along each direction are called the components (i.e. components of the vector going from my office to the plane). Finally, we implicitly assumed the reference frame to be the earth, which means that the orientation of the basis vectors is always the same with respect to the earth.

In the above example we considered translational position, but in the oculomotor system we are interested in angular positions of the eye. Again, at least three

components will be needed to uniquely specify each orientation in 3-D space. Since the eye muscles and semicircular canals have actions fixed with respect to the head, there is general agreement that a craniotopic reference frame is preferable (Fetter et al. 1986; Raphan and Cohen 1986; Robinson 1985; Tweed and Vilis 1987). Previously, the most commonly used coordinate system was the one devised by Fick (Ferman et al 1987a, 1987b, 1987c; Robinson 1963). However, in Fick's system, some coordinate axes are fixed with respect to the head and others are fixed with respect to the eye. This makes the Fick system both un-physiological and difficult to interpret.

To avoid these problems, we will use a coordinate system in which position is described by an angle of rotation relative to some central reference position, about a fixed axis. This will be expressed as components of rotation about three mutually orthogonal, head-fixed coordinate axes: the horizontal component about a head-fixed vertical axis, vertical about an axis parallel to the interaural axis, and ocular torsion as rotation about the forward pointing head-fixed axis, with counterclockwise and clockwise rotation measured from the subjects perspective (these coordinates will be more precisely defined in section 1.4.2 to correspond to coordinates intrinsic to the oculomotor system). As we shall see, the vector parts of the mathematical entities called quaternions provide this representation (Tweed and Vilis 1987; Westheimer 1957).

The use of coordinate systems by the brain is a separate issue. The eye muscles themselves define a head-fixed coordinate system in which simultaneous torque vectors from each muscle are summed componentwise to give a net torque vector (Raphan and Cohen 1986; Robinson 1985; Tweed and Vilis 1987). Since net muscle torques have a fixed ratio to motoneuron activity (Robinson 1970), the latter specifies the components of eye position in muscle coordinates. However, the upstream neural structures need not necessarily utilize an explicit coordinate system. For example, the superior colliculus appears to encode eye displacements in a retinotopic reference frame using a map of all

possible displacements, rather than specifying components of the displacement along a few coordinate axes (Soechting and Flanders 1992; Sparks and Mays 1990).

1.3.2 *The laws of rotational kinematics.*

Although eye position may be expressed as rotation about an axis, this gives no information on the current, or previous history of eye movement. By analogy, the above specification of airplane position relative to my office in U.W.O did not imply that it had taken off from my office, or was heading away from my office at that moment. Instantaneous motion of the eye is best represented by angular eye velocity, in the same head-fixed coordinate system used for position.

An angular velocity vector can be expressed as rotation of a body about a three-dimensional axis at a certain speed (degrees / second). In the case of translational motion, the relationship between velocity and rate of position change is trivial: they are the same thing. However, this is not the case for angular velocity. Rate of rotational position change depends on current eye position as well as current eye velocity in a multiplicative, non-linear fashion that is representation-independent (Tweed and Vilis 1987).

$$\dot{q} = \omega q/2 \qquad (2)$$

Where q is eye position (expressed as a quaternion), $\dot{q}$ is rate of position change (the first derivative of position with respect to time), and ω is angular velocity.

One concrete corollary of Equation 2 is that rotations do not in general commute. That is, rotation A followed by B gives a different final orientation than B then A, except in the case where A and B occur about the same axis (that is why non-commutitivity could be ignored in the previous one-dimensional discussion). To convince yourself of

this non-commutitivity, place your right hand palm-down (thumb to the left) on a table in front of you. Now rotate your hand up by 90° about a space-fixed horizontal axis so that the fingers point to the sky. Second, rotate the hand left 90° about the space-fixed vertical axis. Remember the hand's final position: palm to the left, thumb pointing towards you. Now, repeat these rotations in the opposite order, starting again with the hand palm down and thumb to the left. First, rotate the hand 90° left so that the thumb points towards you, and then rotate the hand upwards (the little finger rising) by 90° about the same horizontal axis (which is now parallel to your middle finger). The final orientation (palm away, thumb downwards) is clearly different this time. Thus, the ordering of a sequence of rotations is critical for determining final position.

1.3.3 *Implications for the oculomotor integrator theory.*

As a result of the specific position dependence of eye position changes embodied in Equation 2, rotation of the eye about fixed axes may have surprising effects on eye position. In order to maintain these final positions, a matching muscular torque must be generated. This in turn requires that the neural position signal generator incorporates the principles of rotational kinematics.

Can the classical neural integrator provide the correct position signal during three-dimensional eye movements? The first derivative of position with respect to time is rate-of-position-change, and so conversely, position is the integral of rate-of-position-change. This poses no problem for one dimensional rotations, in which

$$q = \int \dot{q} = \int \omega \qquad (3)$$

Where q, $\dot{q}$, and ω again represent position, rate-of-position-change, and velocity. However, in three dimensions, rate of angular position change is different from angular

velocity (Equation 2), and thus position is not the integral of the velocity. Rather,

$$q = \int \dot{q} = \int \omega q/2 \qquad (4)$$

Consider the hand rotation experiment described above. If we attempted a component-wise integration of angular hand velocities during the two series of movements, the same final integral would result in either case, whereas two completely different final hand positions were observed.

Tweed and Vilis (1987) were the first to point out this problem to the oculomotor community and give the solution. If the input to the oculomotor indirect path is a velocity signal, then this signal must be multiplied by a current eye position signal to compute the rate of position change, and the latter could then be integrated to give the correct 3-D position signal (Equation 4). The VOR indirect path would have to do this in order to correctly stabilize the eye during and after head movements.

1.4 THREE-DIMENSIONAL ORGANIZATION OF THE OCULOMOTOR SYSTEM

In this section we examine what is known about three-dimensional coordinate systems and rotational kinematics in the oculomotor system.

1.4.1 *The vestibuloocular reflex in three dimensions.*

The VOR is equipped with the sensory and motor structures necessary to compensate for head rotations in any three-dimensional direction. The extraocular muscles are arranged in three pairs of muscles with approximately opposite pulling directions, the medial-lateral rectus pair discussed in section 1.2.2, the superior rectus-superior oblique pair, and the inferior rectus - inferior oblique pair (Fig. 4 A) (Ezure and Graf 1984; Simpson et al. 1986). The latter two pairs produce roughly equal amounts of vertical

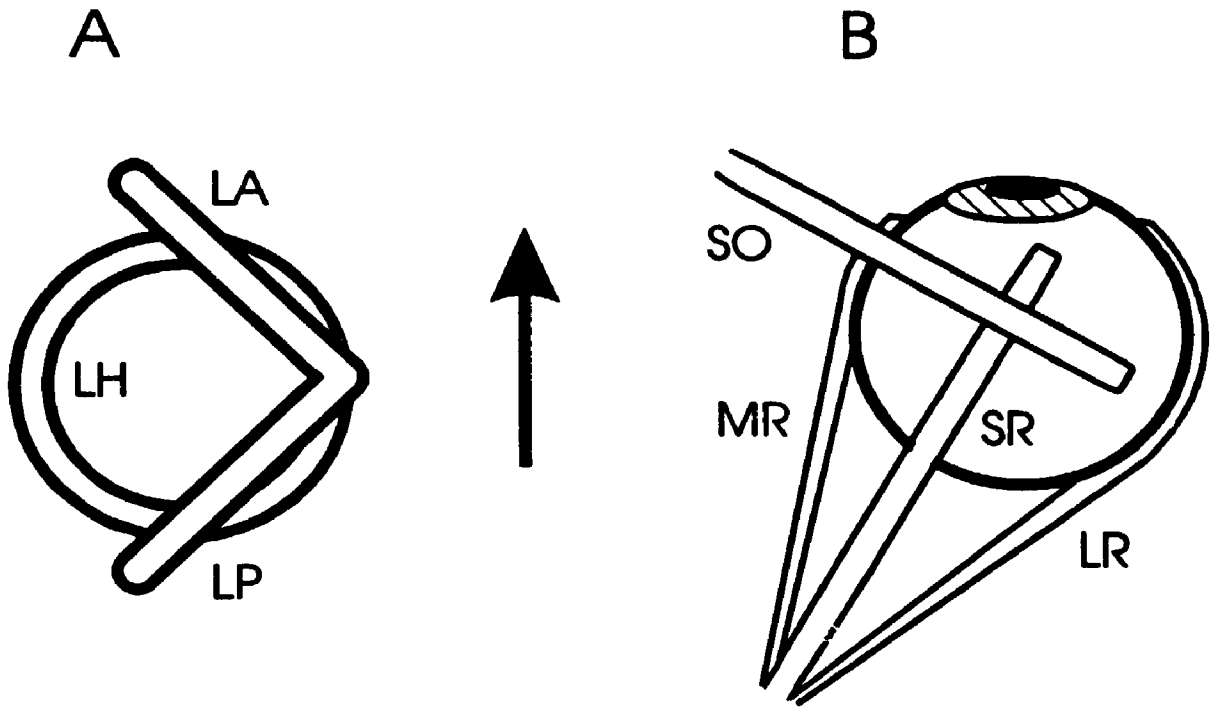

FIGURE 4 Anatomy of eye muscles and semicircular canals in three dimensions. The arrow indicates the forward pointing direction of the subject's head, viewed from above. **A**: Schematic view of the semicircular canals in the left ear. Canals are represented by simple circular tubes: LH: left horizontal. LP: left posterior. LA: left anterior. Each canal senses head rotation about an axis orthogonal to its plane, and these planes are mutually orthogonal. **B:** Schematic view of the extraocular muscles in the right eye. Muscles are represented by strips with closed ends at the ocular insertion and open ends at the functional cranial insertion. The medial rectus (MR), lateral rectus (LR), superior oblique (SO), and superior rectus (SR) are visible. Not visible are the inferior oblique (IO) and inferior rectus (IR), which are directly below the SO and SR respectively, beneath the eye. Thus there are three opposing pairs of muscles, MR - LR, SO - IO, and SR - IR. Each pair controls eye rotations about the axis orthogonal to its head-fixed plane. Note that the spatial arrangement of the muscle planes is similar to that of the canal palnes, but not identical. Structures not shown on the opposite sides of the head are basically mirror images across the sagittal plane of those illustrated.

and torsional rotation in each eye. If we lump the two members of each pair together, then a coordinate system results based aproximately on the following rotations about three mutually orthogonal coordinate axes, (1) left - right, (2) clockwise / up - counterclockwise / down, and (3) clockwise / down - counterclockwise / up. The three pairs of semicircular canals sense head rotations about three similar axes (Fig. 4 B) (Ezure and Graf 1984; Simpson and Graf 1985).

In three dimensions, one must consider not only the gain of the VOR, but also its direction. To stabilize 3-D angular eye position, an optimal VOR would rotate the eye about an axis parallel to that of the head, at the same speed but opposite direction. In other words, the head velocity vector should be reversed. Algebraically, this is achieved by left multiplying the head velocity vector by the negative identity matrix (Robinson 1982):

$$\begin{matrix} -1 & 0 & 0 \\ 0 & -1 & 0 \\ 0 & 0 & -1 \end{matrix}$$

This hypothetical matrix is the 3-D analogue of 1-D VOR gain, which we might therefore call a "gain matrix". The negative ones along the main diagonal of this matrix simply reverse the sign of the head velocity vector components, like 1-D gain elements. What of the off-diagonal components? These are the gain elements that transform one component of head velocity into other components of eye velocity, e.g. horizontal head velocity to vertical and/or torsional velocity. These are generally assumed to be zero, but this need not be the case. For example, by exposing the eyes to consistent vertical visual slip during horizontal head rotations, the VOR can be adapted to produce horizontal and vertical eye rotation in response to purely horizontal head rotation

(Schultheis and Robinson 1981).

The VOR direct path has been modeled using a series of matrices whose overall product is equivalent to the transformation represented by the above gain matrix (Robinson 1982, 1985; Vilis and Tweed 1988). However, such a matrix has never been measured experimentally. Previous three-dimensional studies of the VOR have simply triplicated the 1-D approach, giving three scalar gain values for horizontal, vertical, and torsional VOR (Collewijn et al. 1985; Ferman et al. 1987a; Seidman and Leigh 1989; Skavenski et al. 1979). The main finding of these studies was that the VOR can rotate the eye in all directions, but whereas horizontal and vertical gain are close to ideal in humans and experimental animals, torsional gain is somewhat lower (Berthoz et al. 1984).

The off-diagonal components of the gain matrix in a normal subject have not been investigated. Furthermore, the diagonal components were based on time derivatives of position signals, which do not correctly represent eye velocity (Equation 4) (Tweed and Vilis 1987). Finally, the kinematic properties of 3-D rotations considered in section 1.3.2, and their implications for the indirect path of the VOR (section 1.3.3) have not been examined.

1.4.2 *Kinematic redundancy and Listing's law.*

The VOR is an exceptional case in sensorimotor transformations, because in a given set of circumstances there is only one correct motor solution for any one sensory input. This is because the task of the VOR (image stabilization) requires all three degrees of freedom in the oculomotor plant. In most cases in motor control, the plant is equipped with more kinematic degrees of freedom than are necessary to accomplish the required kinematics of the task in extra-personal space. This is called kinematic redundancy, and it poses a question that has often been called "the over-completeness problem" or the

"degrees of freedom problem" (Pellionisz and Peterson 1988). The question is, given an infinite number of ways to perform a task, does the brain choose the same way every time, and if so, what rule does it choose to follow? The selection it makes should provide insights into brain mechanisms and what they attempt to optimize.

The saccadic system gives a simple example of kinematic redundancy. Its task is to redirect gaze direction. Gaze direction is a 2-D entity, e.g. it may be specified by two angles such as azimuth and elevation in a Fick coordinate system. However, as we have already seen, the oculomotor plant has three degrees of freedom. In particular, it is fully capable (e.g. during the VOR) to rotate the eye about the gaze axis without changing gaze direction. Thus, a potentially infinite number of 3-D eye orientations could be used for any one gaze direction. However, in the previous century Donders found that during visual fixations between saccades with the head upright and still, only one 3-D orientation was assumed for each gaze direction, regardless of previous saccade history (Helmholtz 1925). This has come to be called Donders' law.

Is a consistent rule used to implement Donders' law? This law states that eye position is constrained to a 2-D subspace of the possible set of all 3-D eye orientations. If this 2-D subspace is continuous from one gaze direction to the next, it would be a surface. The question then, is what is the shape of this surface? Helmholtz (1925) and his student Listing answered this question by observing the systematic tilts of visual after-images in various gaze directions. Their result, now called *Listing's law*, states that the position surface is a flat plane (using the convention for expressing eye positions stated in section 1.3.1.).

To be specific, Listing's law states that any arbitrarily chosen (reference) eye position is associated with a particular head-fixed plane, such that the eye only assumes positions that can be reached from this reference position about an axis in that plane (Nakayama 1983; Tweed and Vilis 1990a). These planes may be called *displacement planes.*

Furthermore, there is one special reference position, *primary position*, for which the gaze direction is orthogonal to its displacement plane (Fig. 5). This is called *Listing's plane*. It can be shown that each other displacement plane tilts away from Listing's plane by half the angle between its particular reference gaze direction and the primary gaze direction (Tweed et al. 1990; Tweed and Vilis 1990a).

We can define a special head-fixed orthogonal coordinate system in which the vertical and horizontal coordinate axes are parallel with Listing's plane, and the torsional axis is parallel with the primary gaze direction. Using such *Listing's coordinates*, one can restate Listing's law very simply: the eye only assumes positions with a zero torsional component (Tweed and Vilis 1990a, Westheimer 1957).

Recently, Listing's plane has been measured directly using the 3-D search coil technique (Ferman et al. 1987b, 1987c; Tweed et al. 1990) . In real life Listing's plane has a finite, uniform thickness throughout the oculomotor range. This thickness, expressed as standard deviation of torsional position about a fitted plane, is between 1 and 2 degrees (Ferman et al 1987b; Ferman et al. 1987c; Straumann et al. 1991; Tweed and Vilis 1990a). It is equally thick during saccades and between them (Ferman et al. 1987c; Tweed and Vilis 1990a), even for curving saccades (Van Gisbergen et al 1992). Thus Listing's Law (LL) is important during the generation of saccades as well as for determining final eye position.

Given the laws of rotational kinematics described in section 1.3.2, it should not be so surprising that there is a non-trivial relationship between saccade axes (eye velocity) and eye positions during maintenance of Listing's law. In order to maintain eye position in Listing's plane, saccade axes are geometrically required to tilt torsionally out of Listing's plane (Fig. 6). In fact, the axis for a straight saccade must be the intersection between the displacement planes for the initial and final position (Tweed and Vilis 1987, 1990a, 1990b). Thus, axes of eye rotation during saccades tilt out Listing's plane by a

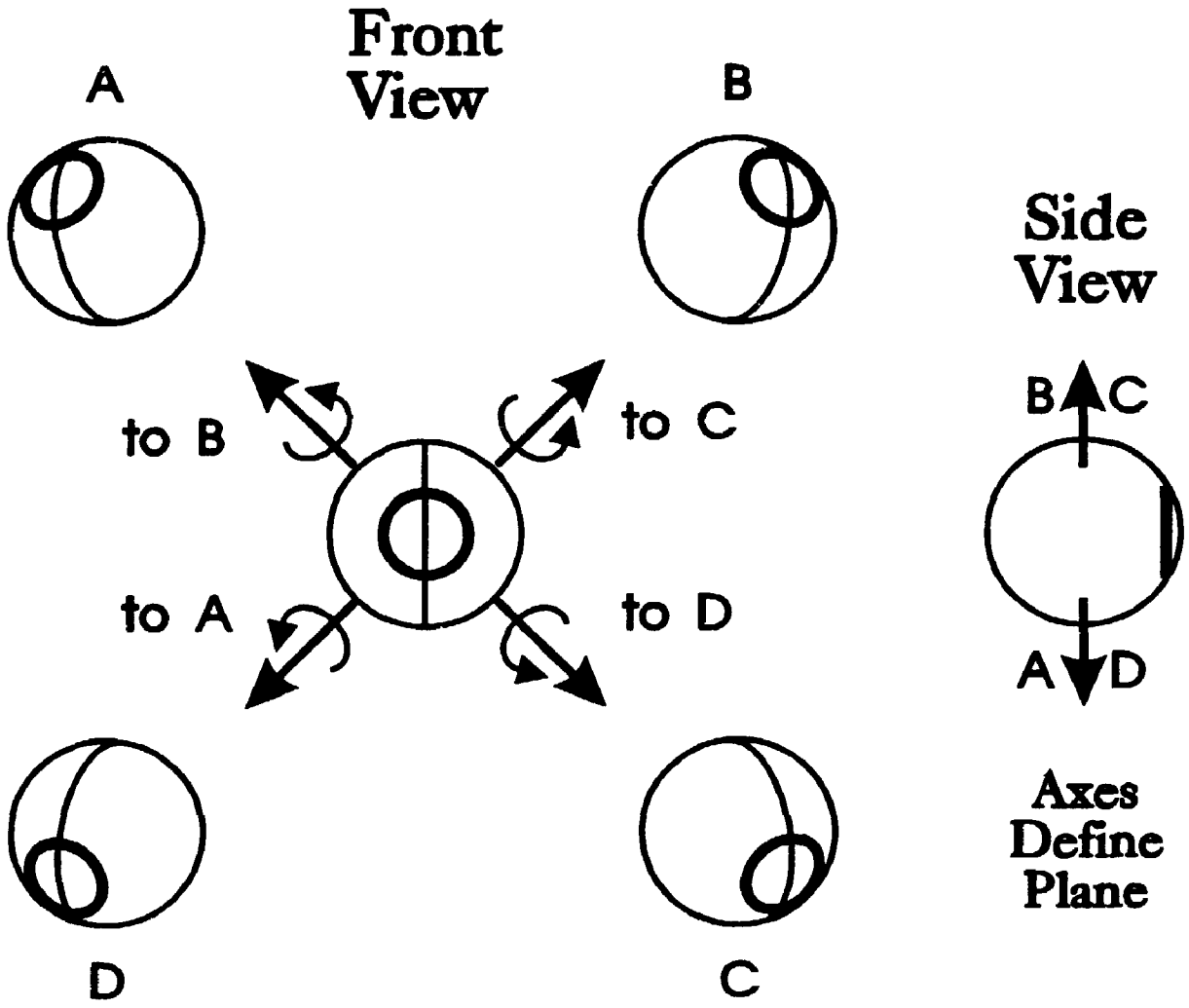

FIGURE 5. Definition of Listing's law. Saccades reach eccentric eye positions (e.g. A, B, C, and D) from the central primary position by rotating the eye about axes that lie in a plane (i.e. the plane of the page in the illustrated front view). This plane can be seen by viewing the axes from the side. These axes of rotation relative to primary position are used to describe three dimensional eye position.

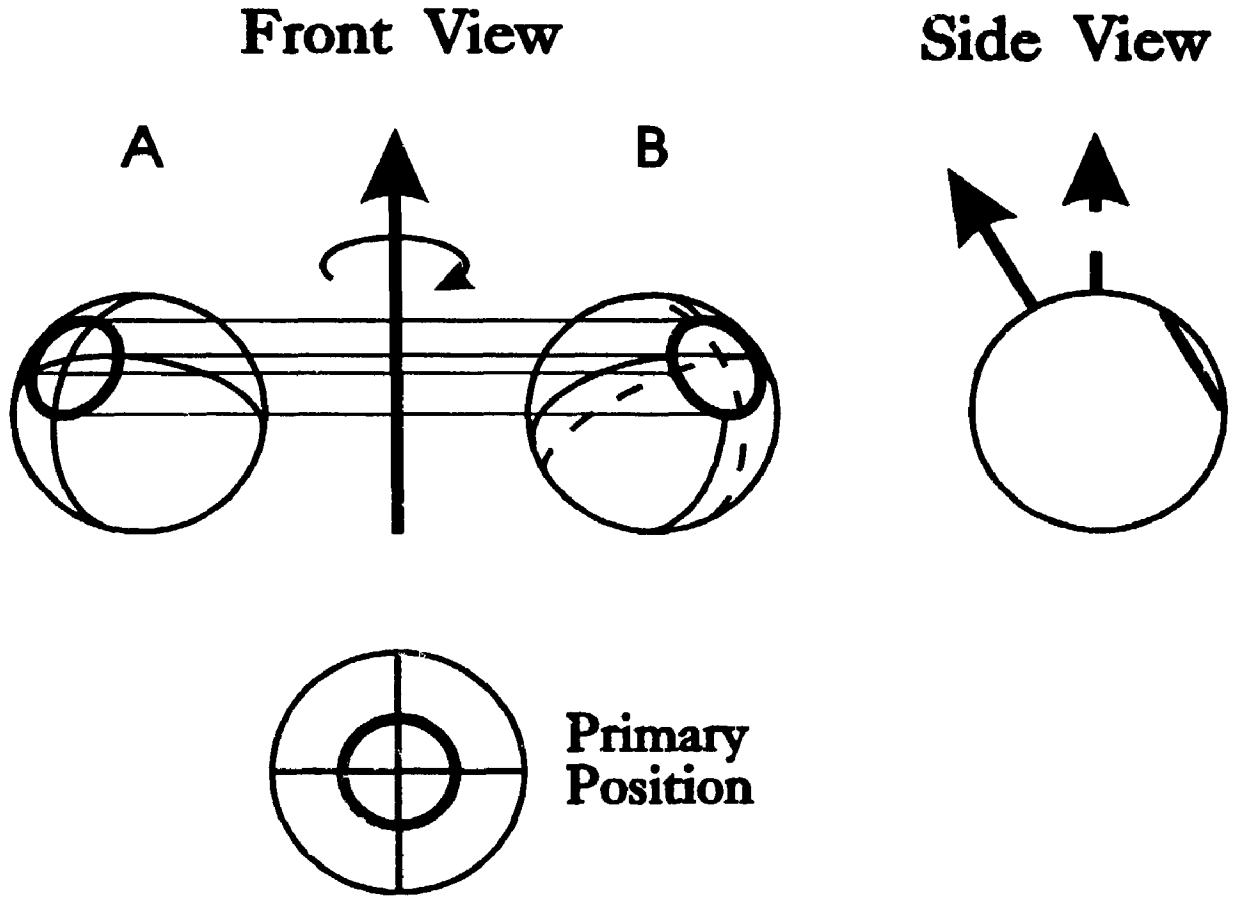

FIGURE 6. Saccade axis tilts required by Listing's law. Eye position is viewed frontally in two positions, (A) up and right from the subjects point of view, and (B) up and left. The side view shows two possible saccade axes, one (dashed line) in Listing's plane and one that tilts counterclockwise (solid line) by half the angle of upward eye position in A and B. The former axis drives gaze direction to the right end point, but 3-D eye position is not in Listing's plane (B, dashed lines). The torsionally tilting axis gives the right gaze and 3-D orientation (B, solid lines).

half-angle rule similar to that described above for displacement planes. Whereas some investigators would suggest that these tilts arise from some mechanical property of the extraocular muscles (Ferman et al. 1987c; Sparks and Mays 1990), others have suggested that Listing's law is implemented by specific neural mechanisms (Hepp 1990; Robinson and Zee, 1981; Tweed and Vilis 1990b).

1.4.3 *Burst neuron coordinates.*

Short lead burst neurons are segregated anatomically into populations of cells with similar directional tuning (King and Fuchs 1979; Luschei and Fuchs 1972). These populations are mainly located in two brainstem nuclei (Fig. 3), (i) the paramedian pontine reticular formation (PPRF) which possesses populations for leftward and rightward movements (Cohen et al. 1968; Cohen and Komatsuzaki 1972; Keller 1974; Luschei and Fuchs 1972; Strassman et al. 1986; Van Gisbergen et al. 1981), similar to the horizontal muscles or semicircular canals and (ii) the mesencephalic rostral interstitial nucleus of the medial longitudinal fasciculus (riMLF), each lateral riMLF side possessing a population for upward movements intermingled with another population for downward movements (Büttner et al. 1977; Büttner-Ennever and Büttner 1978; King and Fuchs 1979; Kompf et al. 1979). There may also be a systematic oblique tilt to the directional tuning of these vertical burst neurons (Büttner et al. 1977). Recent single unit recordings and pharmacological inactivations of the monkey riMLF have suggested that the vertical burst neurons in the right riMLF also produce clockwise (CW) eye rotation, whereas the left riMLF neurons produce counterclockwise (CW) rotations (Henn et al. 1989; Hepp et al. 1988; Vilis et al. 1989). Thus, burst neurons appear to utilize a coordinate system similar to that of the semicircular canals or eye muscles (Büttner et al. 1977; Robinson and Zee 1981).

Theoretical and experimental observations agree the reference frame for burst neuron

coordinates should be the head (Büttner et al. 1977; Pellionisz 1986; Robinson and Zee 1981). However, the above experiments did not distinguish between canal or muscle alignment. These schemes, like most coordinate schemes in motor control, assume alignment with anatomy, whereas some have argued that the intermediate neurons in a sensorimotor transformation utilize "abstract" coordinate systems with no obvious correlates (Masino and Knudsen 1990; Soechting and Flanders 1992). Another possibility is that these so-called abstract coordinates actually align with some aspect of the behaviour produced, in this case Listing's plane, which varies with respect to anatomical coordinates (Tweed and Vilis 1990a). All models of the neural mechanism for Listing's law to date have utilized burst neuron coordinates that were either aligned with or symmetrical about Listing's coordinates, although their authors did not emphasize this point (Hepp et al. 1990; Robinson and Zee 1981; Tweed and Vilis 1990b).

1.5 GAPS IN CURRENT KNOWLEDGE AND SCOPE OF THE THESIS

This thesis is concerned with the brainstem mechanisms for three-dimensional eye movement and fixation in the monkey. The specific questions posed arose from a rich background of theoretical and experimental investigations, but a direct debt is owed to two particular recent advances. First, an understanding of the physical laws governing rotations was required, which has only recently been made accessible (Tweed and Vilis 1987). Second, a new technology was required for correctly measuring the three-dimensional axes of eye velocity and position (Tweed et al. 1990). Previously, this technology had only been used to study the normal behaviour of the saccadic system (Tweed and Vilis 1990a). This thesis describes correct 3-D measurements of the vestibuloocular reflex, and of eye movements during single unit recording, microstimulation, and pharmacological inactivation of neurons.

Chapter 3 examines the basic behaviour of the VOR in three dimensions. This

includes the first precise evaluation of the direction of VOR slow phases, with the goal of experimentally determining the 3-D VOR gain matrix. Next the eye position changes produced by these rotations are considered. If the pattern of position changes predicted by the principles of rotational kinematics are produced and held, then the indirect path of the VOR (which includes the neural integrator) must incorporate these principles. Finally, Chapter 3 examines whether quick phases uphold Listing's law.

The experiments described in chapters 4 - 6 utilized invasive techniques to directly examine the mesencephalic mechanisms for three-dimensional eye movements. One general hypothesis explored in these chapters is that a common canal-like coordinate system is utilized by the brain to generate vertical and torsional eye movements. Chapter 4 explores the coordinate system of oculomotor burst neurons in the riMLF, in particular asking if these coordinates have any relationship to Listing's law.

Section 1.2.4 described the localization of the integrator for horizontal eye position in the prepositus hypoglossi region (Cannon and Robinson 1987). Where are the other integrators for vertical and torsional eye position? Chapter 5 reviews evidence that these are in the interstitial nucleus of Cajal (INC), and presents experiments that strongly support this important hypothesis. Chapter 5 also examines the coordinate system used by the INC. Finally, Chapter 6 uses data from these experiments to test one fundamental aspect of Cannon et al.'s network model (1983): is the neural integrator compartmentalized into parallel, independent modules?

2 METHODS

2.1 RECORDING EYE MOVEMENTS IN MONKEYS

To correctly examine three-dimensional eye movements, we need a representation of eye position that fulfils three requirements: (1) it must be simple and meaningful (see section 1.3.1), (2) it must handle the complex non-commutative properties of rotations (see section 1.3.2), and (3) it must be measurable in the monkey. The following section (and APPENDIX I) shows that eye position quaternions fulfil these requirements.

2.1.1 *Measurement of eye position quaternions and velocities*

A total of six *Macaca fascicularis* (coded MAR, BAR, FAR, LAR, CAS, ART) were prepared for chronic behavioral experiments, each monkey undergoing surgery under aseptic conditions and pentobarbital anaesthesia. During surgery a skull cap composed of dental acrylic was fastened to the animal's head, and two enamelled copper search coils of 5 mm diameter were implanted in one eye for measurement of 3-D eye position. Both coils were positioned nasally, one inferior and one superior. The method used did not require that the coils be aligned orthogonally to each other (Tweed et al. 1990). The leads were extended temporally beneath the conjunctiva and then subcutaneously to sockets secured on the cap. In two of the animals (CAS & ART), coils were implanted in both eyes. During experiments, the head of the alert monkey was immobilized by fixing the skull cap near the centre of three orthogonal magnetic fields. These fields were in phase, but operated at different frequencies (62.5, 125, and 250 KHz). The resultant six coil signals / eye were digitized by a computer at a sampling frequency of 100 Hz during random eye movements, 500 Hz during brain stimulation, and 1000 Hz during trained goal-directed saccades.

The computer was used to convert coil signals into eye position quaternions, both on-

line and after experiments. This computation utilizes Faraday's law that an electric current is produced in each eye coil that is proportional to the sine of the angle between the plane of the coil and the field direction (Figure 7 A). Such signals are used directly to represent one dimensional eye position (Robinson 1963). However, to compute quaternions, the three signals / coil are treated as the components of a vector orthogonal to the coil (Fig. 7 B), multiplied by a gain factor (Tweed et al. 1990). The components of the two coil vectors, and their cross product, constituted a 3 X 3 matrix for each eye position. At the beginning of each experiment such a matrix was recorded while the monkey looked along the forward-pointing field direction. The matrix at every other position was multiplied by the inverse of the reference matrix to give the relative rotation matrix. Eye position quaternions were algebraically derived from the latter (Tweed et al. 1990).

This system required that the coil signals all have the same gains and offsets. This was achieved by rotating a dummy coil within the fields. Gains and biases were adjusted so that each coil signal reached a maximal value of eight volts when the coil was orthogonal to a particular field direction, and a minimal value of zero volts when the coil was parallel to the field. This was the only calibration required by this system (Tweed et al. 1990). Calibrated in this fashion, we have detected measurement errors in eye rotation axes of up to 6°, but errors were usually much smaller than this.

Quaternions are composed of a scalar part q_0, and a vector part $\mathbf{q}$. The scalar part is necessary for the multiplicative operations underlying compositions of rotations, but it is the vector part that is used for representation of data. The vector part has components along torsional, horizontal and vertical axes fixed relative to the head (along basis vectors i, j, and k respectively). In order to interpret the data one need only understand that $\mathbf{q}$ is parallel with the axis of eye rotation relative to reference position, and its length is proportional to the magnitude of this rotation. To be specific, a quaternion is related

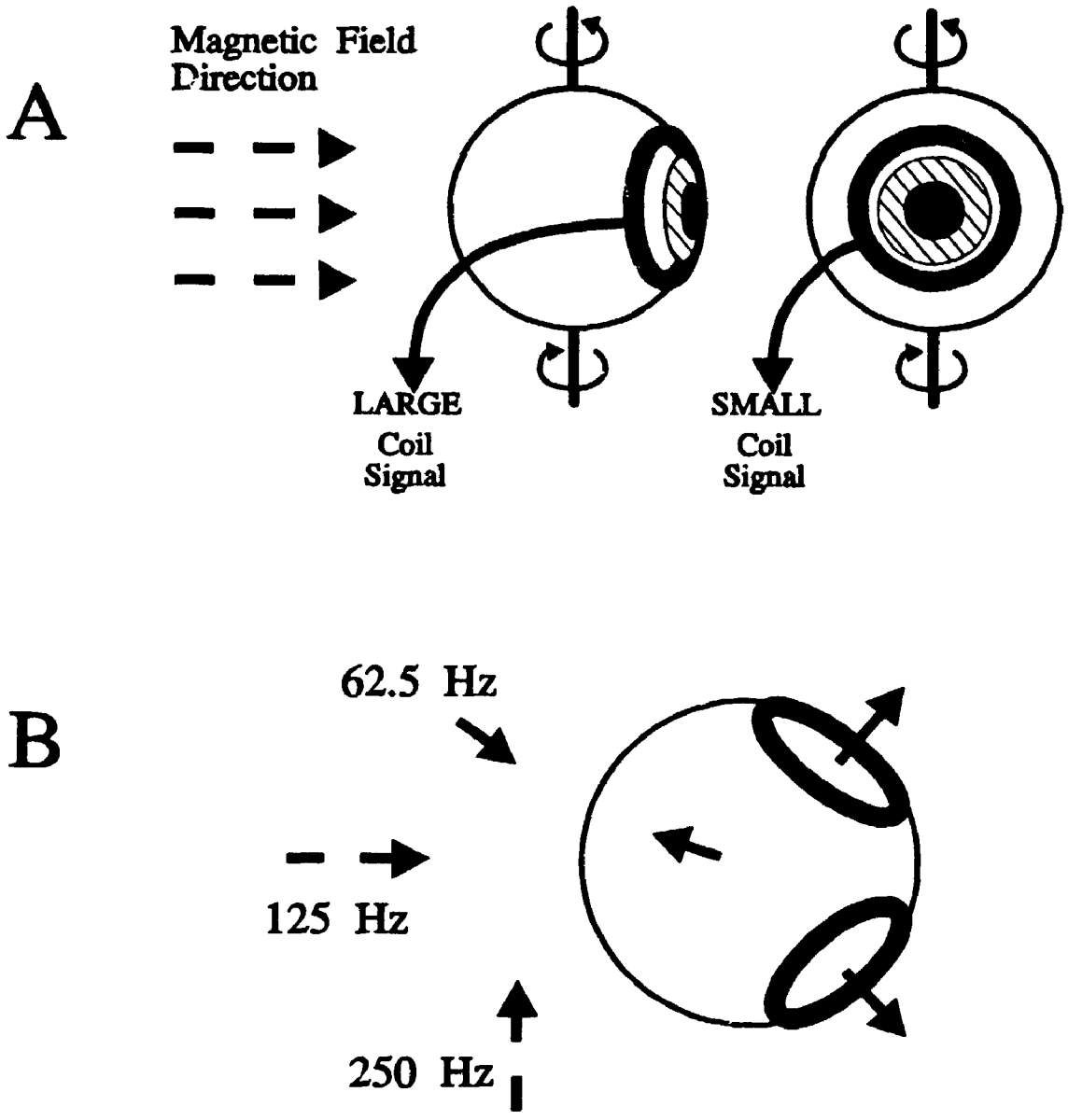

FIGURE 7. Recording eye movements in one and three dimensions. *A*: Recording eye movements confined to one dimension. The coil produces a maximal signal when its plane is orthogonal to the magnetic field direction, and a zero signal when they are parallel. *B*: Recording eye movement in three dimensions. Three magnetic fields produce signals proportional to the components of 2 vectors orthogonal to the 2 coils, and a third vector is computed by taking the cross product of the other two (see text).

to the axis and magnitude of a rotation as follows

$$q_0 = \cos(\alpha/2) \quad (5)$$

$$\mathbf{q} = \mathbf{n} \sin(\alpha/2) \quad (6)$$

The angle α is the magnitude of the rotational displacement and $\mathbf{n}$ is the 3-dimensional unit vector that is parallel to the axis of rotation (Tweed and Vilis 1987). At reference position α = zero and thus $q_0 = 1$ and $\mathbf{q}$ = zero. Direction of rotation from reference position is given by the right hand rule, i.e. if the right hand thumb is pointed from the origin along the quaternion vector, then the fingers curl in the direction of rotation.

Quaternions were also used to compute angular velocities of eye rotation. Angular velocity cannot be computed by simply differentiating coil signals, quaternions, or any other measure of position change, because $\vec{\omega}$ is also dependent on current eye position (Tweed and Vilis 1987). The general relation between angular velocity ($\vec{\omega}$), position quaternions and their rate of change may be expressed by reordering Equation 2,

$$\omega = 2\dot{q}q^{-1} \quad (7)$$

Where juxtaposition of quaternions signifies multiplication and q^{-1} is the inverse of q (the rules governing quaternion multiplication and inversion are described in APPENDIX I). The following variation on this general equation was used to compute the average eye velocity between any two eye positions. If the eye rotates from an initial position q^i to a final position q^f, then this relative displacement can be represented by the quaternion q calculated in Equation 8.

$$q = q^f (q^i)^{-1} \quad (8)$$

The vector part of q gives the axis of the rotation, but q is easily converted to the more familiar angular velocity. The angle α of rotation q may be derived by rearranging Equation 5. This angle is then divided by the time interval between the two eye positions to get the angular speed $\dot{\alpha}$. The axis n is obtained by entering the vector q and angle α into Equation 6. Thus, the direction and magnitude of $\vec{\omega}$ are specified as:

$$\vec{\omega} = \dot{\alpha}\ \mathbf{n} \qquad (9)$$

2.1.2 *Coordinate systems for data representation*

Depending on the question examined, data is presented in field coordinates, Listing's coordinates, or anatomical coordinates. Quaternion and velocity vectors computed from raw coil signals represent rotations in a coordinate system defined by the magnetic fields, ie. the torsional, vertical, and horizontal axes were parallel with the field directions. In some cases, eye positions were recorded after the head had been rotated from the normal upright orientation (during non-horizontal VOR recordings). This required a compensatory rotation of the coil signal matrix vectors V to the orientation they would have with the head upright during recording of the reference position, using simple rotation matrices or quaternion multiplication (APPENDIX I). This field coordinate system was rather arbitrary, since animals were placed within the fields at our best estimate of an upright position.

It was sometimes necessary to rotate these data into a Listing's coordinate system. The arbitrarily determined reference position did not generally align with primary position, so that the associated displacement plane was not Listing's plane. However, it has been demonstrated that the displacement plane will tilt from the horizontal-vertical field coordinate plane by the half-angle rule described in section 1.4.2 (Tweed and Vilis 1990a). Thus, by computing the orientation of the plane with respect to the gaze

direction at reference position, one can determine the orientation of Listing's plane and its orthogonal primary gaze direction. Quaternions and velocities are then easily rotated into a Listing's coordinate system (Tweed et al. 1990).

Data was also rotated into coordinates based on head-fixed anatomical structures. This required determination of the orientation of each animal's stereotaxic coordinates within the field coordinate system. In the four animals (MAR, BAR, LAR, and FAR) this was done by measuring the angle between a line from the centre of the external auditory canal to the orbital canthus, and the horizontal field direction. In the other animals (ART and CAS) search coils, aligned with the stereotaxic horizontal and sagittal planes, were implanted in the skull cap.

Whatever the coordinate system, we view velocity and quaternion axes from three standard perspectives: from above the animal, from the animal's right side, and from behind the animal, depending on which axis components are most relevant. The particular perspectives used on the figures below are initially (Chapters 3 and 4) indicated by head caricatures as a reminder of this fact.

2.1.3 *Elicitation of eye movements*

In all animals, spontaneous saccades were made to visual targets at a distance of 1 to 1.5 meters from the animals head, presented in positions meant to reveal the animal's full range of attainable eye positions and rapid eye movement axes. In four animals (FAR, LAR, CAS, and ART) this was also done while the animal's head was rotated about various axes to elicit compensatory VOR movements. This was done in the light with visual targets to elicit optimal stabilization of the retinal image (Barr et al. 1976; Ferman et al. 1987; Skavenski et al. 1979). Under these conditions, the VOR is assisted by other visual-oculomotor systems, including the optokinetic reflex (OKN) and smooth pursuit.

Angular motion of the head was generated by manually rotating the chair and monkey about an axis parallel to the earth-vertical field direction. A potentiometer detected the angular position of the chair. Since the fields rotated with the monkey, eye coils only detected eye motion relative to the head. The monkey's eyes were always placed near to the axis of rotation in order to minimize translations of the eye relative to visual targets. Orientation of the head within the fields was arbitrary, but Listing's plane was approximately earth-vertical when the monkey was upright. The monkey could be positioned upright, lying on its back, or lying on either side so that the head was rotated about its vertical, torsional or horizontal axis. This was done by repositioning the entire primate chair, i.e. the position of the head relative to the body was not changed. The head was sometimes positioned so that it rotated about axes intermediate between vertical and torsional. At each posture, eye positions were initially recorded with the head immobile, for comparison with eye positions during head rotation. During experiments the monkeys were rotated sinusoidally, usually at a frequency of about 0.5 Hz and amplitude of about 60 degrees.

For some parts of this study, it was necessary to know the intended direction of gaze shifts. Therefore, two animals (MAR and BAR) were trained to saccade between known visual targets. For this, horizontal and vertical eye position signals were monitored by a computer which ran a program controlling activation of LEDs on a target screen one meter from the monkey's face. When the monkey fixated on one LED within a spatial window, the LED turned off and a second LED turned on simultaneous to triggering of data sampling. The program provided the monkey with a drop of grape juice if it properly fixated the second LED within a spatial and temporal window.

Whatever type of eye movement was examined, control eye movements were always recorded at the beginning of each experiment for comparison with movements during brain stimulation and inactivation.

2.2 INVASIVE NEUROPHYSIOLOGICAL PROCEDURES

In order to investigate the mesencephalic structures involved in generating 3-D eye rotations, invasive techniques were required. This constituted a thorough exploration of the midbrain in each animal, with the use of single unit recording, microstimulation, and microinjection of inhibitory drugs, as outlined below.

2.2.1 *General procedures*

When training was completed and coils successfully implanted, a final surgery was performed in animals MAR, BAR, LAR, ART, and CAS, in which a stainless steel recording chamber was mounted stereotaxically over a trephine hole in the skull centred at 8mm anterior and 0mm lateral, directly over the oculomotor nucleus (cranial nucleus III) (Shantha et al. 1968). During experiments, a hydraulic microdrive attached to the recording chamber was used to advance electrodes and cannulas into the midbrain. After the midbrain oculomotor region had been located, one electrode penetration was generally made per day. The regions of oculomotor activity along this penetration were examined using single unit recording and microstimulation and pharmacological inactivation techniques. In this fashion each animal's midbrain oculomotor region (Fig. 3) was systematically explored with an orderly grid of electrode penetrations over a period of several months.

2.2.2 *Unit recording and microstimulation*

Monopolar tungsten electrodes (Frederick Haer, 4 megohms) were used to record from units and to stimulate. The electrode was inserted in an insulated guide cannula which was manually advanced into the brain stem to within 5 mm of the selected oculomotor region. Subsequently the electrode was hydraulically advanced by up to 10 mm from the guide cannula. Oculomotor units were identified by comparing their

discharge patterns with eye movements and positions. Unit recording was performed while the head-stationary animal made saccades in Listing's plane, but not during torsional VOR, so correlations between unit frequencies and torsional eye movements could not be made.

After units were recorded, the same electrode was used to microstimulate at 0.5 mm vertical intervals through oculomotor-related structures. The standard stimulus was a series of monophasic 0.5 ms cathodal square pulses delivered at 20 μA and 200 Hz for durations of 300 to 600 ms. Stimulation was delivered at random intervals while animals spontaneously made saccades to targets throughout their visual range. Mean angular velocity of an individual stimulus-evoked eye movement was computed over the longest interval that was not interrupted by saccades. This involved *division* of final position by initial position, a method that is correct for 3-D and accurate for slow movements (Section 2.1.1, Equations 7-9).

2.2.3 *Pharmacological inactivation of oculomotor neurons*

After completing stimulations, the electrode was pulled out of its guide tube without otherwise disturbing the tube or the microdrive. Then a 30-gauge cannula was inserted into the guide tube and lowered to a depth determined during the unit recording and stimulation phases, usually just above the peak burst region. This did not appear to affect eye movements prior to the subsequent injection. The injection cannula was connected to a hamilton syringe which was used to deliver 0.3 μl of 0.05% muscimol solution (Sigma) to the selected site. For comparison, 0.3 μl of a 2% GABA solution was also injected in two animals. Eye movement recordings commenced immediately after the muscimol injection and continued for 30 minutes or more. These movements were later compared to control eye movements recorded under the same behavioral conditions at the beginning of each experiment. Afterwards the animal was allowed a

48 hour recovery period and then experiments were repeated at an adjacent brain site displaced lateral-medial or rostral-caudal by 1 mm.

Muscimol has a powerful inhibitory effect on neurons which possess γ-aminobutyric acid (GABA) receptors, and neurons in the mesencephalic oculomotor region are known to possess large numbers of such receptors (Wang and Spencer 1992). Since GABA receptors are thought to open Cl^- channels, this would tend to weigh membrane potential towards the equilibrium potential for Cl^-. Since this is very near the resting membrane potential for neurons, the main effect would be prevention of action potentials. At low muscimol concentrations, this might manifest itself as a decrease in post-synaptic gain to all inputs, whereas higher concentrations might lock the membrane potential and prevent all action potentials, effectively removing that neuron from the network.

2.2.4 *Histology*

When the midbrain oculomotor region had been thoroughly explored, the animals were deeply anaesthetized with pentobarbitol and electrolytic lesions (1.5 mA DC anodal current for 15 seconds) were made at a reference microdrive coordinate. Immediately afterwards animals were given a lethal dose of anaesthetic and perfused with an intra-aortic injection of formalin. The brains were removed, sliced into 100 μm sections and stained with thionin. The resulting slides were compared to a stereotaxic atlas of the monkey brain (Shantha et al. 1968) to confirm the anatomical locations of the recording sites.

2.2.5 *Identification of the mesencephalic oculomotor structures.*

Before examining the properties of the riMLF burst-neuron region and INC tonic region, it was necessary to correctly identify these regions, and discriminate them from each other and from nearby motoneurons. Single unit recordings identified a region in

conjugate torsional eye movements which held their final position (Chapter 5, Figure 41), whereas stimulation of the more posterior putative motoneurons produced disconjugate eye rotations in various directions that did not hold their final positions. The latter sort of eye movements were also evoked by stimulation of a region with motoneuron-type unit activity 3mm below the burst region (Chapter 4, Fig. 23 B). These units were encountered and lost within electrode excursions of several microns, suggesting that they were axon fibres of the third cranial nerve.

Injection of muscimol also helped to distinguish between these three areas of oculomotor activity. The initial effect of muscimol injection into the anterior burst region was a conjugate deficit in saccade velocities (Chapter 4). The initial effect of injection into the posterior putative motoneurons was a disconjugate restriction in the position range and saccade velocities. The initial effect of injection into the intervening region, believed to be the INC, was the distinctive conjugate post-saccadic drift described in chapters 5 and 6. This functional identification of the mesencephalic oculomotor structures was consistent with the known anatomy of the region (Fig. 3), as confirmed by our histological procedures (see APPENDIX III).

Injection of muscimol directly into the INC or riMLF region produced immediate oculomotor deficits, whereas it took approximately 30 minutes for a prominent oculomotor deficit to appear after an injection 1 mm lateral to either region. This suggested that in this time period muscimol inactivated oculomotor units within a sphere with a radius slightly more than 1 mm, in agreement with the assessment of Straube et al (1991). Injection of GABA directly into riMLF and INC sites produced the same initial effects reported below for muscimol, but recovery was observed within 10 minutes. The oculomotor effects of muscimol took at least 30 minutes to peak, and judging by other observed deficits (e.g. contralateral tilting of the head), recovery required several hours. For brevity we will henceforth refer to injection of muscimol

the midbrain with a high concentration of short-lead burst neurons, within stereotaxic coordinates extending from 8 mm to 11 mm anterior, 7.0 mm to 5.5 mm vertically, and laterally as far as 2.5 mm. These neurons were classified according to their highly distinctive saccade-related activity, as described previously by several authors (Büttner et al. 1977; King and Fuchs 1979). RiMLF units produced a high frequency burst of action potentials beginning several ms before saccades in their preferred direction, the number of spikes being proportional to the amplitude of the upward saccade component in some units, and the downward component in other units. Up-tuned and down-tuned burst neurons were intermingled on each lateral side. These units were silent during visual fixation. This type of burst activity was recorded at all of the riMLF stimulation and inactivation sites examined in Chapter 4.

Single unit recordings also identified a distinct class of neurons whose activity was correlated to vertical eye position. Neurons that increased their activity either during upward or downward eye positions were intermingled on each side of the brain, and most of these also showed a burst of activity during saccades in these directions, as previously described for the INC region (Fukushima et al. 1990a, King et al. 1981). Such burst-tonic activity was recorded at all of the stimulation and inactivation sites examined in Chapters 5 and 6. Burst-tonic neurons comingled with the posterior third of the riMLF burst neuron region, but were mainly posterior, medial, and ventral to the riMLF, in the region corresponding to the expected stereotaxic location of the INC.

There was less distinction between these putative INC neurons and a posterior-medially adjacent group of putative 3rd cranial nucleus motoneurons, except that the latter strictly possessed burst-tonic type activity that was more regularly related to ocular kinematics and also possessed some neurons whose activity correlated to contralateral horizontal movements. However, electrical stimulation demarcated the border between the former and latter cell groups. Stimulation of the putative INC neurons elicited

into one side of the riMLF (usually 2 mm lateral) as unilateral riMLF inactivation, without implying that every burst neuron on that side had necessarily been inactivated. Similarly, unilateral injection into the INC (usually 1-1.5 mm lateral) will be referred to as unilateral INC inactivation.

3 BEHAVIOUR OF THE VESTIBULOOCULAR REFLEX IN THREE DIMENSIONS

3.1 INTRODUCTION

The vestibulo-ocular reflex (VOR) prevents slip of the retinal image during head rotations. For distant targets, stabilization of this image requires that the eye does not rotate relative to space. To achieve this, the slow phase of the VOR must rotate the eye in the direction opposite to the head, but with the same magnitude. To date most studies have examined the latter; usually expressed as the gain of the VOR (Collewijn et al. 1985; Robinson 1975; Skavenski et al. 1979; Viirre et al. 1986). It is assumed that during normal VOR the eye rotates in the correct direction, ie. about an axis collinear (parallel) with the axis of head rotation. However, there is reason to believe that this ideal state of collinearity may not always be achieved. This is because torsional VOR gain is less than the horizontal and vertical gains (Collewijn et al. 1985; Ferman et al. 1987a; Leigh et al. 1989; Seidman and Leigh, 1989). Rotation of the head about partially torsional axes should result in angular eye velocities with appropriate vertical or horizontal components, but reduced torsional components; ie. non-collinear. The first goal of this investigation was to evaluate the direction of the VOR by examining collinearity between the axes of the rotating eye and head.

The location of the torsional axis, i.e. the axis of minimal gain, will determine where slow phase non-collinearities occur. Where is this axis? Some have expressed torsion as rotation about the line of sight (Helmholtz 1925, Collewijn et al. 1985). Others have argued that a head-fixed coordinate system is more appropriate, since the vestibular apparatus is fixed in the head and the eye muscles exert torques relative to the head (Fetter et al. 1986; Raphan and Cohen 1986; Robinson 1985; Tweed and Vilis 1987). Based on the latter argument, we hypothesized that slow phase non-collinearities would

slow phase, share lower brainstem circuitry with the saccadic system (Chun and Robinson 1978; Ron et al. 1972; Vilis et al. 1989). However, it is not clear at what level these two systems converge. We predicted that, like saccades which obey Listing's law, quick phases would reset any torsional positions by slow phases to zero. This would suggest that the signals that drive saccades and quick phases share the same Listing's law operator (Tweed and Vilis 1990b).

3.2 METHODS

Vestibuloocular eye movements were recorded in four monkeys (FAR, LAR, ART, and CAS), binocularly in the latter two, as described in detail by chapter 2.1. Recall from section 2.1.3 that the turn-table was rotated sinusoidally about the earth vertical axis, and different directions of VOR were produced by repositioning the animals head and body relative to this axis. Note that all data in the present chapter are presented in field coordinates, so that axes of head rotation are parallel with the coordinate axes for data presentation.

3.3 RESULTS

3.3.1 *Slow phase axes.*

The first step in examining slow phase direction was to determine if the axis of eye rotation remained constant during a constant-axis rotation of the head. The constant nature of these axes is illustrated in figure 8. Each point represents an instantaneous angular velocity vector. Thus, a line drawn between zero and any given point would denote the axis of rotation at that time, and the length of this line denotes speed. The right hand convention is used to indicate the direction of rotation about this axis. If the thumb of the right hand is pointed along the axis towards the data point (eg. downward for the eye velocities in figure 8), then the fingers curl in the direction of rotation

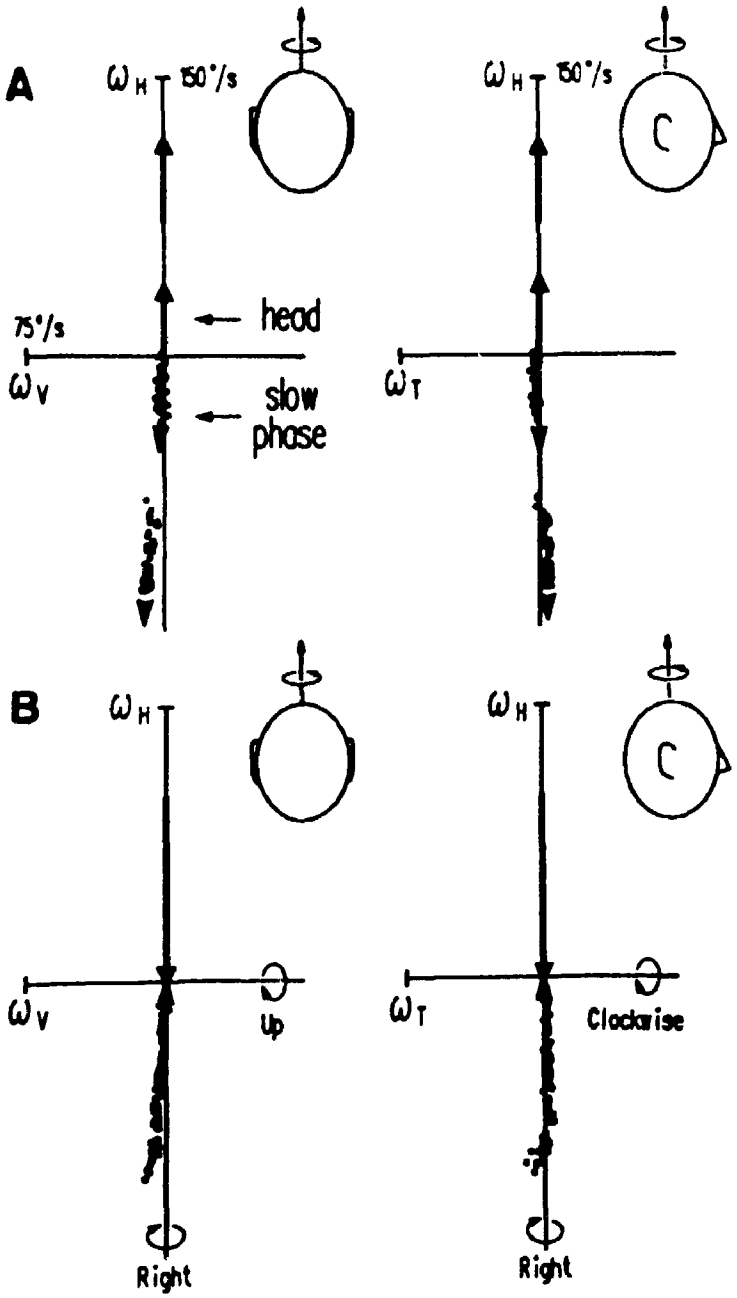

FIGURE 8. Instantaneous angular velocities of VOR slow phases. A single leftward rotation of the head is shown (■ velocity points during slow phases, quick phases not shown). The *heavy arrows* indicate head velocity during the slow phases. *Row A*: increasing velocity. The same data is viewed from behind the subject (*left column*) or from the side (*right column*), as indicated by the *Head caricatures*. *Row B*: decreasing velocity. *Axes* are labelled according to the direction of rotation (*curving arrows*).

follow a pattern consistent with gain being lowest about some head-fixed torsional axis.

The axes that the eye rotates about determine the positions that the eye will assume. What positions will be observed if the eye rotates about the same axis as the head? During saccades, eye positions conform to Listing's law. If eye position is described in Listing's coordinates, as defined in sections 1.4.2 and 2.1, then this law states that eye position is confined to Listing's plane of zero torsional positions. (Ferman et al. 1987b; Nakayama 1983; Tweed and Vilis 1990a; Westheimer 1957). Recently, a surprising aspect of Listing's law has been confirmed. In order to keep the torsional component of eye position at zero, saccade axes must have a position-dependent torsional tilt (Helmholtz 1925; Tweed and Vilis 1990a). Conversely, should the eye always rotate about an axis within Listing's plane, as in a collinear horizontal VOR, then position-dependent violations of Listing's law are expected. If the latter situation occurs, Listing's law must be a product of the neural saccadic system, contrary to the mechanical hypothesis proposed by some investigators (Ferman et al. 1987b; Sparks and Mays 1990).

The pattern of eye position changes predicted by rotational kinematics should enable discrimination between alternative models of the oculomotor position-signal-generator (Robinson 1975; Tweed and Vilis 1987). During horizontal head rotation, the classical Robinson integrator would convert velocity to position in the horizontal dimension, but would be unaware of any torsional changes in eye position that occur when the eye is above or below primary position. The resulting mismatch between motoneuron firing rates and eye position would result in positional drift. If no such drift occurs, then the VOR indirect path, i.e. the brainstem position signal generator, must incorporate the correct laws of rotational kinematics.

The final goal of this study was to examine the action of VOR quick phases on ocular torsion, as compared to saccades. Quick phases, which reset eye position following the

(rightward in this case). As head velocity increased or decreased, so did slow phase velocity in the opposite direction. The straightness of the path followed by these velocity vectors indicates that the axis of rotation remained relatively constant.

Figure 8 also suggests that the slow phase axis was not precisely collinear with that of the head. To determine whether this was a consistent phenomenon, the mean velocities of 400 slow phases were examined for each axis of head rotation (Fig. 9 *A*, *B*, *C*). On average, the slow phase axes were closely collinear with the head axes. However, two types of non-collinearity were evident. The first was a random variability most prominent during torsional head rotations (Fig. 9 *C*). The second was a small systematic tilt, in this case most prominent in the behind view of Figure 9 *A*. Neither of these appeared to depend on eye speed.

The apparently random variation in non-collinearities was examined for eye position dependence. Robinson has predicted that, if uncorrected, position dependent changes in muscle pulling directions should result in axis tilt. For example, a 30° elevation of the eye should result in a 25° vertical tilt of the torsional slow phase axes (Robinson 1985). There did not appear to be any such pattern in our data. Third order surfaces were fitted to axis tilt as a function of eye position. The computed position dependence of axis tilt did not follow a consistent pattern between animals, and was generally small compared to the standard deviations for any one position.

Since the trial-to-trial change in axes appeared to be random, this variation was removed by averaging, leaving only the systematic non-collinearity. Several hundred mean slow phase axes were averaged for each axis of head rotation, in each monkey (Figure 10). Rotations of the head in opposite directions tended to produce eye rotations about parallel axes, with less asymmetry than previously observed for gains in opposite directions (Snyder and King 1988). For example, when leftward slow phase axes tilted back, rightward axes tilted forward (Fig. 10, side view). Axis tilts were most consistent

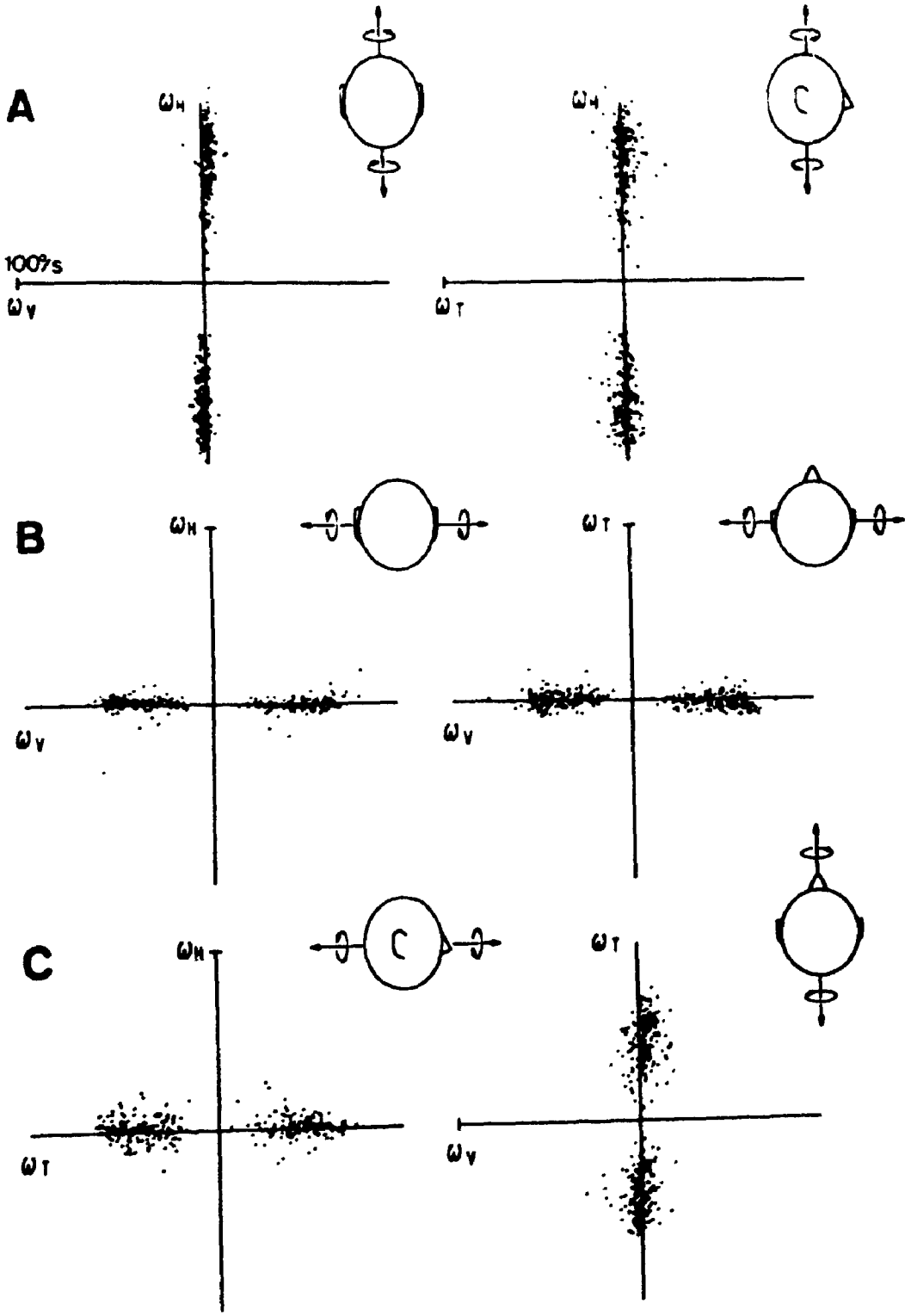

FIGURE 9. Mean velocities of slow phases during fixed-axis head rotations. *Row A*: horizontal VOR. *Row B*: vertical VOR. *Row C*: torsional VOR. Two views of the data are given in each row, as indicated by the *head caricatures.*

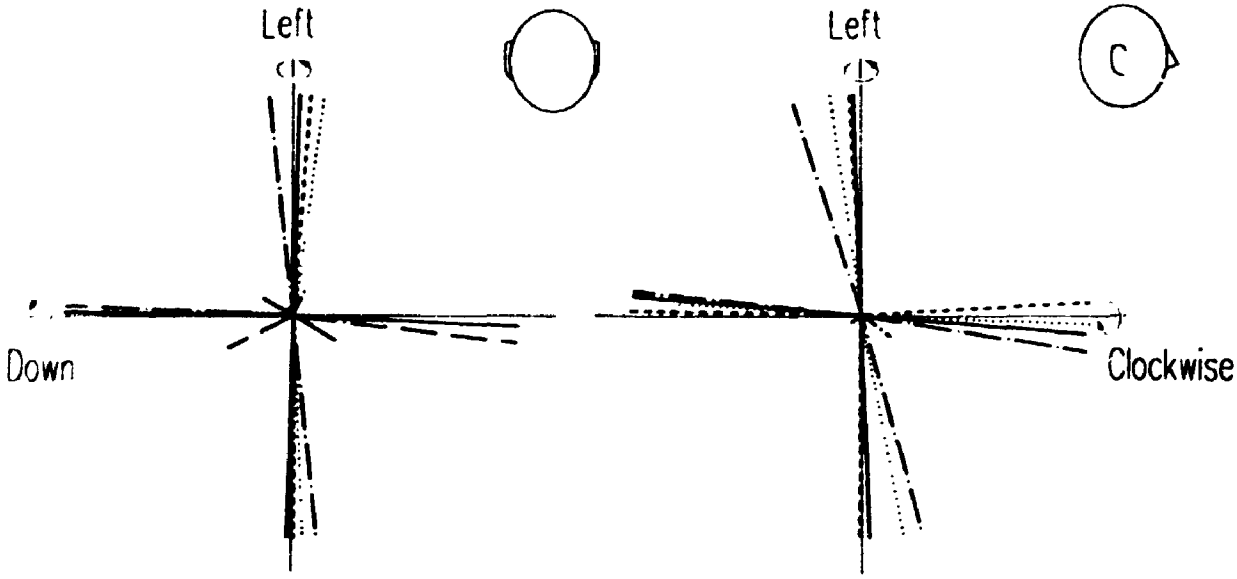

FIGURE 10. Average torsional, horizontal and vertical slow phase axes of all four animals. For each axis of head rotation, the axes of negative and positive slow phase directions are plotted separately. Subject Key: *solid line* ART, *dotted line* FAR, *dashed line* LAR, *interrupted line* CAS.

between monkeys from the side view, ie. vertical axes tilted backwards and torsional axes tilted forward. However, the amount and direction of tilt varied from animal to animal.

How could such systematic non-collinearities arise? One possible source of non-collinearity might be differences in gain between various VOR directions. This hypothesis was tested by rotating the head about an axis that was partially vertical (high gain) and partially torsional (low gain). This test is illustrated in figure 11 *A*. The unit torsional and vertical head rotation vectors $\mathbf{h}_t$ and $\mathbf{h}_v$ have been reversed (multiplied by -1) for better comparison with the eye vectors. Four hundred average slow phase velocities were divided by head speed and averaged to get each of the resultant eye vectors $\mathbf{e}_t$ and $\mathbf{e}_v$. These can be thought of as the average VOR output resulting from one unit of head rotation in a given direction, or a three-dimensional version of gain. Note that the length of $\mathbf{e}_t$ is significantly less than the length of $\mathbf{e}_v$, and that both are very near to being collinear with the axes of head rotation. The third solid arrow $\mathbf{h}_*$ illustrates an intermediate axis of head rotation. The resultant eye rotation $\mathbf{e}_*$ was always less collinear with the axis of head rotation than the other vectors and its direction of tilt was towards the vertical axis.

To test whether this non-collinearity was the result of linear vector summation, a 3 X 3 VOR "gain" matrix G was computed for each eye. The components of the torsional eye vector $\mathbf{e}_t$ constituted the first column of G, those of horizontal vector (not shown) formed the second, and the components of the vertical vector $\mathbf{e}_v$ formed the third column. Multiplication of $\mathbf{h}_*$ by this matrix gave the predicted 3-D eye rotation $\mathbf{e}_p$. In other words, each component of head rotation was multiplied by the individually computed 3-D "gain" for that direction of VOR, and the resulting three vectors were then summed linearly. Figure 11 is used to illustrate this process qualitatively in two dimensions.

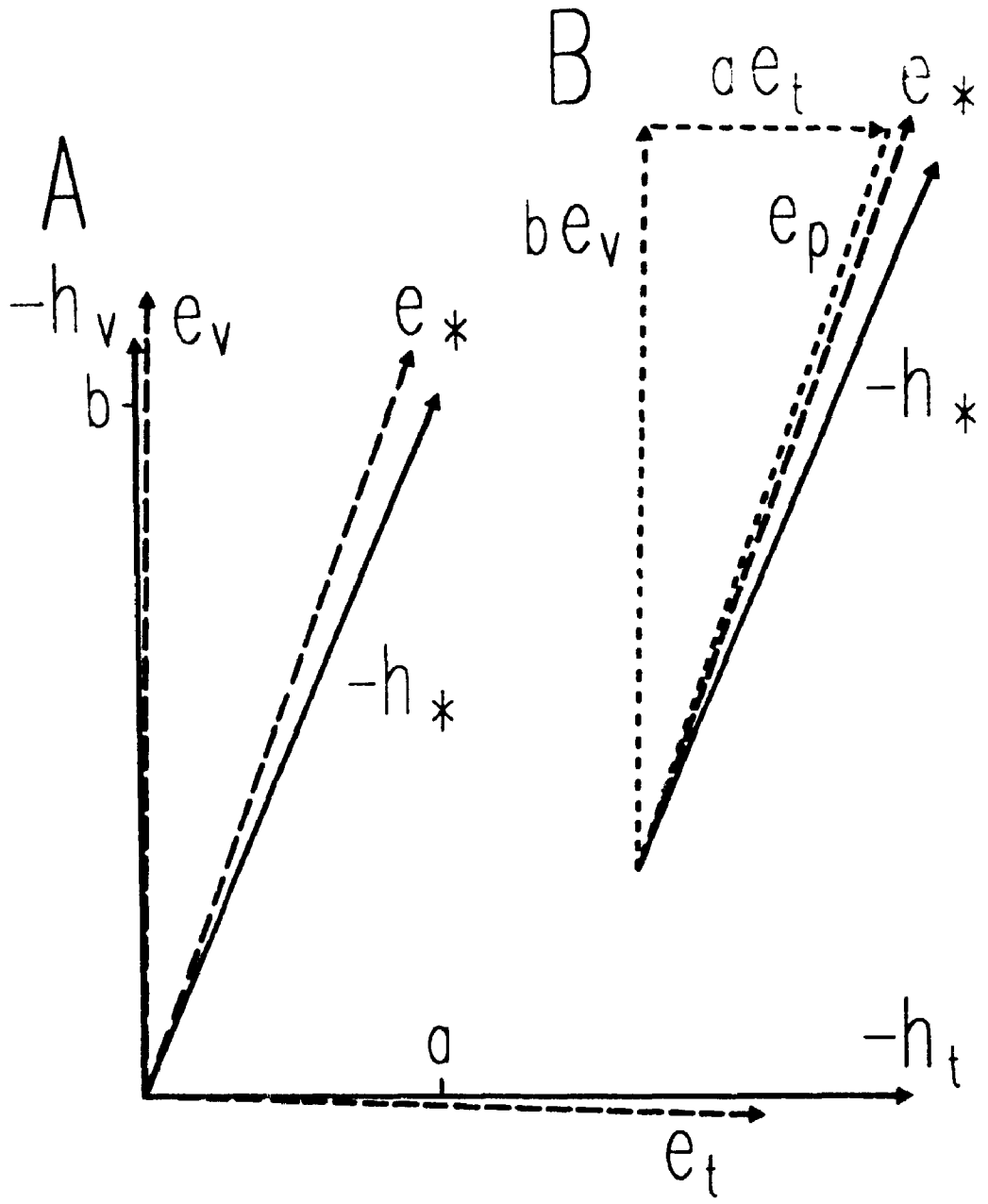

FIGURE 11. Axis tilts caused by low torsional gain. *A*: Torsional, vertical and intermediate axes of head rotation (*solid vectors* $\mathbf{h}_t$, $\mathbf{h}_v$, $\mathbf{h}_*$) and the resultant axes of eye rotation (*dashed vectors* $\mathbf{e}_t$, $\mathbf{e}_v$, $\mathbf{e}_*$). The torsional and vertical components of the intermediate axis of head rotation are indicated as a and b. *B*: Prediction of $\mathbf{e}_*$ by vector summation. The products $a\mathbf{e}_t$ and $b\mathbf{e}_v$ are summed linearly to produce $\mathbf{e}_p$. Unlike the other figures, the vertical axis is labelled as such, rather than by the direction of rotation.

Orthogonal projections were made from $\mathbf{h}_s$ to the torsional and vertical axes to get the components, a and b (Fig. 11 *A*). These components were then multiplied by the appropriate vectors ($\mathbf{e}_t$ and $\mathbf{e}_v$, ie. columns 1 and 3 of G) to estimate the eye movements that they would have produced individually (Fig. 11 *B*). Vector summation of these predicted vectors $a\mathbf{e}_t$ and $b\mathbf{e}_v$ gave the theoretical eye rotation vector $\mathbf{e}_p$. The theoretical eye vector $\mathbf{e}_p$ always predicted the deviations in magnitude and direction of the real eye vector $\mathbf{e}_s$ from the corresponding head vector $\mathbf{h}_s$. This analysis suggested that most of the non-collinearity between $\mathbf{h}_s$ and $\mathbf{e}_s$ resulted from low torsional gain. In general, whenever the torsional, vertical and horizontal gains were not equal, the slow phase axis tilted towards the axis of highest gain, exactly as predicted by the assumption of linear vector summation.

While differences in gain appear to produce non-collinearities during head rotations about intermediate axes, how can this explain the non-collinearities illustrated in figure 11? It is quite probable that the axes of maximal and minimal gain were not perfectly aligned with the arbitrary coordinate axes about which the heads were rotated. If so, the vertical and torsional axes of rotation were really intermediate axes, and the observed non-collinearities were the result of vector summation as illustrated in figure 11. In order to test this hypothesis, an attempt was made to locate a physiologically meaningful torsional axis.

First, one must exclude the hypothesis that gain is lowest about the axis of gaze direction, that is, in retinal coordinates rather than head coordinates. This hypothesis suggests that during rotations of the head about the torsional axis, VOR gain should be lowest when the eye looks straight ahead along the axis of rotation. Similarly, during horizontal or vertical head rotations, gain would drop as the eye looks away from straight ahead, towards the axis of rotation. If the VOR was 0.7 about the line of sight and 1.0

about axes orthogonal to the line of site, then head-fixed gain would be expected to rise or fall with eye position by 0.15 within the oculomotor range. The theoretical relationship is not exactly linear, but is close enough to yield a correlation coefficient of 0.98. No such systematic correlation was found in the monkeys. Actual correlation coefficients ranged from -0.306 to 0.264 with an average of 0.006. The application of more complicated curvilinear fits to the data did not improve this relationship.

It thus appeared that by default, gain was minimal about some head-fixed axis. The next step was to determine the orientation of this axis in the head. Theoretical axes of minimal gain were computed by multiplying different head rotation vectors of unit length by each G matrix, until the axis that produced the smallest eye rotation was found. The axis of maximal gain must be orthogonal to this axis, as was confirmed by similar computations. In the 6 eyes monitored, the direction of the axis of minimum gain varied from almost straight ahead to tilting upwards by 22°. The orientations of these axes were not consistently related to any anatomical landmark fixed in the head.

The coordinates of the saccadic system, ie. Listing's plane and the orthogonal direction of primary gaze, have also been demonstrated to vary with respect to anatomical landmarks (Tweed and Vilis 1990a). Surprisingly, we found a strong positive correlation ($r = .904$; $p < 0.05$) between the upward tilt of the minimal VOR gain axis and the primary gaze direction of the saccadic system (Fig. 12). In three of the 4 animals these angles were within 2° of each other. Similarly, the axes of maximal gain were aligned closely with Listing's plane. Apparently the axis of minimal gain and the primary gaze direction share the same internal physiological coordinate system.

The tilt of the torsional (minimal gain) axis provided the necessary rationale for the systematic non-collinearities seen in figure 10. If this axis was neither parallel nor orthogonal to the axis of head rotation, then non-collinearities are expected. Figure 12 gives an example of the correspondence between Listing's coordinates and the axis of

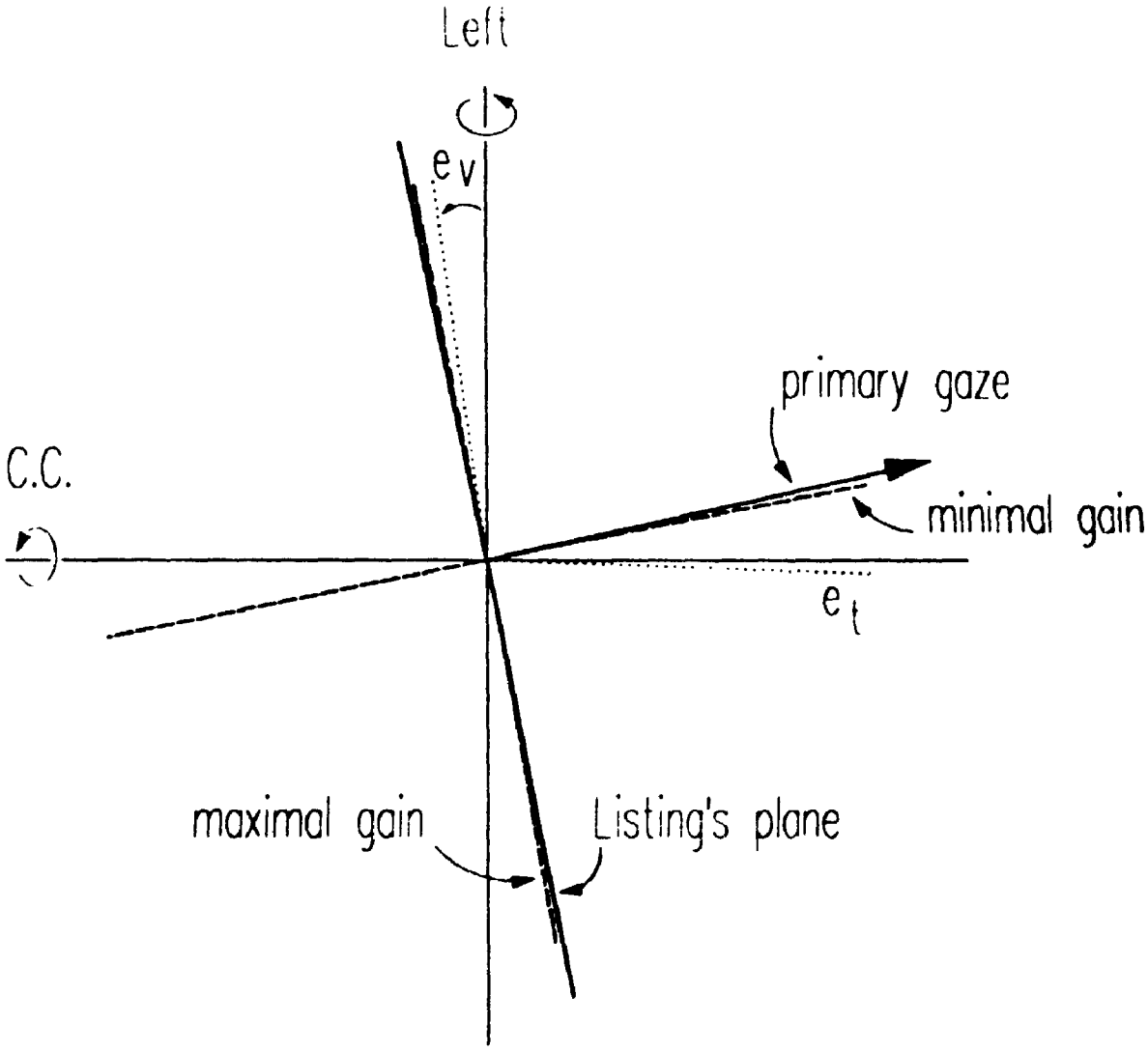

FIGURE 12. Correspondence between slow phase axes and Listing's coordinates. Data from animal FAR is plotted in standard field coordinates. *Solid lines*: Listing's plane and primary gaze direction. *Dashed lines*: the computed axes of maximal and minimal gain. *Dotted lines*: slow phase axes during rightward and counterclockwise head rotations about the coordinate axes.

minimal gain, with non-collinearities in the expected directions. The upward tilt of the primary gaze direction was related to the backward tilt of the axis of horizontal VOR e_y by a correlation coefficient of $r = .928$ ($p < 0.05$). This indicates that 86% of the variation in this non-collinearity could be explained by its relationship to the primary gaze direction. Thus, much of the observed non-collinearity appeared to be due to directional gain differences and an arbitrary choice of coordinates. In order to more thoroughly determine the contribution of this effect to the results, the VOR gain matrices were re-examined.

The results suggested that VOR gains are aligned with the orthogonal coordinates dictated by Listing's law. Would transformation into Listing's coordinates simplify the G matrices into three gain numbers along mutually orthogonal axes? As expected, this coordinate transformation tended to reduce the torsional gain while increasing vertical and horizontal gain. The average magnitude of all off-diagonal components of the matrices was reduced by 30% to 0.040. These residual entries mostly represent non-systematic axis tilts which will not be eliminated by any choice of orthogonal coordinates, and were so small and inconsistent between animals that they were probably due to measurement error. Finally, the standard deviations between corresponding elements of the G matrices were reduced from an average of 0.11 to 0.07. Thus, transformation into Listing's coordinates appeared to standardize the matrices and increase their diagonality.

Averaging the G matrices of all subjects after transformation into Listing's coordinates further reduced the off diagonal elements (Fig. 13). This matrix provides a desription of our data under these specific circumstances, and is not a static description of all VORs. One-dimensional gain magnitudes along the main diagonal of this matrix were: .664 (torsional); .869 (vertical); .917 (horizontal). Since the off-diagonal components were very close to zero (and were smaller than the measurement error of our

	h_T	h_V	h_H
e_T	−.664	−.013	−.018
e_V	−.012	−.869	−.025
e_H	−.004	−.010	−.917

FIGURE 13. Average **G** matrix in Listing's coordinates. The nine elements of the **G** matrix are necessary to relate each of the three components of head rotation to each of the three components of eye rotation. If a given component of head rotation is selected (*columns* h_T, h_V, h_H), and a given component of eye rotation is chosen (*rows* e_T, e_V, e_H), then the intersection of the row and column gives the appropriate gain element. The entries along the main diagonal correspond to one-dimensional VOR gains, while entries off the main diagonal correspond to non-collinearities. Vertical gain may have been reduced by the head posture used for this VOR direction (Hain and Buettner 1991).

recording system), the average G matrix was essentially composed of three orthogonal columns. Thus, it would appear that the overall action of the VOR under these conditions was best expressed as three gains along the mutually orthogonal axes aligned with Listing's coordinates.

3.3.2 *Slow phase eye positions.*

Having determined the axes of slow phase eye rotation, the resulting changes in eye position were examined. This question is not as trivial as it may seem. The laws of rotational kinematic require that when the eye is rotated about a fixed vertical axis while gazing upward or downward, its position must change not only in the horizontal direction, but also vertically and torsionally. The latter change in eye position would be a violation of Listing's law. On the other hand, current models of the VOR suggest that only horizontal position will change.

In order to determine whether the slow phases violate Listing's law, it was first necessary to determine Listing's plane with the head stationary. The typical range of eye positions during saccades and fixations is illustrated in Figure 14. The upper row of Figure 14 gives a component vs. component plot of eye position quaternion vectors. The data points can be interpreted as the tips of vector "arrows" extending outward from the origin. Recall from section 2.1.1 that each arrow is parallel to the axis of rotational displacement from reference position, and the length of the arrow is proportional to the angle of this rotation. The right hand rule requires that when the thumb is pointed in the direction of this arrow (e.g. up for the top-most points in Figure 14), the fingers curl in the direction that position is displaced (e.g. leftward in this example). As reported elsewhere, the range of obtainable eye positions was distributed within a nearly flat two-dimensional surface with a finite torsional width of about 3° (Tweed and Vilis 1990). Third-order curved surfaces were fitted to the data as illustrated in the lower row of

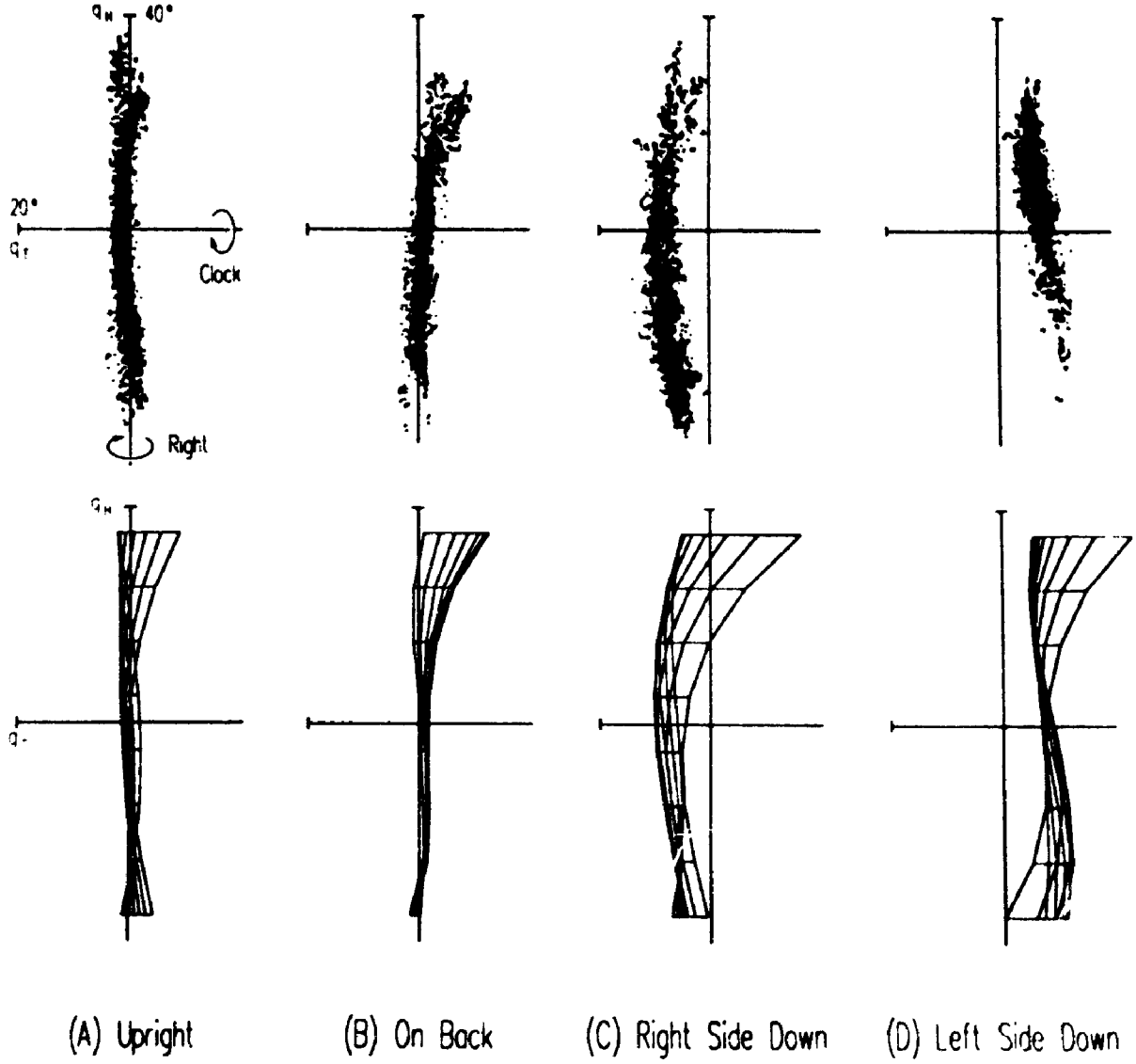

FIGURE 14. Eye positions with the head in different stationary postures. Data during and between saccades is viewed from the right side of the head in each case. *Top row*: 10,000 eye position quaternions during 100 seconds of random visually guided saccades. *Lower row*: Third order curved surfaces fit to the above data. All positions were computed relative to the same reference position recorded with the head upright. The curvature of the co nterrolled surfaces was not an artifact of the shifted reference position.

figure 14. These show that when the monkey was upright, eye position was confined to the highly planar surface defined by Listing's law.

Was Listing's plane constant during the other head positions used in this study? Eye positions were also recorded while the animal lay on its back, right, and left sides (figure 14 *B, C, D* respectively). With the monkey on its back, Listing's plane remained intact, with a slight forward tilt. When the monkey was lying on its side, the head was tilted 90° torsionally from the upright position. During such postures the tonic *ocular counterroll* reflex occurs, resulting in a torsional shift of Listing's plane in the direction opposite to head rotation (Collewijn et al 1985). These surfaces appeared to be thicker than the standard Listing's plane. However, surface fits revealed that this was partially due to distortion of the plane into a bowl-like surface, ie. the torsional shift was not as great for eccentric gaze directions. The standard deviations of torsional position from the surfaces of best fit illustrated in figure 14 were 0.872 degrees with the monkey upright, 1.246 degrees with the monkey on its back, 1.141 degrees with the monkey right-side-down, and 1.116 degrees with the monkey left-side-down. Thus, aside from small shifts and distortions of the plane, eye position during and between saccades remained confined to an essentially planar surface despite tonic head tilt.

Figure 15 illustrates the changes in eye position produced by rotations of the head about fixed vertical, horizontal, and torsional axes. These slow phase axes were nearly collinear with the axis of head rotation. As expected, the main change in orbital eye position was in the direction opposite to that of head rotation (Fig. 15, left hand column). If the right hand thumb is pointed in the direction of the quaternion vectors, the curl of the fingers indicates that eye positions changed leftward in row *A*, upward in row *B*, and counterclockwise in row *C*. Not surprisingly, the latter drove eye position counterclockwise out of Listing's plane.

FIGURE 15. Slow phase eye position changes. Each series of quaternion vectors forms a dotted line representing one complete slow phase. *Small arrow heads* at the final position indicate direction. *Row A*: Rightward head rotation. *Row B*: downward head rotation. Eye positions are shifted torsionally as in figure 6 *C* due to the tilted head posture used. *Row C*: clockwise head rotation. *Head charicatures* indicate that data are viewed orthogonal to (left column) and down (right column) the axis of head rotation.

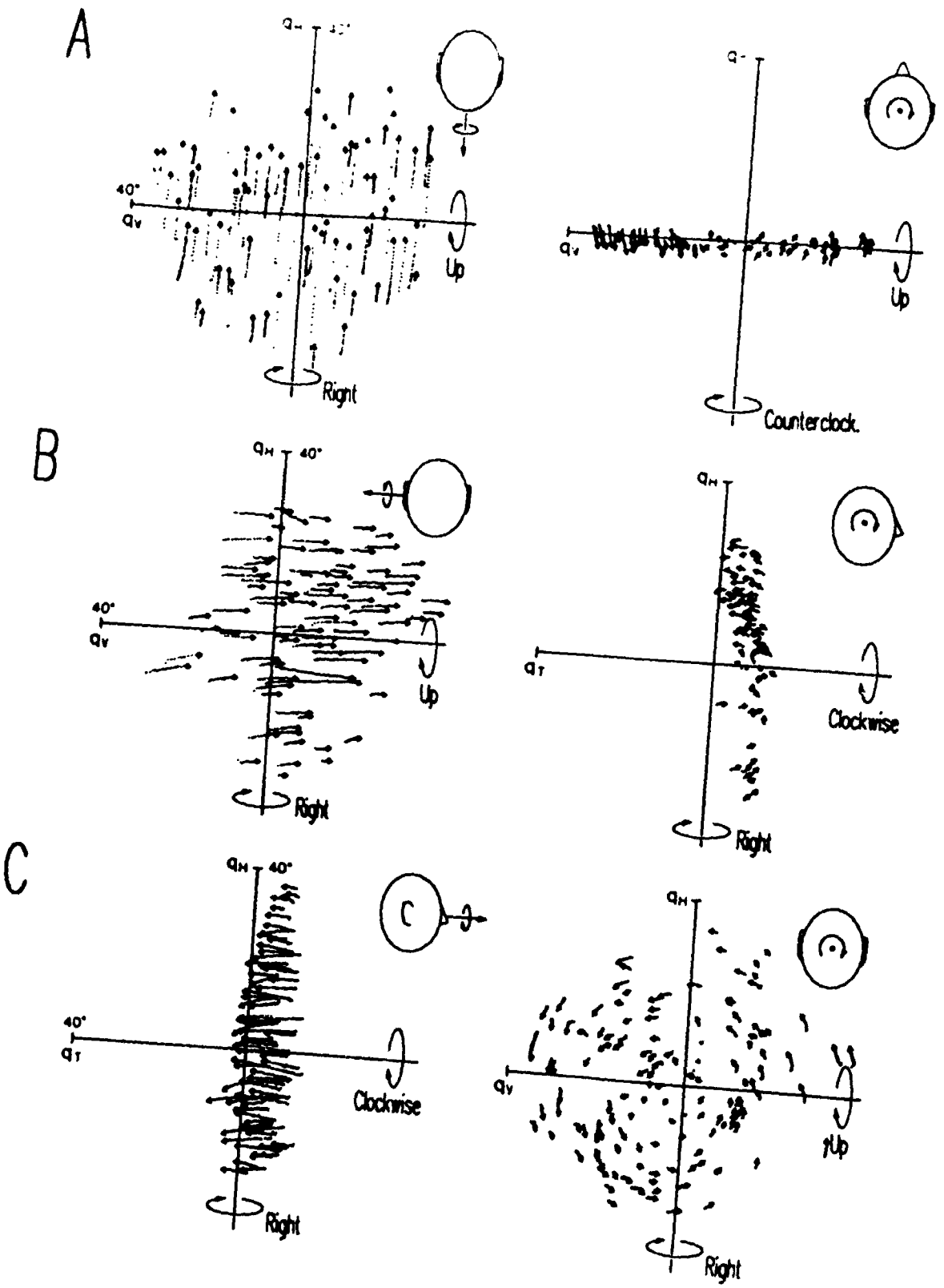
A
40°
Up
Right
Counterclock.
B
40°
Up
Right
Clockwise
C
40°
Clockwise
Right
Up
Right

As required by rotational kinematics, changes in eye position vectors (the vector part of quaternions as defined in METHODS) did not only occur along the axis of head rotation, but also in a systematic manner in the orthogonal directions. In the right column of figure 15, data is viewed orthogonal to the axis of rotation, with eye velocities pointing towards the reader. In the case of horizontal VOR (figure 15 *A*), there was a change in torsional position whose direction and magnitude depended on vertical eye position. For example, during leftward slow phases, clockwise position accumulated when the eye looked up and counterclockwise position accumulated when the eye looked down. The opposite pattern occurred during rightward slow phases. Vertical slow phases produced a similar pattern of position changes (figure 15 *B*), except that in this case the direction and magnitude of torsional position change was dependent on *horizontal* eye position. Thus, rotation of the eye about axes in Listing's plane produces violations of Listing's law, when that rotation is not directly towards or away from primary position. Section 3.4.2 will show that this is not an unexpected observation.

Torsional VOR clarified the pattern of 3-D eye position change that was only partially discernable for the other VOR directions. When counterclockwise slow phase positions are viewed down the axis of rotation (figure 15 *C*, right column), changes in vertical and horizontal eye position are evident. The change in vertical position depended on initial horizontal position, and the change in horizontal position depended on initial vertical position. As a result, a circular pattern of position change is observed. The pattern of position changes can be summarized as follows. If one points the thumb of the right hand in the direction of the eye velocity vector, eg. out of the page in the right hand column of figure 15, then position vectors changed mostly in this direction. However, the position vectors also circled around reference position in the direction of finger curl. The same circular pattern was followed during horizontal and vertical VOR, but only a slice of the family of circles was present because the onset of quick phases

restricted the range of torsional eye positions.

As described in the discussion section below, this pattern of position change was actually a necessary condition for stabilization of gaze. It was not a consequence of axis non-collinearities but rather the expected result of rotating the eye about a fixed axis, based on the principles of rotational kinematics. Do the brainstem circuits of the VOR incorporate these principles? The conventional view is that during a horizontal rotation of the head, it is only necessary for the indirect pathway of the VOR to accumulate a horizontal signal. Vertical and torsional position signals would not be generated in this example. The current results show that this would usually result in a mismatch between the position signals encoded by motoneurons and actual eye position. Any post-rotational torsion should decay exponentially in a fraction of a second. However, no such post-rotational drift was observed in our data. When head rotation stopped, any accumulated torsion held until the next eye movement (Fig. 16). Thus, position signals from ocular motoneurons appear to be perfectly matched to actual eye position. This suggests that, contrary to the conventional view, the neural circuit of the indirect pathway which converts velocity to position incorporates the principles of rotational kinematics.

3.3.3 *Quick phases.*

AXES OF ROTATION. As expected, quick phases almost always reversed the direction of eye rotation generated by slow phases, and often caused gaze to lead in the direction of head motion. Therefore, mean angular velocities of such quick phases had a significant component in the direction of head rotation. However, quick phases also directed gaze to specific visual targets. Because of this, quick phase axes had almost every combination of vertical and horizontal components (Fig. 17). Therefore, unlike slow phase axes (Fig. 9), quick phase axes did not line up with the axes of head rotation. A comparison of these two figures also reveals that during horizontal and especially

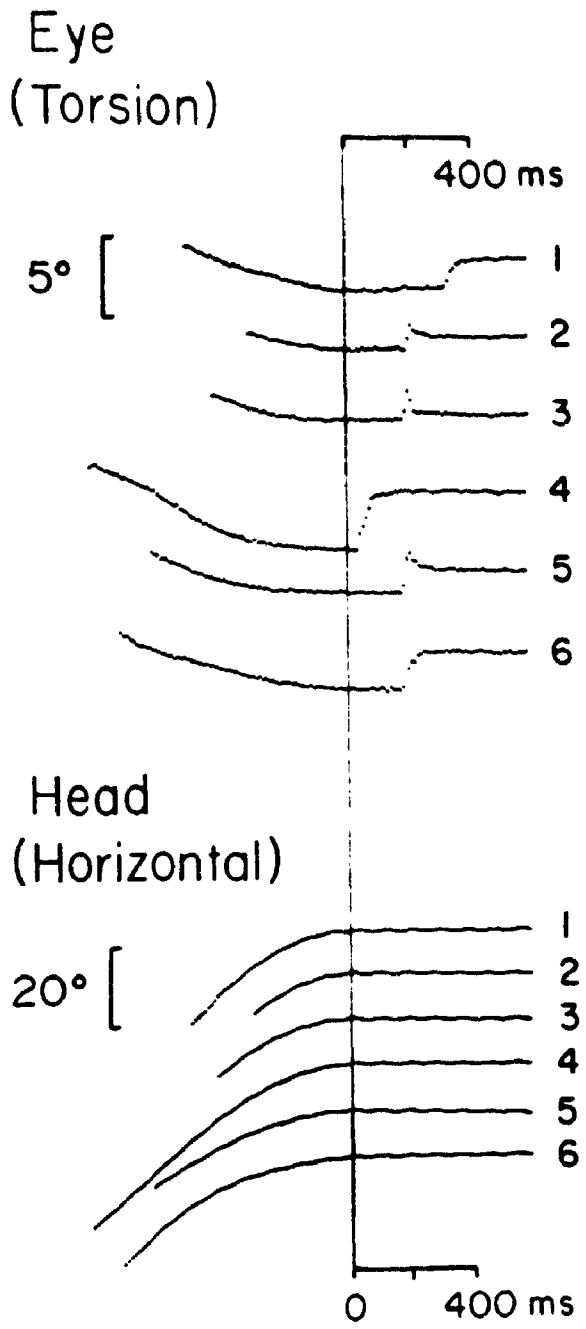

FIGURE 16. Maintenance of accumulated torsional position after horizontal head rotation. The change in eye position was due to the position-dependent effect described in the text, not axis non-collinearity. Counterclockwise changes in eye position during six slow phases are shown *above*. The corresponding rightward changes in head position are sh.. .. *elow*. The monkey was looking downward in each case. Position traces have been aligned at the time when head movement stopped (*vertical line*).

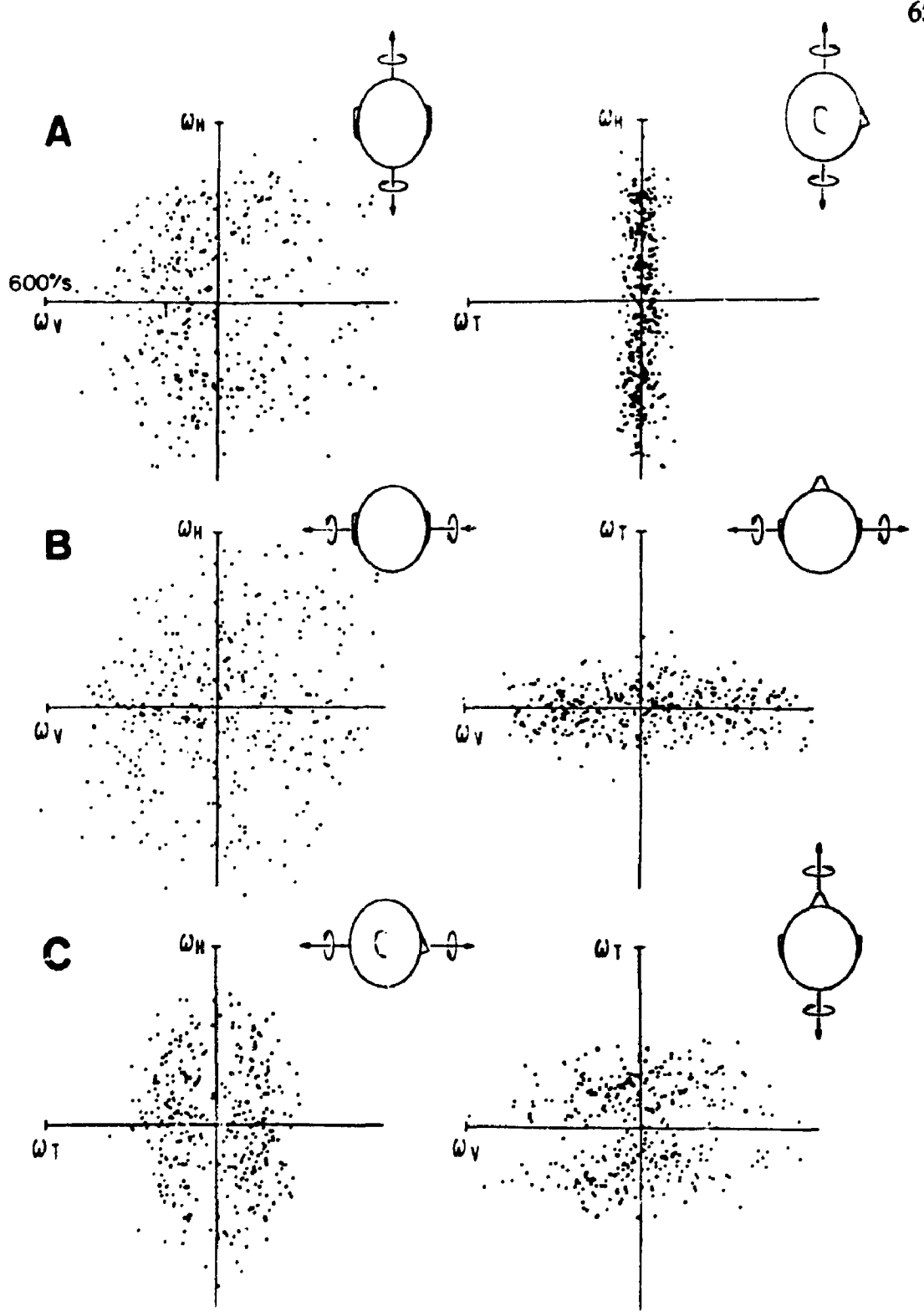

FIGURE 17. Mean velocities of quick phases during fixed-axis head rotations. *Row A*: horizontal head rotation. *Row B*: vertical head rotation. *Row C*: torsional rotation. *Head caricatures* and *Arrows* indicate the viewing perspective and axis of rotation.

vertical VOR, the quick phase axes exhibited a larger distribution in the torsional direction than the slow phase axes. Thus, quick phase axes tilt out of Listing's plane in a manner similar to saccades, which do so in order to obey Listing's law.

QUICK PHASES AND LISTING'S LAW. As we have seen, slow phases usually violate Listing's law. However, large torsional components did not accumulate after several slow phases. Therefore the quick phases must have been correcting the torsion produced by slow phases. In the case of torsional VOR, the slow phases drove eye position almost perpendicularly out of Listing's plane. The torsional quick phases not only corrected these violations of Listing's law, but overshot Listing's plane by an approximately equal amount (Fig. 18). Thus, the eye was directed to a range of positions rotated torsionally in the direction of head rotation. This range of positions appears as a plane *shift* in three dimensional plots. The surfaces fit to this data (Fig. 18, *bottom row*) had a bowl shape similar to ocular counterroll surfaces (figure 14). The magnitude of this plane shift increased with frequency and speed of head rotation. At the standard frequency of head rotation (0.5 Hz), the torsional quick phase planes were shifted from Listing's plane by an average of 5.5° across subjects. As a result of starting and ending at positions with opposite torsional components, the torsional slow phases tended to straddle Listing's plane.

Is this torsional overshoot by quick phases a violation of Listing's law, or does the plane of desired eye positions shift in order to keep slow phases centred on Listing's plane? Examination of horizontal and vertical VOR revealed that the latter strategy was followed. Quick phases not only corrected violations of Listing's law but, as in torsional VOR, crossed Listing's plane (Fig. 19 *A*). Recall that leftward slow phases drove the eye counterclockwise when looking down and clockwise when looking up. In order to reverse this torsion, quick phases had to direct eye position to a plane that was rotated horizontally, again in the direction of head rotation. Each quick phase drove the eye to

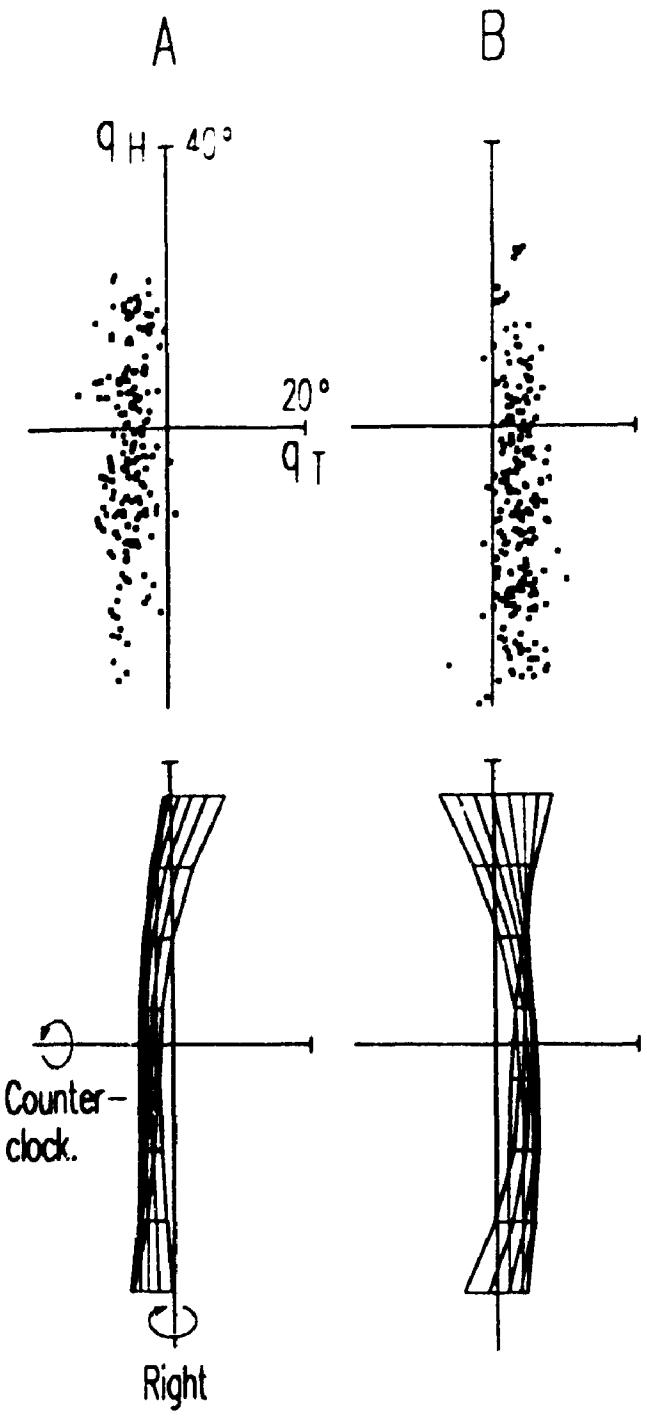

FIGURE 18. Final positions of quick phases during torsional VOR. *Upper row*: eye positions at the end of counterclockwise (*A*) and clockwise (*B*) quick phases. *Lower row*: Third order curved surfaces fit to the above data.

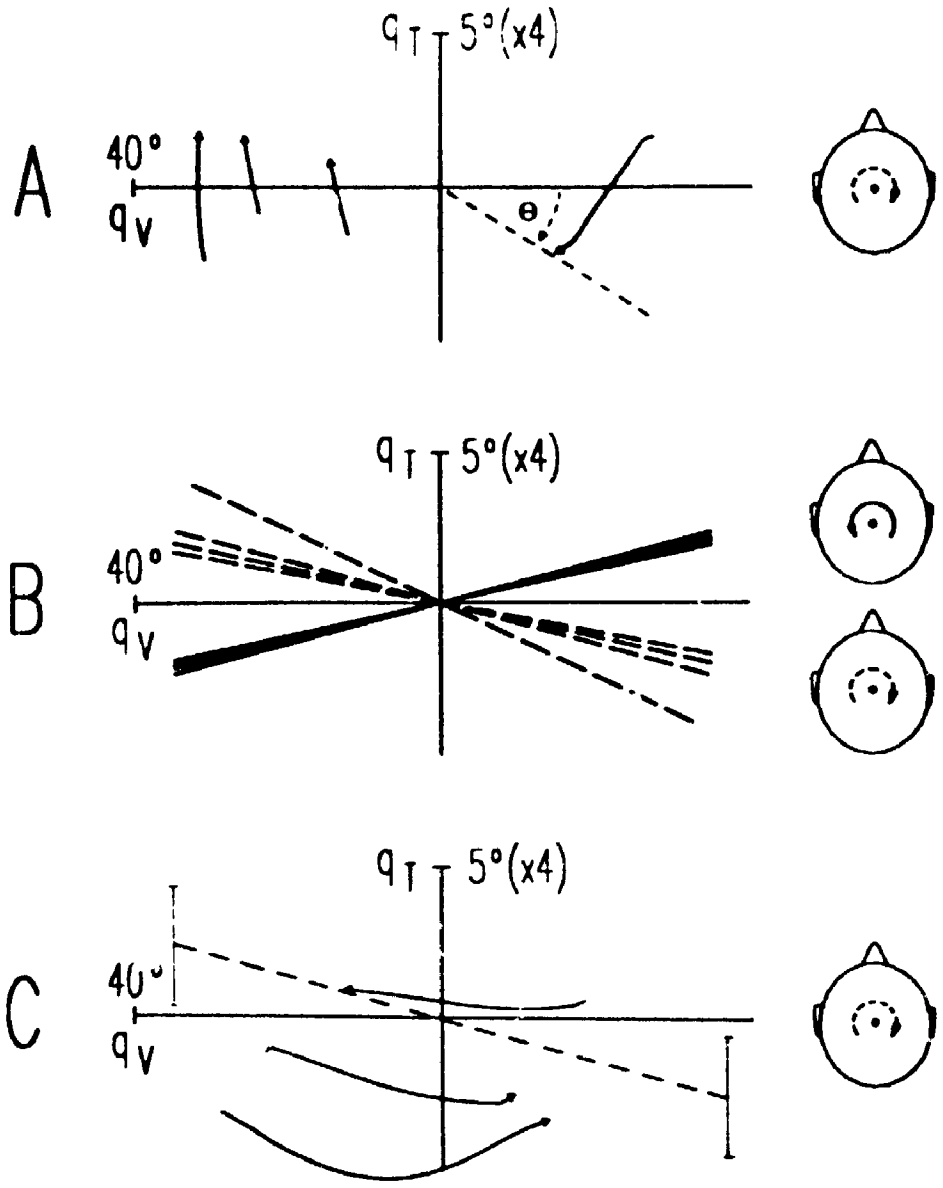

FIGURE 19. Quick phase eye positions during horizontal VOR. Standard above views of the data are used except that torsional position scaled up four times for clarity. ***A***: typical quick phases during rightward head rotation. The angle Θ quantifies the amount that the quick phase overshot the standard Listing's plane. ***B***: Average rotation of quick phase planes from Listing's plane. *Solid lines*: planes during leftward head rotation in all four animals. *Broken lines*: planes during rightward head rotation. ***C***: Quick phases that reversed the vertical component of eye position. The *dashed line* is the average plane of quick phase final positions from ***B***. *Error bars* indicate the width of this plane.

a plane rotated from Listing's plane by an angle we called Θ. The average rightward and leftward quick phase plane tilts for these animals are illustrated in figure 19 *B*. There was a significant difference between the Θ's of rightward and leftward quick phases in all animals ($p < .05$). The mean Θ across subjects was 3.8°.

Thus, quick phases appear to direct the eye to a plane of positions that anticipated violations of Listing's law produced by subsequent slow phases. This is most convincingly illustrated by quick phases such as those shown in figure 19 *C*. Take, for example, the case in which the eye initially looked downward, and a leftward slow phase had just driven eye position counterclockwise out of Listing's plane. Subsequent quick phases that redirected gaze to an upward direction maintained that counterclockwise torsion, instead of driving the eye clockwise. Had these quick phase crossed Listing's plane, as in figure 19 *A*, the next slow phase would drive the eye further clockwise, resulting in a large violation of Listing's law. Thus, by taking eye position to the *same* side of the plane, such quick phases anticipated the action of the subsequent slow phase. For all VOR's, quick phases directed the eye towards a plane of positions rotated in the direction of head rotation, so that the torsional component of the subsequent slow phase straddled Listing's plane.

3.4 DISCUSSION

Three separate but interrelated findings are reported in this chapter. First, the data suggests that the slow phase axis is remarkably collinear with the axis of head rotation, when the latter is either within or orthogonal to Listing's plane. However, rotation of the head about any other intermediate axis results in non-collinearity. This appears to the result of low gain about the head-fixed torsional axis orthogonal to Listing's plane. As demonstrated below, these results corroborate Robinson's diagonal VOR matrix, provided the matrix is expressed in Listing's coordinates (Robinson 1982, 1985).

The second finding is that these slow phase axes do not only change eye position in the direction opposite to head rotation. A position-dependent pattern of changes is also observed in the other components. Even rotation of the eye about axes in Listing's plane, eg. vertical and horizontal, produces torsional deviations in eye position, and this torsion appears to be held by tonic motoneuron signals. To produce this pattern, the VOR must incorporate the principles of rotational kinematics into the velocity-to-position transformation of the indirect path.

Finally, quick phases appear to not only reset these torsional components, but drive the eye to the torsional position that anticipates the action of the subsequent slow phase. This observation is explained below by a model of the saccade / quick phase generator which implements Listing's law *above* the level of convergence with the slow phase generator.

3.4.1 *Directions of slow phase eye movement.*

The essential feature of slow phase axes was their close alignment with the axes of head rotation. Thus, slow phases rotated in the correct direction to minimize slip of the retinal image. Observed errors in direction took the form of small random variations in slow phase axes, and systematic non-collinearities.

The origin of the random variation in slow phase axis orientation remains uncertain. It has been suggested that the mechanics of the muscles might result in a dependence of the VOR on orbital eye position (Robinson 1985). However, in the present study, deviations from collinearity did not follow the pattern predicted by Robinson for a VOR which did not correct for such a dependence. In general, the data agreed with the previous observation that slow phase direction (in head-fixed coordinates) is independent of eye position (Fetter et al. 1986). This is consistent with recent anatomical experiments which suggest that muscle pulling-directions, at least those of the recti, are

relatively independent of horizontal and vertical eye position (Miller and Robins 1987). Alternatively, if a significant pattern of eye position dependence in muscle pulling-directions does exist, our data would suggest that it is compensated for by the VOR.

The combination of two conditions confirmed by this study make systematic non-collinearities inevitable. First, as predicted by Robinson's matrix model, slow phase axes can be predicted by applying predetermined vertical, horizontal, and torsional gains to the components of head rotation, and then summating the resulting vector products (Robinson 1982, 1985). Second, as observed previously, torsional gain is low (Berthoz et al. 1984; Collewijn et al. 1985). Consequently, rotation of the head about a partially torsional axis will produce a slow phase axis with proportionately small torsional components, such that this axis tilts away from the torsional axis.

If slow phase axes tilt away from the torsional axes, there is practical value in determining the location of this special axis. The intrinsic coordinate systems of the VOR, including those of the semicircular canals, extra-ocular muscles, and the position-signal-generator do not encode torsion along a single independent channel (Baker et al. 1984; Peterson and Baker 1991; Simpson, 1983; Simpson et al. 1989; see also Chapters 5-6). What is the appropriate coordinate system for the overall action of the VOR, which is the product both of these intrinsic coordinates and the transformations that occur between them (Robinson 1982)? The Robinson model arbitrarily puts VOR gain into Cartesian coordinates with the torsional axis pointing straight forward. The main diagonal-elements of this matrix were taken from the best available 1-D measures of gain, and the other elements were set at zero; ie. the VOR was assumed to be collinear about the head-fixed torsional, vertical and horizontal axes. Our data confirms that VOR gain is organized in head-fixed orthogonal coordinates, and furthermore suggests that these coordinates align with those designated by Listing's law of the saccadic system.

The full implications of this remarkable coincidence between the coordinates of the

saccadic system and the VOR are not yet clear. Visual maintenance of VOR gain may be the key. Retinal slip is necessary for calibration of gain, and velocity of slip near the fovea is relatively small during rotations of the eye about the line of sight (Gonshor and Melvill Jones 1976; Miles and Fuller 1974; Schultheis and Robinson 1981). If the monkey's preferred range of gaze directions was centred around the primary direction, then calibration of gain about this axis might consequently suffer. This effect may be compounded by avoidance of large torsional head rotations during visual orientation (Glenn and Vilis 1992). However, this hypothesis appears to be contradicted by the frequent eccentricity of experimentally determined primary positions (Tweed and Vilis 1990a). If primary position does not correspond to the preferred gaze direction, then some other internal factor must be responsible for its significance in the VOR: perhaps sharing of saccadic and VOR coordinate systems at the indirect path, or interaction with the smooth pursuit system, which has recently been shown to obey Listing's law (Tweed et al. 1992).

In summary, the gain of the visually assisted VOR appears to be lowest about an axis parallel with the primary gaze direction and highest about axes in Listing's plane. Systematic non-collinearities arise as follows. Axes of head rotation that were neither in nor orthogonal to Listing's plane produced axes of eye rotation that tilted towards Listing's plane. As the axis of head rotation tilts out of Listing's plane to a peak of 45 degrees, the contribution of axis non-collinearity to instability of the retinal image increases. The VOR is apparently most accurate in direction and magnitude when the head is rotated about an axis within Listing's plane.

3.4.2 *Changes in Eye position during slow phases.*

The pattern of position changes observed during slow phases was the consequence of rotating the eye about a single fixed axis, as predicted by the principles of rotational

kinematics. Equation 2 (section 1.2.3) showed that rate of position change is proportional to eye velocity multiplied by eye position. This clearly shows that rate of change in eye position depends on both the velocity (axis) of rotation and the current eye position. Thus, even rotations of the eye about axes within Listing's plane are expected to violate Listing's law in a position-dependent manner. The fact that they do shows unequivocally that Listing's law is not a product of plant mechanics.

Figure 20 illustrates the sort of three-dimensional position changes that can result from rotations about two-dimensional axes. The eye is viewed from a frontal perspective. Initial position *A* (gaze directed straight ahead) is chosen as the reference position, and a symbol is superimposed over the pupil. The eye first rotates 90° horizontally about a fixed vertical axis to position *B*, as it would during an oversized slow phase or saccade. Clearly, eye position relative to reference position has a significant horizontal component, but no torsional or vertical components.

When rotation is neither towards or away from reference position, the relationship between motion and position is not so trivial (Tweed and Vilis 1987, 1990a). This is most easily illustrated by an extreme case. In the bottom row of Figure 20, the eye starts from position *C*, which is rotated 90° upward from the initial reference position. A 90° leftward slow phase rotates the symbol about the line of sight to position *D* without changing its location. What is the overall change in eye position relative to the head-fixed reference position *A*? It is that rotation that will take the eye from initial position *A* to final position *D*. A purely upward rotation will take the symbol to the correct location, but in the wrong orientation. Any combination of upward and leftward rotation without torsion will take the symbol to the wrong location. Thus, the axis of rotation from reference position must also tilt forward torsionally, as indicated. This is not so-called false torsion; a clockwise torque relative to the torque in *A* must be

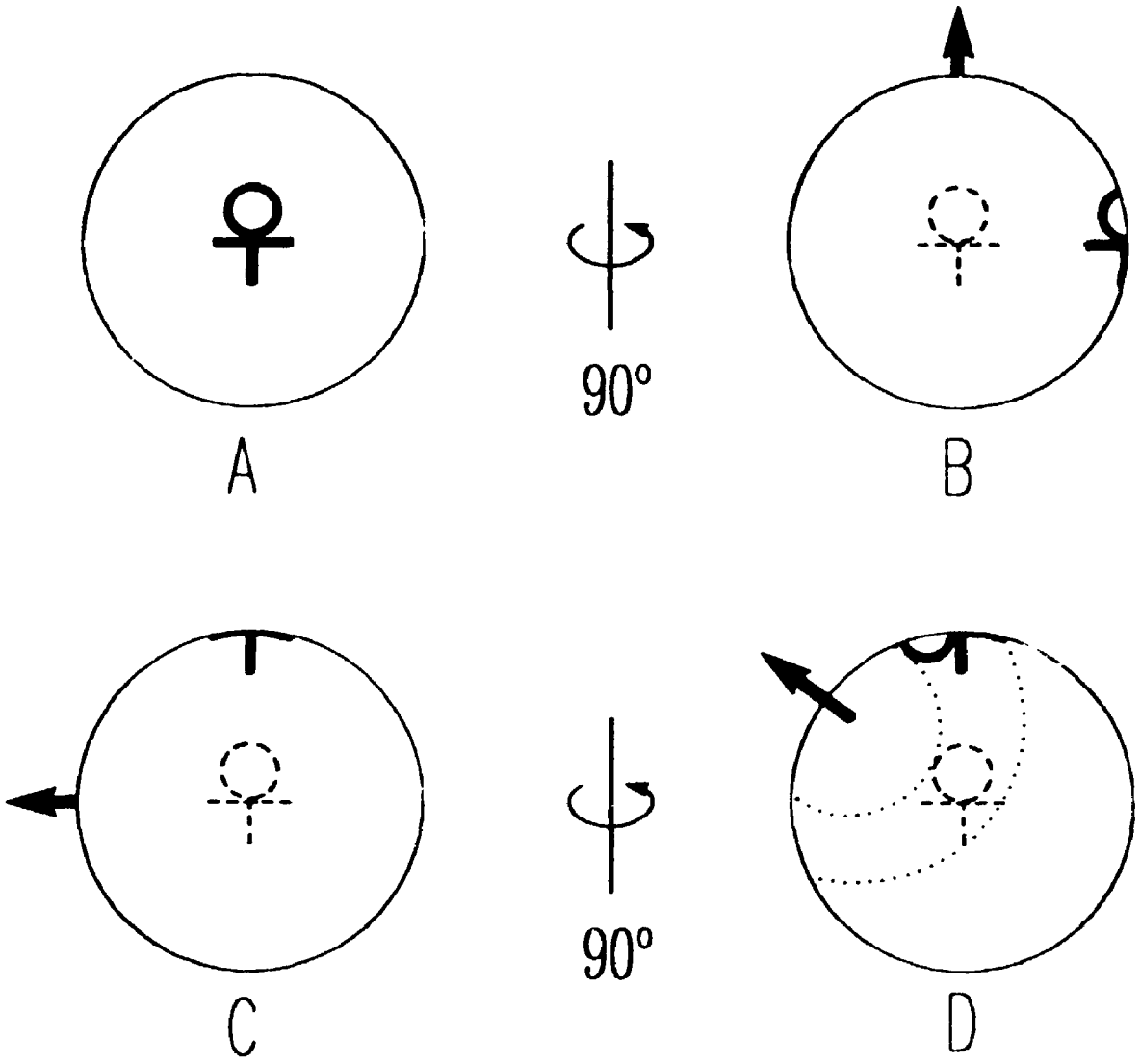

FIGURE 20. The effects of fixed-axis rotation on 3-D position of a sphere. *Upper row; **A***: Initial position. A symbol is painted onto the sphere to indicate rotational position. ***B***: The sphere has undergone a 90° leftward rotation from the initial position. The original position of the symbol is outlined for reference. *Lower row; **C***: The sphere is rotated 90° upward about a horizontal axis from the reference position. ***D***: the sphere in *C* is further rotated 90° to the left. *Heavy arrows* embedded in the spheres indicate the axes of rotation that would take the eye from initial position *A* to each of the other positions. *Dotted lines* indicate the resultant trajectories of points on the surface of the sphere. *Axes* between the two columns show that the same rotation occurs in both rows.

generated by the extra-ocular muscles if position *D* is to be maintained.

The complete pattern of torsional changes expected during more realistic eye positions was simulated using a model of the three-dimensional VOR (Fig 21 *A*). This model is similar to the more familiar one-dimensional Robinson model, but incorporates the principles of rotational kinematics stated above in Equations 2 and 4 (Robinson 1975; Tweed and Vilis 1987). The important modification occurs in the three-dimensional model of the oculomotor plant, where the rate of change in eye position **E** is the product of ω_c and current eye position **E**. Similarly, in the indirect pathway to the brainstem the vestibular eye velocity command ω_{c^*} is multiplied by an internal estimate of eye position $\mathbf{E}^*$ prior to integration. These computations are all performed in head-fixed coordinates. The unique property of this model which is not shared by any previous model is that when gains are set to 1.0 (ideal), it will perfectly stabilize the eye relative to space for any axis of head rotation.

The results of simulating the VOR during rightward head rotation are shown in figure 22. The angular velocity of the eye, ω_{eye}, is equal and opposite to ω_{head}. The important feature of this figure is the dependence of change in eye position quaternions on initial position. When eye position starts from zero (a central reference position) it changes only horizontally, along the axis of rotation. If the initial eye position is above or below centre, then components of position orthogonal to the axis accumulate. The position vectors actually followed an elliptical pattern. As the vertical eccentricity of the initial position increases, so does the tilt and width of the ellipses; ie. the change in torsional and vertical eye position increases. When viewed down the axis of rotation, these components project onto the horizontal plane as circles of increasing radius. This circling pattern occurs because this orthogonal component of rate-of-position-change is proportional to the cross product of the eye velocity vector and the vector part of the eye position quaternion (Tweed and Vilis 1987). This is the same pattern of eye position

FIGURE 21. Kinematically correct models of the oculomotor system. ***A***: Model of the slow phase generator and 3-D oculomotor plant. The vestibular eye velocity signal ω_{e^*} is sent directly to the motoneurons, and also to a velocity-to-position transform (VPT) in the indirect path. The VPT represents current eye position $\mathbf{E}^*$ as the tonic output of an integrator. Rather than inputting ω_{e^*} directly into the integrator, this signal is first multiplied by $\mathbf{E}^*$ to give the estimated rate of eye position change $\dot{\mathbf{E}}^*$, which is then integrated. The plant model incorporates the principals of rotational kinematics with a similar VPT. Subtraction of current eye position from the plant input signal leaves only changes in input, which are converted to velocity signals, multiplied by current eye position, and then integrated. *k*: plant elasticity constant. *r*: plant viscosity constant. *Superscript asterisks* denote neural estimates of real variables. ***B***: VOR model which incorporates a circuit for generation of quick phases in 3-D. Additions to the previous model are drawn in solid lines. Desired gaze direction $\mathbf{g}^*$ is input to the Listing's law operator *LL*, which computes the desired eye position $\mathbf{E}_d^*$. This is then compared to the indirect path's estimate of current eye position $\mathbf{E}^*$ to determine motor error, which is encoded topographically in the deep layers of the colliculus. Motor error drives the brainstem saccade generator (*BSG*). For more details, see Tweed and Vilis (1990b). A feedback signal from the vestibular eye velocity comm-and ω_{e^*} to the *LL* operator has been added to allow rotation of the position plane in the appropriate direction.

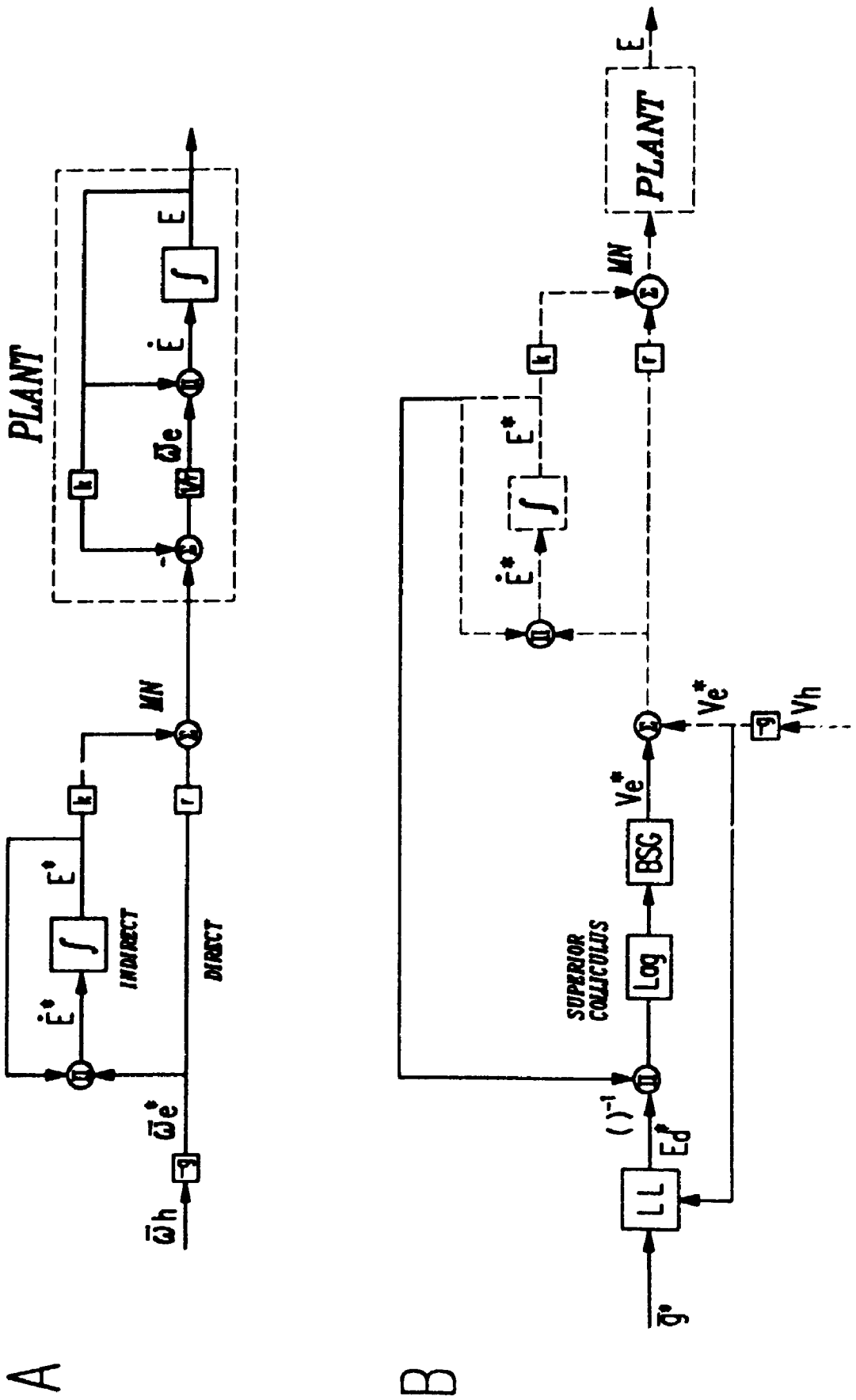
A
PLANT
E
ω̇e
ωe
MN
INDIRECT
DIRECT
Ė*
E*
ω̄e*
ω̄h
B
PLANT
E
MN
Ė*
E*
Ve*
Vh
SUPERIOR COLLICULUS
Log
BSG
Ed*
LL
g*

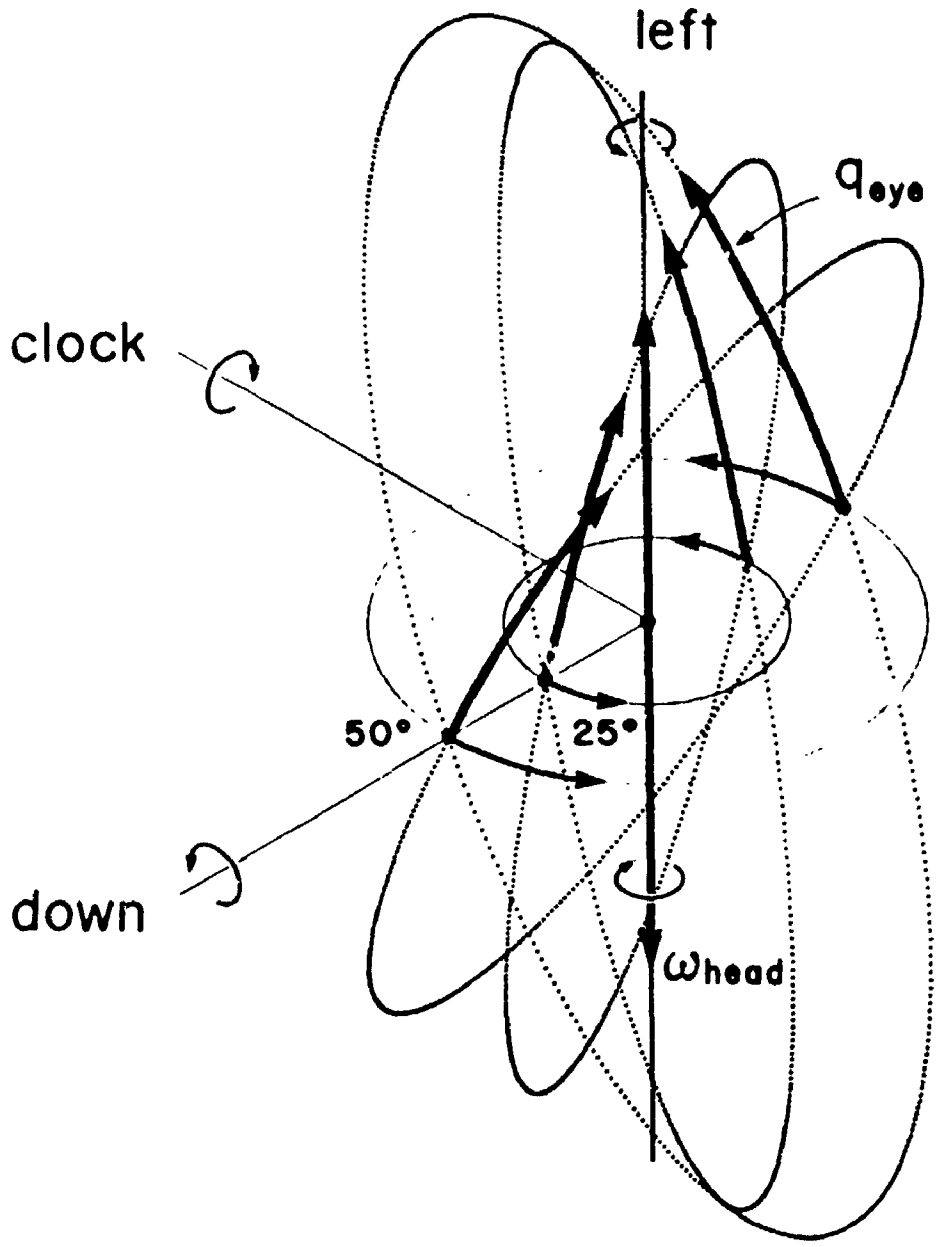

FIGURE 22. Simulation of eye positions during rotations about the vertical axis (horizontal VOR). The eye begins at different vertical positions between 50° down and 50° up. *Heavy lines with arrows*: Realistic paths that eye position would follow during rightward head rotations. *Dotted lines*: elliptical paths that eye position quaternions would follow beyond the oculomotor range. *Solid circles*: projections of eye position onto the plane orthogonal to the axis of rotation.

changes that was observed experimentally. The use of ideal gains in the model demonstrates that this is the pattern that is appropriate for stabilizing the eye in space.

An important feature of this model is that when head rotation stops, accumulated changes in eye position are held; ie. in figure 22 the positions at the end of the arrows are maintained. If the indirect brainstem pathway was ignorant of the properties of rotational kinematics and simply used the integral of the velocity command to estimate position, then during horizontal rotation only the horizontal integrator would change activity. Simulations of such a model showed that after rapid head rotations, the eye should show post rotational drift towards a point on the zero torsion plane. No such drift was observed in the experiment. Thus the indirect path must make the correct velocity-to-position transformation. This suggests that the brainstem structures involved in generation of the position signal, including the nucleus prepositus hypoglossi and the interstitial nucleus of Cajal, must take current eye position into account before integrating velocity (Cannon and Robinson 1987; Crawford et al. 1988).

3.4.3 *Quick phases and Listing's law.*

The function of the quick phase is to reset eye position changes produced by slow phases of the VOR. This appears to include resetting of torsional deviations produced by slow phases. Furthermore, the results show that quick phases direct the eye to a position that anticipates the effects of the subsequent slow phase. Clearly, this is not accomplished by simply reversing the slow phase (Figure 17). Instead, this anticipation appears to be accomplished by directing eye position towards a specific plane that is rotated in the direction of head rotation. This anticipatory interaction is reminiscent of anticipatory interactions that occur between VOR slow phases and vergence movements (Snyder et al. 1992). For quick phases to anticipate slow phase eye positions in such a manner, the brain must choose different planes of desired eye position, depending on

head velocity.

How are the axes of quick phases selected in order to accomplish this? One possibility is that they are produced by the same premotor mechanisms which determine saccade axes. In the previous section we have seen that slow phase axes which do not tilt out of Listing's plane violate Listing's law. By the same token, saccade axes must tilt systematically out of the plane in order to obey Listing's law (Tweed and Vilis 1990b). This tilt depends on both the initial and final position of the saccade. A neural circuit that will compute the correct tilt of these axes has recently been proposed (Tweed and Vilis 1990b).

The main elements of this circuit have been incorporated into the previously discussed slow phase generator (Figure 21 *B*). The input to this circuit is desired gaze direction relative to the head ($\mathbf{g}^*$). This input specifies only two of the three components necessary to define eye position. The brain must select the third component such that the desired eye position E_d^* lies on Listing's plane. This process is denoted by the box labelled *LL*, the Listing's law operator. The next step is to select the rotation (initial motor error) that will take the eye from its present position E^* to the desired position. Recently it has been suggested that such error signals are derived from 2-D retinal error signals, without requiring knowledge of position (Goldberg and Bruce 1990; Waitzman et al. 1991). However, the variable position-dependent displacements produced by a single slow phase eye velocity command show that such a model will not work. The correct computation of initial motor error is achieved by dividing desired position by current position. The axis of rotation is thus dependent on both these positions. Thus, in this model the neurons explicitly compute the torsional saccade axis tilts required to maintain Listing's law, and these axes must be specified by correct input to the extra-ocular muscles.

Figure 21 illustrates this model as it was originally proposed, with the *LL* operator

upstream from the output layer of the superior colliculus. A recent test of this model has suggested that *LL* is downstream from the colliculus (Van Opstal et al. 1991). This requires some changes to the model, but analogous computations must still be made. Since there is no fundamental difference between these computations and those necessary to determine quick phase axes, we propose that the oculomotor system makes use of the same circuit for generation of quick phases to visual targets in the light.

To correctly simulate quick phases, the model must be able to direct eye position to a plane rotated in the direction of the head, or more precisely, in the direction opposite to the eye. The vestibular velocity signal to the eye specifies this information, and also is a good predictor of subsequent slow phase magnitude. Therefore, a vestibular signal to the *LL* operator has been added (Figure 21 *B*). This operator treats plane shifts and tilts equally as rotations in the 4-D space of quaternions. The Listing's law operator then determines the position that is the intersection between this rotated plane and the line of correct gaze positions.

This 3-D VOR / quick phase model suggests that any mechanism involved in stabilization of gaze in space, including the optokinetic and otolith-ocular reflexes (Morrow and Sharpe 1989; Viirre et al. 1986), will produce violations of Listing's law identical to those observed in the present study. Furthermore, these violations should be minimized by anticipatory plane shifts or tilts. Why would the oculomotor system take such measures to minimize torsion? Listing's law appears to optimize several variables from motor and sensory perspectives (Helmholtz 1925): 1. maintenance of the extra-ocular muscles at the centre of their torsional range of motion confers a mechanical advantage; 2. the eye moves to and from a preferred central position (primary position) along the shortest possible path; 3. interpretation of monocular information is simplified by reducing the degrees of freedom of eye position with respect to visual space; 4. binocular vision is facilitated by maintenance of a constant positional relationship between

the two eyes. For example, the pattern of corresponding points on the two retina's gives rise to a tilted vertical horopter (Nakayama 1982), which may disintegrate during large conjugate torsion. Although these may all be important consequences of Listing's law, the key determinant of this law remains unknown.

The plane shifts observed during VOR quick phases also raise the possibility that the ocular-counterroll reflex might be accomplished by a similar plane shift. This is consistent with the similarity between the quick phase end-position surfaces and counterroll surfaces observed in this study. According to this new view, after the dynamic component of a torsional VOR, the end points of subsequent saccades would be determined solely by the saccadic system, without evoking the need for an otolith-ocular direct path. Is this a vestigial righting reflex (Collewijn et al. 1986), or might it serve some more precise function? Recently it has been shown that head position obeys a Fick gimbal-like position constraint during gaze movements (Glenn and Vilis 1992). A torsionally tilted head posture is thus not really allowable during gaze movements, and the first true gaze movement should correct this with a torsional head movement. If Listing's plane is shifted to anticipate the expected torsional slow phase, as we have observed during the dynamic torsional phase, then the predicted anticipatory shift would resemble the phenomenon now known as ocular counterroll. In general, a significantly tilted static head posture will be followed by a head movement in the opposite direction. Thus, Listing's plane should rotate / shift by a small amount in the direction opposite to that of static head tilt to anticipate slow-phase violations of Listing's law. This predicts the plane shifts that were observed here during both vertically and torsionally tilted head postures.

To summarize, the results of this investigation stress the importance of maintaining zero torsion. VOR slow phases violate this state of zero torsion, but this effect appears to be minimized by keeping eye position centred across Listing's plane. This suggests

that Listing's law is not simply a default solution to the degrees of freedom problem. Rather, it appears that minimization of ocular torsion is a specific mandate of the oculomotor system, although the object of physiological optimization remains elusive. Furthermore, this illustrates a remarkable sophistication in even this relatively simple system. By minimizing ocular torsion and retinal slip, while permitting foveation of visual targets, VOR slow phases and quick phases maintain normal orienting functions despite the challenge of operating from an unstable platform.

4 THREE-DIMENSIONAL COORDINATES OF THE SACCADIC BURST GENERATOR

4.1 INTRODUCTION

Oculomotor short-lead burst neurons provide an excellent experimental model for examining the nature of brain coordinate systems. Burst neurons, which produce the phasic command for conjugate rapid eye movements, are named for the brief burst of action potentials that they produce before and during movements in a preferred direction (Fuchs et al. 1985; Luschei and Fuchs 1972; Sparks and Mays 1990). For such phasic movement commands, coordinates are essentially a set of one-dimensional movement directions (the directions generated by individual burst neuron populations) that can be combined to express a movement in any given direction. To determine the overall movement, the magnitudes of movement along each coordinate direction must be specified as components (by discharge rate of various burst neurons). Thus, components are only meaningful if the associated coordinates are understood. Moreover, one must understand the frame of reference in which these coordinates are imbedded, such as the head, the body or gravity fields. Recent theoretical models and behavioral experiments have frequently emphasized the importance of neural coordinate systems and their reference frames (Hollerbach and Atkeson 1987; Pellionisz and Peterson 1988; Raphan and Cohen 1986; Robinson 1985; Simpson and Graf 1985; Soechting and Flanders 1991), but there is less direct experimental data (Anderson et al. 1985; Mays and Sparks 1980; Peterson and Baker 1991; Simpson et al. 1989). The purpose of the present study was to determine the coordinate directions utilized by oculomotor burst neurons, and how this system is oriented within its reference frame.

For at least 15 years, there has been debate between two schools of thought that would align burst neuron coordinates either with eye muscle pulling directions (Büttner

et al. 1977) or the maximal sensitivity vectors of semicircular canals (Robinson and Zee 1981). Why has this question not been resolved? Single unit recording has provided most of our knowledge of burst neuron physiology, but is not suited to the precise determination of coordinates. The movement directions that correlate best to unit activity can deviate from the directions of rotation that are generated by neurons (Pellionisz and Peterson 1988). Furthermore, individual units may show variations unrelated to the overall behaviour produced by the population, as demonstrated clearly by neural network models (Anastasio and Robinson 1990). Another problem is that burst neurons are generally thought to encode eye velocity (Robinson 1975; Tweed and Vilis 1990a), i.e. three dimensional (3-D) axes of eye rotation, but previously such axes were not correctly recorded. We attempted to avoid these pitfalls by electrically microstimulating and pharmacologically inactivating various riMLF burst neuron populations while correctly recording axes of eye rotation (Chapter 2).

In contrast to the multiple classes of oculomotor-related activity found in the PPRF (Raybourn and Keller 1977), the riMLF appears to be almost exclusively comprised of short-lead burst neurons (Büttner et al. 1977; King and Fuchs 1979). Our preliminary goal was to corroborate the accepted theory that the riMLF produces saccadic velocity signals, upstream from the neural "integrator" that generates tonic eye position signals (Fuchs et al. 1985; Robinson 1975). If so, then a constant stimulus input should result in a ramp - like change in eye position that holds at the end of stimulation (Fig. 2 B). Eye movements of various directions, including torsion, have been observed previously during midbrain stimulation (Westheimer and Blair 1975; Hassler 1972; Kompf et al. 1979).

The first step in determining coordinates is to establish the directions of eye rotation controlled by individual riMLF burst neuron populations. The behaviorally measured canal / muscle - like scheme described above differs from a more recent scheme based

on the anatomical projections of functionally identified riMLF burst neurons (Moschovakis et al 1991a, b). Downward burst neuron projections to motoneurons were consistent with the canal / muscle scheme, but the projections of upward burst neurons suggested that they do not produce torsion. The behaviorally and anatomically determined schemes agree in predicting that stimulation of the right riMLF should produce CW eye rotations and left stimulation should produce CCW rotations about a head-fixed axis roughly orthogonal to the face. Both schemes also predict that CW saccade / quick phase components will be abolished after right inactivation, and CCW rotations lost after left inactivation. However, the anatomical evidence (Moschovakis et al. 1991a) predicts that during unilateral riMLF inactivation upward saccades will be relatively normal, whereas the behavioral evidence predicts that both upward and downward saccades will be made with equal amounts of abnormal torsion (Vilis et al 1989). This chapter will experimentally test the predictions of these two schemes.

Neither scheme explains the suggestion of early single unit investigations that riMLF neurons may also carry a small horizontal component (Büttner et al. 1977), or the anatomical projections that have been observed from the riMLF to the abducens nucleus (Büttner-Ennever and Büttner 1988). These observations suggest that the coordinate axes defined by the riMLF burst populations may also have a horizontal component. If so, then we hypothesize that inactivation of the riMLF should also affect horizontal saccades.

Finally, we will examine the orientation of the burst neuron coordinate system with respect to its reference frame. Theoretical and experimental observations agree the reference frame should be the head (Büttner et al. 1977; Pellionisz 1986; Robinson and Zee 1981), but to determine precise orientation within the head, direct observations are required. Unilateral stimulation of the riMLF should reveal the torsional coordinate axis, while the intact vertical axis following riMLF inactivation should reveal the coordinate specified by the remaining PPRF burst region. These axes might align with sensory

canal coordinates (Robinson and Zee 1981), downstream muscle coordinates (Büttner et al. 1977), or something intermediate. Another possibility is that such motor coordinate systems do not align best with associated anatomical structures, but rather with some parameter of the behaviour produced. It is the behavioral synergy called Listing's law which determines the axis of rotation for a saccadic gaze shift, and thus the required ratio of activity between the various burst neuron populations (Hepp 1990; Helmholtz 1925; Tweed and Vilis 1990 a,b; Westheimer and Blair 1972). Therefore we hypothesized that the coordinate axes controlled by oculomotor burst neuron populations are related to Listing's plane and its perpendicular primary gaze direction.

4.2 METHODS

The riMLF burst region was identified and thoroughly explored in 4 monkeys, MAR, BAR, ART, and CAS, as described in chapter 2. Recall that spontaneous eye saccadic eye movements to visual targets were recorded in all animals, MAR and BAR were trained to make saccades between LED targets, and the VOR was tested about various axes in ART and CAS. Binocular recordings were made in the latter two animals.

4.3 RESULTS

4.3.1 *Microstimulation of the riMLF*

Electrical microstimulation of identified burst neurons was performed at 26, 39, 13, and 17 sites in animals MAR, BAR, CAS and ART, respectively. Ten to twenty stimulations were typically delivered at each of these sites, sometimes up to 100. The results reported below were observed consistently in all of these trials, except where specifically stated otherwise. As explained in the METHODS, when burst neurons were recorded during saccades the two sides of the riMLF appeared to be similar, each possessing intermingled up and down tuned neurons. During unilateral riMLF

stimulation these vertical components appeared to cancel each other, and the remaining components emphasized the difference between the two sides. The primary change in eye position during stimulation was torsional, out of Listing's plane of normal saccadic eye positions. The direction of movement was clockwise during right riMLF stimulation and counterclockwise during left riMLF stimulation. We will first consider the time course of stimulus-evoked eye position changes, and then precise directions of rotation.

TIME COURSE OF EYE POSITION CHANGE Figure 23 A illustrates the conjugate nature of a typical eye movement recorded during right riMLF stimulation. Data are plotted in Listing's coordinates, so that torsional position is relative to Listing's plane. For contrast, eye movements evoked by stimulation of putative motoneuron fibres several mm below the riMLF (Fig. 23 B) are also shown. During such stimulations and during stimulations of the more posterior third cranial (oculomotor) nucleus, the eye movement was not conjugate. In the illustrated case only the ipsilateral eye moved, as would be expected from stimulation of the third cranial nerve below its decussations. Furthermore, during application of the stimulus, the eye drifted exponentially towards a new position. Upon termination of the stimulus, the eye drifted rapidly back towards its original position. This is the behaviour expected from a step input directly to the motoneurons supplying one eye, downstream from the neural integrator.

RiMLF stimulation produced changes in eye position at a much more constant rate than motoneuron stimulation. Plots of eye position as a function of time during application of the standard step-like stimulus to the riMLF resembled a ramp (Fig. 24). Another important observation was that upon termination of the stimulus, eye position stopped abruptly and held, without the rapid drift observed during motoneuron stimulation. The consistency of these observations is emphasized in figure 24 A, which shows torsional eye position (in Listing's coordinates) as a function of time for a series of 20 consecutive right riMLF stimulations. Eye positions have been truncated at the

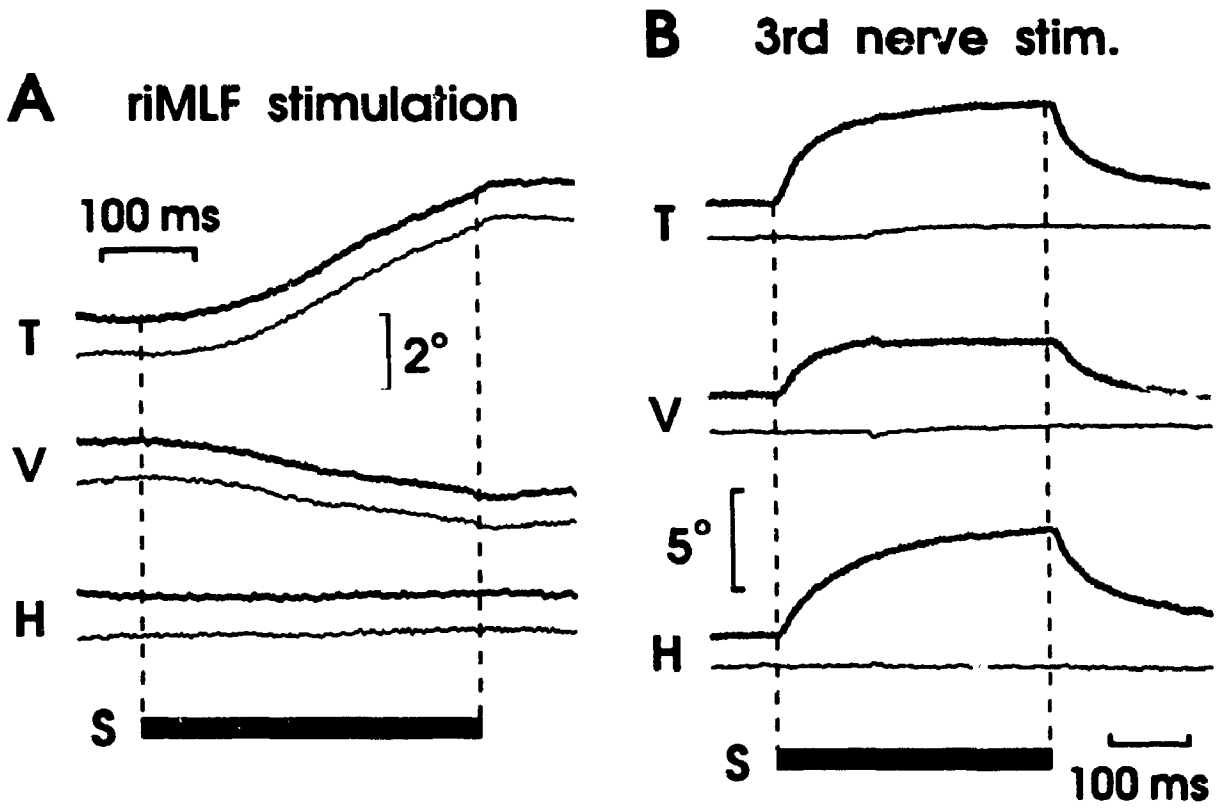

FIGURE 23. Burst neuron vs. motoneuron stimulation. Binocular eye position during unilateral microstimulation of the (A) right riMLF and (B) third cranial nerve are shown. Torsional (T), vertical (V) and horizontal (H) eye positions are plotted as a function of time. Thick lines: left eye; Thin lines: right eye. The duration of the standard stimulus (S) (20 μA, 200 Hz) is indicated by the bar. Data is plotted in Listing's coordinates, so that torsion is equivalent to violation of Listing's law. Animal: ART

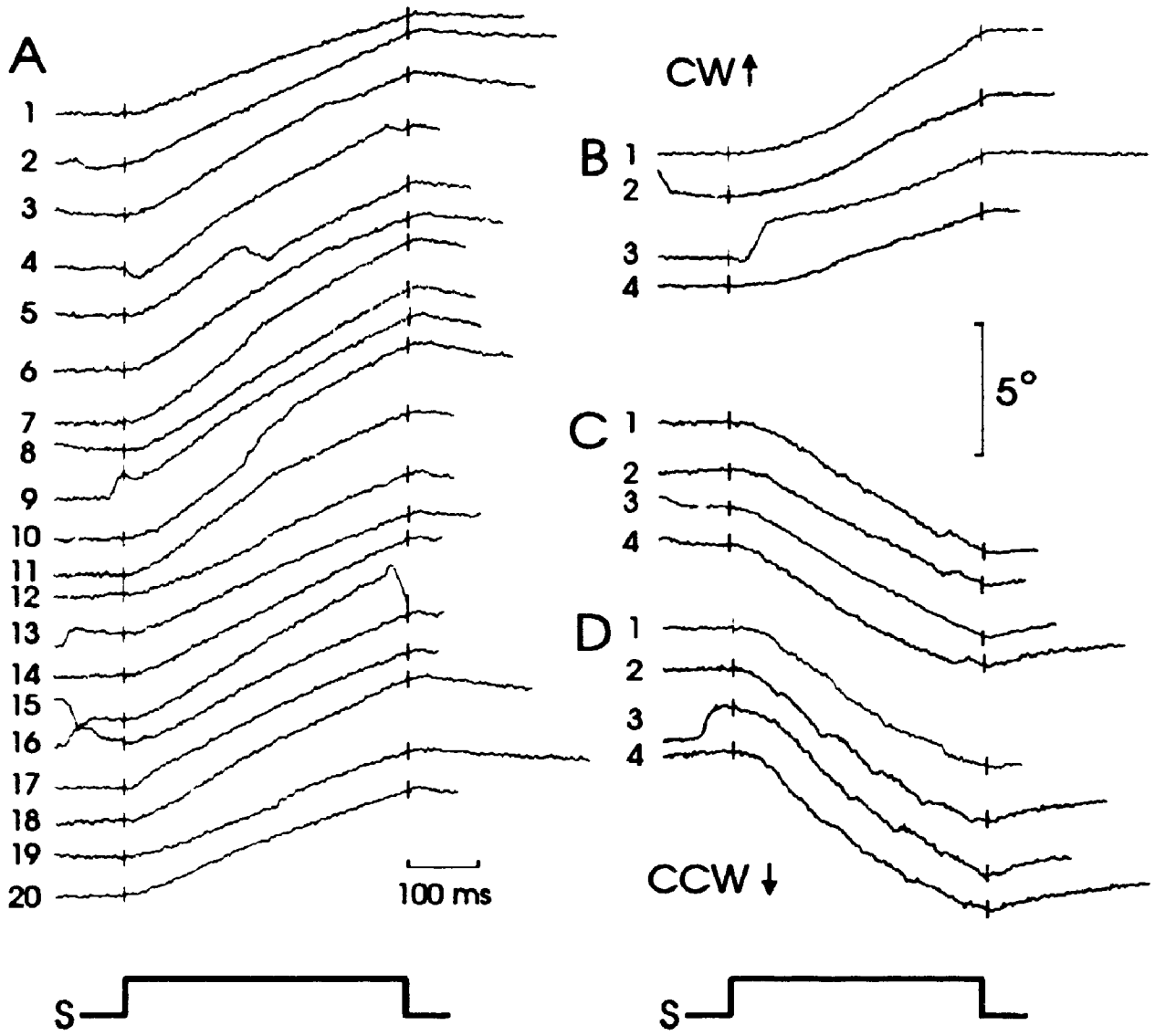

FIGURE 24. Ramp-like torsional eye position changes during step-like riMLF stimulation (S). Right rimlf stimulations are shown for animal CAS (A) and animal ART (B). Left riMLF data are also shown for CAS (C) and ART (D). Stimulations were performed in the light at random gaze directions. CW: clockwise. CCW: counterclockwise.

occurrence of the first post-stimulus saccade, which will not be considered here. Also shown are several right riMLF stimulations from a second animal (Fig. 24 B), and several left riMLF stimulations from the same two animals (Fig 24 C, D). The latter also exhibit the typical ramp-like response and stability of post-stimulus eye position.

The ramp-like response was most clear when no saccades occurred during the stimulus (Fig 23 A). However, the ramp was usually superimposed on horizontal and vertical saccades, which occurred frequently during the relatively long stimulus. The directions and sizes of these saccades were not consistent, and neither was their affect on the torsional ramp. For example, many saccades occurred during the movements illustrated in figure 24, some reducing torsion (eg. mid-movement A5), some increasing the torsion (eg. early in movement B3), but more often inducing random noise as in figure 24 D.

DIRECTION OF EYE ROTATION Stimulations throughout one side of the riMLF consistently produced eye rotations that were mainly torsional, clockwise during right stimulation and counterclockwise during left stimulation. Figure 25 illustrates the mean eye velocities produced by multiple stimulations at 0.5 mm vertical intervals through the right riMLF. Eye velocities are viewed from a perspective above the animal, as indicated by the head caricature, in magnetic field coordinates. A line drawn from the origin to each data point defines the axis of rotation, the length of the line is the speed, and direction of rotation is defined by the right-hand convention. If the thumb of the right hand is pointed along this line away from the origin, then the fingers curl in the direction of rotation. As the stimulation electrode was vertically advanced, the onset of eye movement was abrupt, going from no response at 0.5 mm above the illustrated range to a large response (Fig 25 A, B), and then becoming smaller (Fig 25 C). This transition was similar for both eyes, which always rotated with similar directions and speeds. The observed variations in eye speed and direction for any one stimulation site

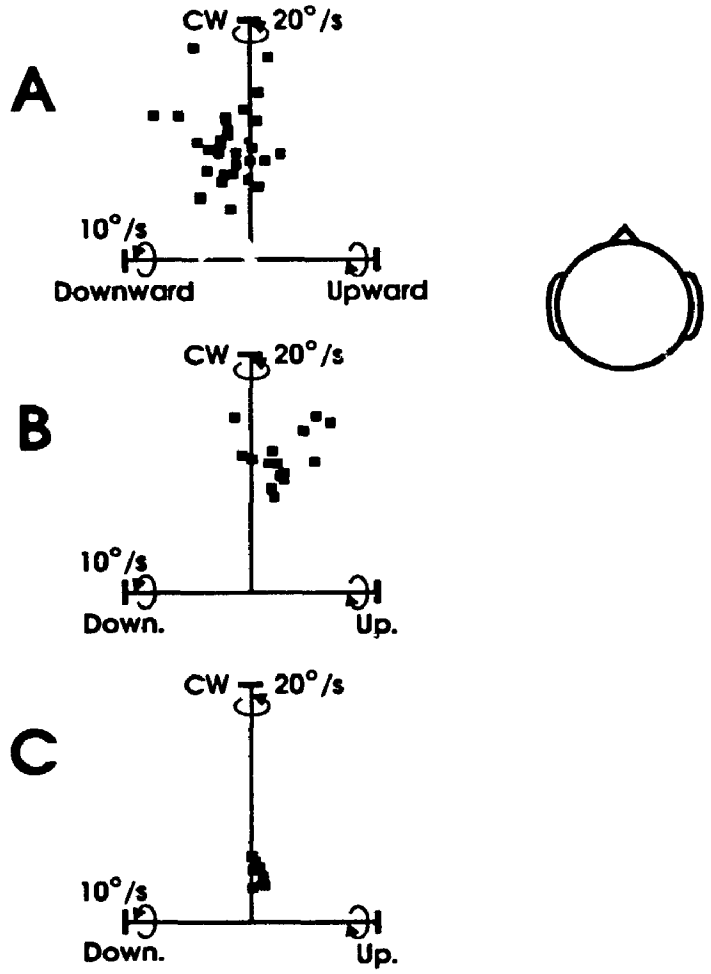

FIGURE 25. 3-D riMLF stimulation axes. Mean eye velocities are shown during multiple stimulations at 0.5 mm vertical intervals along one right riMLF electrode penetration in animal ART. Stereotaxic coordinates: anterior 10 mm, lateral 2 mm, vertical (**A**) 7.0 mm, (**B**) 6.5 mm, (**C**) 6.0 mm. Movement was not evoked 0.5 mm above **A** or 0.5 mm below **C**. Data points are the mean velocities of individual stimulus-evoked movements, plotted in field coordinates, and viewed from a perspective above the subject (indicated by head caricature). Stimulations were performed in the light at random gaze directions. Although care was taken not to include saccadic movements in the data, axis variability increased with the frequency of spontaneous saccades, perhaps because of variable natural neural inputs to the burst neurons during intersaccadic intervals.

were not correlated with eye position. Again, the primary direction of eye rotation was torsional, clockwise for the right riMLF sites illustrated. A small tendency towards vertical rotation was also observed, eg. downward in figure 25 A and upward in figure 25 B, but these directions did not appear to follow a consistent anatomical pattern. Similar results were observed during left riMLF stimulation, except that the main component of eye velocity was counterclockwise.

In order to compare data between animals, the mean stimulation velocities from each site (eg. Fig 25 A) were averaged to get a representative stimulation velocity in field coordinates. Such representative velocities are illustrated in figure 26 for right riMLF and left riMLF sites of all four animals. The criterion used for choosing these sites was that they gave the largest responses of those sites removed by at least 1 mm anterior from areas where cell recording revealed tonic oculomotor activity and muscimol injection produced positional drift. Velocities in figure 4 have been normalized to unit vectors using division by average speed ($\bar{s}$). Error bars show the small standard errors of the torsional, vertical, and horizontal components. Figure 26 illustrates the main points described above, showing the dominance of the torsional component over the others, its consistency of direction (CW(+) for right riMLF and CCW(-) for left riMLF) and the variability of the vertical response.

Stimulation velocities plotted in field coordinates also had a consistent pattern of horizontal components (Fig. 26). Right riMLF stimulation velocities had a leftward (+) component and left riMLF velocities had a rightward (-) component. Recalling that horizontal rotation occurs about a vertical axis, this means that the forward pointing (clockwise) right riMLF stimulation vectors also pointed slightly upwards, and the left riMLF stimulation vectors pointed in the opposite direction. In other words, the stimulation axes were rotated upwards from the forward pointing torsional field coordinate.

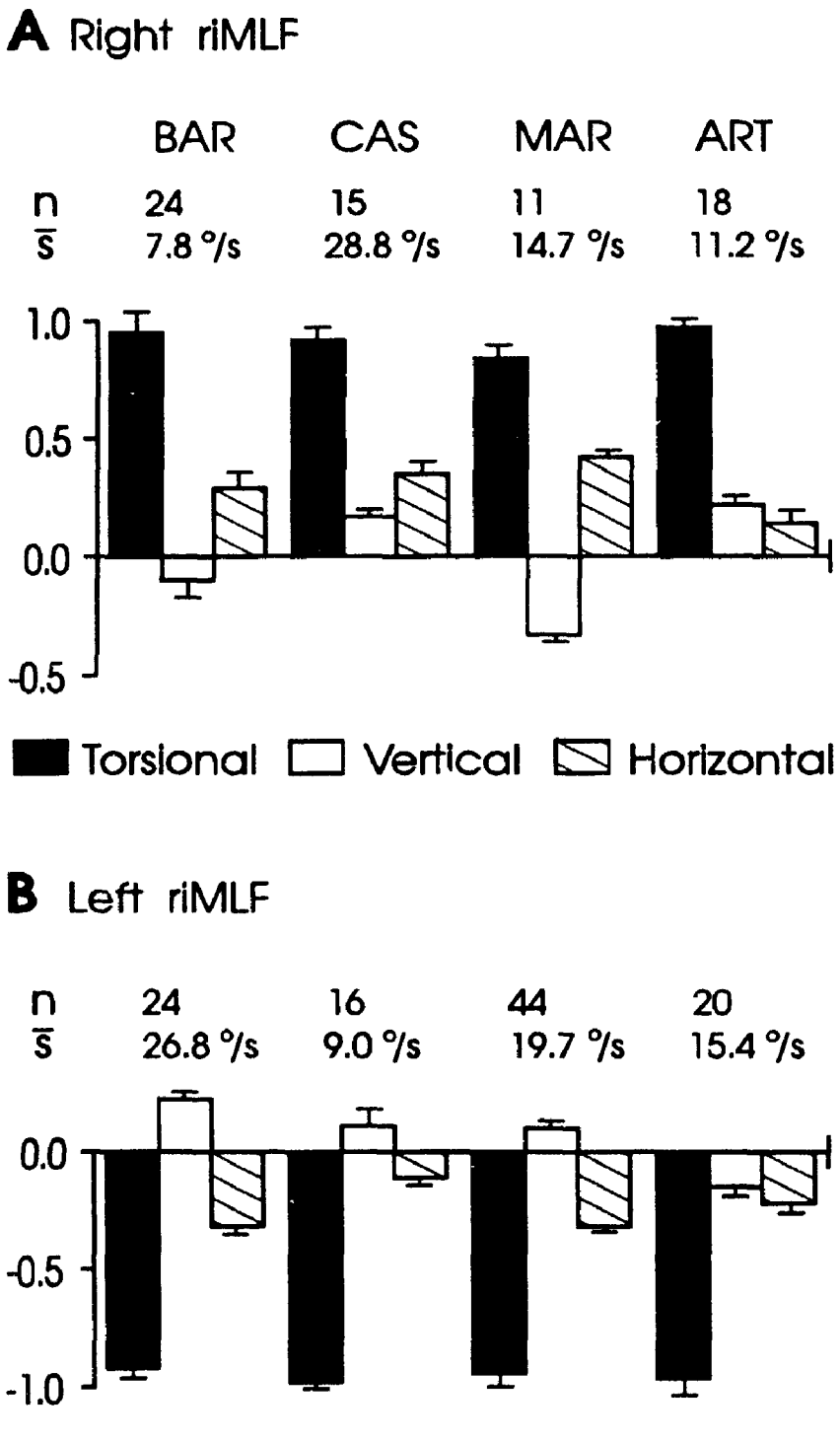

FIGURE 26. Normalized components of representative eye velocities from right (**A**) and left (**B**) riMLF stimulation of the four animals. Positive deflection denotes clockwise, upward, or leftward rotation. See text for explanation.

Listing's plane and its orthogonal primary gaze direction also tended to be rotated upwards compared to the arbitrary field coordinate system, as indicated schematically in figure 27 A. That is to say that during and between saccades, eye position was confined to an upward-rotated plane (Fig. 27 B). Figure 27 C shows a computer fit of Listing's plane and primary gaze direction to normal saccadic eye positions (Fig. 27 B) and also the mean velocity vectors of a series of stimulations from the optimal right and left riMLF sites of the same animal. There was a remarkable alignment between primary gaze direction and the riMLF stimulation axes viewed from the side.

To quantify this alignment, we plotted the upward tilts of the optimal stimulation axes from figure 26 as a function of the upward tilt of the primary gaze direction (Fig. 28 A) and as a function of the upward tilt of the horizontal stereotaxic plane (Fig 28 B), each relative to the field coordinate system for a given experiment. Statistically, the upward tilt of Listing's coordinates accounted for 82% ($r^2 = 0.82$) of the variability in stimulation axis tilt (Fig 28 A). Furthermore, one can see that the points align closely with the line of equality. As reported previously (Tweed and Vilis 1990b), the orientation of Listing's plane varied with respect to anatomical landmarks (not illustrated). The Listing's planes used for these computations tilted upward from the stereotaxic horizontal plane by $10.4 \pm 6.9^{\circ}$ (mean $\pm$ SD), and the tilts of these two systems relative to field coordinates were not highly correlated ($r^2 = 0.24$). The correlation between upward tilts of the stimulation axes and upward tilts of the horizontal planes (Fig. 28 B) was even lower ($r^2 = 0.09$), much lower than the correlation between stimulation axes and Listing's planes. Henceforth data are plotted in Listing's coordinates, unless stated otherwise.

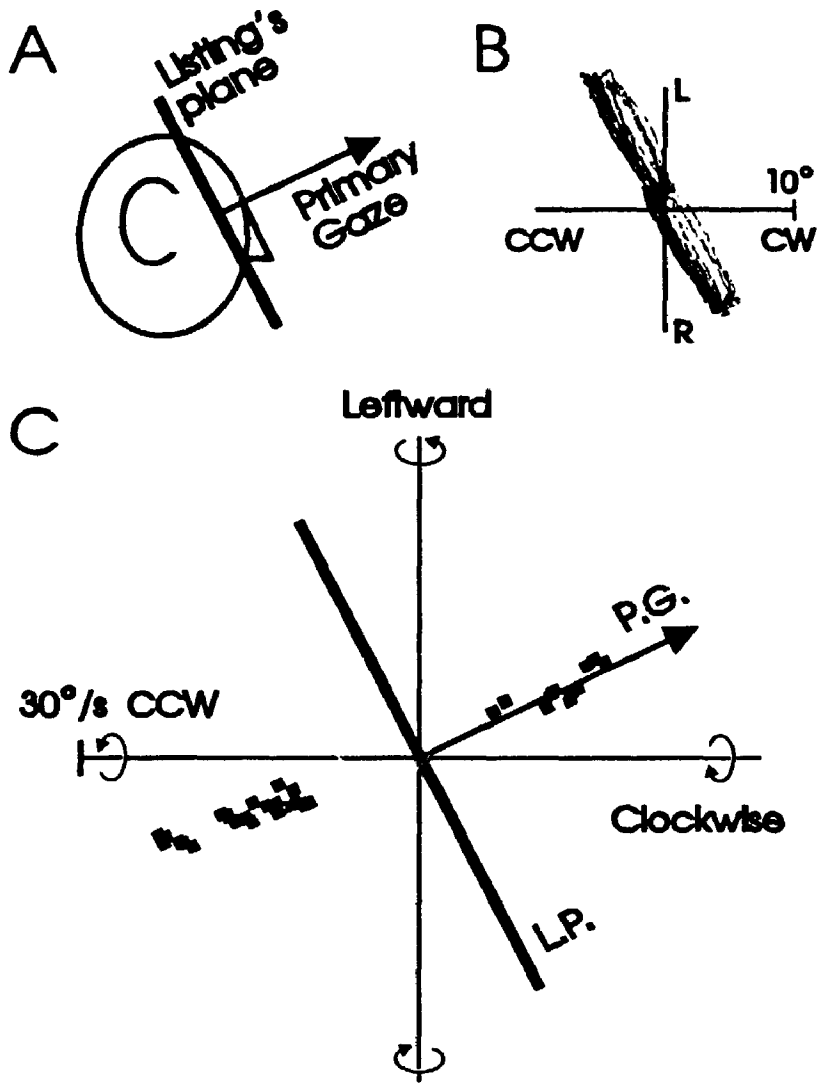

FIGURE 27. Correspondence between riMLF stimulation axes and primary gaze direction. **A:** Schematic drawing of upward tilt of Listing's plane and its orthogonal primary gaze direction relative to the head when viewed from the side. **B:** A real Listing's plane, viewed edge-on from the side in field coordinates. Eye positions during forty saccades between a central target and four diagonal targets are plotted relative to the computed primary position. Animal: MAR **C:** Side views of mean eye velocities during a series of stimulations of the left (CCW points) and right (CW points) riMLF of animal MAR. A plane of best fit (L.P.) to the data in **B** and its orthogonal (primary gaze direction; P.G.) are overplotted. Data are plotted in field coordinates.

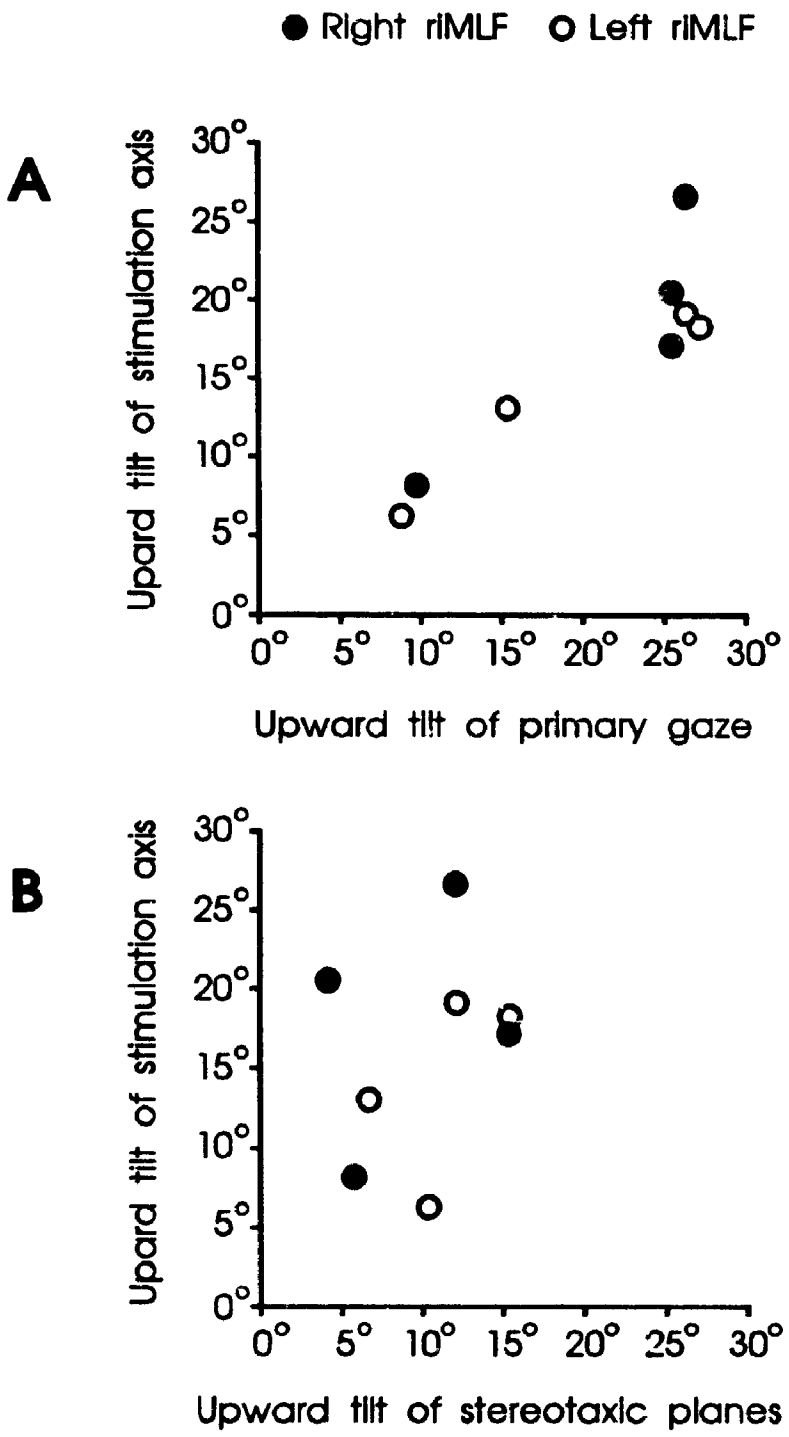

FIGURE 28. Alignment of stimulation axes with Listing's plane rather than anatomy. Plot of upward tilt of representative stimulus axes from optimal sites of all four animals (Fig. 26) as a function of upward tilt of (**A**) primary gaze direction (orthogonal to Listing's plane) and (**B**) stereotaxic planes, relative to magnetic field directions.

4.3.2 *Muscimol inactivation of the riMLF.*

AXES OF EYE ROTATION. Muscimol was injected directly into 9, 6, 7, and 9 identified burst neuron sites in animals MAR, BAR, CAS and ART respectively, as well as a greater number of immediately adjacent sites. Unilateral riMLF inactivation produced a conjugate deficit in vertical and torsional rapid eye movements, and a smaller deficit in horizontal rotations that was observed consistently in the spontaneous saccades of all four animals. The nature of the deficit was most clear during trained saccades between LED's (animals MAR and BAR) and during torsional VOR quick phases (animals CAS and ART), as illustrated below.

Which axis will the eye rotate about if a trained animal attempts a vertical saccade during unilateral riMLF inactivation? Saccades between vertically displaced LED targets were normally made about a horizontal axis (Fig. 29 A). This is illustrated using the instantaneous velocities of these saccades which, starting from zero, grew to a maximal value and then looped back to zero along the horizontal axis. During unilateral riMLF inactivation the velocity of saccades between vertically displaced LED's was reduced by 50% or more (Fig. 29 B, C, *upper row*). Furthermore, animals were unable to make purely downward or upward saccades without large torsional components. During right riMLF inactivation both downward and upward saccades had an inappropriate counterclockwise velocity component as large as the vertical component (Fig. 29 B, *upper row*). Similarly, during left inactivation upward and downward saccades had an inappropriate clockwise velocity component as large as the vertical component (Fig. 29 C, *upper row*). Following bilateral riMLF inactivation, vertical saccades were practically abolished (Fig. 29 D).

When these same saccade velocities were examined from a perspective behind the subject, ie. vertical vs. horizontal velocity, a surprising linkage between vertical and horizontal velocity was observed (Fig. 29 B, C, *bottom row*). During right riMLF

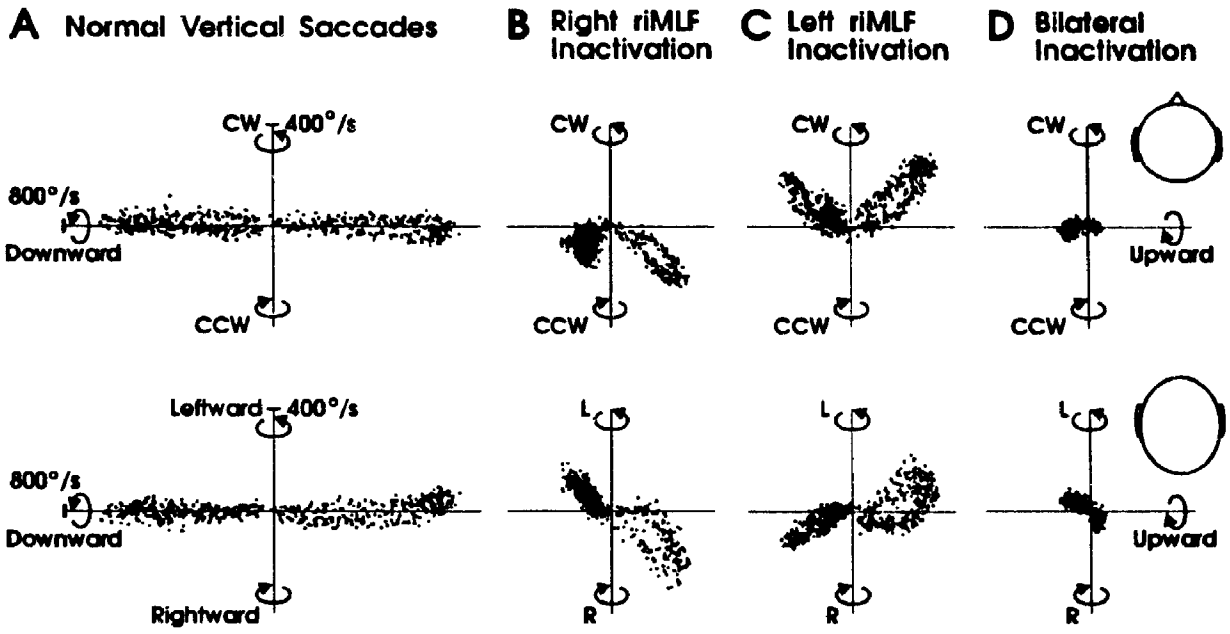

FIGURE 29. Axes for saccades between vertically dispaced targets after riMLF inactivation. Instantaneous velocities are shown for saccades that attempt to shift gaze between targets displaced vertically by 20°, (**A**) normally, (**B**) after right riMLF inactivation, (**C**) after left riMLF inactivation, and (**D**) after bilateral inactivation. For each saccade, velocity begins at zero and then loops out and back along the axis of rotation. Overlapping velocity loops of eight consecutive upward and downward saccades are shown in each case, constituting four individual data files. Data is viewed from a perspective above (*top row*), and behind (*Bottom row*) the animal, in Listing's coordinates. Animal: MAR.

inactivation, upward saccades rotated the eye rightward and downward saccades rotated the eye leftward (Fig. 29 B, *bottom row*). During left riMLF inactivation the symmetrically opposite vertical-horizontal linkage was observed (Fig. 29 C, *bottom row*). These horizontal components were observed consistently, but were usually smaller than the torsional and vertical components. Thus, when the two trained animals attempted vertical saccades during right riMLF inactivation, CCW-upward-rightward and CCW-downward-leftward rotations occurred, and during left riMLF inactivation CW-upward-leftward and CW-downward-rightward rotations occurred.

One interpretation of the above data is that the axes used for vertical saccades during unilateral riMLF inactivation are the coordinate axes controlled by the upward and downward burst neuron populations of the opposite intact side. This would suggest that these burst populations are not only involved in generating vertical and torsional saccade components, but also horizontal components. If so then riMLF in-activation should reduce horizontal saccade velocity. Furthermore, the riMLF would normally have to participate in horizontal saccades in such a way that its vertical components would cancel, and these should no longer cancel during unilateral inactivation. The predicted pattern was consistently observed when the two trained animals saccaded between horizontally displaced LED's (Fig. 30). During right riMLF inactivation, rightward saccades had an inappropriate upward component and leftward saccades had an inappropriate downward component (Fig. 30 B). The symmetrical pattern was observed during left riMLF inactivation (Fig. 30 C). Horizontal velocity was slightly reduced by unilateral riMLF inactivation (Fig. 30 B, C), and further reduced by bilateral inactivation (Fig. 30 D).

We examined this further in the other two animals (CAS & ART) by eliciting the maximal possible range of velocities before and after muscimol injection. To elicit the maximal range of movement the monkey was rotated sinusoidally about a torsional axis,

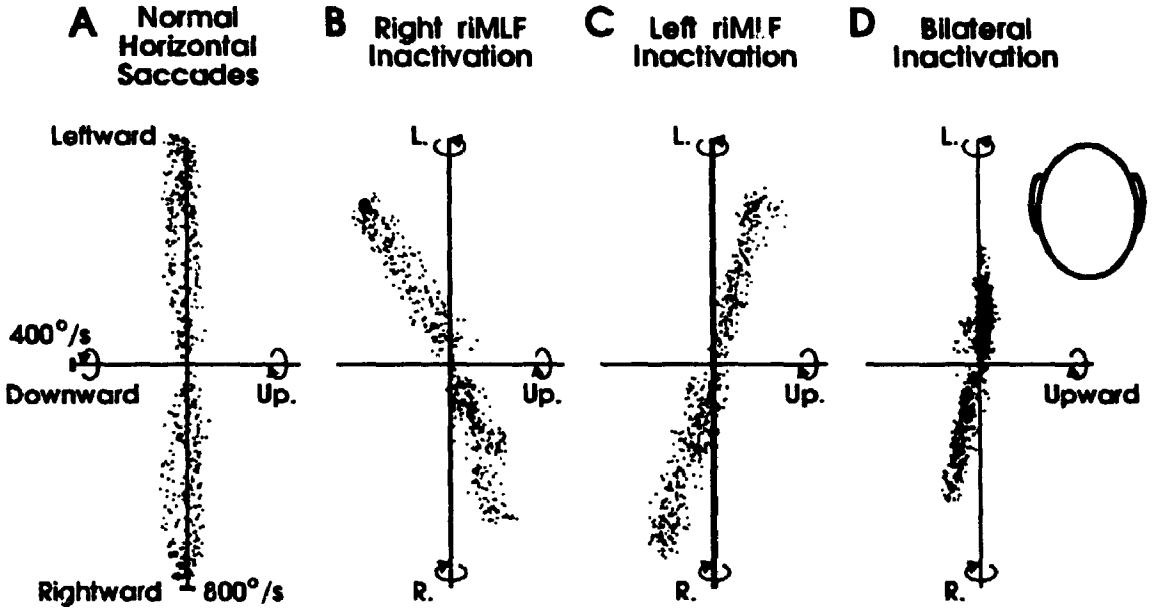

FIGURE 30. Axes for saccades between horizontally displaced targets after riMLF inactivation. Each panel displays overlapping velocities of eight leftward and rightward saccades viewed from a behind perspective in Listing's coordinates.

which elicited large torsional quick phases. At the same time visual targets were presented to encourage large movements in all combinations of vertical and horizontal directions. Normally, the range of velocities fell within a flattened sphere of dimensions ± 400°/s torsional, ± 800°/s vertical, and ± 800°/s horizontal (Fig. 31 A).

Following unilateral riMLF inactivation, there was a stereotyped conjugate reduction in the quick phase velocity range of both animals. Eye velocities on one torsional side of Listing's plane was practically obliterated, the clockwise side during right riMLF inactivation (Fig. 31 B, *above views*), and the counterclockwise side obliterated during left inactivation (Fig. 31 C *above view*). The upwards and downward range of velocities were equally reduced, usually by slightly more than 50% (Fig. 31 B, C, *both views*), while the horizontal range was only slightly reduced (Fig 31 B, C, *behind views*). The remaining instantaneous eye velocity vectors formed an overall 3-D range resembling a 90° wedge cut out of the normal spherical range. These wedges fanned out torsionally from an inner narrow edge aligned with the vertical axis (Fig. 31 B, C, *above views*), and were elongated along this axis (Fig 31 B, C, *behind views*). From the behind perspective these wedges had a tilt that ranged from small (Fig. 31 B) to quite prominent (Fig. 31 C). Horizontal and vertical velocity appeared to be impaired more for oblique movements along one diagonal than along the other, an effect that was also consistently observed during trained oblique saccades. Velocities of both eyes are shown during right riMLF inactivation to illustrate the essentially conjugate nature of the deficit. The same basic deficit was observed in the velocities of head-fixed spontaneous saccades during all riMLF inactivations in all four animals, the main difference being that both the normal and abnormal torsional ranges were smaller in the absence of a vestibular stimulus.

INTERACTIONS BETWEEN EYE VELOCITY AND POSITION As expected from the torsional velocity imbalance described above, vertical saccades always drove eye

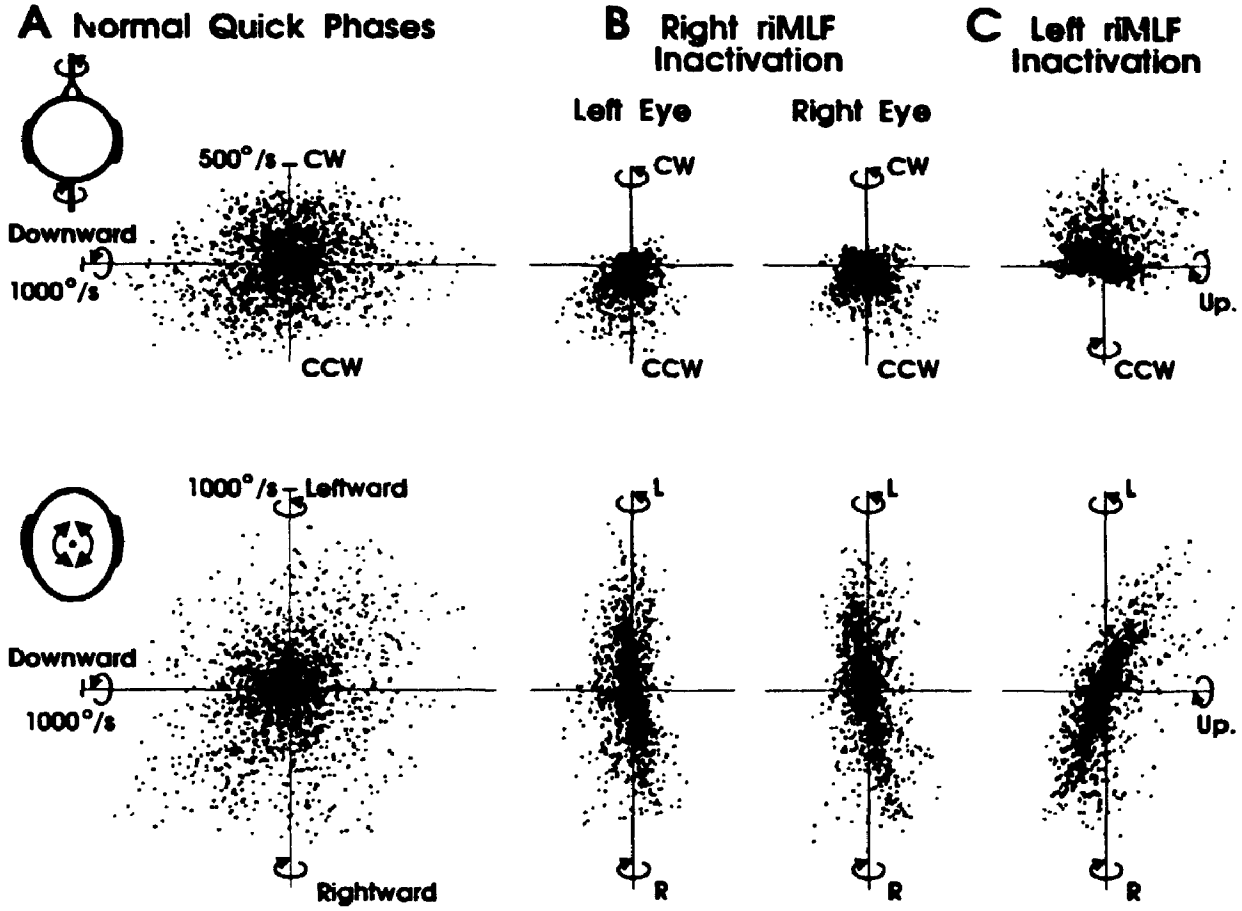

FIGURE 31. VOR quick phases axes before and after unilateral riMLF inactivation. Instantaneous velocities of rapid eye movements during 100 seconds of torsional VOR, normally (**A**), 22 min after injection of muscimol into the left riMLF (**B**), and 14 minutes after right riMLF injection (**C**). Data is plotted in Listing's coordinates from the above view (*upper row*) and behind view (*lower row*). Head caricatures indicate both the perspective of view and the axis of head rotation. Animal: ART

position out of Listing's plane immediately after unilateral riMLF inactivation (Fig. 32). These torsionally deviated positions were then held, unless the muscimol injection was placed at the border of the interstitial nucleus of Cajal (Chapters 5, 6). As a result, the overall distribution of eye positions appeared to shift torsionally from the normal Listing's plane (Fig. 33 B), CCW during right inactivation (Fig. 33 A) and CW during left inactivation (Fig. 33 C). The position range shifted rapidly at first and then settled after 15 - 20 minutes, with a final mean torsional shift of 10 to 25 degrees.

Was the linkage between horizontal and vertical saccade velocities (Fig. 29 B, C; Fig 30 B, C; Fig. 31 B, C, *behind views*) a mechanical effect of the concurrent torsional eye positions? We hypothesized that during tonic torsional deviations the horizonal recti might take on elevator and depressor properties. To test this possibility, horizontal VOR slow phases axes were recorded during unilateral riMLF inactivation in animals CAS and ART. If there was an effect due to muscle mechanics, then slow phase axes should tilt like the saccade axes. This was not the case (Figure 34). Vertical axes of horizontal slow phases w re not affected by the torsional eye positions produced by unilateral riMLF inactivation.

ALIGNMENT WITH LISTING'S PLANE. During unilateral inactivation, Listing's plane appeared to demarcate the division between the range of intact and missing torsional axes. This is most clear when viewing instantaneous eye velocities from the side, in Listing's coordinates (Figure 35). Thus, the deficits produced by injection of muscimol into one side compared to the other were symmetrical across Listing's plane and the inner edge of the remaining velocity range is aligned closely with this plane.

To quantify this alignment in all animals, an axis was fit to the inner edge of the velocity range. A computer algorithm rotated a vertical axis about the origin to the orientation that maximized the number of velocity points on the intact side. Each computation was performed in field coordinates using instantaneous velocities of

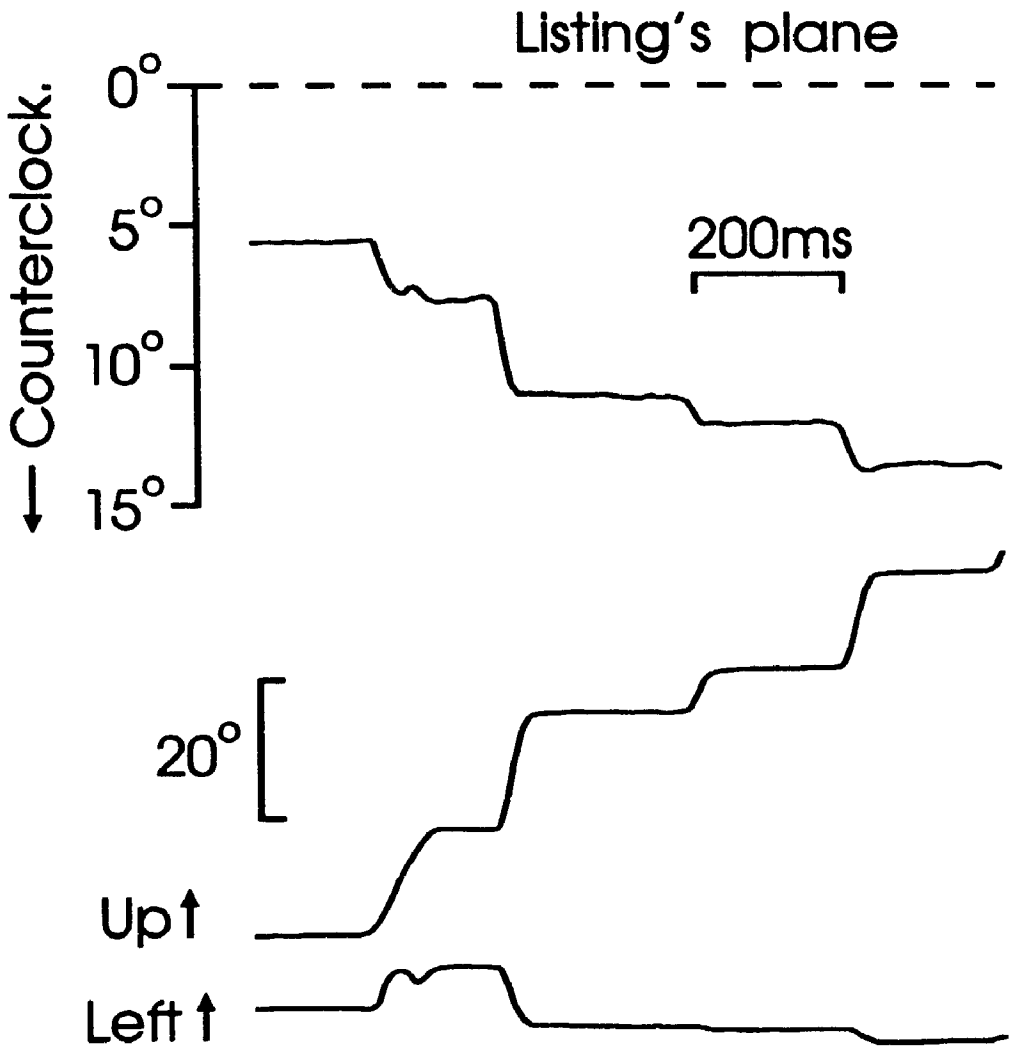

Fig. 32 Saccades drive position out of Listing's plane during unilateral riMLF inactivation. Eye position plotted as a function of time, three minutes after injection of muscimol into the right riMLF. Vertical and horizontal components of eye position quaternions have been shifted to avoid overlap and scaled down 4X tc conserve space. Data are plotted in Listing's coordinates. Animal: BAR.

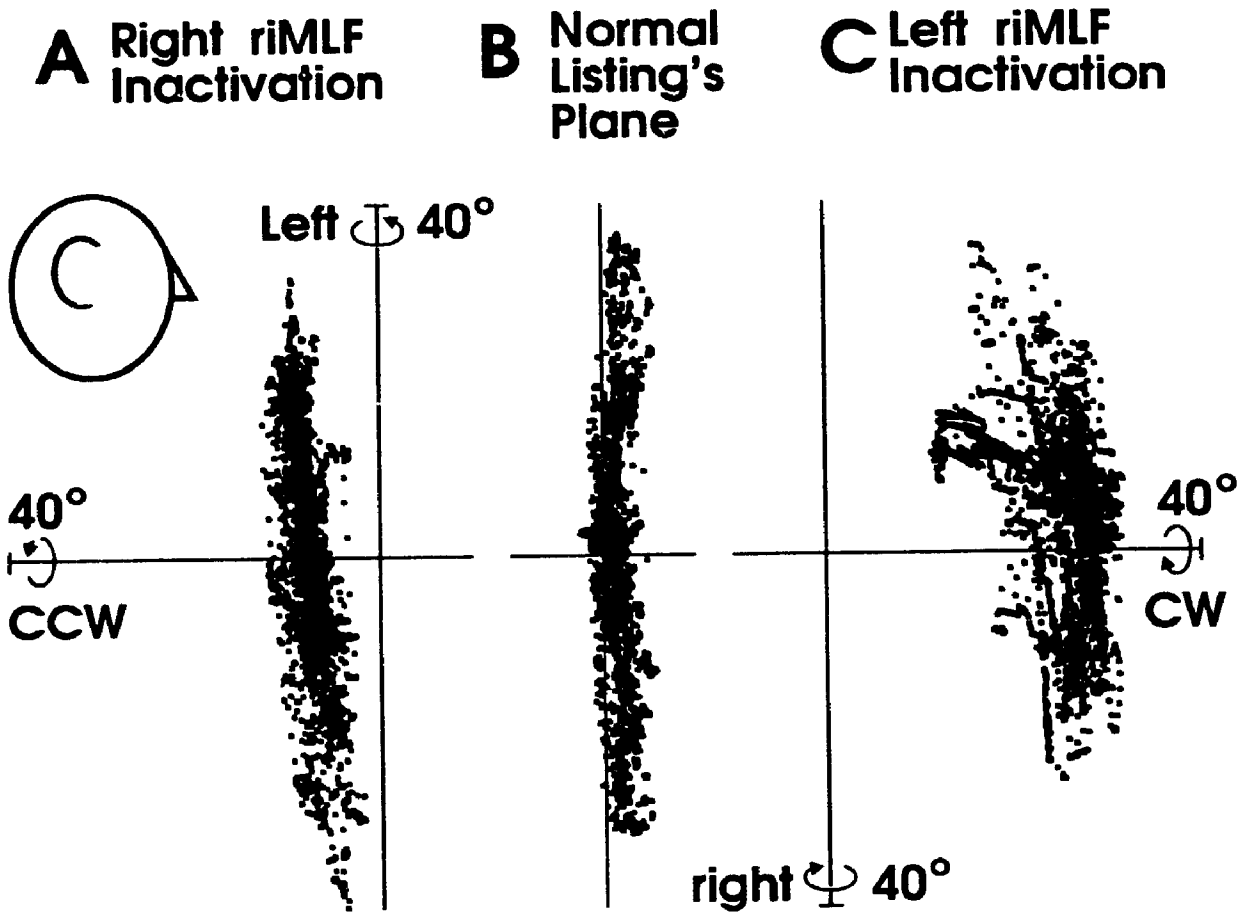

FIGURE 33. Torsional shifting of the eye position plane after unilateral riMLF inactivation. Eye position quaternions from 100 seconds of visually guided, head-fixed saccades are plotted, (A) normally, (B) after right riMLF inactivation, and (D) after left riMLF inactivation. Data are viewed from the right side perspective in Listing's coordinates, so that normal positions are confined to the vertical-horizontal plane perpendicular to the page. Data points are the tips of quaternion vectors which give the axis and magnitude of rotation from primary position, following the right hand rule. Animal: ART

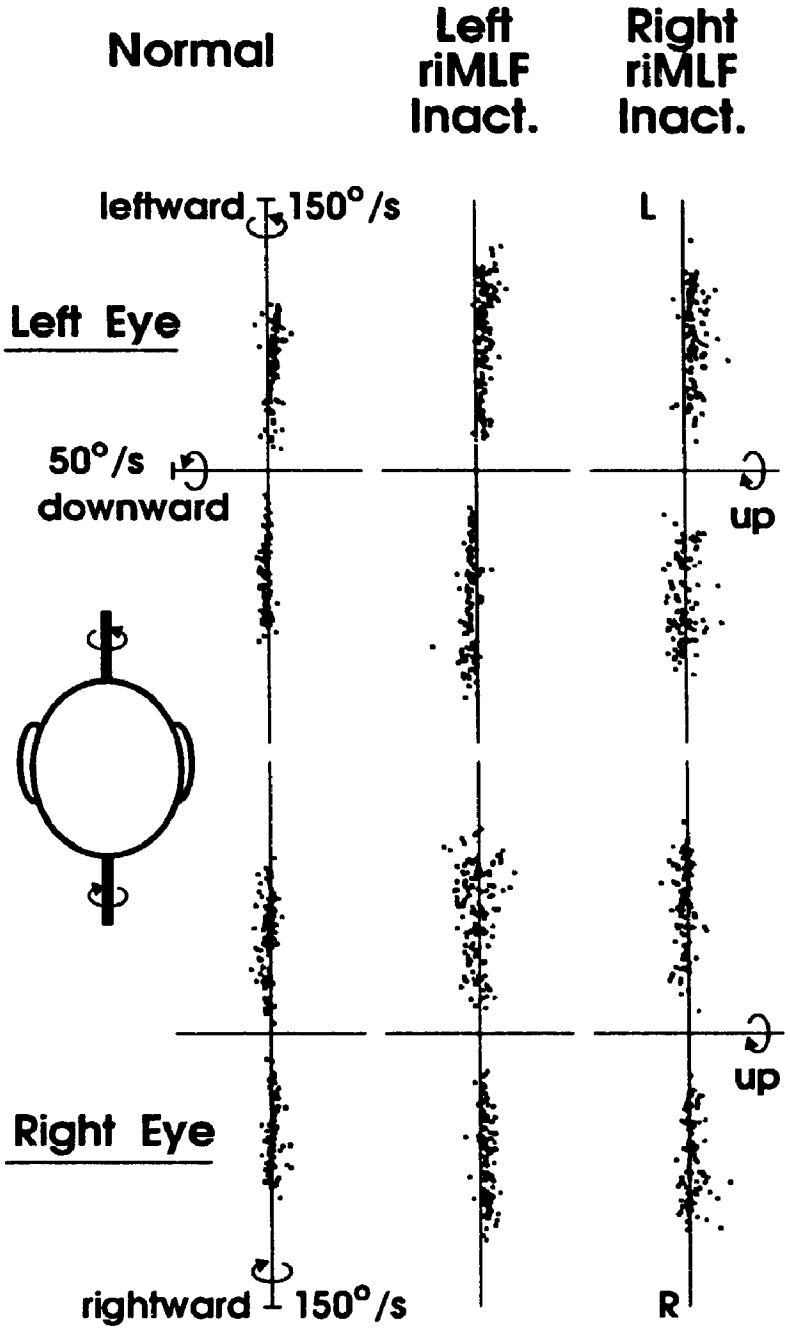

FIGURE 34. Horizontal slow phase axes are normal during unilateral riMLF inactivation. The post-injection data was measured in animal ART at the time of the torsional eye position shifts illustrated in figure 33, and the saccade axis tilts illustrated in figure 31. Normal tilts in slow phase axes of the left eye (*upper row*) and right eye (*lower row*) were symmetrical across the midsaggital plane.

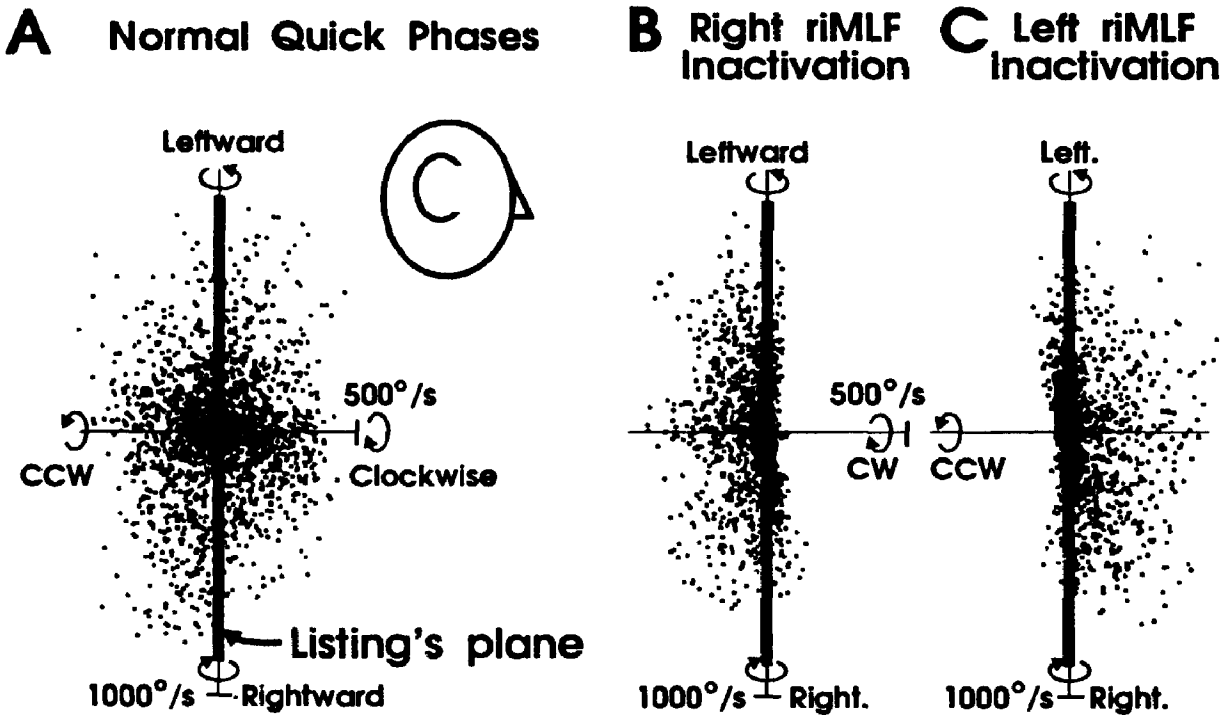

FIGURE 35. Correspondence of saccade axes with Listing's plane after riMLF inactivation. Instantaneous eye velocities are plotted during (A) normal visually guided torsional quick phases, (B) following right riMLF inactivation, and (C) following left riMLF inactivation. Data are plotted in Listing's coordinates, ie. Listing's plane (LP) is orthogonal to the page from these side views (thick line). Axes are largely confined behind Listing's plane during right riMLF inactivation (B) and in front of Listing's plane during left inactivation (C), ie. Listing's plane aligned with the inner edge of the intact wedge of velocities illustrated in figure 31. Animal: ART.

approximately 500 saccades recorded over 100 seconds. Collection of this data was initiated at 31 ± 5 minutes (mean ± SE) after injection of muscimol into the optimal riMLF sites discussed above. As done for the stimulation data, the upward tilts of these axes were then plotted against the upward tilts of Listing's plane (Fig 36 A), and the upward tilts of the stereotaxic planes (Fig 36 B) relative to field coordinates. Again, the relationship between the anatomical landmarks and the measured axis tilts was poor (r^2 = 0.18; Fig 36 B), worse than the relationship between the anatomical landmarks and Listing's plane (r^2 = 0.24; not illustrated). Again, the correlation between tilts of the inactivation-fit axes and Listing's plane was high (r^2 = 0.80), and the tilts of riMLF data and Listing's plane were approximately equal (Fig. 36 A).

Alignment of riMLF stimulation and inactivation axes with Listing's coordinates is summarized in Figure 37. Axes from the optimal riMLF sites of all animals (Figs. 26, 28, 36) are viewed from the side. First, data are plotted in the field coordinate system in which the head was initially placed (Fig 37 A). This illustrates the variable upward tilts of the data in field coordinates, 16.2 ± 6.3° for stimulation data and 17.0 ± 6.1° for the inactivation data (mean ± sample SD). Transformation into Listing's coordinates aligned the data with the coordinate axes and removed most of its variability (Fig 37 B). Stimulation axes now tilted downward by 4.0 ± 3.1° and inactivation axes tilted downward by 3.3 ± 3.2° (mean ± sample SD). The similarity of these two numbers in either coordinate system was related to the mutual orthogonality of the stimulation and inactivation data, ie. 88.7 ± 3.4° apart for the left riMLF and 89.8 ± 3.4° for the right riMLF (mean ± sample SD). Furthermore, in Listing's coordinates (Fig. 14 b) it is clear that data from the left and right riMLF were nearly collinear; axes produced by left and right stimulation were 1.7 ± 2.9° apart, and axes fit to eye velocities during left and right riMLF inactivation were 4.7 ± 0.7° apart (mean ± sample SD). Thus, the data formed an orthogonal system that was aligned aligned with Listing's coordinates.

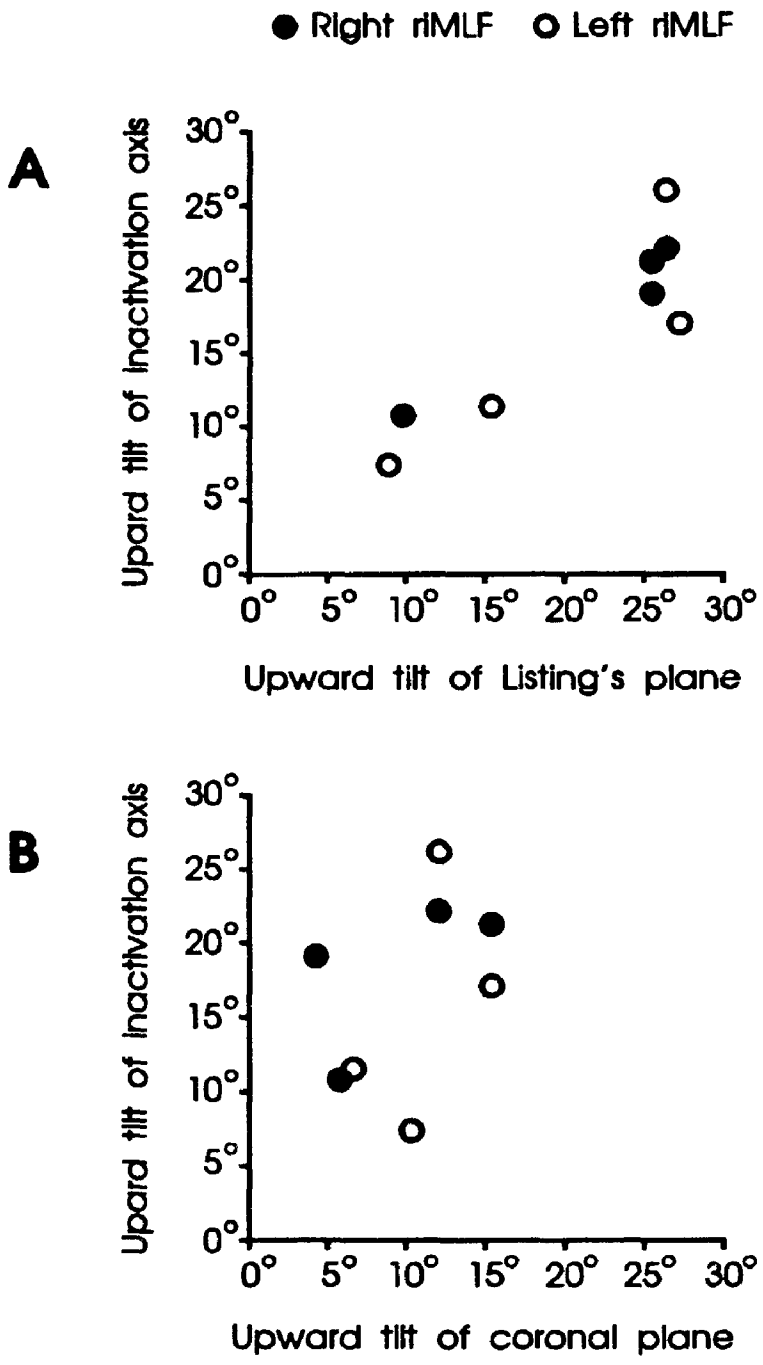

FIGURE 36. Alignment of post-inactivation axes with Listing's plane rather than anatomy. Plot of upward tilts of axes fit to inactivation data (Fig. 35) as a function of upward tilt of (A) Listing's planes and (B) stereotaxic planes of all four animals, relative to magnetic field directions.

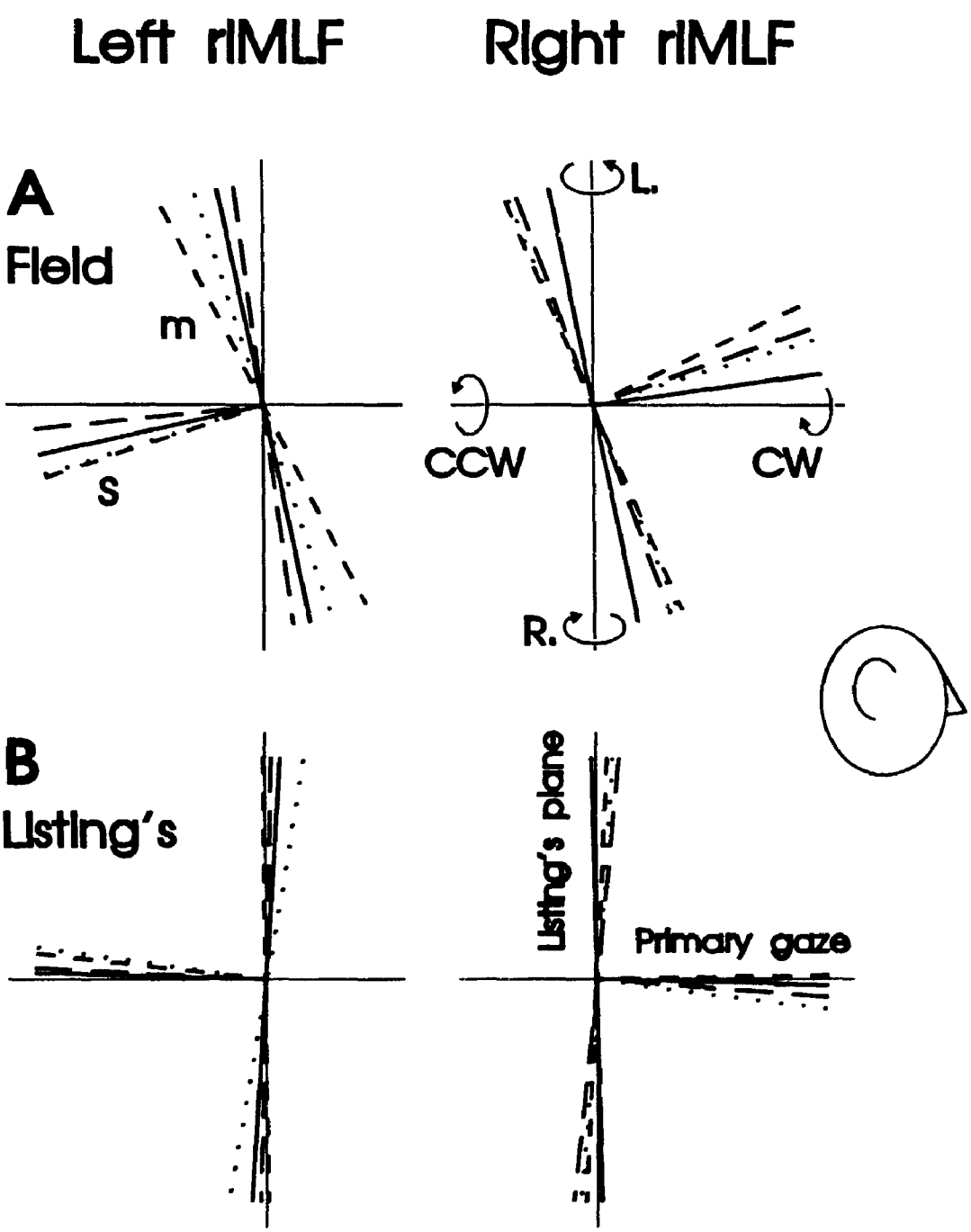

FIGURE 37. Summary of alignment between riMLF data and Listing's coordinates. Representative torsional stimulation axes (s) and vertical axes fit to unilateral inactivation data (m) of optimal left and right riMLF sites of all four animals are shown. Data were computed in field coordinates (Row **A**) and then rotated into Listing's coordinates (Row **B**). Each animal's data are assigned a consistent line style throughout.

4.4 DISCUSSION

4.4.1 *General Comments*

The oculomotor system appears to be an example of a neural network that expresses movement kinematics explicitly, and does so in a relatively clear hierarchy. Before considering burst neuron coordinates, it was necessary to corroborate several assumptions concerning the riMLF's position in this hierarchy. First, short-lead burst neuron firing rate appears to be related to eye velocity (King and Fuchs 1979; Van Gisbergen et al. 1981). If this relationship is causal, it follows that a constant stimulus input to burst neurons should produce a ramp-like change in eye position. This was indeed observed during riMLF microstimulation. Second, since burst neurons are not active during fixation, their direct projections to motoneurons cannot hold eye position. Therefore it is thought that burst neurons have an indirect path through a neural velocity-to-position transformation, which maintains motoneuron activity between saccades (Robinson 1975). This accounts for the observation that eye position held after each riMLF stimulation, as was observed for the PPRF (Cohen and Komatsuzaki 1972). Finally, injection of muscimol into the riMLF did not reveal any oculomotor deficits that could not be accounted for by burst neuron inactivation. The torsional deviations in eye positions observed during unilateral riMLF inactivation were the expected geometric consequence of a more fundamental deficit in saccade velocities, rather than positional drift. This supports the suggestion of single unit recordings that this structure is homogenous in function, at least with respect to eye movements (Büttner et al. 1977; King and Fuchs 1979)

4.4.2 *Axes of eye rotation generated by riMLF burst neuron populations.*

To specify the angular velocity of a rigid body such as the eye, at least three coordinate axes are required. Thus, in an orthogonal system there must be at least 6

classes of excitatory short-lead burst neurons, ie. three opponent pairs such as leftward - rightward, upward - downward, and CW - CCW. Although the techniques available (single unit recording, electrical microstimulation and injection of inhibitory drugs) each have their well known limitations, together they provide strong evidence for six characterizable burst neuron populations. Burst neurons in the pontine PPRF mainly produce the horizontal component of saccades, each side containing a population which produces ipsilateral rotation (Cohen et al. 1968; Cohen and Komatsuzaki 1972). The present study confirms that each side of the riMLF contains two intermingled populations which produces upward and downward rotation (King and Fuchs 1979), the difference between the two sides being the effect on torsional rotation (Vilis et al. 1989).

Previous 3-D unit recording and riMLF inactivation studies (Henn et al. 1989; Hepp et al. 1988; Vilis et al. 1989) suggested that the four riMLF burst populations rotate the eye in directions similar to those that maximally activate the ipsilateral vertical semicircular canals (Blanks et al. 1985), ie. CW-upward / CW-downward on the right side and CCW-upward / CCW-downward on the left. This organization also resembles the pulling directions of the vertical muscles controlled by the ipsilateral motoneurons, in agreement with the primarily ipsilateral motoneuron projection sites of downward-tuned riMLF burst neurons (Simpson et al. 1986; Moschovakis et al 1991b). However, recent anatomical evidence suggested that upward-tuned burst neurons project to upward-tuned motoneurons on both sides of the brain (Moschovakis et al. 1991a), which would presumably cause their torsional components to cancel and result in purely upward rotation. According to this scheme, upward and CW-downward rotations would be encoded by the two right riMLF populations whereas upward and CCW-downward would be encoded on the left. This assumes that the synaptic efficacies of burst neuron projections are all functionally equal, but this need not be the case. The presence of an anatomical connection says little about its functional efficacy. For example, vestibular

neurons from each semicircular canal have an anatomical input to the motoneurons of every extraocular muscle, but only a minority provide a strong functional drive. There is reason to suspect that the contralateral synapses of upward burst neurons are not as efficacious as the ipsilateral synapses. For example, if these efficacies were equal and the upward neurons did not produce torsion, then downward-torsional burst neurons would have to be coactivated to a very high degree to produce upward-torsional rotations, which is not compatible with the cell recording literature (Vilis et al. 1989).

Our riMLF stimulations (clockwise for right riMLF, CCW for left) were consistent with both the behaviorally and anatomically determined schemes. However, contrary to the anatomically determined scheme of Moschovakis et al., there did not appear to be populations of burst neurons encoding purely upward saccades. When animals attempted to saccade between vertically displaced targets during unilateral inactivation, they could not produce vertical eye velocities without equal amounts of torsion (and some horizontal rotation). This suggests that the contralateral excitatory connections of riMLF burst neuron axons observed by Moschovakis et al. (1991a) have low synaptic weightings. Assuming that animals solely used either the up or down - related burst population of the intact riMLF side when saccading between vertically displaced targets, the four riMLF burst populations appeared to generate the following rotations: CW-up-left and CW-down-right in the right riMLF, and CCW-up-right and CCW-down-left in the left riMLF.

This proposed organization of riMLF burst neuron populations is illustrated schematically in figure 38, along with the previously described PPRF populations (Cohen et al. 1968; Cohen and Komatsuzaki 1972; Luschei and Fuchs 1972; Van Gisbergen et al. 1981). Since the activity of some PPRF burst neurons correlates best with oblique or even near-vertical directions (Keller 1974; Luschei and Fuchs 1972; Strassman et al. 1986), the characterization of these populations as purely horizontal may well be an over-simplification. Figure 38 also indicates which of these populations

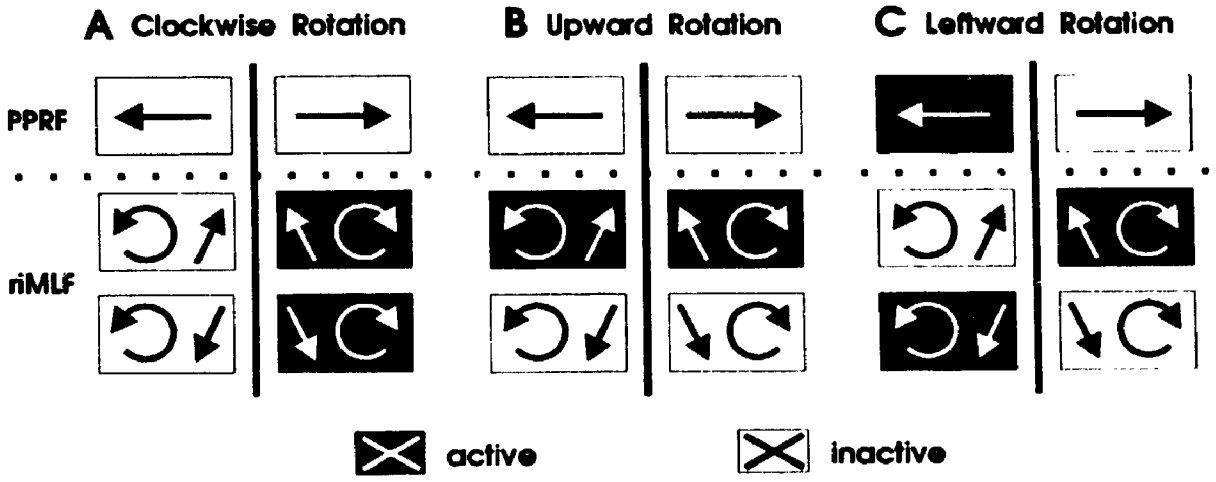

FIGURE 38. Directions of eye rotation controlled by burst neuron populations. Our experimentally determined scheme for directions of eye rotation generated by the six known excitatory short-lead burst neuron populations is shown, indicating the patterns of activation that should occur during torsional (A), vertical (B), and horizontal (C) rapid eye movements. Each rectangular box represents one burst neuron population, illustrated in symmetry across the midsagittal plane (vertical lines). Arrows indicate the direction of eye movement produced by the population. Dotted lines divide between the upper two PPRF populations and the lower four riMLF populations. Activation is defined as greater activity relative to the inactive populations. Single unit recordings suggest that riMLF neurons are activated more for torsional (A) and vertical (B) rotations than for comparably sized horizontal (C) rotations (Büttner et al. 1977; Hepp et al. 1988).

should be activated during clockwise (A), upward (B) and leftward (C) rapid eye movements. To illustrate how this scheme fits with the data, imagine that an upward saccade is attempted in the absence of the right riMLF, assuming normal ratios of input to the burst neuron populations (see APPENDIX II). The eyes should rotate in the upward-counterclockwise-rightward direction controlled by the population on the intact side, as observed experimentally. This scheme provides a unifying interpretation for the results in this investigation.

The above organization surprisingly suggests that riMLF burst neurons might contribute to normal horizontal rotations, which were previously thought to be generated exclusively by PPRF burst neurons. If so, then riMLF inactivation should reduce horizontal saccade velocity (although not to the extent of torsional and vertical velocity). Furthermore, riMLF populations would have to be bilaterally activated during normal horizontal saccades in order to cancel out their major torsional and vertical components, and these components should no longer cancel during unilateral inactivation. For example, if a leftward saccade is attempted in the absence of the right riMLF, Figure 38 C predicts that the downward component produced by the opposite intact side will no longer be cancelled. The predicted impairment of horizontal velocity and patterns of inappropriate vertical rotations were indeed observed. Initially, we thought these abnormal axis tilts might be a mechanical product of the abnormal torsional eye positions that existed concurrently. Muscle pulling directions appear to be relatively independent of two-dimensional eye positions (Miller and Robins 1987), but torsional dependence has not been examined. However, VOR slow phase axes did not exhibit the tilts observed in saccade axes. Barring the unlikely possibility that the VOR makes position compensations that the saccadic system does not, eye muscle pulling directions do not appear to be dependent on the torsional deviations produced by unilateral riMLF inactivation.

Is involvement of riMLF burst neurons in generating horizontal saccades consistent

with previous literature? Early single unit studies of riMLF burst neurons (with 2-D eye recordings) suggested oblique tilts in directional tuning that agree with our data (Büttner et al. 1977), and anatomical studies have identified projections from the riMLF to the abducens nucleus that were previously difficult to explain (Büttner-Ennever and Büttner 1988). Our observation appears to contradict the finding that PPRF lesions can completely obliterate horizontal saccades (Cohen et al. 1968; Henn et al. 1984), but interpretation of this is problematic. The PPRF possesses short and long-lead burst neurons (Raybourn and Keller 1977) and the latter are thought to project to the riMLF (Büttner-Ennever and Büttner 1978, 1988). Thus, PPRF inactivation might remove the inputs that normally activate riMLF burst neurons during horizontal saccades.

To summarize how the figure 38 scheme accounts for the remaining results, first, stimulation of the two (intermingled) riMLF populations on one side of the brain should result in torsional eye rotation, while vertical and horizontal components cancel (as in Fig. 38 A). Second, the linkage between horizontal and vertical rotation in riMLF burst populations accounts for the greater difficulty in saccading along one oblique diagonal than the other during unilateral riMLF inactivation. Finally, if one side of the schematic riMLF is eliminated, the set of all possible combinations of the remaining directions resembles the full range of velocities that we observed after unilateral riMLF inactivation. Thus, the distribution of intact eye velocities during visually guided torsional quick phases tilted obliquely, showed a reduction in vertical velocity by at least 50%, and a total absence of rotation in one torsional direction.

Why is it that burst neurons are basically organized into a separate horizontal saccade generator, and a combined vertical-torsional saccade generator in the midbrain? Since these directions are similarly combined in the eye muscles (Simpson et al. 1986), the semicircular canals (Blanks et al. 1985), and (as we shall see in Chapter 5) the oculomotor integrator, it would appear that there is something fundamental about

orienting rotations of the eye and head that makes this organization optimal. By post-hoc arguments, it can be shown that this unique near-orthogonal arrangement optimizes several important principles, including signal-to-noise ratio, bilateral symmetry, non-redundancy, and energy efficiency. Figure 39 illustrates and explains the basic arguments. In particular, this discussion shows how the bilateral symmetry of burst neuron coordinates allows their anatomical outputs to vertical eye muscles to follow a simple rule: excite the ipsilateral inferior muscles and contralateral superior muscles. Figure 39 E also shows that the measured riMLF axes deviate slightly from the ideal orthogonal system in figure 39 D, as indicated by the horizontal tilts in the vertical arrows. These additional horizontal signals appear to satisfy bilateral symmetry, but introduce non-orthogonality and redundancy.

Why would the saccadic system sacrifice orthogonality to introduce signals that are apparently redundant? Thus far, our theoretical discussions have mainly considered orthogonal burst neuron coordinate systems, which require three opponent pairs of populations encoding opposite directions of rotation about the same axis. By encoding rotations about four different axes in the experimentally measured arrangement, the riMLF gains the potential to generate eye rotations about any 3-D axis. For example, by picking various combinations of two out of the four riMLF populations, purely torsional, vertical or horizontal rotations could be made (consider figure 38, in absence of the PPRF populations). These results are an illustration of a theoretical possibility that was first pointed out to me by Doug Tweed, but has otherwise been ignored in the motor control literature, determination of 3-D rotations with a minimum of four neuron populations. Such a scheme might explain how some aquatic organisms achieve a three-dimensional VOR with only four semicircular canals (Simpson and Graf 1985). Since two-dimensional experiments suggest that the PPRF may control horizontal and vertical rotations and this structure has not been explored three-dimensionally, it is possible that

FIGURE 39. Hypothetical coordinate schemes for the burst neuron populations. Burst neuron populations are represented as in figure 17. It is assumed that orthogonal coordinates are optimal because they enhance the signal to noise ratio, ie. the angle between any two coordinate axes in such a system is large compared to the biological noise in the individual channels (Robinson 1985). A Cartesian scheme (**A**) would divide the vestibular-oculomotor systems into three structures for torsional, vertical, and horizontal rotations, with one direction of each rotation represented per side, eg. clockwise on the right and counterclockwise on the left brain. The problem with this representation is that up and down are not mirror - symmetric between the two sides of the head across the midsaggital plane (Robinson 1985). With a Cartesian system the neurons of the right brain would have to make anatomically asymmetric connections to sensory and motor structures compared to the left brain. In order to maintain symmetry, up and down have to be equally represented on each side of the brain, but the cost of simple duplication (**B**) is redundancy (Simpson and Graf 1985). Another way to achieve symmetry is to combine vertical with one of the other directions, either horizontal (**C**), or torsional (**D**). Which choice is optimal? Terrestrial animals live in a primarily horizontal environment defined by the earth's surface. Thus, they make primarily horizontal orienting movements, whereas torsional movements are minimized. The horizontal-vertical combination (**C**) requires coactivation of two oblique eye muscles during every horizontal rotation. The torsional-vertical system (**D**), which resembles eye muscles and canals, would not require coactivation during horizontal rotations, and so has the advantage of energy efficiency. The symmetry of this system allows a simple anatomical rule; excite the ipsilateral inferior (oblique and rectus) muscles and contralateral superior (oblique and rectus) muscles. Our experimentally determined scheme for the riMLF (**E**) is similar to **D**, but has additional horizontal signals that introduce redundancy and non-orthogonality.

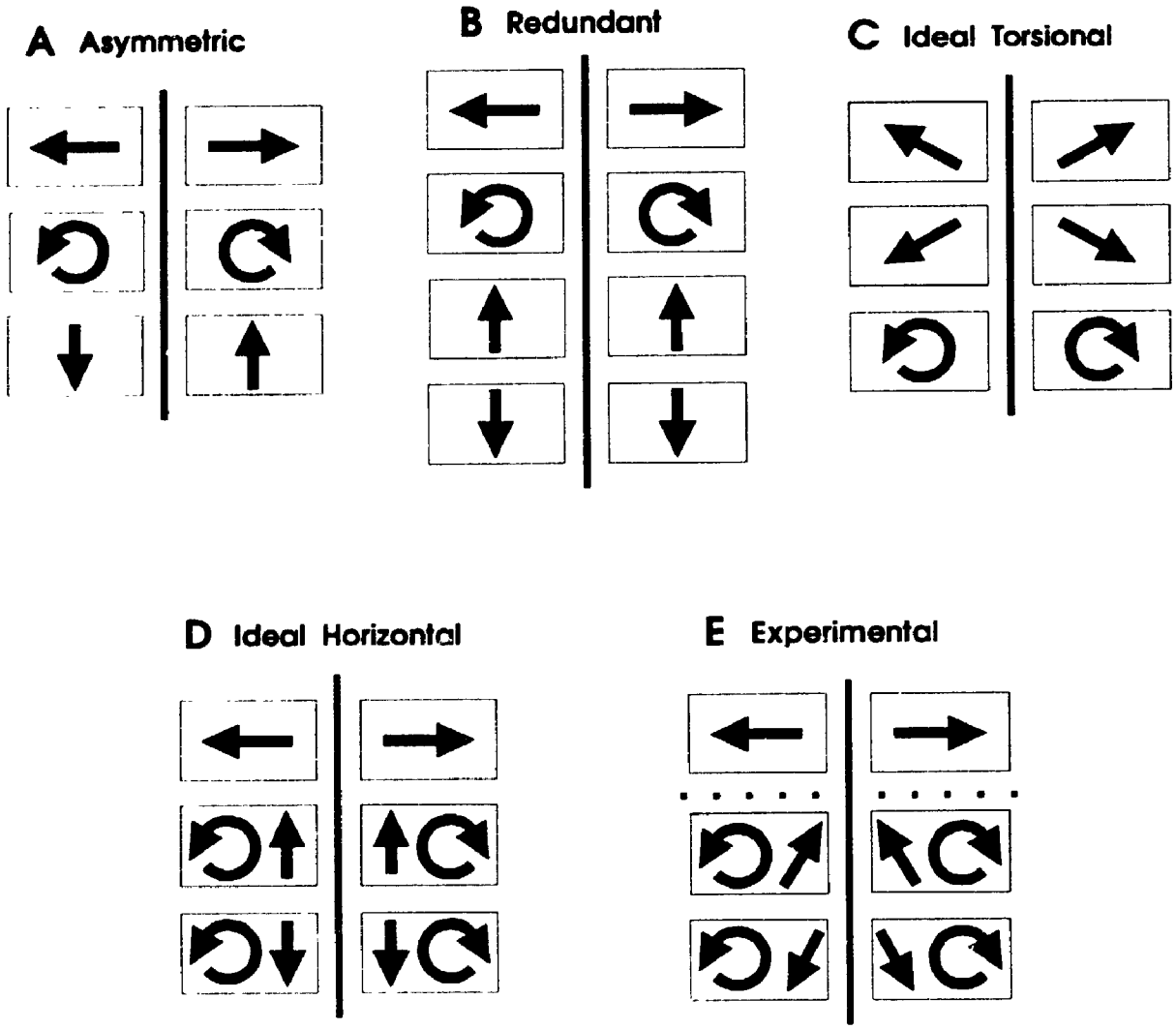
A Asymmetric
B Redundant
C Ideal Torsional
D Ideal Horizontal
E Experimental

this nucleus has a similar 3-D arrangement, but with more emphasis on horizontal. Thus, it appears that motor control systems may use simple 3-D coordinate systems embedded within more complex overall coordinate systems, although the functional utility of this is not presently clear.

4.4.3 *Alignment with Listing's plane.*

It is clear that motoneuron and sensory afferent coordinates are determined by the anatomical structures they innervate, but it is less clear what coordinate systems are used by the intervening structures. Previous theoretical and experimental investigations of motor coordinates have argued between various systems based on anatomical parameters, including muscle pulling directions (Büttner et al. 1977; Pellionisz 1986), other parameters of the physical plant (Hollerbach and Atkeson 1987, Soechting and Flanders 1991), sensory anatomy (Robinson and Zee 1981), or intermediate stages between sensory and motor structures (Peterson and Baker 1991). However, we found that the orientation of rotation axes controlled by burst neuron populations did not correlate well with externally measured anatomical landmarks. Furthermore, when the full compliment of torsional, vertical and horizontal elements of riMLF burst population coordinates are considered, they did not resemble either vertical eye muscles or vertical canals as much as previously expected (Büttner et al. 1977; Robinson and Zee 1981).

Another possibility is that motor systems sometimes utilize coordinates that align with some property of behaviour such as Listing's plane of saccadic eye positions, which varies with respect to anatomical landmarks from subject to subject (Tweed and Vilis 1990b). We found that burst neuron coordinates did correlate well with the orientation of Listing's plane. Clearly, the individual riMLF burst populations did not produce rotations about axes parallel or orthogonal to Listing's plane. However, both stimulation and inactivation experiments suggested that these axes are symmetrical across Listing's

plane, and about the primary gaze direction orthogonal to Listing's plane. During unilateral riMLF stimulation the vertical and horizontal components of two populations appeared to cancel, leaving a torsional axis of rotation orthogonal to Listing's plane, ie. parallel to the primary gaze direction. Normally, rapid eye movement axes are not confined to Listing's plane (Tweed and Vilis 1990b). After riMLF inactivation horizontal saccade axes, presumably produced primarily by the PPRF, appeared to align with Listing's plane. These stimulation and inactivation axes were mutually orthogonal, aligned well between the two sides of the brain, and collapsed along the coordinate axes when transformed into Listing's coordinates. Thus, the behaviour of burst neuron populations appeared to be more amenable for interpretation than activity of single units studied previously.

Figure 40 summarizes the axes of eye rotation controlled by the six known burst neuron populations, plotted symmetrically about Listing's coordinates. The PPRF appears to mainly rotate the eye about the vertical axis in Listing's plane (*solid lines*). The mainly torsional and vertical role of the left riMLF (*dashed lines*) and right riMLF (*dotted lines*) populations is best seen from the above view (Fig. 40 A), while the other views also show the smaller horizontal component. Although the illustrated riMLF axes do not align with Listing's plane (L.P.) or the primary gaze direction (P), they are symmetrical about these coordinates.

Had this data aligned with either canal or muscle coordinates, one would expect that the stimulation axes would lay in the plane of the horizontal canals / muscles with the inactivation axes extending orthogonally. When our data (Fig. 37) was replotted into coordinate systems based on anatomical data measured previously in rhesus monkeys, the stimulation / inactivation data tilted by 15.7 $\pm$ 6.3° / 14.9 $\pm$ 5.7° downward from canal coordinates (Blanks et al. 1985) and 8.6 $\pm$ 6.3° / 7.8 $\pm$ 5.7° downward from muscle coordinates (Simpson et al. 1986), compared to 4.0 $\pm$ 3.1° / 3.3 $\pm$ 3.2° from Listing's

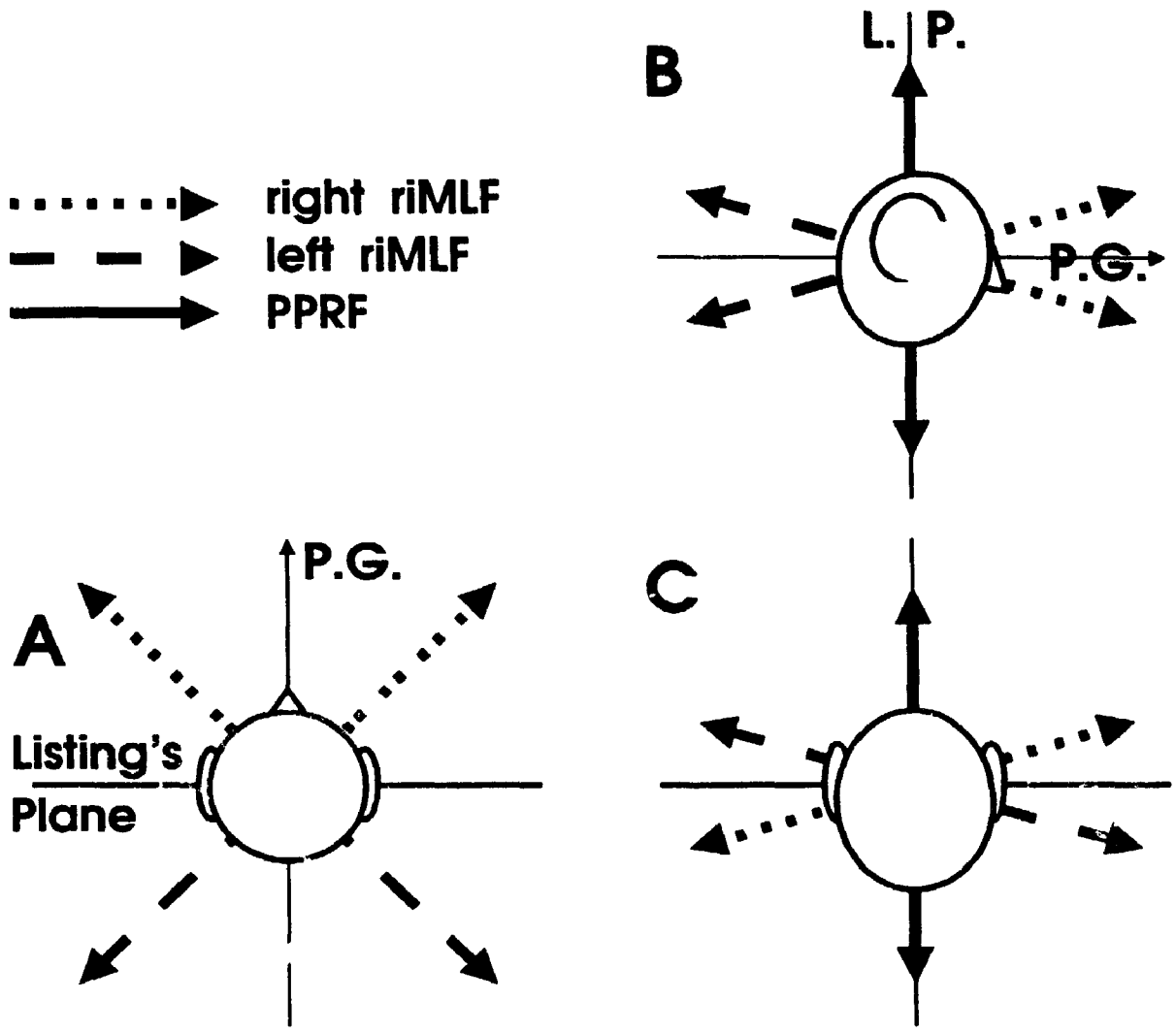

FIGURE 40. Relationship between short-lead burst neuron coordinates and Listing's plane. Axes controlled by burst populations are plotted in Listing's coordinates and viewed from (A) above Listing's plane with the primary gaze direction (P.G.) pointing up on the page, (B) the side of Listing's plane (L.P.) with P.G. pointing rightward, and (C) behind Listing's plane. Note that these axes define a coordinate system that is symmetrical about Listing's coordinates, but do not all align with Listing's plane or the primary gaze direction. The PPRF is treated as having only two distinguishable populations, although this may be an oversimplification. Directions of rotation are defined by the right hand rule.

coordinates (mean ± sample SD). Thus, of these two anatomical schemes, muscle coordinates on average aligned better with the riMLF data and Listing's plane. Since we did not directly measure muscle pulling directions, we cannot eliminate the possibility that they also varied with respect to stereotaxic coordinates as much as Listing's plane. However, the Listing's coordinates we measured varied with respect to stereotaxic coordinates with a standard deviation of ± 6.9°. This appears to be much larger than the variations of muscle coordinates reported between three cats (Ezure and Graf 1984), but a study of variations between a larger population of primates would be welcome. To ideally resolve these issues, the present study should be repeated with additional measurements of canal and muscle planes relative to stereotaxic coordinates.

In retrospect, a relationship between burst neuron coordinates and Listing's plane makes sense. Such a relationship might be expected if the functional anatomical connections underlying specific neural coordinate systems arise as a result of some activity-dependent developmental process. Burst neurons are primarily devoted to saccade production, and saccades are constrained by Listing's law. To have such a behavioral constraint, there must be a constraint on neural activity (Chapter 3). Given any one coordinate system, it is Listing's law that determines the axis of rotation for a given saccadic gaze shift, and thus the extent to which each burst population is activated (Consider the visual system precedent that neural activity determines the details of functional connectivity; Shatz 1992). Conversely, given Listing's law, the coordinate system used will determine the extent to which each population is activated. For example, burst coordinate symmetry about Listing's plane is required to allow symmetrical pulse activity between the two sides of the riMLF during saccades to and from primary position. Therefore one might expect an alignment between coordinates and the directions of movements that are preferentially optimized, e.g. the head-fixed vertical and horizontal axes in Listing's plane. Unfortunately, direct alignment of burst

coordinates is not possible or desirable given the other constraints mentioned above (Figure 16), and so symmetry about Listing's plane is the next best choice.

IMPLICATIONS FOR OTHER MOTOR CONTROL SYSTEMS If the saccadic system is a model for movement systems in general, we should be able to generalize from the above observations. In particular, one predicts a relationship between solutions to the degrees of freedom problem, and coordinates used for coding of kinematics prior to the inverse dynamic stage. In controlling 3-D orientation of any one body segment, neural coordinate axes should align with, or be symmetrical about the coordinate axes that are optimized by a particular solution to kinematic redundancy. Thus, direct measurements of movement constraints might indirectly elucidate the associated coordinate system. The smooth pursuit system, which has the same kinematic redundancy as the saccadic system, is constrained even more closely by Listing's law (Tweed et al. 1992) and so might be expected to utilized a Listing - based coordinate system. In contrast, optimal vestibuloocular and optokinetic responses are essentially dictated by a 3-D sensory input (assuming their function is to stabilize retinal slip), and do not require additional constraints (Chapter 3). As might be expected, their interneurons appear to utilize coordinates similar to those of the semicircular canals, eye muscles, or some combination of these (Baker et al. 1984; Peterson and Baker 1991; Simpson et al. 1989). Surprisingly, chapter 3 of this thesis suggests that VOR coordinates may not be completely independent of Listing's law, because the axis of minimal VOR gain appeared to align with the primary gaze direction in the monkey.

What then of skeletomotor systems whose circuits generate multiple, complex behaviours? Recent 3-D measurements during gaze movements showed that the head moves like a Fick gimbal (Glenn & Vilis 1992). Furthermore, measurements of arm orientations during pointing also revealed a Fick-like constraint (Hore, Watts & Vilis 1992), and these Fick-like properties also emerged during throwing movements (Hore,

Watts & Tweed 1992). In a Fick gimbal, horizontal rotations occur about a fixed vertical axis, but vertical rotations occur about an axis that rotates with the head or arm. In other words, orientations are constrained to a 2-D sub-space in which the two coordinates are azimuth and elevation. In these systems, to follow the oculomotor example, azimuth and elevation should also form the basis for the neural coordinate system.

Remarkably, this is the same scheme that Soechting and Flanders (1992) have proposed for arm movement on the basis of their psychophysical observations, but is based on more direct manipulations of the brain and measures of kinematic variables. Separation of neural movement commands into azimuth and elevation coordinates has not been directly tested for arm movements, but neural commands for head movement are apparently partitioned into horizontal and vertical channels (Masino & Knudsen 1990), which might correspond to azimuth and elevation. Because these recently identified intermediate sensorimotor coordinate systems did not correspond to any known sensory or motor anatomy, they have been described as abstract (Masino & Knudsen 1990). The present argument suggests that such abstract coordinates reflect the behavioral coordinate axes that emerge from the rules that constrain body segment orientations.

Burst neurons occupy a very interesting stage in the broader scheme of movement production: the transformation from a 2-D retinotopic vector map, the superior colliculus (Sparks and Mays 1990; Van Opstal et al. 1991) into a 3-D coordinate system in motoneuron space. This chapter suggests that issues such as transformation from extra-personal space to intra-personal space, transformation from vector coding to coordinate systems, the degrees of freedom problem, and choices of kinematic coordinate systems are probably functionally inter-related, and should not be considered in isolation. Understanding these complex problems seems daunting in complex skeletomotor systems involved in a multitude of kinematic tasks. The oculomotor system, with only two basic 3-D strategies (Listing's law and visual stabilization) provides us with a valuable model.

5 LOCATION OF THE VERTICAL AND TORSIONAL OCULOMOTOR INTEGRATORS

5.1 INTRODUCTION

The eye movement commands discussed in the preceding chapter encode eye velocity signals (Büttner et al. 1977; King and Fuchs 1979; Luschei and Fuchs 1972). These alone would move the eye to the desired position, but afterwards would not prevent the muscles from relaxing and thus allowing the eye to drift back towards some resting position. Since this does not occur, it appears that such velocity-related pulse commands are converted into position-related step commands by a neural integrator (Robinson 1968, 1975, 1989). Chapter 3 demonstrated that in three dimensions, angular velocity is different from rate-of-position-change, and the former must be converted into the latter before integration will yield a correct position signal (Tweed and Vilis 1987, 1990a), but the integrator remains as the heart of this transformation.

As explained in section 1.2.4, the integrator for horizontal eye rotations appears to be located in the nucleus prepositus hypoglossi region of the medulla (Cannon and Robinson 1987; Cheron and Godaux 1987). Chemical inactivation of this site produced a profound deficit in ability to hold horizontal eye positions, without affecting rapid eye movements. However, much of the vertical position signal remained intact, and more recent lesion studies in that area have reported almost complete sparing of vertical position holding (Yokota et al. 1992). Furthermore, torsional eye rotations were not examined in these studies.

Previous chapters of the this thesis have demonstrated the necessity for integration in three dimensions. Integration in the torsional direction is necessary to explain the tonically deviated torsional positions observed during unilateral stimulation / inactivation of the riMLF. For a more physiological example, correct torsional integration is

necessary for normal function of torsional VOR slow and quick phases. Furthermore, chapter 3 demonstrated that maintenance of torsional eye position changes is even necessary during horizontal / vertical rotations of the head about axes within Listing's plane. Finally, given the way in which the oculomotor system combines control of vertical and torsional movement in the eye muscles, semicircular canals, and burst neurons, it is unlikely that vertical integration is achieved in isolation from torsional integration.

Where then are the vertical and torsional integrators? The best candidate at the inception of this study was the mesencephalic interstitial nucleus of Cajal (INC). King et al. (1981) suggested that the INC might be the vertical integrator after identifying the requisite vertical eye position - related activity in the monkey. Since then, others have identified similar activity in the cat INC (Fukushima et al. 1990a, Le Taillanter 1991a), in addition to saccade and VOR - related activity that may not be related to integrator function (Fukushima et al. 1990a, 1991; Fukushima and Fukushima 1992). A role in vertical integration was also suggested by phase advances and gain decreases observed in the sinusoidal vertical VOR and OKN of cats with chemically lesioned INC regions, as though only the direct path velocity signal remained (Anderson et al. 1979; King 1982; Le Taillanter 1991b). Finally, neurotoxin / electrolytic lesions of the INC region produced a failure to hold the vertical components of post-saccadic eye positions (Fukushima 1987; King 1982; King and Leigh 1982), although the time constants of drift did not indicate total integrator failure, and fibres of passage may have been affected.

Although the experiments above did not examine torsional eye position, others have implicated the INC in torsional eye movement. Torsional eye deviations have been evoked by stimulation in what may have been the INC of the monkey (Westheimer and Blair 1975), and after lesions in the cat INC (Anderson 1981). Furthermore, the INC receives input from structures involved in both vertical and torsional eye rotations

(midbrain burst neurons and vertical semicircular canals) and projects to motoneurons that rotate the eye both vertically and torsionally (Büttner-Ennever and Büttner 1988; Moschovakis et al. 1991a, 1991b). We therefore hypothesized that the interstitial nucleus of Cajal is involved in generating both the vertical and torsional eye position signals.

5.2 METHODS

The INC region was identified in five monkeys, MAR, BAR, LAR, ART, and CAS. Binocular recordings were made in the latter two animals. As described in chapter 2, three dimensional eye positions were recorded during single unit recordings, microstimulations, and microinjections of muscimol. In order to show that INC is part of the neural integrator, two results were required: (1) stimulation of this nucleus should evoke constant-velocity eye rotations that hold their final eye position, and (2) inactivation of this nucleus should cause a failure to maintain post-saccadic eye positions, resulting in centripetal drift at an exponential rate. Thus, in this chapter, we examine severe inactivation results in which muscimol was injected directly into the INC and allowed time to spread through one side of the INC circuits.

5.3 RESULTS

5.3.1 *Microstimulation of the INC*

Single unit recordings confirmed the previous finding that INC neuron firing frequencies were correlated to vertical eye position (Fukushima 1987; King et al. 1981). Neurons that increased their activity either during upward or downward eye positions were intermingled within the INC, and most of these also showed a burst of activity during saccades in these directions. Activity in the left INC was indistinguishable from that of the right INC. However, we were unable to correlate changes in neural activity to changes in ocular torsion since Listing's law kept that value at a constant zero value.

Based on the vertical intermingling of cells, and results of stimulating riMLF neurons in chapter 4, one might expect vertical components to cancel during unilateral INC stimulation, revealing the net torsional command. Such stimulations (20μA, 0.5ms cathodal pulses, 200 Hz, for 300 to 600 ms) were delivered at 41, 22, 4, 17, and 28 sites respectively in animals CAS, BAR, MAR, LAR, and ART, with a normal range of 10-20 stimulations per site. INC stimulation produced a stereotypical pattern of eye movements in all animals (Fig. 41). Speed of rotation was constant during stimulation, and then final eye position was maintained, indicating that the stimulus input had been integrated. Both eyes rotated with the same direction and magnitude. In contrast, stimulation of the adjacent motoneurons produced exponential monocular rotation that did not hold.

The direction of eye rotation was always clockwise during right INC stimulation and counterclockwise during left stimulation. Torsional velocities were as great as 50° per second during stimulation 1 mm lateral of brain midline, but dissipated at 2 mm lateral. Vertical rotation was occasionally almost as large as the torsional rotation (Fig. 41 B), but was usually much smaller (Fig 41 A), with a variable direction. Thus, intermingled "up" and "down" neurons appeared to cancel each other's effects. Very little horizontal rotation was observed.

5.3.2 *Muscimol inactivation of the INC*

One interpretation of these results is that (i) the INC integrates its inputs for motoneurons of both eyes, and (ii) like the adjacent midbrain oculomotor structures, the INC is organized into clockwise-up and clockwise-down neurons on the right side, and counterclockwise-up and counterclockwise-down neurons on the left side (which may operate in bilateral interdependent pairs, as argued in section 6.4.3). This interpretation required confirmation because (1) stimulation may have affected fibres of passage and (2) stimulation may have activated other structures such as the riMLF orthodromically.

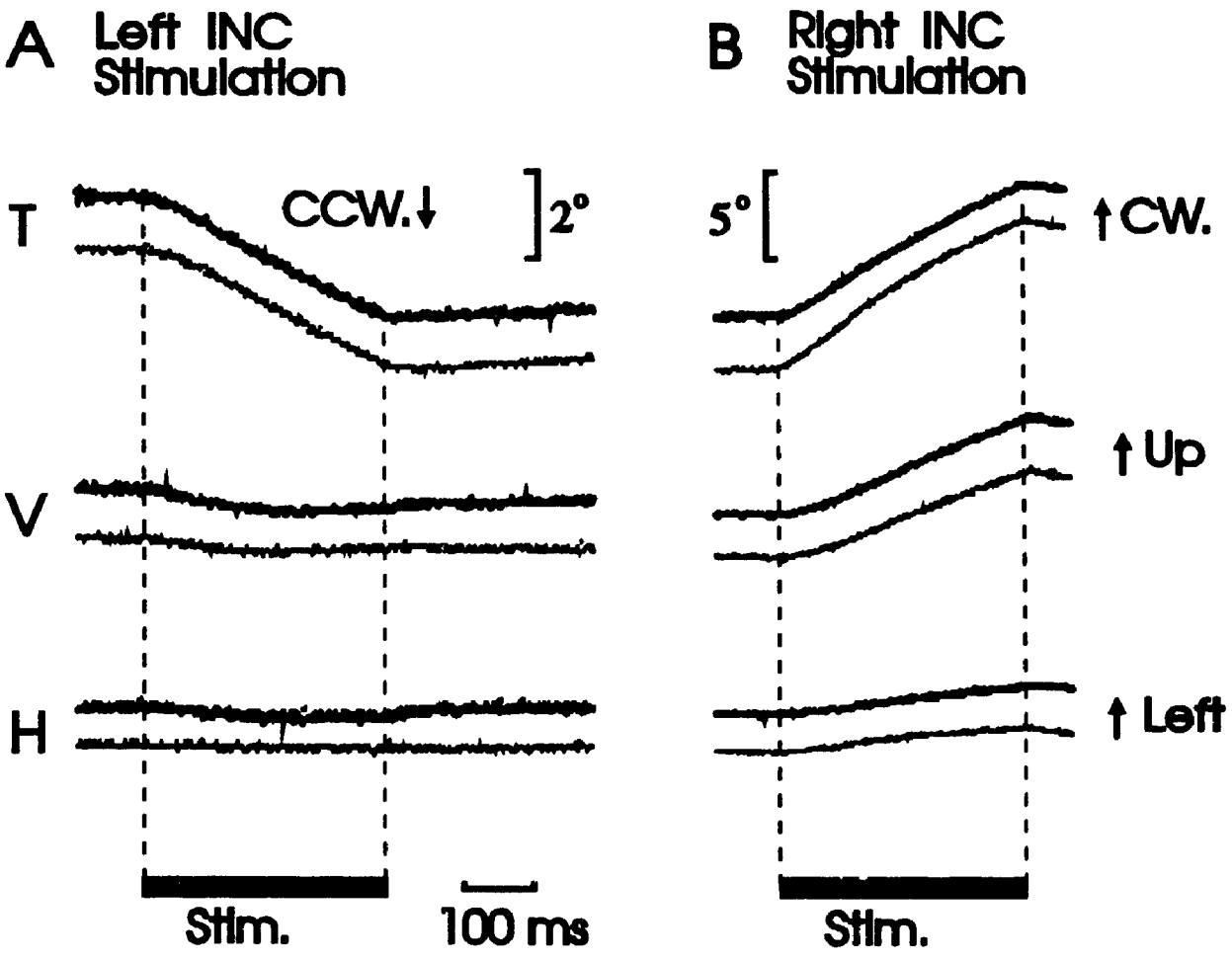

FIGURE 41. Eye position during unilateral microstimulation of the (A) left and (B) right interstitial nucleus of Cajal. Position of left eye (*thicker lines*) and right eye (*thiner lines*) are plotted as a function of time. The standard stimulus was delivered during the time indicated by the bar. The ramp-like change in position indicates relatively constant velocity. Eye position traces are truncated at the first saccade. T, V, H: torsional, vertical and horizontal position. CW, CCW: clockwise and counterclockwise.

This confirmation was realized by using pharmacological inactivation of cell bodies within the INC region. Muscimol was injected unilaterally into the mesencephalic region identified as the interstitial nucleus of Cajal (INC) 14, 8, 3, 3, and 10 times in animals BAR, CAS, MAR, LAR, and ART respectively. This was in addition to 1, 1, and 2 bilateral injections in animals BAR, CAS and ART respectively, and several injections of GABA in each of the latter two animals. Unilateral injection of muscimol into the INC resulted in an immediate failure to hold eye positions, without profoundly affecting saccades. This deficit was characterized by a failure to hold vertical positions of both eyes, and a conjugate torsional nystagmus (Fig. 42 B). The deficit reached a peak within half an hour, and recovered after several hours.

Figure 43 plots the horizontal component of eye position against vertical component during unilateral INC inactivation. Note that vertical eye position is plo..ed along the horizontal axis, and horizontal eye position is plotted along the vertical axis. This is a reminder that these data are actually eye position quaternions, which give the axes of rotation relative to the reference position using the right hand rule. After vertical saccades, eye position drifted exponentially towards a central vertical null value (Fig. 43), so that drift was either upward or downward, depending on initial position. This is in contrast to the constant-velocity drift expected from vestibular lesions. Horizontal positions did not exhibit centripetal drift.

The eye also exhibited an immediate torsional drift (Fig. 44), away from the plane of zero torsion positions normally maintained by saccades (Tweed and Vilis 1990). At this time, rapid eye movements returned the eye to Listing's plane, resulting in the torsional nystagmus pattern shown in Fig. 42. These results were observed in both eyes. Thus, the animals could only hold a line of horizontal positions at the intersection of the torsional and vertical null values. The vertical position of this line was usually above the center of the eye's range of motion, such that upward drift was most prevalent. The null

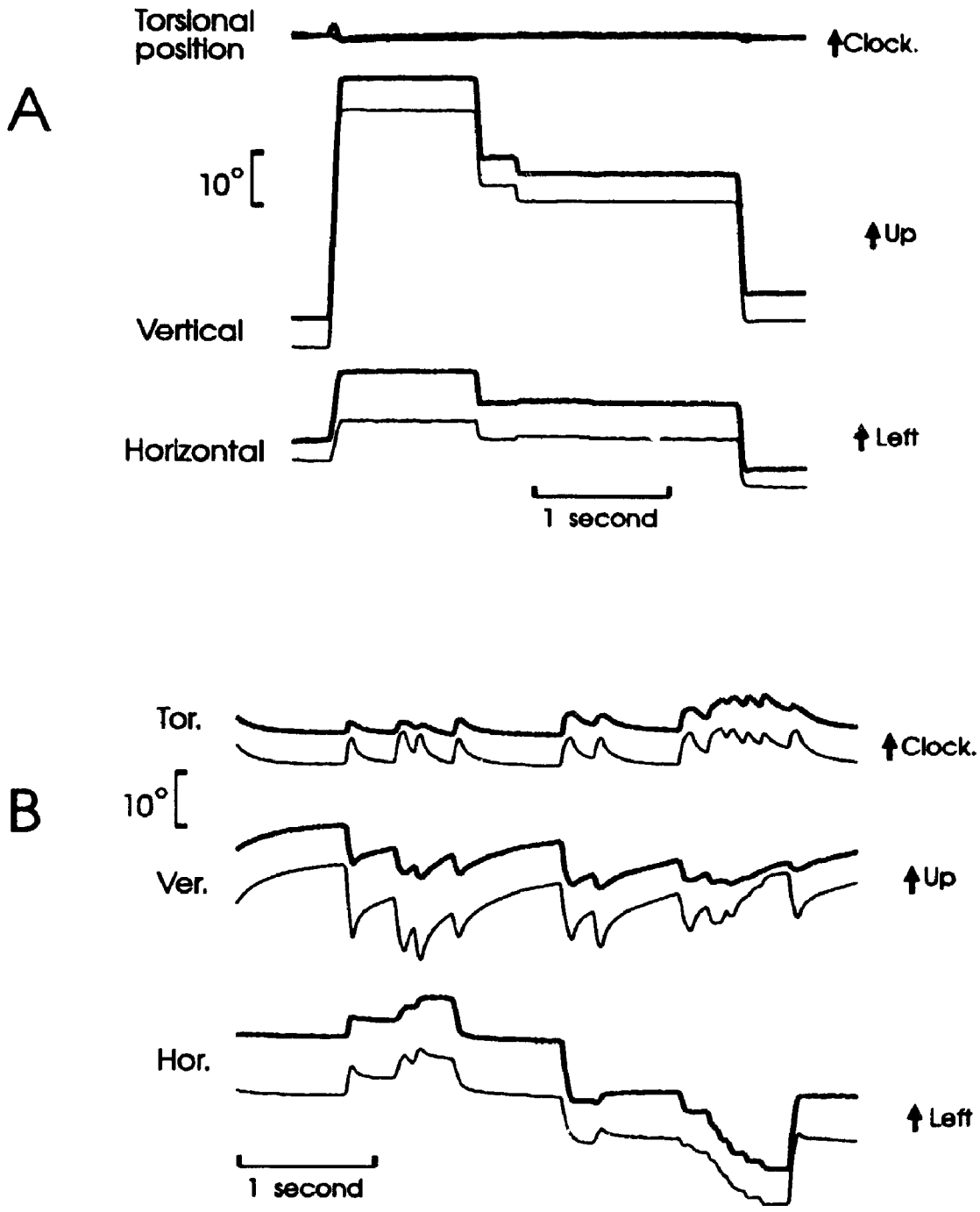

FIGURE 42. Deficit in holding position of both eyes during interstitial nucleus of Cajal (INC) inactivation. Positions of the left eye (*thick lines*) and right eye (*thin lines*) during random saccades with the head still are plotted against time. **A**: Normal saccades. **B**: Position after INC inactivation with muscimol. This illustrates the basic observation of drift between saccades, primarily in the vertical and torsional directions.

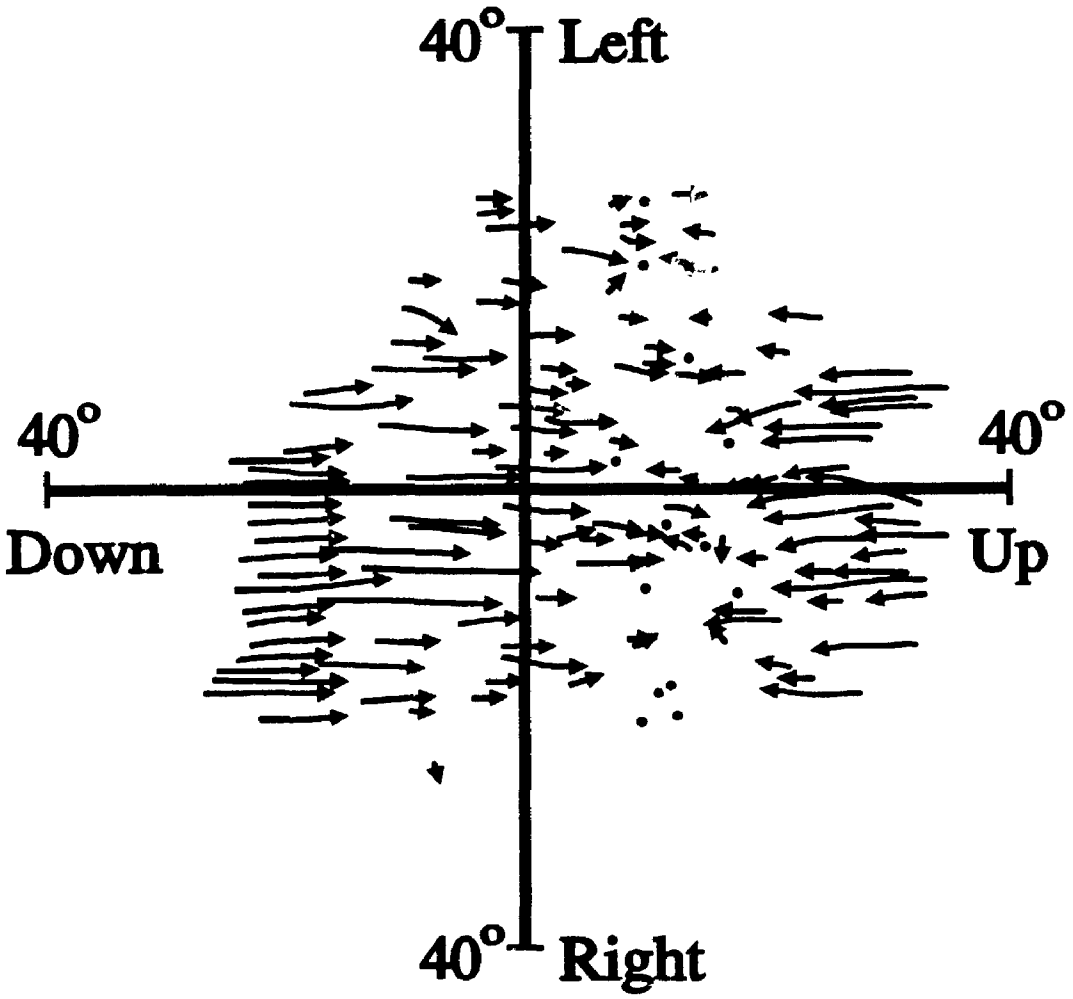

FIGURE 43. Direction of vertical eye position drift during unilateral INC inactivation. Only positions between voluntary eye movements are shown, with arrows indicating direction of drift. Horizontal and vertical components of eye position are shown 38 min after muscimol injection. Torsional drift is not visible in this view.

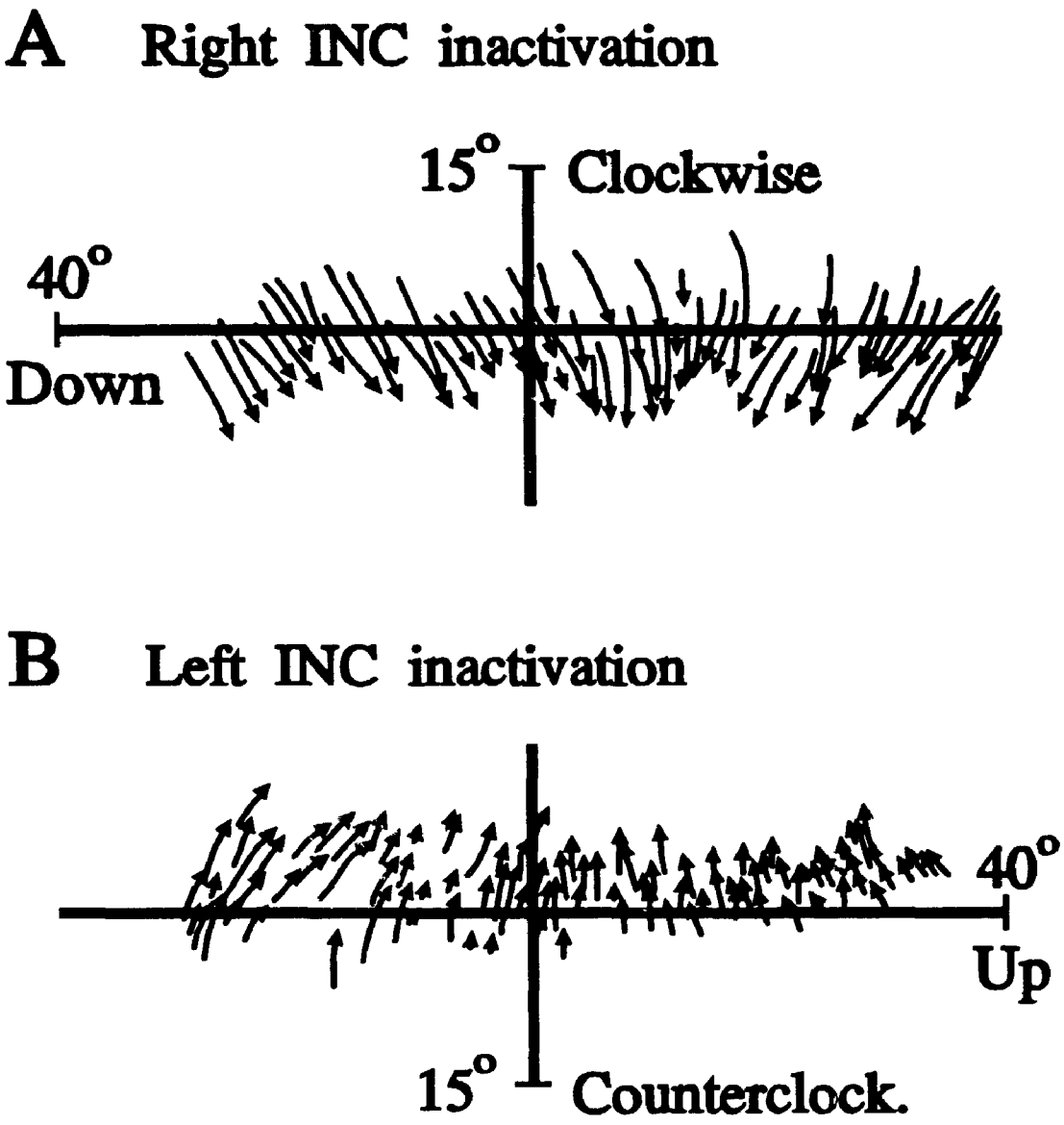

FIGURE 44. Direction of torsional drift immediately after unilateral muscimol injection. Torsional drift was counterclockwise after right INC inactivation, and clockwise after left INC inactivation (saccades returned the eye towards Listing's plane). This direction pattern was later obscured by spread of muscimol to the riMLF, which causes saccades to drive position away from Listing's plane (Chapters 4 and 6).

line was almost always shifted clockwise during left INC inactivation (Fig. 44 B), and counterclockwise during right INC inactivation (Fig. 44 A), as treated in more detail in Chapter 6. Thus, the torsional drift produced by unilateral INC inactivation was in the direction opposite to the rotation produced by comparable unilateral stimulation.

To quantify the severity of this position deficit, we computed the time constants of drift. Figure 45 A illustrates the exponential nature of the drift. After a saccade, vertical and torsional positions drifted towards their final resting point at a rate proportional to their distance from this line. The time constant is defined as the time required to drift two thirds of this distance. Complete failure of the integrator should result in drift with the intrinsic time constant of the eye, approximately 200 ms (Robinson 1970, 1975). Time constants of torsional drift tended to be slightly lower than those of vertical drift, but both suggested total integrator failure in four out of five animals (Fig. 45 B).

5.4 DISCUSSION

The results of this study suggest that the INC is an essential component of the oculomotor integrator. Previous work suggests that integration is distributed between several regions, including the vestibular nuclei (Fukushima 1987; King, cited in Robinson 1987; Tweed and Vilis 1987). As a simplification, we can divide the brainstem oculomotor circuitry into two groups, each consisting of a saccade burst generator, an integrator and motoneurons. The pontine / medullar group consists of neurons which drive the eye horizontally towards the side of the brain activated (Cannon and Robinson 1987; Cheron and Godaux 1987; Cohen et al. 1968; Cohen and Komatsuzaki 1972; Henn et al. 1984; Keller 1974; Luschei and Fuchs 1972; Robinson 1970; Robinson and Keller 1972; Skavenski and Robinson 1973; Strassman et al. 1986a, 1986b). The midbrain group is organized so that each neuron influences both vertical and torsional eye position (Anderson 1981; Büttner et al. 1977; Fukushima et al. 1990a, 1991; Fukushima and

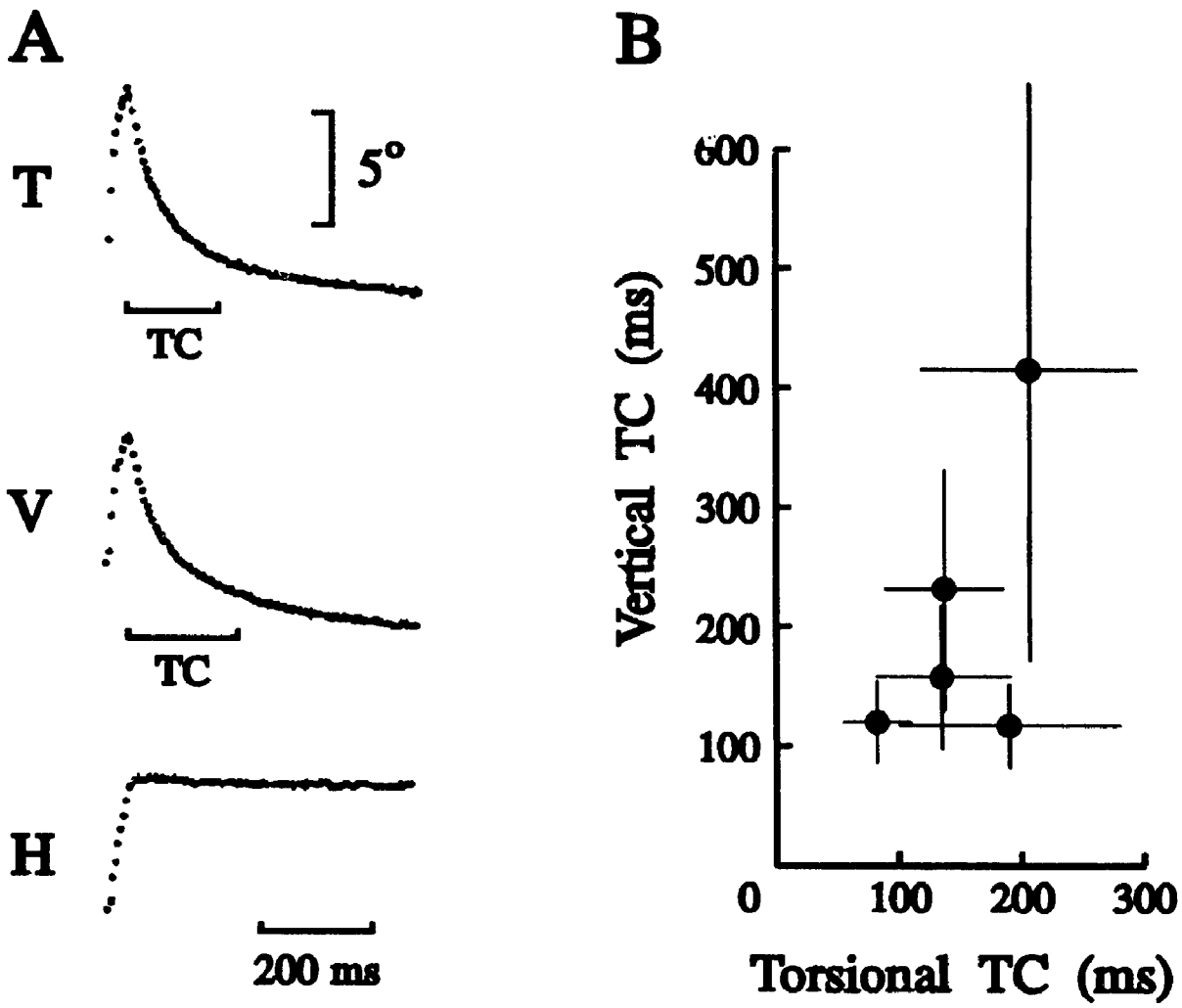

FIGURE 45. Time constants (TC) of exponential drift during unilateral INC inactivation. **(A)** Eye position is plotted as a function of time to illustrate an example of the exponential drift that followed saccades. TC's are illustrated for reference. T, torsional eye position; V, vertical; H, horizontal. **(B)** Vertical and torsional time constants of drift from all five animals. *Solid circles*: mean TC for each animal, obtained from an experiment in which a severe eye position deficit was present ~ 30 min after muscimol injection. TCs of vertical and torsional drift were then computed for a series of individual examples and averaged. *Error bars* give standard deviations of these TCs.

Fukushima 1992; Henn et al. 1989; Hepp et al. 1988; King et al. 1981; King and Fuchs 1979; Vilis et al. 1989). Our data confirms earlier suggestions that the integrator for this group is the interstitial nucleus of Cajal. These circuits utilize the same organization that is observed in the vestibular canals, which provide a velocity signal to the integrator for the vestibulo-ocular reflex.(Ezure and Graf 1984; Simpson and Graf 1985). Having localized vertical and torsional integrator function to the INC, we may not turn our attention to more detailed questions concerning the neural mechanism of oculomotor integration. This subject is taken up in the following chapter.

6 PARALLEL PROCESSING IN THE OCULOMOTOR INTEGRATOR

6.1 INTRODUCTION

The first stage in pursuing the oculomotor integrator theory was the demonstration of a neural integrator for horizontal eye movement in the nucleus prepositus hypoglossi region (Cannon and Robinson 1987; Cherron and Godaux 1987) and the integrators for vertical and torsional position in the INC, as demonstrated in the previous chapter. The next stage, the focus of the present chapter, is to determine how such a neural integrator works. It follows that incorporation of different basic principles in the mechanism will have different clinical and theoretical implications. One principle that has been embraced as fundamental for other parts of the brain is parallel distributed processing.

In the last few years much attention has been focused on the principle of parallel distributed processing in the brain, mainly with reference to "connectionist" or "neural network" models (Sejnowski et al. 1988; Zipser and Anderson 1988; Crick 1989; Morris 1989; Anastasio and Robinson 1990; Van Leeuwen 1990). These models emphasize the importance of lateral connections between parallel channels. They suggest that experimental neuroscientists must not only confirm the existence of lateral connections, but to assess their patterns of connectivity and the functional implications of these patterns. Modular connectivity, e.g. the columns of sensory cortex (Mountcastle 1957; Hubel and Weisel 1959), is one such basic pattern that has been observed throughout the brain, without any clear rationale for its significance (Purves et al. 1992). This pattern is not as obvious in motor systems, but has been proposed for the oculomotor integrator network on theoretical grounds (Cannon et al. 1983; Cannon and Robinson 1985). If true, the integrator would provide a simple experimental model for exploring the implications of modularity. The purpose of the present study was to experimentally test this hypothesis.

The neural mechanism of integration has been modeled using a number of approaches (Cannon et al 1983; Cannon and Robinson 1985; Galiana and Outerbridge 1984; Kamath and Keller 1976; Robinson 1989; Rosen 1972; Tweed and Vilis 1987). At the core of most integrator models is a simple positive feedback loop that retains a constant level of neural activity when input is zero. Damage to such an integrator would produce a simple position-dependent exponential drift of the eye towards a unique "null" position, with a time constant that is inversely proportional to the amount of damage (Robinson 1989). Cannon et al. (1983) have pointed out that integration with a single positive feedback loop is not a robust scheme, because extremely small errors in the gain of this feedback would cause the integrator either to rapidly leak to inactivity or continuously drive its neurons to the upper limit of their frequency.

The solution to this problem clearly involves increasing the number neurons in the network. Although it is obvious that integration is not achieved by a single neuron, it may not be as obvious that a multi-neuron network can be computationally equivalent to a single-neuron model. For example, a network with uniformly distributed connections would suffer from a similar lack of robustness, because damage to any one synapse would affect overall gain in the distributed feedback loop, causing a failure to maintain activity levels throughout the network.

Cannon et al. (1983) addressed this problem using an integrator network model with parallel units that indirectly excited themselves though mutually inhibitory lateral connections (Cannon et al. 1983; Cannon and Robinson 1985). The key point for this discussion is that the lateral connections were organized so that connections were dense between neighbouring units, but sparse between distant units. This was based partially on experimentally observed patterns of lateral connection in the visual system (Ratliff et al. 1969). Taken to an extreme, such a pattern would result in numerous parallel and independent sub-integrators within the entire integrator network. This model was much

more robust. Simulations showed that significant post-saccadic drift only occurred during systematic localized damage, and this did not affect integration in other regions of the network. The simulated drift was initially rapid, but then stabilized within a second, essentially holding at a slightly less eccentric position maintained by the undamaged integrator circuits (Cannon et al 1983). These circuits could eventually be recalibrated to compensate for the damage. The oculomotor community has accepted this theory in principle, but the implications of this simple connectivity pattern are obscured by the complexity of the neural network models and, surprisingly, an experimental test of the model has not been performed (Robinson 1989). The aim of the present study was to test the fundamental predictions of this parallel integrator model against those of a single integrator by examining post-saccadic drift during partial inactivation of the INC.

6.2 METHODS

Whereas the preceding chapter emphasized complete failure of the torsional and vertical oculomotor integrators ~30 minutes after injection of muscimol into the INC, the present study examined the more modest initial effects of the same experiments, and the time course of their progression. In particular, we examined parameters of drift that should distinguish between models equivalent to a single integrator, and models in which the velocity-to-position transformation is distributed across a bank of parallel integrator modules. Observations that would suggest parallel integration would include (1) a rapid drift towards a position that is some fraction of initial post-saccadic position, rather than slower drift towards a single null position, (2) as a consequence of #1, a dependence of drift rate on previous saccade magnitude as well as current eye position, and (3) a drift that has multiple time constants, determined by a combination of inactive and partially active integrators. In 6 experiments in animal BAR and 1 in LAR this analysis was applied to data collected during spontaneous saccades in the dark as well as visually

evoked saccades.

6.3 RESULTS

6.3.1 *Progression in Time of Drift Magnitude and Direction.*

TWO-DIMENSIONAL OBSERVATIONS When viewing 2-dimensional gaze direction following injection of muscimol into the INC region, the first effect to manifest itself was a position-dependent inability to maintain vertical gaze. This effect is illustrated in Figure 46 by an experiment in which an injection delivered at the lateral edge of the INC region produced a steadily progressive effect. Each part of this figure shows eye positions recorded over the course of 100 seconds. In this and all other cases below, the data is plotted in Listing's coordinates. Thus, the reference position (the origin) is primary position, which is usually located high in the oculomotor range of *Macaca fascicularis* (Chapters 3 and 4). In the control case (Fig. 46 A) one views Listing's plane of normal saccadic eye positions as if from behind the subject.

Each cluster of dots in Figure 46 gives eye positions during the first 100 milliseconds (ms) after each saccade. As expected, post saccadic position was constant before muscimol injection (A) and thus the figure shows a clump of overlapping dots at each fixation point. However, 9 minutes after muscimol injection adjacent to the INC (Fig. 46 B), some of these position clumps became slightly elongated, particularly in the downward gaze direction. The larger symbols, which indicate eye position at 100 ms after the previous saccade (i.e. the last illustrated position of each sequence), show that in these lower positions the drift is largely upward. After 19 minutes (Fig. 46 C), this drift became more pronounced. The greater length of the 100 ms position sequences indicates that the magnitude of drift had increased. Furthermore, the magnitude of this drift is larger for eccentric vertical positions, clearly being directed towards a central range of positions where post-saccadic gaze was still quite stable. At the 30 minute mark

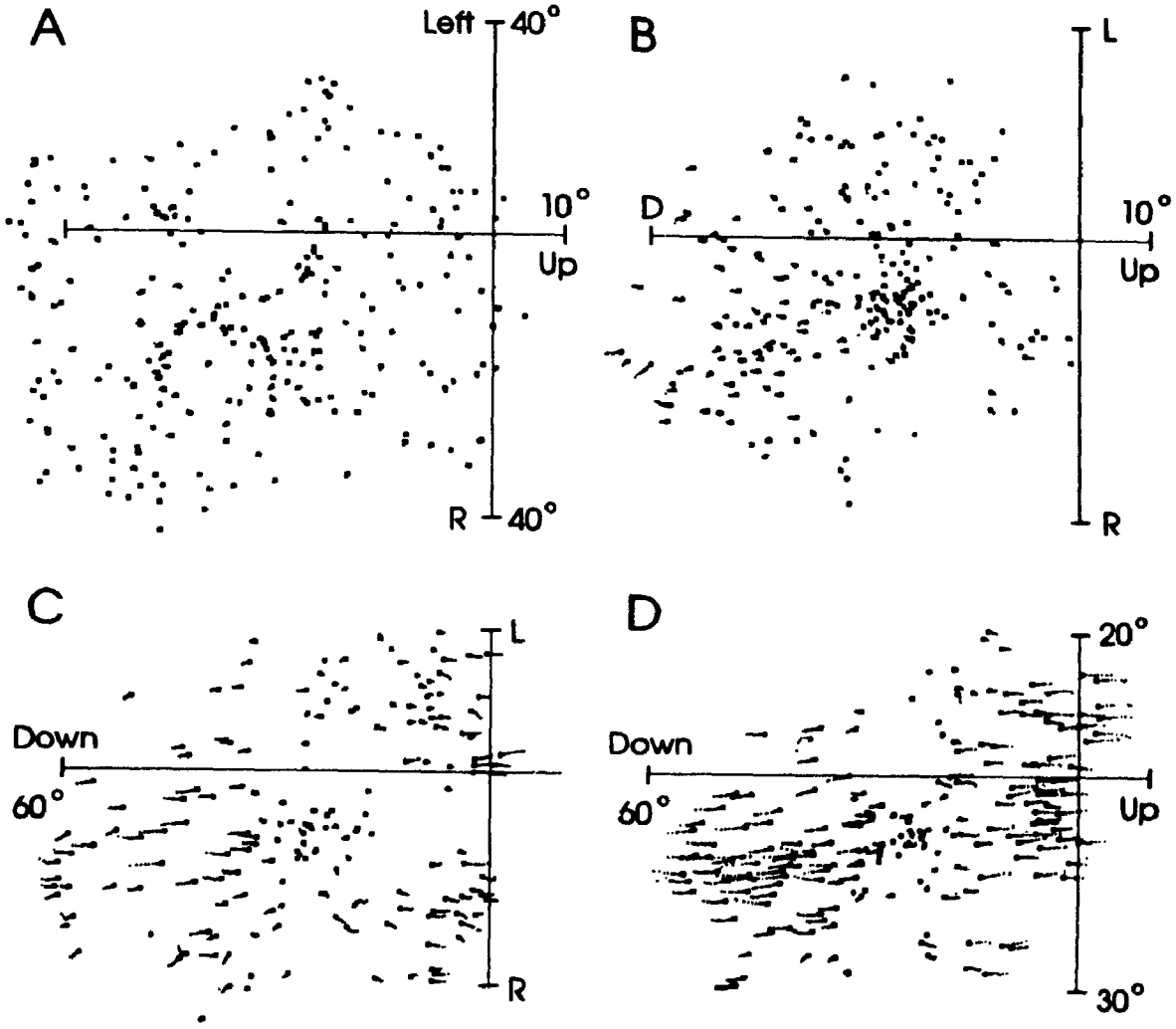

FIGURE 46. Time course of deficit in holding vertical and horizontal eye position after a muscimol injection adjacent to the right interstitial nucleus of Cajal. The first 100 milliseconds of eye position quaternions are shown after each of several hundred randomly directed saccades (A) before injection and (B) 9 minutes, (C) 19 minutes, and (D) 30 minutes after injection. Larger data points demarcate the last position of each 100 millisecond sequence. Animal: BAR.

(Fig. 46 D) these effects have again become more pronounced. Note that even at this point the magnitude of horizontal drift was small compared to the vertical drift, without any clear position-dependence. Thus, eye position appeared to drift towards, and hold steady at a line of horizontal eye positions at a central vertical level (Chapter 5). Similar results were consistently observed during injection of muscimol into either side of the INC.

WHERE DOES THREE-DIMENSIONAL POSITION SETTLE? Currently accepted models of the oculomotor system predict that during integrator failure, the direction of position drift will depend on (1) initial post-saccadic position (a function of the saccade generator) and (2) the point where eye position eventually comes to rest (a function of neural integrator output). We examined final resting eye positions by plotting eye position only during intervals when velocity was below a threshold, focusing our attention on the non-horizontal components of drift. Figure 47 gives a vertical vs *torsional* view of eye position quaternions during an experiment in which muscimol was injected directly into a concentrated group of oculomotor-related neurons in the left INC. The left column (A-D) shows eye positions when overall eye velocity (speed) had dropped below a 2.5° / second threshold, as an indication of where position was settling. Within an oculomotor range of $\pm$ 50°, this threshold would exclude drift with a time constant less than 25 seconds, a value typical for normal fixation (Robinson 1989). As expected, almost all positions between saccades were included in the control case, spread across a large ($\sim$70°) vertical range and a narrow ($\sim$3°) torsional range. Thus, these positions formed a plane (Listing's plane) that is viewed edge on, as if from above the subject.

Immediately after injection of muscimol (B), eye position began to settle towards positions that were shifted progressively more torsionally from Listing's plane, up to about 7° CW within 100 seconds. Simultaneously, the vertical range of positions that

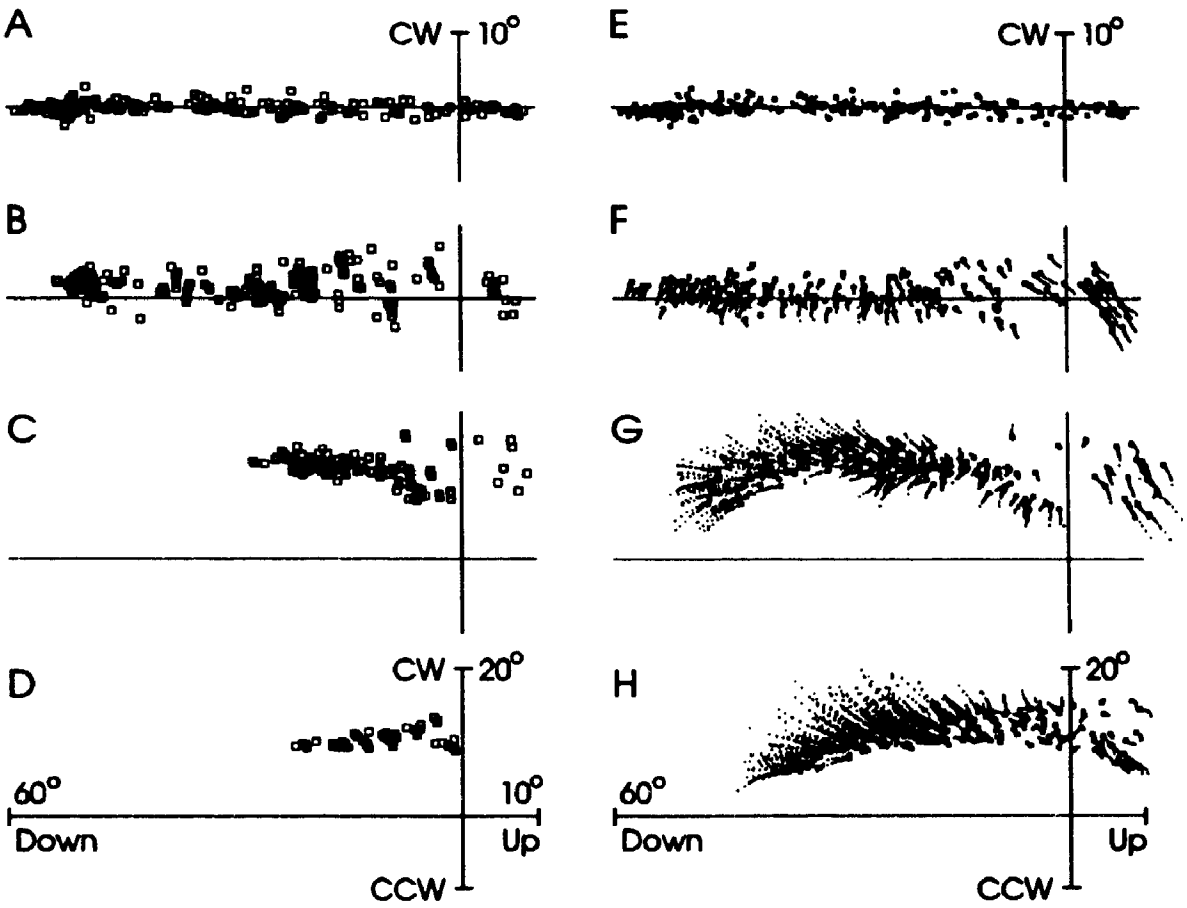

FIGURE 47. Typical time course of deficit in holding torsional and vertical eye position after injection of muscimol directly into the left interstitial nucleus of Cajal. **A-D**: Eye positions during which eye speed was less than 2.5° per second **(A)** before injection and **(B)** 0-2 minutes, **(C)** 14 minutes, and **(D)** 23 minutes after injection. **E-H**: The first 100 milliseconds of eye positions are shown after each of several hundred randomly directed saccades, computed from the same data as A-D. Larger data points demarcate the last position of each 100 millisecond sequence. Animal: ART.

held (beneath the speed threshold) began to diminish. After 14 minutes (C) this vertical holding range was clearly restricted, particularly for downward gaze directions, but was still more than half of the normal range. At this time the torsional range of position holding appeared to settle within a range with almost normal width, but shifted by 10-15° CW. Henceforth we will refer to this range of position holding during drift as the "null range". The final null range after 23 minutes (D) was further reduced in the vertical direction, and the shifted torsional range was comparable in thickness to the normal Listing's plane. This progressive reduction in the vertical null range together with a torsional offset was typical of all unilateral muscimol injections, as quantified below.

How did post-saccadic eye positions influence rate and direction of drift? The right hand column of Figure 47 (E-H) was computed from the same data, but gives the first 100 ms of post-saccadic eye position, showing the end positions of saccades and also the initial direction and magnitude of post-saccadic drift. As the null range diminished (A-D) relative to the range of post-saccadic positions (E-H), the magnitude of torsional and vertical drift increased markedly. Initially, saccades terminated near the normal Listing's plane (F), but as the muscimol spread further they drove the eye progressively further in the CW direction, beyond the null range (G and H). Such anti-corrective torsional saccades appeared between 0 and 30 minutes after muscimol injection, depending on proximity to the anteriorly adjacent riMLF, whereas injections into the posterior riMLF produced the saccade deficit immediately and afterwards produced positional drift (Chapter 4). Since the torsional null range was relatively stable on the CW side of Listing's plane, the torsional direction of post-saccadic drift changed from clockwise (F), to bidirectional (G), to counterclockwise (H). Figure 47 emphasizes that the null range was relatively independent of saccade behaviour, and that both influence the direction of drift.

A second example (Fig. 48) shows the effects of injection on the right side of the

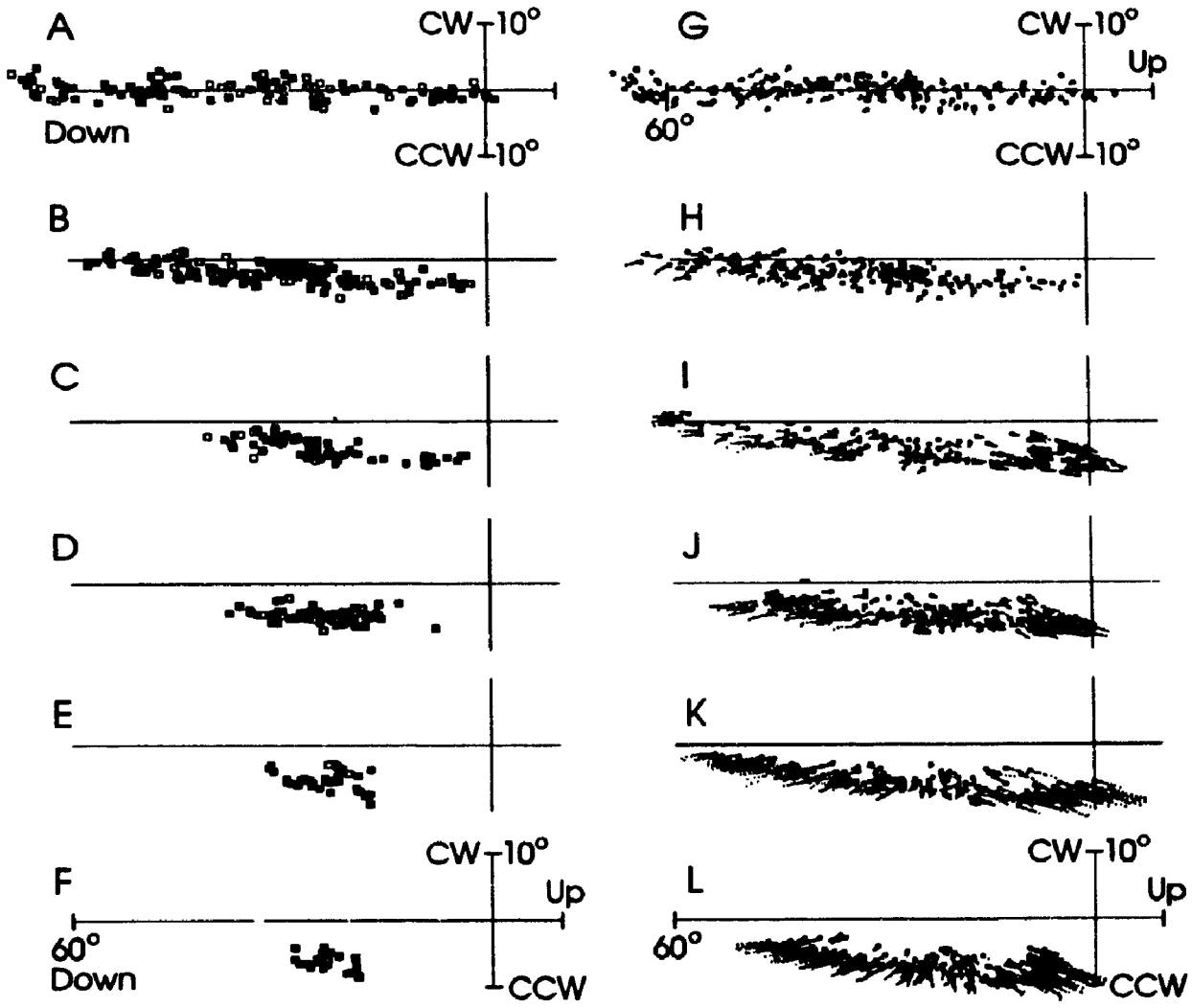

FIGURE 48. Time course of torsional and vertical eye position holding and drift after injection of muscimol adjacent to the anterior-lateral pole of the right interstitial nucleus of Cajal. **A-F**: Eye positions during which eye speed was less than 2.5° / second **(A)** before injection and **(B)** 9 minutes, **(C)** 19 minutes, **(D)** 21 minutes, **(E)** 30 minutes, and **(F)** 38 minutes after injection. **G-L**: The first 100 milliseconds of positions are shown after each of several hundred randomly directed saccades, computed from the same data as A-F. Larger data points demarcate the last position of sequence. Animal: BAR.

brain. This is the same experiment illustrated in Figure 46, which can be referred to for a complete three-dimensional view. In this case, muscimol was injected just outside the anterior-lateral pole of the right INC, which resulted in a more gradual and uniform progression of the deficit. As with left INC injections, a thin torsional null range appeared, but now on the CCW side of Listing's plane, in this case stabilizing within 19 minutes (C) and changing little thereafter. As with all other unilateral injections, the vertical null range began to decrease with the first signs of positional drift (B). This range decreased progressively (B-F), presumably as muscimol progressively diffused through the INC, until the remaining vertical-torsional range of position holding approximated a point. In view of the fact that there was little horizontal drift, the null range has become a null line of positions, shifted CCW and viewed end-on.

The muscimol injection illustrated in Figure 48 was near the right riMLF, and was associated with a more rapid CCW shifting of initial post-saccadic positions that kept pace with the developing position deficit (H). Again, as the torsional imbalance in saccades progressed (H-L), eye position was driven farther away from the null range, resulting in increasing torsional drift. However, the vertical range of post-saccadic positions remains constant compared to the progressively diminishing vertical null range. Concurrently, the magnitude of drift increased markedly, always directed towards the null range.

The above examples show that the null range most simply and directly characterizes the position deficit that resulted from INC inactivation, despite complicated and variable saccade deficits that may have arisen from adjacent structures. Null ranges measured at the end of experiments are summarized for all animals in Figure 49. Figure 49 A shows a vertical vs. torsional plot of the final null ranges from 8 individual experiments, for example as illustrated in Fig. 48 F. A typical left INC injection (○, ▵, x, ◐, □) is illustrated for each animal , and typical right injections (▲, ■, ●,) are illustrated for

FIGURE 49. Summary of the torsional-vertical "null ranges" observed during unilateral interstitial nucleus of Cajal (INC) inactivation in all animals. Torsional position is plotted as a function of vertical position in Listing's coordinates, i.e. the horizontal axis (for vertical rotation) is embedded in Listing's plane and the origin is primary position. Eye position holding is defined as periods during which eye speed was less than 2.5° per second, as in Figures 2-3. **A**: Means and standard deviations for the range of torsional and vertical eye positions that held following representative INC inactivations from each animal. Data from the last file recorded was used. Key with animal code and N values (# eye positions that held) for left INC inactivation: (○: CAS, 331 ▵: ART 270 ×: LAR, 258 ◐: MAR, 152 □: BAR, 33) and for right INC inactivation: (▲: ART, 233 ■: BAR, 148 ●: CAS, 42). **B**: Averages and standard deviations (between experiments) of "null range" means, as illustrated above, calculated from all unilateral experiments that resulted in moderate to extreme positional drift. Key with animal code and N values (# experiments) for left INC inactivation: (○: CAS, 2 ▵: ART, 4 ×: LAR, 3 ◐: MAR, 3 □: BAR, 5) and for right INC inactivation: (▲: ART, 5 ■: BAR, 6 ●: CAS, 4).

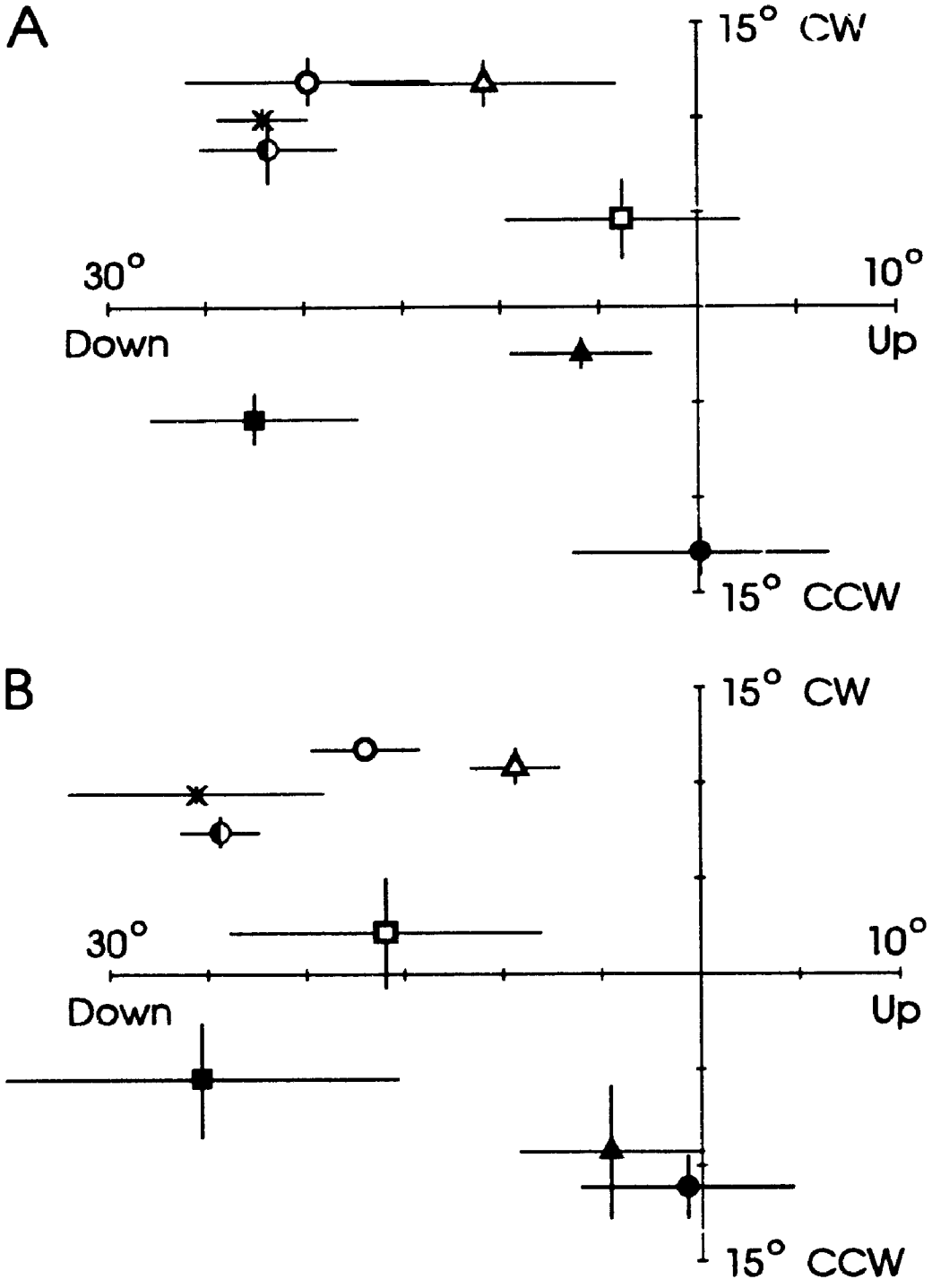
A
15° CW
30°
10°
Down
Up
15° CCW
B
15° CW
30°
10°
Down
Up
15° CCW

the three animals in which this side was explored. Symbols give the mean value of the positions that held (< 2.5°/s) while error bars give the standard deviations of the torsional and vertical range. As illustrated above, the torsional range was shifted but remained small in all cases, and although the vertical range was greatly reduced compared to normal, it typically retained a finite value.

Figure 49 B summarizes the null range data across all unilateral INC injection experiments that produced moderate to extreme position holding deficits. In this case the symbols give the average of the mean values of the null position range, as illustrated in part A, across all experiments in each animal, and the error bars give the standard deviations between the means of these experiments. Note the torsional value of the null range mean was almost always (16 / 17 experiments) shifted clockwise after injection of muscimol into the left INC region (○, ▵, x, ◐, □). In contrast, right INC injection always resulted in values that were shifted in the CCW direction (▲, ■, ●,). The vertical value of the means was more variable, but tended to range between our arbitrarily set straight ahead gaze direction, and the primary gaze direction (the origin in the figure), which ranged about 25° upwards from the former in these animals (Crawford and Vilis 1992). Thus, eye position settled towards multiple null positions within a decreasing vertical range in the upper half of the oculomotor range, and a more narrow torsional range that was shifted clockwise during left INC inactivation, and counterclockwise during right INC inactivation.

Of particular relevance to the central question of this study is the time course over which the vertical null range progressively decreased after muscimol injection into either side of the INC. Figure 50 illustrates this decrement for one experiment from each animal that produced a strong effect, expressed as a percentage of the pre-injection range. In this case, the threshold value used for position " holding" was 1°/s in the vertical component of velocity (a lower threshold could be used here because there was

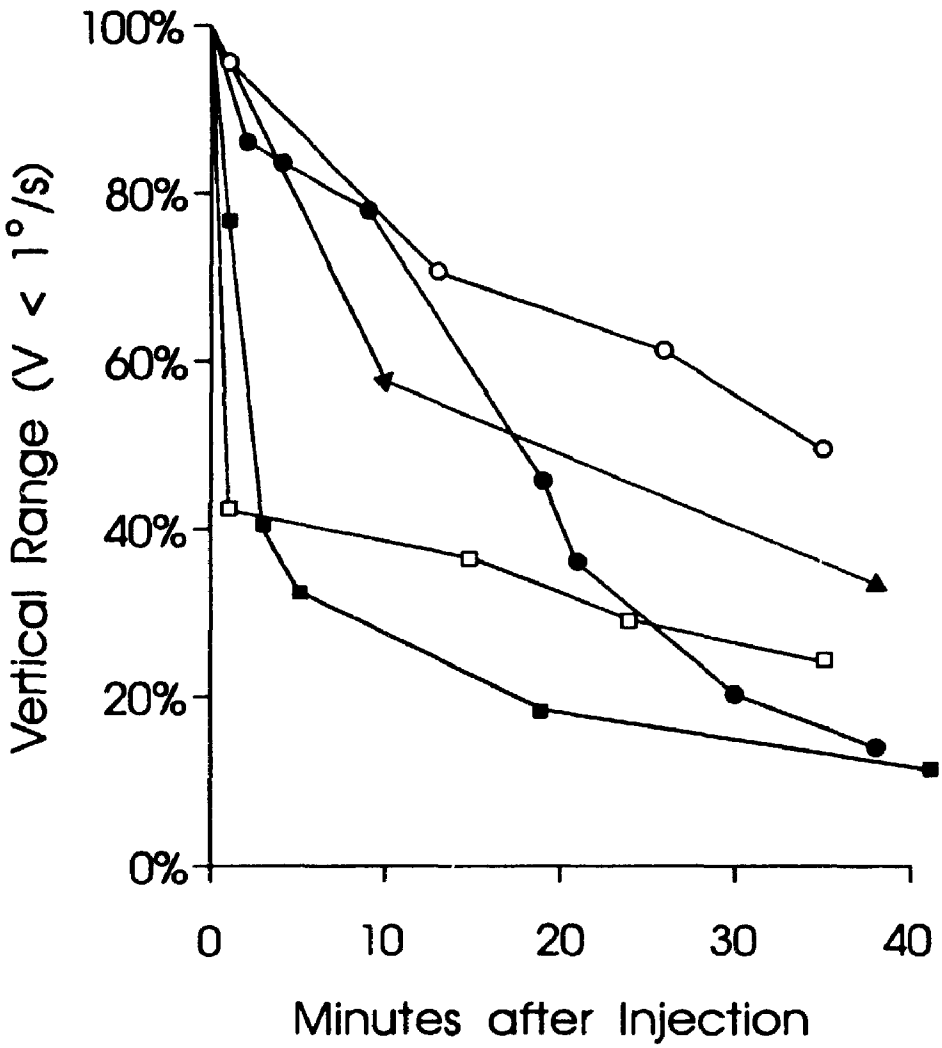

FIGURE 50. Time course of decrement in vertical "null range". An experiment that resulted in a strong position deficit is shown for each animal. The vertical range of positions that held (farthest upward - farthest downward) is expressed as a percentage of the control range of that day and is plotted as a function of time after muscimol injection. Eye position holding is defined here as periods during which the vertical component of velocity was less than 1.0° per second. ○: CAS ●: BAR ▲: MAR □: ART ■: LAR.

less noise in vertical velocity than in three-dimensional velocity). At this threshold, simple exponential leak of a single integrator predicts a very narrow null range (2 x threshold x time constant)° (Cannon and Robinson 1987). The figure shows a rapid and progressive decrement in the vertical range of position holding, presumably related to the spread of muscimol in the region of the injection. However, even the final null ranges varied between 7.4° and 27.0°, whereas the corresponding time constants of drift determined by traditional methods were less than 0.5 seconds (Chapter 5, Fig. 45), predicting null ranges of less than one degree. The remainder of the RESULTS is a detailed examination of the phenomena underlying the progressive decrement and persistence of these vertical null ranges.

6.3.2 *Determinants of vertical drift rate.*

IS DRIFT RATE A SIMPLE FUNCTION OF EYE POSITION? If the mechanism that transforms eye velocity commands to position commands is computationally equivalent to a single integrator circuit, then damage to this structure should result in a simple exponential drift that is proportional to eccentricity of eye position. Theoretically, the rate of this drift for any one position would increase as muscimol spread through the integrator, disrupting more and more of its circuits.

Was a simple position-dependent drift produced by injection of muscimol into the INC? This was examined by plotting a number of post-saccadic intervals at various vertical levels, with their initial post-saccadic positions aligned to the left (Fig. 51). The typical initial effects of muscimol injection into the INC region are illustrated in Figure 51 A. In the normal pre-injection state (A_1) eye position held steady at various vertical levels. Immediately after injection (A_2) vertical drift appeared, but there was not a clear-cut relationship between eye position and the magnitude of the drift. At any one vertical level there was a mixture of positions that held and others that exhibited post-saccadic

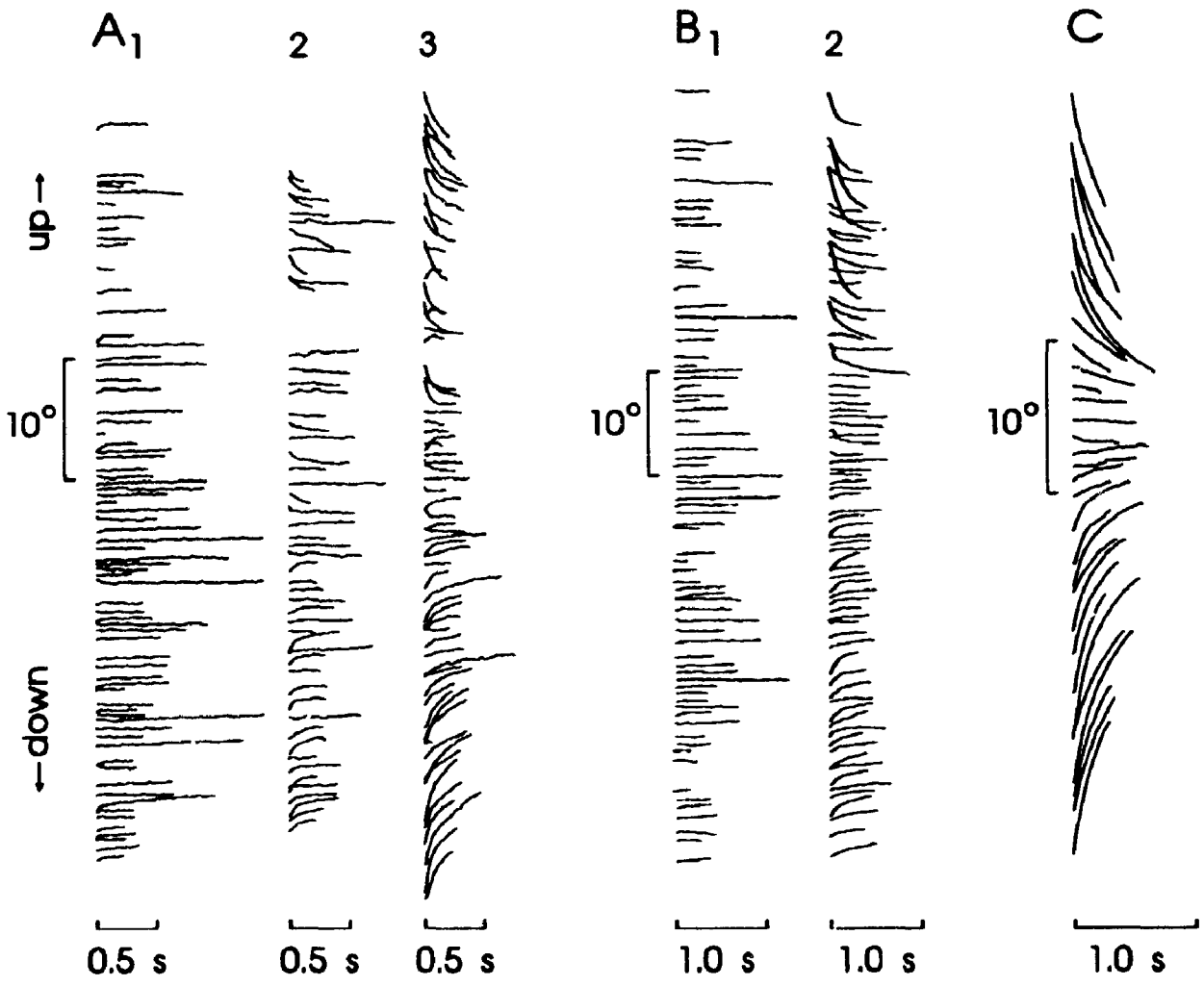

FIGURE 51. Vertical eye position (plotted as a function of time) after INC inactivation. Inter-saccadic intervals at various vertical levels are shown, aligned to the left. **A**: Typical injectio. effects in the light, showing position (1) before, (2) immediately after, and (3) 9 minutes after injection. Animal: CAS. **B**: Positional drift during spontaneous saccades in the dark, (1) before, and (2) 30 minutes after injection. Animal: BAR. **C**: A large effect, 38 minutes after muscimol injection, in which rate of drift appears to be a fairly simple exponential function of eye position. Animal: BAR.

drift. After 9 minutes (A_3) the effect was stronger but qualitatively similar. Different rates of drift were observed at any one vertical level of eye position. This was not because the magnitude of the effect was changing over the course of data collection; random rates of drift relative to any one position were observed throughout the period of each 100 second data file. Furthermore, examination of individual sequences of drift (A_2 and A_3) did not reveal the almost linear segments that should be observed for small segments of drift with a long time constant. Instead, most of these sequences had a rapid initial rate of drift that then settles almost completely within approximately 0.5 seconds. These effects were not restricted to saccades in the light. Figure 6 B illustrates an example with similar pre- (B_1) and post-injection (B_2) data, during spontaneous saccades in the dark. Again, there appeared to be neither a unique null position, or a simple position dependence in drift rate.

Eye position drift began to approximate a simple position dependent exponent only during the advanced stages of the effect (Fig. 51 C), at least from a superficial examination. During strong position deficits there was a rapid centripetal (towards center) vertical drift with a rate that appeared to be determined by eccentricity of eye position. In one animal (LAR), this drift type appeared at earlier stages, with a time constant of 5-6 seconds. However, as we shall see below, the apparent simplicity of even these examples did not endure a more careful quantitative analysis.

The time course of the effect for a typical experiment is further illustrated in figure 52. For comparison, the same data is used as presented in Figure 47. The initial effects of muscimol injection were similar to those described above. After each brief period of variable post-saccadic drift, eye position appeared to settle, at various vertical levels. As the deficit progressed (Fig. 52 C and D) the central range of vertical position retained this quality, but drift at the eccentric positions, particularly downward, no longer settled during the time allotted. This evidently relates to the restricted "null ranges" illustrated

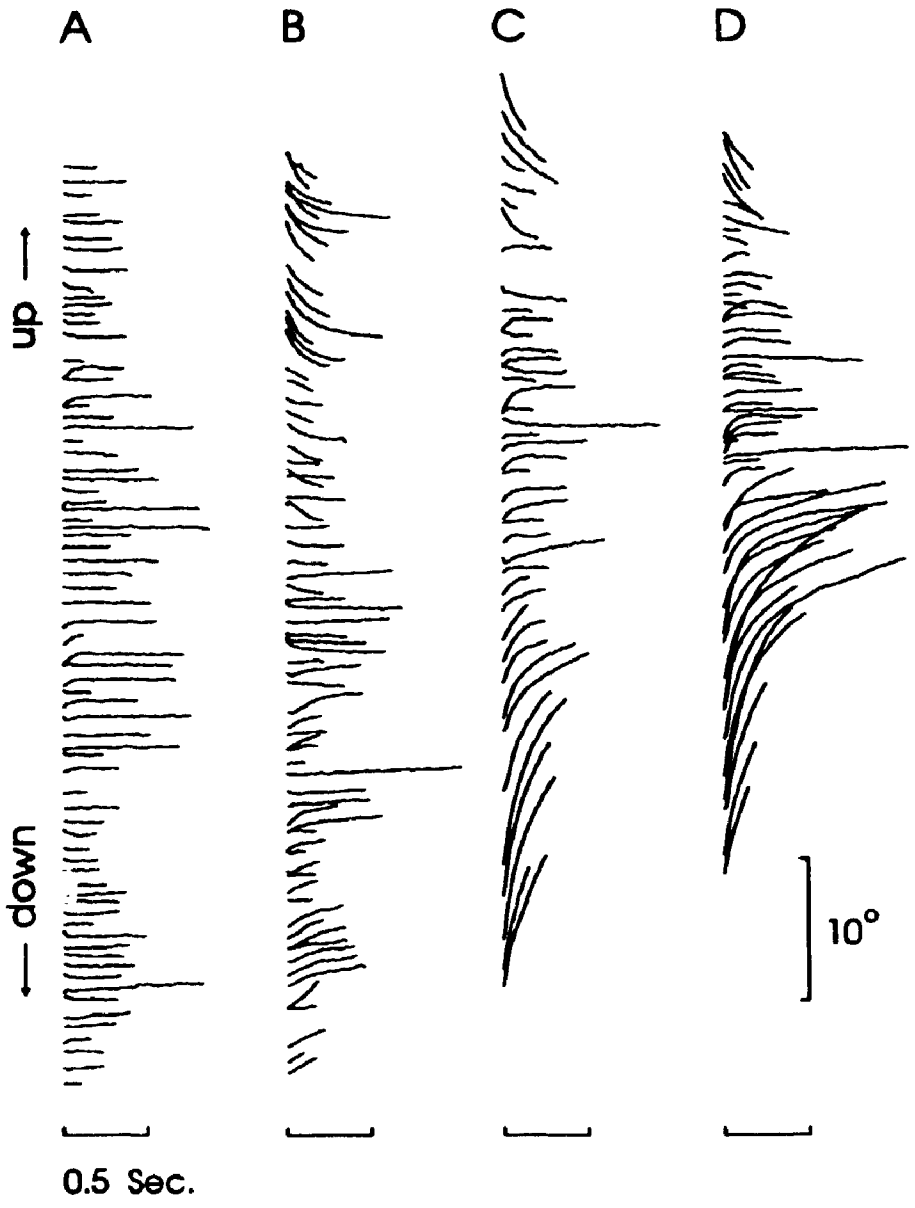

FIGURE 52. Typical time course of increasing vertical position drift (plotted as in the previous figure). Eye positions are illustrated (A) before, (B) immediately after, (C) 14 minutes after, and (D) 23 minutes after injection of muscimol into one side of the INC. Animal: ART.

in Figures 49 and 50.

MULTIPLE TIME CONSTANTS IN THE DRIFT Figure 52 D illustrates another aspect of drift that was frequently encountered during intermediate stages of the position deficit. Close inspection of the figure suggests that this drift has more than one time constant (illustrated in more detail in Fig. 53). First, there are instances in the upward levels of Figure 52 in which the direction of drift appears to reverse about 200 ms after the saccade. Second, the upward drift from the lower vertical levels seems too rapid initially, and then too slow to fit a simple exponential curve with one time constant.

Multiple time constants were difficult to quantify because, as shown above, they did not have a single, unique null position. However, the effect could be demonstrated qualitatively (Fig. 53). Figure 53 A shows several examples in which an animal made a downward saccade towards a position that was still above the center of the null range. In these cases, there was an initial segment of rapid post-saccadic drift in the direction opposite to the previous saccade, which then reversed direction and drifted more slowly towards the centre of the null region. Figure 53 B shows two more downward saccades from the same experiment, but this time their final position was beneath the center of the null range. Ideal exponential curves with one time constant (····) have been fitted to the initial component of the upward post-saccadic drift. The real drift initially aligned with the ideal exponent, but then diverged and followed an almost linear path. This demonstrates the presence of a fast time constant and one or more slower time constants. Figure 53 also suggests that previous saccadic history as well as current eye position may have been important in determining drift. Note that in both A and B the initial segments of drift tended to be in the direction opposite to that of the preceding saccade, while the final direction of drift was always towards the center of the null region. Thus, there were at least two time constants of drift present, the shorter one somehow linked to the previous saccade, and the longer one linked more to eye position.

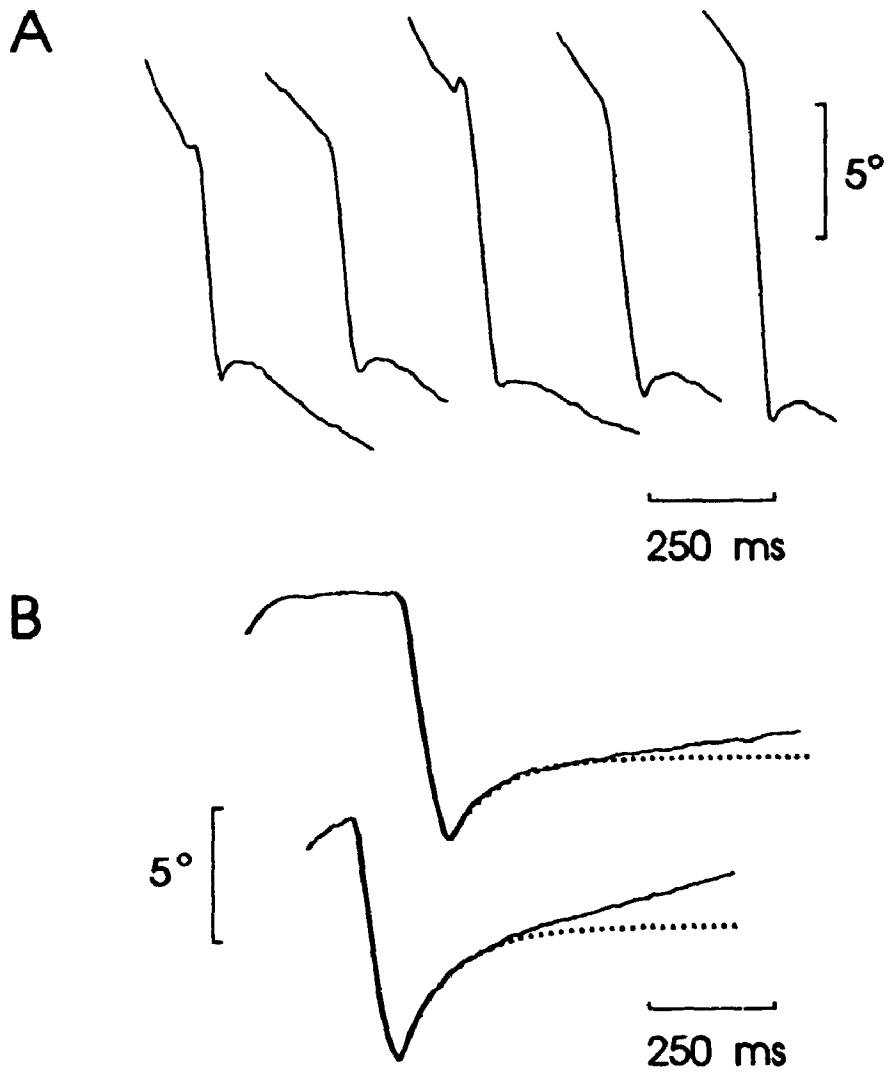

FIGURE 53. Multiple time constants in post-injection vertical position drift. **A**: Five downward saccades that started near the upward edge of the position range and ended still above the central "null range". Each saccade was preceded by downward drift, and was immediately followed by a brief but rapid drift that then reversed direction and slowly drifted downward towards the null range. **B**: Two downward saccades, plotted on the same position scale, which started below the center of the null range. A simulated segment of drift with a single 100 millisecond time constant (·····) has been fit to the initial portion of the post-saccadic drift. Animal: ART.

RELATIONS BETWEEN EYE POSITION, SACCADE MAGNITUDE, AND RATE OF DRIFT By taking saccade history into account as well as eye position, the irregular relationship between eye position and drift rate in the initial post-injection effects can be explained. Figure 54 (A-D) illustrates the saccade dependence of positional drift in an animal that was spontaneously making saccades in the dark. Vertical eye position is plotted against time for saccades converging on four different vertical levels. At any one of these levels, the size of the post-saccadic vertical drift appeared to be negatively correlated to the vertical component of the previous saccade. For example at 2° above primary position (A), which was near the top of the position range, the magnitude of downward post-saccadic drift increased with the magnitude of the previous upward saccade. At intermediate vertical levels (B), the direction of post saccadic drift would even reverse depending on the direction of the previous saccade. In these respects, and in the rapid settling of the post saccadic drift, this resembled the phenomena known as pulse-step mismatch, a mismatch between the oculomotor commands for movement and position holding.

In another respect the drift did not resemble as pulse-step mismatch, because the drift was also dependent on eye position. As one proceeds downward in the position range form Fig. 54 A to D, there is a change in weighting from downward to upward drift. This is illustrated most clearly by comparing drift at different positions while keeping saccade magnitude constant. Figure 54 E shows drift following a series of saccades with similar vertical magnitude that terminated at different vertical levels. The gradual transition from upward to downward drift between the lowest and highest saccade could only be accounted for by a position-dependence.

If the magnitude and null point of post-saccadic drift is partially dependent on magnitude of the previous saccade as shown above, then it is expected that an animal could approximate fixation of any target by a succession of progressively smaller

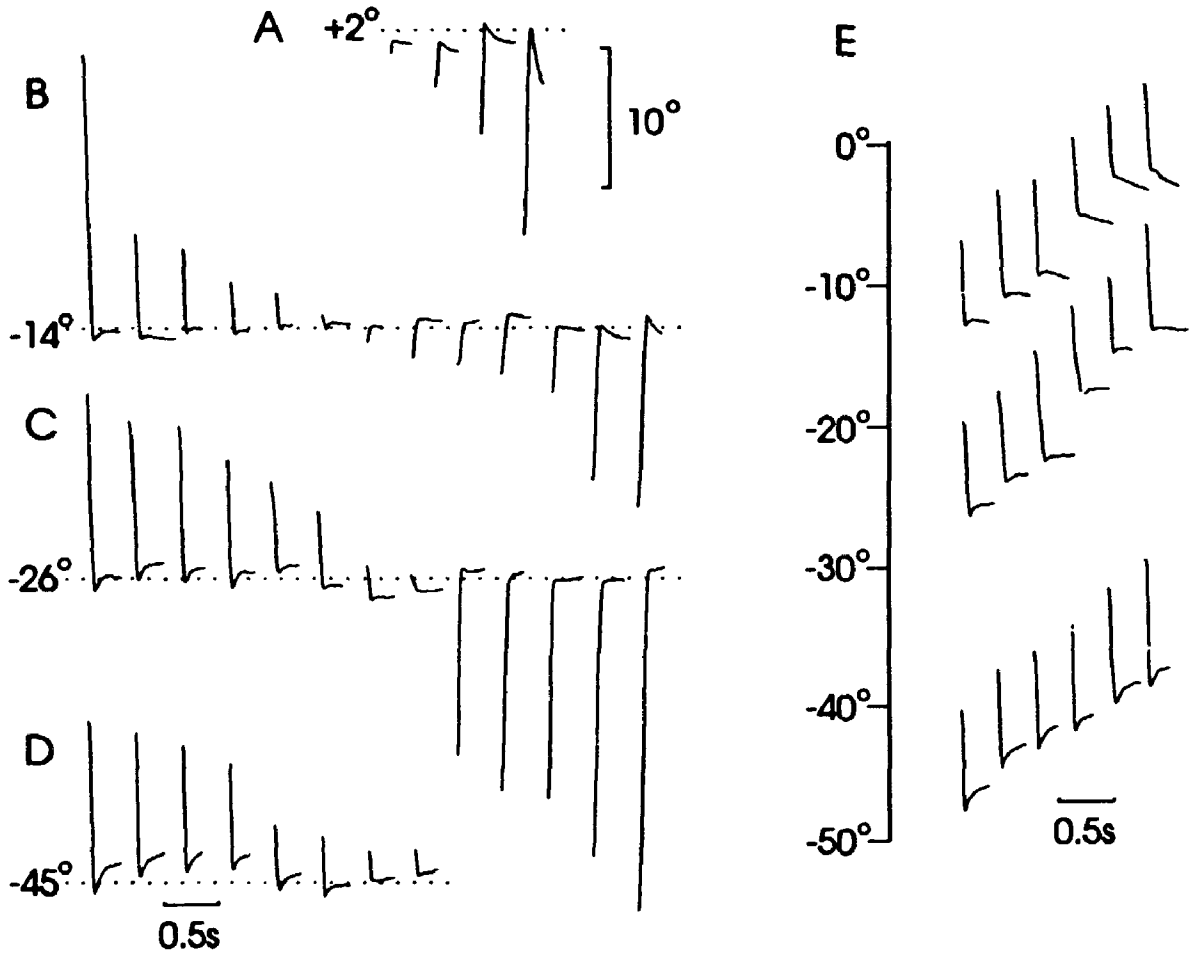

FIGURE 54. Dependence of vertical drift both on vertical eye position and vertical magnitude of the previous saccade. Data was recorded while the animal spontaneously made saccades in the dark. **A-D**: In each case vertical eye position is plotted against time for saccades with a range of vertical magnitudes and directions, but which ended at a common labelled vertical position ( ). **E**: A series of vertical saccades with similar magnitudes, but different final positions. The particular choice of alignment is simply for conservation of space. Animal: BAR.

saccades to that spot. Such was the case during mild initial post-injection effects. An exampie is illustrated in Figure 55 A, in which the animal is able to achieve reasonably good stabilization of eye position 48° degrees below primary position using a sequence of downward saccades. The magnitude of post-saccadic drift decreased after each of the progressively smaller saccades. However, this strategy no longer worked for eccentric eye positions when the deficit progressed further (Figure 55 B). Although position would still settle within a central vertical range (eg. 10° - 20° below primary position in the illustrated example) during a moderate to strong deficit, no number of saccades could stabilize eye position beyond the null ranges quantified above. In Fig. 55 B, there is no sign of stabilization at the lower extremity after the 9 saccades illustrated, or indeed over the next 10 seconds of similar saccades (not illustrated). Thus, this inability to hold any eye position beyond an ever-narrowing central region, ultimately limited the size of the null ranges.

In order to quantify the relations between vertical saccade magnitude, initial post-saccadic vertical eye position, and vertical drift, we computed these three parameters for a series of 200-300 saccades measured over 100 second time spans. Drift magnitude was quantified by the vertical position change in the first 100 ms of post-saccadic drift. Fig. 56 A plots drift magnitude (D) from one experiment as a function of initial post-saccadic position (P) on the left side, and as a function of saccade magnitude (S) on the right side. Standard statistical analysis (between two variables at a time) showed the expected correlation between drift magnitude and both position (e.g. $r = -.971$ in the illustrated case) and saccade magnitude (e.g. $r = -.842$). However, this is clearly a three-way ...em in the three-dimensional space defined by drift (D), position (P), and saccade magnitude (S). One can think of 11 A as two views of this D-P-S space from perspectives orthogonal to its axes. In particular, P and S were always correlated (e.g. $r = .765$, in the illustrated case), which could influence the two-dimensional results.

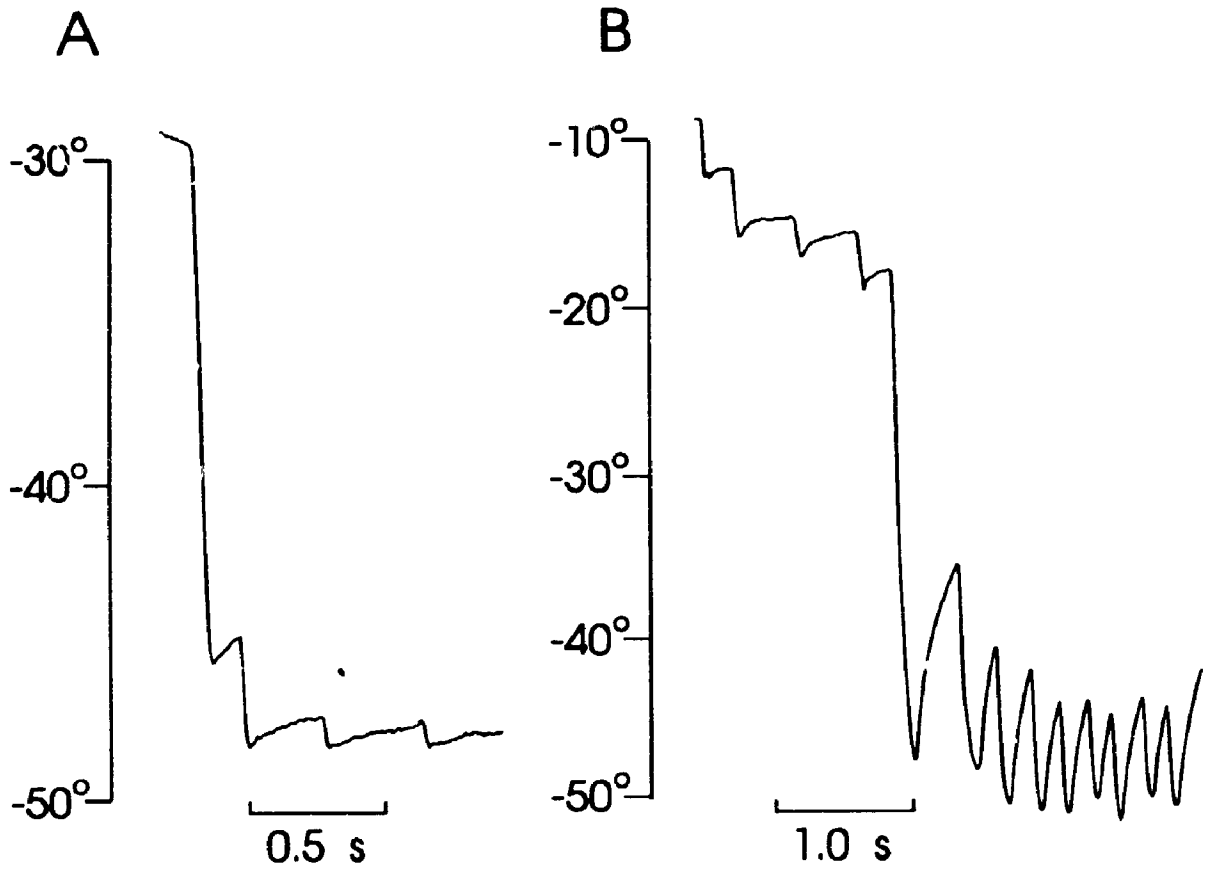

FIGURE 55. Eye drift following a series of saccades to the same eccentric vertical position. **A**: Vertical position as a function of time during the initial effects of muscimol injection. **B**: Similar saccades after further progression of the deficit. Animal: ART.

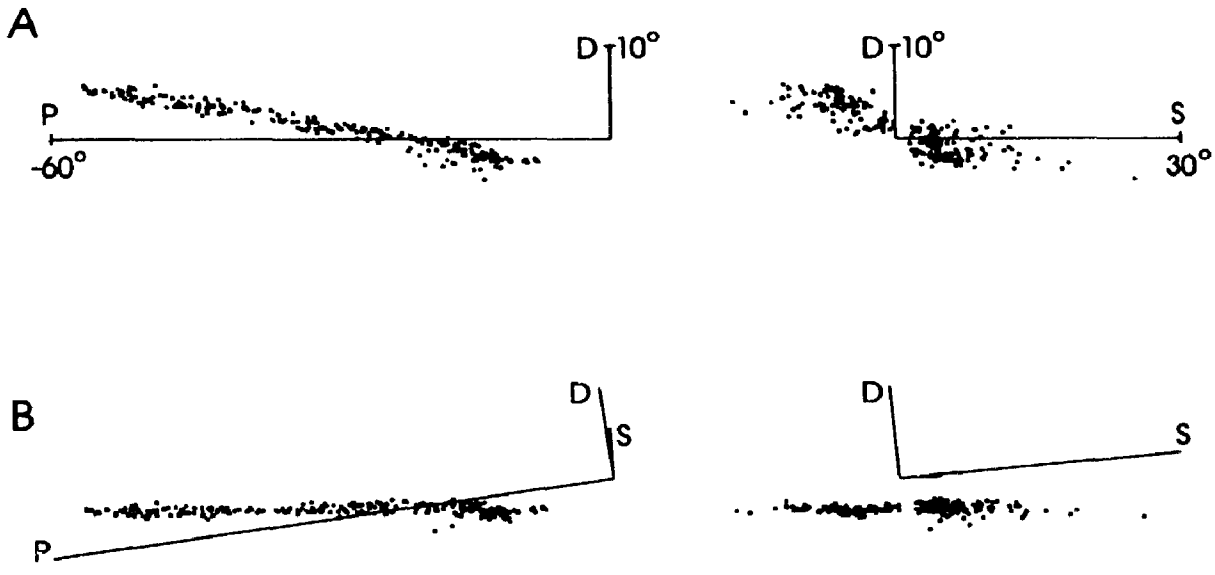

FIGURE 56. Geometric relationship between drift, position, and saccade magnitude. Magnitude of post-saccadic vertical eye position drift (D) in 100 milliseconds is plotted as a function of the initial post-saccadic vertical eye position (P) and of the vertical magnitude of the previous saccade (S). **A**: The three-dimensional relationship is viewed orthogonal to the coordinate axes from two views. **B**: The same data and coordinate axes have been rotated so that now apparent planar distribution of data is viewed edge on. N = 230. Animal: BAR. See text for explanation.

Therefore a multiple-regression analysis was performed (Bevington 1969), which utilized the above correlation coefficients and a plane fit to the data points in the three-dimensional space of D, P, and S. This revealed that the data fell within a planar distribution (in D-P-S space - nothing to do with eye position planes). In Figure 56 B, the data and axes from A have been rotated so that this plane is viewed edge-on, revealing the narrow orthogonal variance from this perspective. The multiple correlation coefficient (R) fit to this data was 0.983. The F value for this experiment showed that this R, and all others computed including experiments in light and dark, was significant far below the 1% level of error. This indicates that both independent variables P and S were required to explain the distribution of the dependent variable D (Bevington 1969).

A summary of our statistical analysis for all animals is presented in figure 57. Separate error bars give average statistical values for the initial effects of muscimol injection into the INC (hatched bars), and the last-recorded effects (solid bars). Standard two-way correlation coefficients (r) are shown for the relationship between eye position and drift magnitude (r[pd]), between saccade and drift magnitudes (r[sd]), and between the two independent variables, position and saccade magnitude (r[ps]). The correlations were much higher at the end of the experiment than during the initial effects. The three-way multiple regression analysis gave the slopes (m) of drift vs. position for a constant saccade size (m[pd]), and drift vs. saccade size for a constant position (m[sd]). Not surprisingly, these slopes became steeper between the initial and finally measured effects, as drift magnitude increased. Finally, the average multiple correlation coefficients (R[psd]) were 0.610 for the initial effects (when slopes m[pd] and m[sd] were changing rapidly), and 0.941 for the final, more stable effects. The latter was clearly higher, suggesting almost all variability had been accounted for. However, all individual R values were significant ($P < 0.01$), even for drift which had seemed a simple position-dependence at first glance (e.g. Fig. 6 C). This quantitative analysis strongly suggests

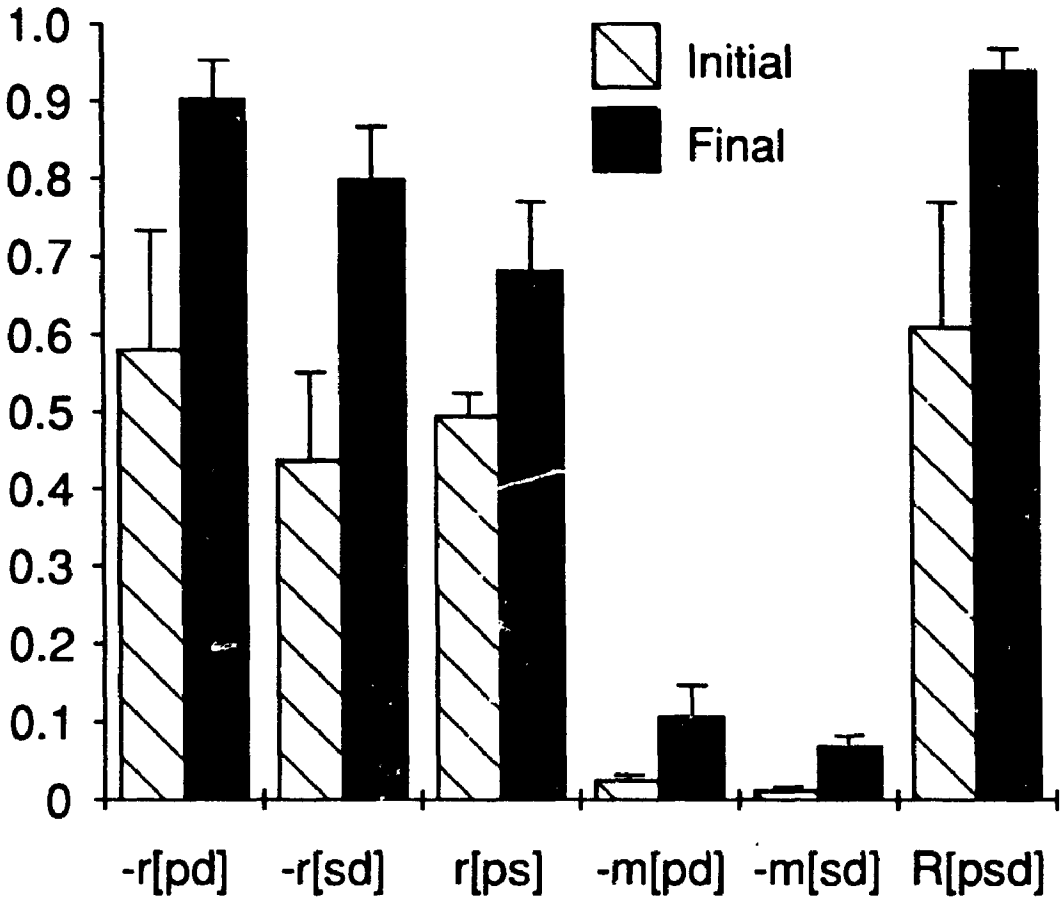

FIGURE 57. Summary of the multiple regression analysis between post-saccadic vertical drift (d) magnitude in 100 milliseconds, initial vertical position (p), and vertical magnitude of the previous saccade (s). Initial and finally recorded data (see key) were analyzed for a typical experiment from each animal. Bars illustrate the averages across all animals. Plotted are the average correlation coefficients between position and drift (r[pd]), average correlations between saccade magnitude and drift (r[sd]), average correlations between position and saccade magnitude (r[ps]), the average "slopes" of the former two relationships (m[pd] and m[sd]), and the average multiple correlation coefficients (R[psd]). Negative correlation coefficients have been reversed to conserve space, and error bars indicate the standard deviations of the values between animals.

that not only initial post-saccadic eye position but also previous saccadic history are necessary to account for the observed post-saccadic drift.

6.4 DISCUSSION

6.4.1 *Simulation of the data using single and parallel integrator models.*

The purpose of this investigation was not to develop a new model of the oculomotor integrator, but rather to test one fundamental principle incorporated into a previously described network model (Cannon et al. 1983). Does the integrator react to damage like a network that utilizes a modular pattern of lateral connections, or like a network with uniformly distributed connections? To answer this question we tested the data against two models that were compuationally equivalent to these network configurations but isolated their key features more clearly. A one-dimensional model of the brainstem saccade generator was developed that incorporated either a simple perfect integrator (Fig 58 A) or one in which integration was distributed across a parallel array of perfect integrators (Fig. 58 B). The latter model utilized a number (n) of simple positive-feedback integrators, each receiving a copy of the burst neuron velocity signal and contributing 1/n of the position signal to motoneurons. Ten parallel integrators were used in the simulations illustrated below. This model was basically the same as that used by Abel et al. (1978) to simulate partial integrator failure, except that they only used two parallel integrators. Progressive disruption to a single neural integrator was simulated by causing an integrator to leak with progressively lower time constants. The effect of muscimol spreading through parallel neural integrators was simulated by inactivating an increasing number of local integrators, and introducing leak in an increasing number of surrounding integrators.

FIGURE 58. Models of the brainstem saccade generator incorporating a single velocity-to-position integrator (**A**), and multiple parallel integrators (**B**). **A**: Main elements of the saccade generator. Current motor error (e_m•) is converted to a velocity command (V) by a saturating gain element, the burst neurons (BN). V• is then sent directly to the motoneurons (MN) and in parallel to an integrator which produces and maintains the position signal (P•). V• and P• were multiplied by the plant viscosity constant (r) and elasticity constant (k) and then summed as input to the motoneurons (MN). The viscosity and elascticity constants were set to 1 and 5 respectively, giving an intrinsic plant time constant of 200 milliseconds (Robinson 1970, 1975). e_m• is the difference between desired displacement (desired position - current position) and displacement feedback that is derived upstream from the main integrator (Jürgens et al. 1981). Thus, simulated integrator failure will not affect e_m• during saccades, as suggested by the lack of saccade overshoot observed during integrator failure (see APENDIX I; Kaneko and Fuchs 1991). **B**: Parallel array of n integrators used to replace the single integrator in A. Each integrator contributes 1/n of the position signal to the motoneurons.

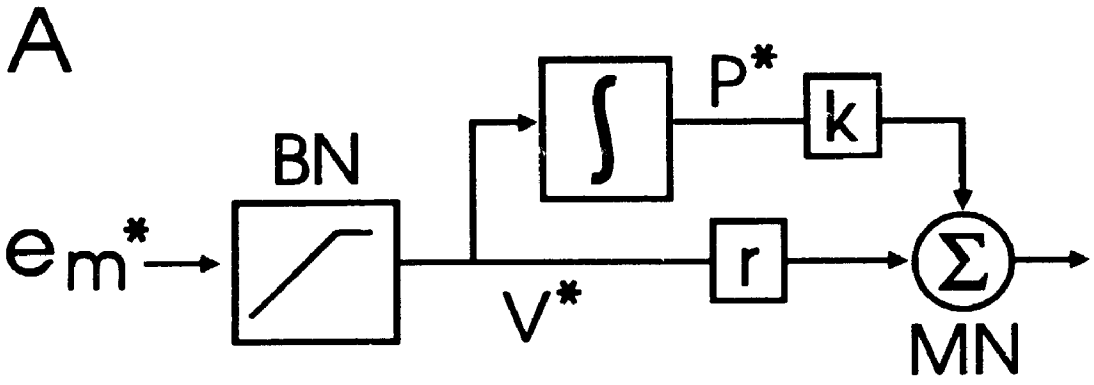
A
BN
em*
V*
P*
k
r
Σ
MN

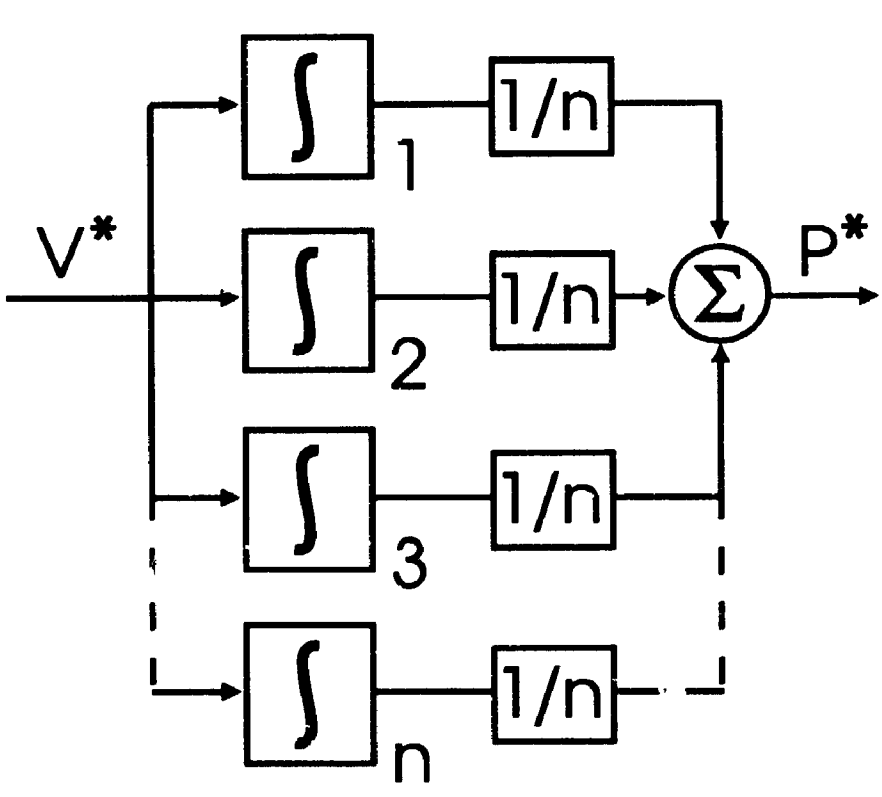
B
V*
1/n
1/n
1/n
1/n
1
2
3
n
Σ
P*

Figure 59 illustrates the essential differences between simulated damage to the two integrator models. When the eye position signal was generated by a single leaky integrator (Fig. 59 A) position always drifted towards a unique null position (----), at a rate determined uniquely by current eye position. Finite segments of slower drift appeared to be almost linear. However, the drift was exponential with a single time constant. This constant was primarily determined by the time constant of integrator leak, until this became small compared to the time constant of the plant, which set the lower limit.

As expected, the parallel integrator model produced more complex effects. When some integrators remained intact, and the intersaccadic interval was long compared to the time constants of drift, this model gave an effect equivalent to a pulse-step mismatch (Fig. 59 B). For example, if 30% of the integrators were completely inactivated and the others left intact, each saccade was followed by a reversing drift with the time constant of the plant, towards a position 30% of the way back to the start. This final resting position (----) could then hold indefinitely. Thus, there was no longer a unique null position, but rather brief, rapid drift towards multiple null positions. As long as the eye was allowed to settle between saccades, post-saccadic drift was determined uniquely by the magnitude and direction of the previous saccade, rather than eye position.

The parallel integrator model no longer produced a simple pulse-step mismatch when position was not allowed to settle between saccades. Figure 59 C illustrates this with 50% of the integrators leaking with a 2 second time constant, like that used for the single integrator in 59 A. At the second saccade, the leaky integrators still maintain some neural activity from the first saccade, and similarly they maintain activity from the previous two saccades at the third saccade. With more frequent saccades and slower integrator leak, the post-saccadic drift became indistinguishable from the position dependent drift produced by leak in a single integrator. However, unlike the leaky single integrator, when saccades suddenly ceased, eye position did not settle to a unique null

FIGURE 59. Theoretical relationships between saccade magnitude, eye position, and drift using the single integrator model (**A**) and using the multiple integrator model (**B-D**). Simulated vertical eye position is plotted (at 2 millisecond intervals) as a function of time. In each case the eye is initialized at the zero position and then makes three saccades towards targets 15°, then 30°, then 45° down at one second intervals. (——): the position that the eye is currently settling towards. **A**: The position signal is generated by a single integrator that leaks with a time constant of 2 seconds. **B**: The position signal is generated by ten parallel integrators, of which 30% have been completely inactivated. **C**: 50% of the parallel integrators leak with a time constant of 2 seconds. **D**: A combination of B + C, i.e. 30% of the integrators are inactivated, 50% leak with a 2 second time constant, and 20% remain intact.

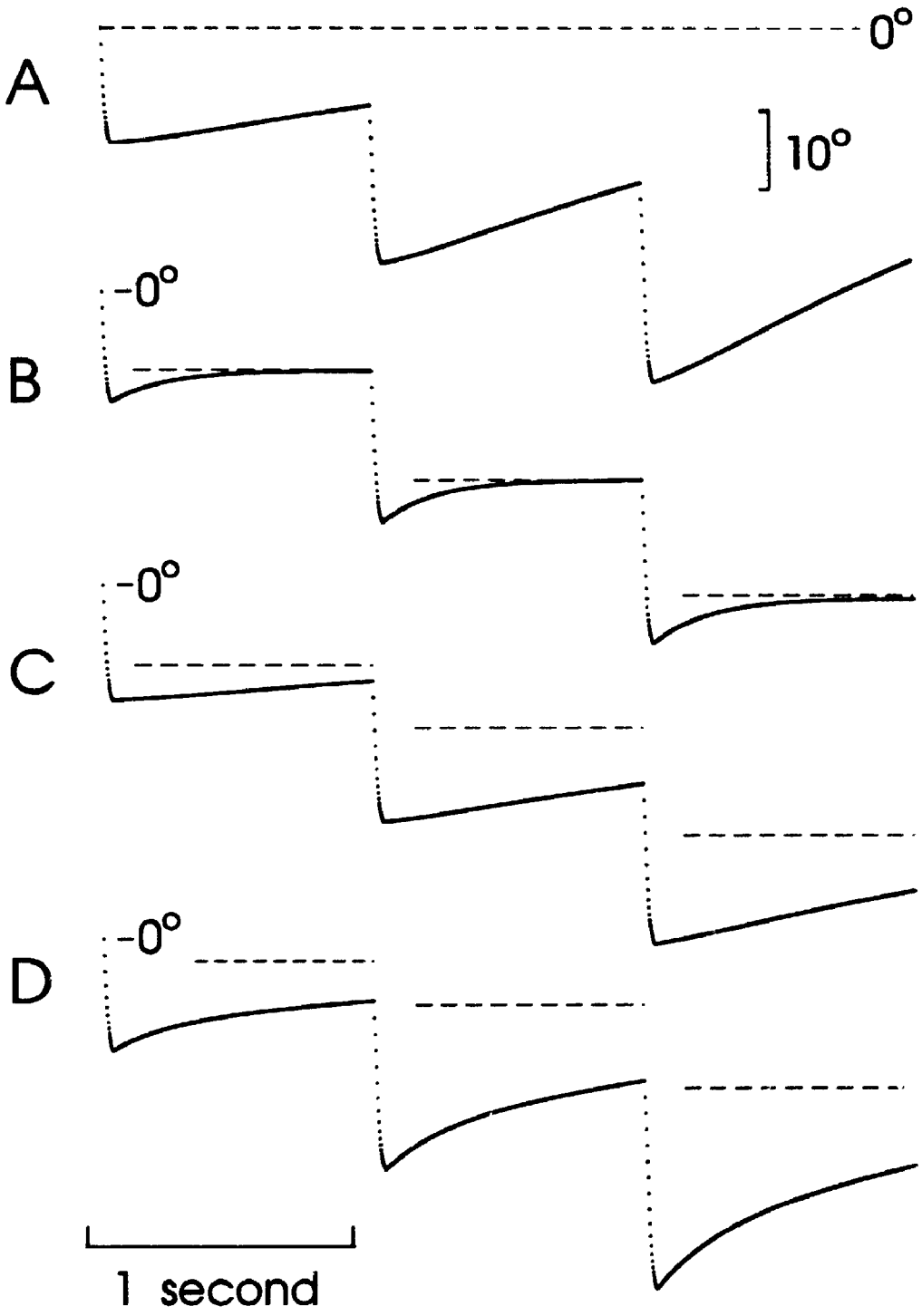
0°
A
10°
-0°
B
-0°
C
-0°
D
1 second

position, but rather to a value determined by charge in the intact integrators (----).

Finally, if some integrators leak rapidly, others slowly, and others not at all, (Fig. 59 D), there was a combination of the position and saccade related effects illustrated in B and C. The drift still had multiple null positions. Moreover, the drift then had more than one time constant, with the rapid drift correlated more to the saccade (for reasons discussed above) and the slow drift correlated more to current position. Thus, this model predicts three features of the experimentally observed drift that could not be accounted for by a single leaky integrator[1]: multiple null positions (Figs. 47-55), multiple time constants (Figs. 52, 53), and dependence of drift rate on the previous saccadic history as well as current eye position (Figs. 54-57).

One limitation of this study was that most of the experiments were performed in the light, which may have affected stabilization of the eye (Straube et al. 1992). However, turning off the lights during experiments in animals LAR and BAR did not affect the

1 Manipulations of the single integrator model can simulate some of the results, but this model still fails for fundamental reasons. Post-saccadic drift can be simulated by two means with a single integrator: (1) reducing the gain of saccade velocity input to the integrator produces a pulse-step mismatch with saccade-related drift, and (2) reducing the gain of the positive feedback loop that maintains integrator activity produces a leaky integrator and position-dependent drift. In the illustrated simulations, both gains were equally reduced to simulate post-synaptic inhibition, but the integrating positive feedback loop was so much more sensitive that the position-dependent drift completely dominated. By adding a much greater pulse-step mismatch (decreasing input gain to the integrator by 1000 times the decrease in feedback gain), the model was able to simulate a combined position-dependent and saccade-dependent drift like the data. However this model still failed to maintain eye positions at multiple null positions, because the single integrator will always leak to zero activity. In order to simulate the multiple, saccade-related null positions observed in the data, there must be a different DC bias in the integrator pathway after each saccade. Such a tonic non-zero level of activity can only be maintained by another non-leaky integrator that also receives input from the saccade generator. However, a second integrator above or below the first would not allow normal saccadic behaviour, because the output of the indirect pathway would no longer be position. Therefore, this non-leaky integrator must be in parallel with the leaky integrator, returning us to the other model.

fundamental characteristics of the drift (e.g. Figs. 51 & 54). Furthermore, visualstabilization does not the explain sudden reversals in drift direction (Fig.53 A), or the saccade dependence of very rapid drift (Fig. 57) (Cannon and Robinson 1987). Thus, the data strongly suggests that the integrator is divided into parallel independent sub-integrators, requiring a restricted, i.e. modular pattern of lateral connections.

6.4.2 *Rebound nystagmus, integrator saturation, and the null range.*

Rebound nystagmus has been reported during recovery from damage to the integrator for horizontal eye position (Cannon and Robinson 1987), in cerebellum-damaged patients (Bondar et al. 1984), in normal subjects in the dark (Gordon et al. 1986), and was also observed in the present investigation. Rebound nystagmus is characterized by a progressive decrement in drift towards center during a series of eccentric saccades (Fig. 55 A), and then a drift away from center after the subsequent central saccade (Fig. 53 A) (Gordon et al. 1986; Leigh and Zee 1991). This deficit could result from a simple pulse-step mismatch, but also emerges from the equivalent deficit that occurs during partial inactivation integrators in parallel. Whereas a single leaky integrator cannot simulate rebound nystagmus after a saccade towards center (Fig. 60 A), this is an inherent prediction of the parallel integrator model (Fig. 60 B). The parallel model also simulates the subsequent reversal of drift direction towards center observed in Figure 53 A. Drift is dominated first by the faster, more saccade-dependent drift and then by the slower, seemingly position-dependent drift. This model suggests that the mechanism for rebound nystagmus depends on function of intact portions of the integrator, as suggested previously (Leigh and Zee 1991).

The presence of intact integrators is particularly important for stabilization of gaze during a series of saccades to the same target. With a single leaky integrator model there is no opportunity to stabilize gaze, for example at 20° or 40° down (Fig. 61 A). With

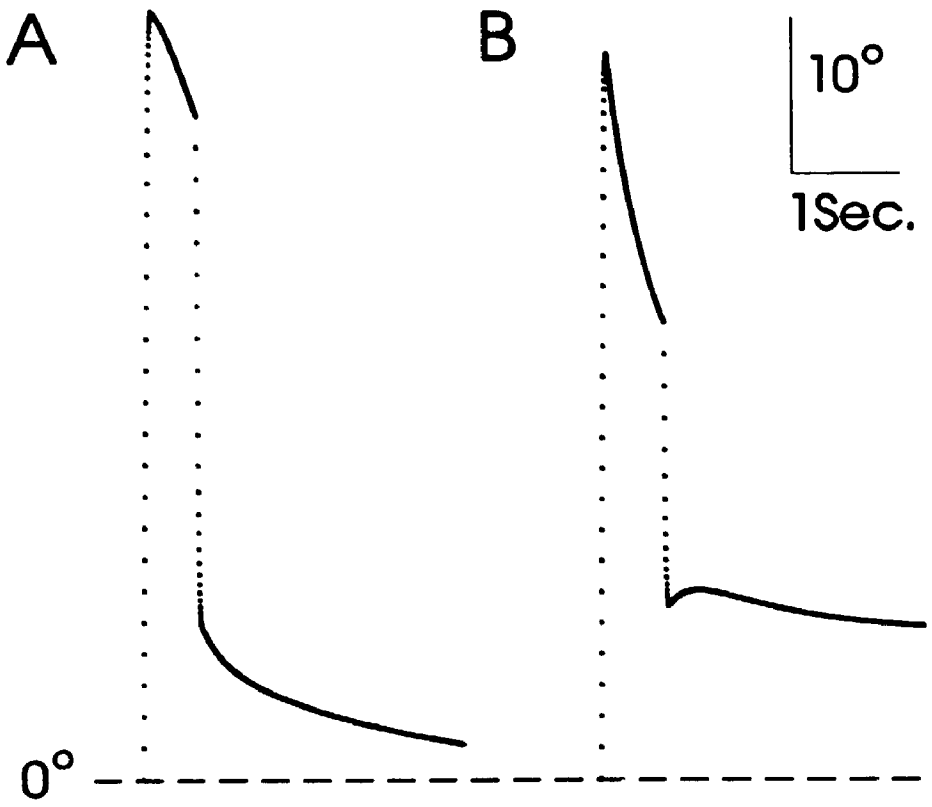

FIGURE 60. Reversal of drift direction with the multiple integrator model, but not the single integrator model. Simulated eye position is plotted (at 4 millisecond intervals) against time. In each case the eye first saccades upwards from zero towards 50° up, and then after 600 milliseconds saccades downwards towards a position 10° up from zero. **A**: The position signal is generated by a single integrator leaking with a 2 second time constant. **B**: The position signal is generated by 10 parallel integrators of which 30% are completely inactivated, 40% leak with a 1 second time constant, and 30% are intact.

20% of the parallel integrators completely inactivated and 30% leaking with various time constants (100, 200, and 500 ms), simulated eye position stabilized within ~3 seconds, no matter how eccentric the target (Fig. 61 B). This stabilization occurred because the intact integrators "charged up", while the damaged integrators leaked to a stable level.

In the experimental data, animals could not use this strategy to stabilize gaze beyond the progressively decreasing null range (Fig. 55 B). The model used in Figure 61 B failed to show this behaviour because its intact integrators were allowed to charge up indefinitely. Real neurons cannot charge up indefinitely; their firing rates must saturate at a some maximum, and a minimum obviously limited at zero. Figure 61 C is the same simulation as B, except the integrator neurons now saturate at -300 or 300 Hz (comparing to 0 and 600 Hz in more realistic neurons that modulate about a baseline). With our model parameters, this corresponds to a maximal total position signal of $\pm$ 50°. With such a saturation, and 50% of the integrators leaking, the intact neurons could only maintain a maximal total position signal of $\pm$25°. Therefore, the series of saccades towards 20° down are unaffected by this saturation, but eye position can no longer be stabilized at 40° down, no matter how many saccades occur. Figure 61 D uses the same saturating model, but now only 20% of the integrators are intact, increasing the magnitude of drift and further limiting the maximal range of eye stabilization to $\pm$10°. Thus, the percentage of intact integrator units and their saturation limit ultimately determines the null range.

If we assume that integrators normally saturate near the boundary of the oculomotor range, as simulated above, then the fraction of intact integrator units could be estimated as null range / oculomotor range / 2. This assumption is supported by our observation that the null range begins to decrease with the first signs of ocular drift. It is also supported by the rapid increase in drift velocity (end point nystagmus) observed near the oculomotor limits of normal humans, particularly under fatiguing conditions that

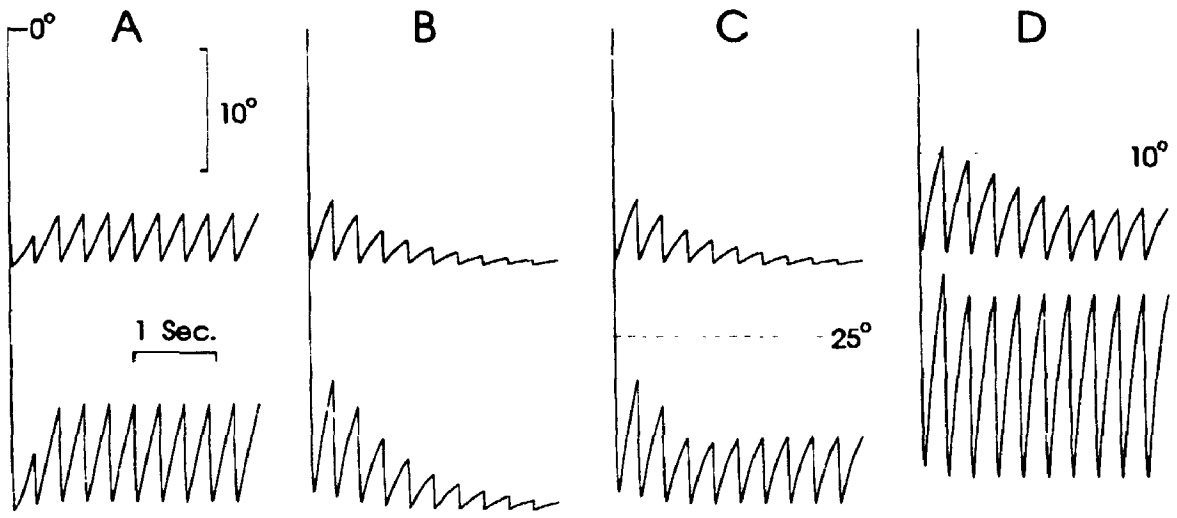

FIGURE 61. Vertical nystagmus patterns using the single integrator model (**A**) and the multiple integrator model (**B-D**). Simulated eye positions are initialized to zero and then plotted during three seconds of saccades occurring at intervals of 300 milliseconds. In each case a series of saccades directed towards 20° down is superimposed over a second series towards 40° down. **A**: The position signal is generated by a single integrator which leaks with a time constant of one second. **B**: The position signal is generated by ten parallel integrators of which 50% are intact, 20% have been completely inactivated, and the other three leak with various time constants (100, 200, 500 milliseconds). **C**: Same as previous simulation, except that the integrating tonic neurons have been given a saturation at 300 Hz (normally corresponding to 50° eccentricity). **D**: As in previous simulation, except that three additional integrators have been inactivated. The horizontal lines (—) in C and D indicate the maximal eccentricity of eye position that can be maintained by the intact integrators.

might reduce the saturation point (Eizenman et al. 1990). Such boundary saturation would confer a useful safety feature to the oculomotor system: eccentric eye movements, such as an uninterrupted VOR slow phase, would be prevented from over-charging the integrator to represent positions beyond the plant's mechanical range. In general, such a feature would prevent excessive muscular torques against an unyielding mechanical limit, and likewise prevent errors in position feedback signals that are thought to be important for programming of various movements (Flanders et al. 1992; Jürgens et al. 1981; Robinson 1975; Zipser and Anderson 1988).

6.4.3 *Anatomical organization of integrator coordinates.*

The oculomotor velocity-to-position transformation is thought to be distributed between several interdependent brainstem nuclei (King and Leigh 1982; Cannon and Robinson 1987; Cherron and Godaux 1987; Fukushima 1987; Tweed and Vilis 1987; Crawford and Vilis 1991). If our above discussion is correct (# intact integrator units = null range / oculomotor range / 2), then Figs. 49A and 50 suggest that 10-50% of the vertical integrators were unaffected by unilateral muscimol injections. These intact integrators may have resided in unaffected parts of the INC or in other nuclei. Torsional null ranges were consistently narrow (Fig. 49 A), and torsional drift was more rapid than vertical drift during INC inactivation (Crawford et al. 1991; Crawford and Vilis 1992). This suggests that torsional integration may be more completely localized to the INC than vertical integration.

The observation that unilateral INC inactivation abolished both clockwise and counterclockwise position holding supports the view that the two sides of the integrator are interdependent (Cannon et al. 1983; Galiana and Outerbridge 1984: Cannon and Robinson 1987; Anastasio and Robinson 1991). Despite this interdependence, their inputs appear to be symmetrically opposite. Unilateral stimulation suggests that the

integrator receives its main excitatory input from the contralateral semicircular canals and ipsilateral burst neurons (Cannon and Robinson 1987; Chapter 5, Figure 41). Unilateral injections of kainic and ibotenic acid did not consistently support this scheme, but the excitatory / inhibitory effects of these neurotoxins is not clear (Cannon and Robinson 1987). However, injections of the inhibitory GABA agonist muscimol gave results that agreed with the stimulation data. Unilateral injections into the nucleus prepositus hypoglossi produced contralateral shifts in the null position of horizontal drift (Yokota et al. 1992). Similarly, injection into the left INC gave a CW shifted null range and right injection gave a CCW shifted null range. Similar torsional shifts were reported after unilateral inactivation of the INC in normal and labyrinthectomized cats (Anderson 1981; Fukushima et al. 1992). These shifts and concomitant torsional drift were also reported in humans diagnosed with "see-saw" nystagmus, who had unilateral damage to the INC region (Halmagyi et al. 1990, Halmagyi and Hoyt 1991).

These null point shifts can be accounted for by Cannon et al.'s (1983) scheme of a bilateral, mutually inhibitory pair of neurons with opposite inputs, in this case with excitatory CCW inputs on the left and CW on the right. Inhibition of one side should disrupt both CW and CCW integration, and block transmission on that side. The remaining contralateral channel would allow background activity of integrator neurons and their inputs to simply pass through, and the unopposed net output would produce the observed shifts in the torsional null position (Anderson's 1981; Fukushima et al. 1992).

6.4.4 *General implications of integrator modularity.*

It is a dogma in neuroscience that the brain improves signal-to noise ratios by using a large number of channels (e.g. axons in a tract). This is sometimes called redundant coding, although this incorrectly implies an unnecessary duplication. The present investigation illustrates that a similar principle holds for the neural computations

preformed within the grey matter. In particular, the data suggests that neural velocity-to-position integration is distributed across an array of parallel independent sub-integrators. This requires that lateral connections within the integrator network are restricted, yielding a modular pattern similar to that proposed by Cannon et al. (1983). The advantages of such modular channels in parallel processing include a relative immunity to microlesions and other random computational errors, maintenance of some fraction of function after more extensive damage, and potential for functional recovery through local parametric adjustments (Cannon et al. 1983). Similar principles may hold for a variety of computational tasks performed by the brain. For example, with local damage to a retinotopic map, a small scotoma would be preferable to degradation of the entire visual image. This may be an important consequence of the modular patterns of neural connectivity observed throughout the brain (Mountcastle 1957; Hubel and Weisel 1959; Purves et al. 1992)

7 SUMMARY AND CONCLUSIONS

7.1 INTRODUCTION

The experiments described in this thesis used correct recordings of 3-D eye movements to examine four major questions that were either neglected or unanswerable by previous one and two-dimensional recordings: (1) the implications of rotational kinematics for motor control, (2) the location and organization of the vertical / torsional oculomotor integrator, (3) the coordinate axes utilized by this integrator and the saccadic burst generator, and (4) the relationship between these intrinsic coordinate systems and constraints on the behavior they produce, i.e. Listing's law.

7.2 KINEMATICS OF THE VESTIBULO-OCULAR REFLEX

Chapter 3 represents the first correct evaluation of VOR slow phase axes. Previously it was assumed that VOR slow phases rotate the eye about axes that are collinear with those of the head, which would be optimal for stabilization of eye orientation in space. This thesis shows that slow phases are collinear for some axes of head rotation, but for other directions systematic deviations from collinearity occur. Slow phase axes tend to tilt away from axes with low gain. In this respect, the VOR acts like a linear operator (i.e. a matrix) on its vector input (head velocity) as predicted by Robinson (1982). Gain appears to be lowest about an axis fixed in the head. We observed a remarkable coincidence between the location of this axis and the primary gaze direction orthogonal to Listing's plane, suggesting that the saccadic and VOR systems share intrinsic coordinates. As a result, the VOR is most accurate in both magnitude and direction for head rotations about axes in Listing's plane.

Contrary to previous suggestions (Ferman et al. 1987b), Listing's law cannot be a product of plant mechanics, because even slow phase axes in Listing's plane violate

Listing's law. This is the consequence of the laws of rotational kinematics (Tweed and Vilis 1987), and is required for proper stabilization of the retinal image. The fact that these positions were held at the end of head rotation shows that the indirect pathway of the VOR is more complex than the simple integrator proposed by Robinson (1975). This pathway must also incorporate the laws of rotational kinematics by multiplying the eye velocity signal by position feedback at a point upstream from the integrator.

Finally, violations of Listing's law that occur during slow phases are corrected by quick phases. They do this by directing the eye to a plane of positions that anticipates the slow phase violations. This suggests that saccades and quick phases utilize common brainstem circuitry at the Listing's law operator, and that maintenance of zero torsion is not just a default strategy, but rather a specific mandate of the oculomotor system.

7.3 COORDINATE SYSTEM OF THE BURST GENERATOR

The object of the experiments described in chapter 4 was to determine the axes of eye rotation generated by burst neuron populations in the rostral interstitial nucleus of the medial longitudinal fasciculus (riMLF), and the coordinate system that they collectively define. Preliminary to this task, we used electrical microstimulation and pharmacological inactivation to confirm that the riMLF provides velocity signals for rapid movements to both eyes, upstream from the neural integrator (King and Fuchs 1979).

Our data shows that the riMLF is functionally segregated into four burst populations. These populations control rotations similar to those controlled by the vertical eye muscles and semicircular canals (Büttner et al. 1977; Robinson and Zee 1981), but differ because they also control horizontal rotations. Units which burst before upward or downward saccades were recorded intermingled in each side of the riMLF, as previously reported (Büttner et al. 1977; King and Fuchs 1979). Similarly, unilateral inactivation reduced vertical velocities by $\sim 50\%$. However, unilateral inactivation also abolished one

direction of torsional rapid eye movements, and unilateral stimulation produced torsional rotations in the opposite direction: clockwise during right stimulation and counterclockwise for the left. Surprisingly, unilateral riMLF inactivation also reduced horizontal velocities, and induced contraversive oblique tilts in the axes of vertical and horizontal saccades. This suggests that the riMLF uses a coordinate system that enables it to generate rotations about any axis: the two right populations generate clockwise-upward-leftward and clockwise-downward-rightward rotations respectively, and the left riMLF populations generate counterclockwise-upward-rightward and counterclockwise-downward-leftward rotations.

Finally, we found a remarkable alignment between oculomotor burst neuron and Listing's plane, which varies with respect to anatomical landmarks. Unilateral riMLF stimulation rotated the eye about an axis aligned with the primary gaze direction orthogonal to Listing's plane. Furthermore, the intact rapid eye movement axes after unilateral riMLF inactivation aligned with Listing's plane, rather than external anatomical landmarks. Thus, the coordinate system of burst neurons is symmetric across Listing's plane, a product of their own emergent behaviour.

7.4 THE NEURAL INTEGRATOR: 3-D ORGANIZATION AND MECHANISM.

Two results reported in chapters 5 and 6 show that the interstitial nucleus of Cajal (INC) is the neural integrator that holds vertical and torsional eye positions. First, electrical stimulation of the INC produced conjugate, constant - velocity torsional eye rotations that held their final position. Second, INC inactivation produced an almost complete failure to hold post-saccadic vertical and torsional eye positions, without abolishing saccades themselves. Based on previous experiments (e.g Cannon and Robinson 1987) this suggests that the INC is the integrator for all vertical and torsional eye movements.

These experiments also suggest that the functional coordinate system of the INC is similar to that of the muscles, canals, and riMLF. Single unit recordings confirmed that upward and downward position-related activity was intermingled on each side (King et al. 1981). However, right INC stimulation and left INC stimulation evoked clockwise and counterclockwise movements respectively, whereas the null point of torsional drift was shifted in the opposite direction during unilateral inactivation. Thus the right INC controls clockwise-up / clockwise-down signals, and the left INC controls counterclockwise-up / counterclockwise-down.

The positional drift observed during INC inactivation showed several characteristics that could not be accounted for by leak in a single integrator. Vertical eye position did not drift with a simple position - dependent exponential rate towards a single null position. Rather, position drifted toward multiple resting positions within a range that decreased as the deficit progressed. In addition, the drift appeared to have multiple time constants. Finally, the rate of post-saccadic drift was dependent on metrics of the previous saccade as well as current eye position. This suggests that INC neurons do not utilize an evenly distributed pattern of connections that would respond to damage like a single leaky integrator. Rather, the integrator network uses a compartmentalized or modular pattern of connectivity, as proposed by Cannon et al. (1983). Such modularity confers a relative immunity to microlesions and other random localized computational errors, and partial conservation of function after larger lesions.

7.5 BASIC AND CLINICAL IMPLICATIONS FOR OCULOMOTOR CONTROL

With the inclusion of the experiments described in this thesis, oculomotor physiologists can now explain the basic premotor mechanisms involved in generating vertical and torsional eye movements. Each side of the riMLF burst generator and INC position generator excites the ipsilateral inferior eye muscles and contralateral superior

muscles (Fig. 62). This requires that burst neurons on both sides of the riMLF be coactivated to generate a purely vertical saccade, in order to cancel out the torsion that they generate. For example, to make an upward saccade from primary position, upward-tuned burst neurons on both sides are equally activated. These excite motoneurons for the inferior oblique and superior rectus muscles of both eyes, whose torsional torques would cancel, leaving a net upward torque (Figure 62). The burst neurons also excite the INC ipsilaterally, which generates the signal necessary to sustain the muscle tone that holds post-saccadic eye position. To generate torsional quick phases, burst and tonic neurons on just one side of the brain are activated so that the vertical signals cancel.

This scheme also gives a simple paradigm for localizing and interpreting midbrain damage in clinically observed oculomotor disorders, as detailed in chapters 4 through 6. Damage to the riMLF should be associated with deficits in vertical and torsional rapid eye movements, whereas INC damage should produce a vertical or torsional gaze-evoked nystagmus and affect slow eye movements in these directions. The rebound and end-point components of such nystagmus are accounted for by partitioning the integrator model into parallel independent sub-units. Finally, unilateral damage should cause eye drift and/or abnormal saccades to shift torsional eye position towards the other side.

7.6 GENERAL IMPLICATIONS FOR SYSTEMS NEUROSCIENCE

In this thesis, I have attempted to use eye movements as a window into general principles governing brain function. For example, maintenance of the position-dependent torsional eye position produced by VOR slow phases showed that the VOR indirect path incorporates the correct 3-D model of the oculomotor plant. This requires multiplication of the velocity signal by position signal feedback, which contradicts the recent suggestion that neural commands for movements in space are based on 2-D retinal error signals, without requiring knowledge of position (Goldberg and Bruce 1990; Waitzman et al.

FIGURE 62. Midbrain structures involved in generating vertical and torsional saccades. Brain structures and eyes are viewed from above the subject. Only excitatory connections are illustrated, but symmetrically opposite inhibotory connections would be expected to operate in push-pull fashion. During a saccade, neurons in the riMLF send a burst of activity directly to ipsilateral motoneurons of the third and fourth cranial nerve nuclei and to the ipsilateral INC (see Figure 38 for more detail). The INC converts this burst signal (and similar net velocity inputs from the contralateral semicircular canals) into a position signal which tonically excites the ipsilateral motoneurons. Motoneurons of the right brain innervate eye muscles that rotate the eyes clockwise and vertically, while motoneurons of the left brain innervate the counterclockwise-vertical muscles. Thus, the riMLF, INC and moto-neurons excite the ipsilateral inferior muscles and contralateral superior muscles. *Thick lines* projecting from the eyes show the axes and direction of rotation produced by the individual muscles. The *small axes* at the top of the figure summarize the rotations controlled by neurons on each side. **riMLF**, rostral interstitial nucleus of the medial longitudinal fasciculus; **INC**, interstitial nucleus of Cajal; **III**, oculomotor nucleus; **IV**, trochlear nucleus; **SO**, superior oblique muscle; **SR**, superior rectus; **IR**, inferior rectus; **IO**, inferior oblique.

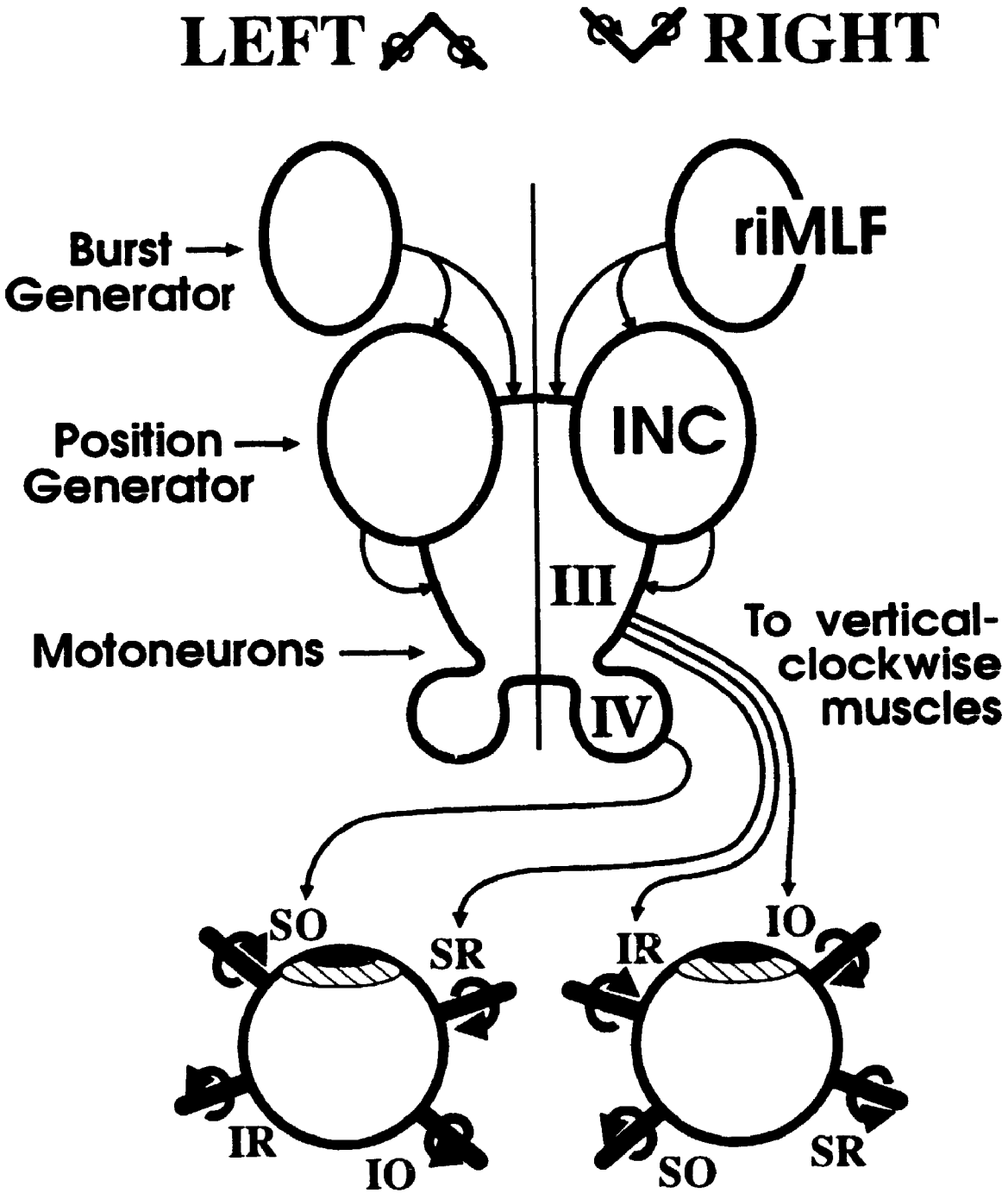
LEFT
RIGHT
Burst Generator
riMLF
Position Generator
INC
III
Motoneurons
To vertical-clockwise muscles
IV
SO
SR
IR
IO
IR
IO
SO
SR

1991). Furthermore, since multiplication is non-linear, this is contrary to the commonly held view that the brain makes linear approximations to non-linear problems (Flanders et al. 1992). The position feedback loops required by the laws of rotational kinematics should be even more critical for movements produced by large limb rotations about multiple joints.

Our measurement of burst neuron coordinates suggests that wherever intrinsic kinematic constraints on motor behaviour are observed, they will have correlates in neural coordinate systems. A combination of two factors might explain this association. First, VOR Kinematics (Chapter 3) show that behavioral constraints reflect a constraint on neural activity, and second, studies of the visual system have shown that neural activity influences development of functional connections (Shatz 1992). Therefore, constraints on neural activity may interactively influence the development of motor coordinate systems.

Finally, it has been suggested that many neural tone generators may utilize neural integrators (Robinson 1989). For example, integrators could be used to maintain the set point for the stretch reflex. If so, then principles observed in the oculomotor integrator will provide a blueprint for further investigations. Functional compartmentalization of network connections is of particular interest, because it confers robustness for computations such as integration that are highly sensitive to random errors in distributed network activity. This may be an important consequence of the modularity (e.g columnar organization) observed throughout the brain.

APPENDIX I. QUATERNION MULTIPLICATION

This section defines multiplication and division of quaternions. Recall that quaternions are composed of a scalar component (q_0) and a three components (q_1,q_2,q_3) along vector bases (i,j,k). Quaternions are multiplied componentwise like polynomials (Tweed 1987; Westheimer 1957). Multiplication of the scalar component q^1_0 at q^2 is indistinguishable from scalar multiplication of a vector. Components of the vector part are multiplied like scalars, but the basis is governed by the following rules:

$$i^2 = j^2 = k^2 = -1$$

$$ij = -ji = k \qquad jk = -kj = i \qquad ki = -ik = j \qquad (10)$$

Thus, multiplication between vector components contributes to a different component in the product. Furthermore, the order of the two quaternions gives different results, i.e. quaternion multiplication does not commute.

Division by a quaternion (q) is achieved by multiplying by the inverse of q (q^{-1}). As with scalars, the product of a non-zero quaternion and its inverse is one, i.e. (1,0,0,0). The inverses of the unit quaternions used for this thesis were derived simply by multiplying the vector components of q by negative one.

In addition to representing rotational displacements, quaternions (q) were used to implement coordinate transformations by rotating another quaternion (p) about the axis n and angle α of q (from equation 6), as follows:

$$qpq^{-1} \qquad (11)$$

Where p can also be a vector, treated as a quaternion with a zero scalar component.

APPENDIX II. INTERNAL FEEDBACK LOOPS

In this thesis data has been interpreted according to two implicit assumptions: (1) the saccade generator upstream from the riMLF is updated between saccades about abnormal eye positions produced by electrical / pharmacological perturbation of the INC and riMLF, and attempts to correct these, and (2) the INC and riMLF operate in feed-forward during saccades. Specifically, these assumptions were incorporated in the model used to simulate neural integrator failure (Chapter 6), and when interpreting the axes of rotation generated by intact burst neurons during partial riMLF inactivation. Although feedback control of saccades is not a central issue in this thesis, some preliminary data is presented here to justify these assumptions.

Current models of the brainstem saccade generator place burst neurons within two functionally different internal feedback loops. The first loop computes the initial motor error that drives burst neurons by comparing desired eye position to an estimate of current position that arises from the output of the neural integrator (Jürgens et al. 1981) This comparison and the resultant initial motor error must be three-dimensional in order to generate saccades that correct violations of Listing's law produced by head movements (Chapter 3), as predicted by Tweed and Vilis' (1990) 3-D model of the saccade generator. Such a model predicts that the initial motor error that drives burst neurons will attempt to correct torsionally deviated eye positions produced by INC / riMLF stimulation or inactivation.

There are several reasons to believe that the INC and riMLF are within such a feedback loop. First, following unilateral stimulation of either the INC or riMLF, the ocular torsion that resulted was negated by the next saccade. Second, during the initial stages of torsional drift following INC inactivation, a nystagmus pattern resulted with the quick phases directing the eye back to Listing's plane. Finally, such a feedback loop in

3-D would explain why after our unilateral riMLF inactivations the intact burst neurons appeared to be less active and effective than might be expected, for example producing less than 50% normal vertical eye velocity (Figs. 29, 31). After the intact neurons drove the eye torsionally out of Listing's plane, a torsional error signal would arise which would tend to inhibit the intact neurons. Thus, the INC and riMLF appeared to be within the feedback loop that determines initial saccadic motor error, and this error signal appeared to be three-dimensional, rather than the two-dimensional signal proposed by some (Hepp 1990; Van Gisbergen et al. 1992).

Most models also place the burst neurons within a short - latency "local" feedback loop which guides an ongoing saccade to the desired eye position (Becker et al. 1981; Van Gisbergen et al. 1981; Scudder 1988). In its original form, Robinson's model subtracted feedback from the integrator from the desired eye position signal to get the current motor error signal that drives burst neurons during a saccade (Van Gisbergen et al. 1981). To date, only a few investigations have directly tested the local feedback model (Becker et al. 1981; Jürgens et al. 1981). This model predicts that during integrator failure, the feedback signal will underestimate the saccadic displacement, and so saccades will undershoot.

To test this prediction, we examined the vertical metrics of trained saccades between LED targets in animals MAR and BAR, during INC inactivations that gave apparent vertical integrator failure. We found that such saccades did not overshoot vertically (Fig. 63). Rather, they tended to be vertically hypometric. Similar results were obtained in horizontal saccades by Kaneko and Fuchs (1991) during inactivation of the prepositus hypoglossi region in the monkey. This slight saccade undershoot was in qualitative agreement with that produced during our simulations in chapter 6, using a model in which the integrator is downstream from the local feedback loop. The undershoot in the simulation was simply due to an insufficient position signal, which normally made a

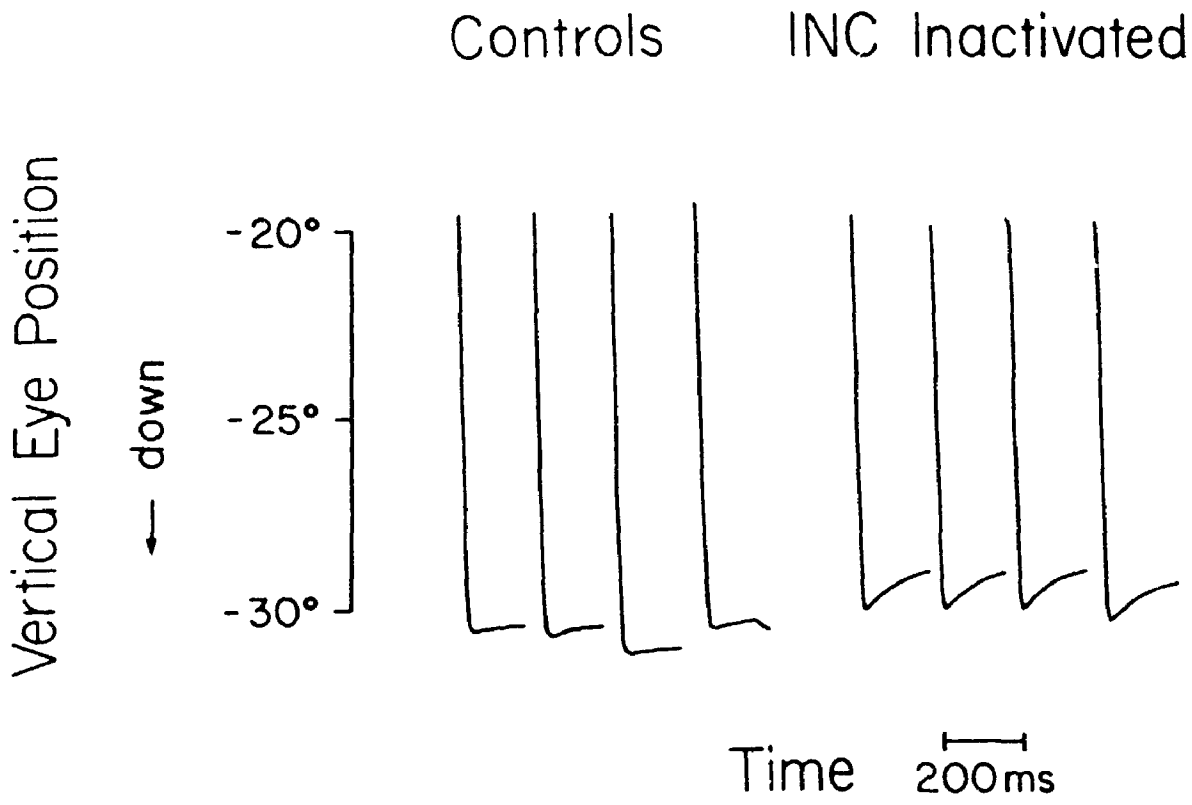

FIGURE 63 Failure of vertical saccades to overshoot during INC inactivation. Vertical eye position is plotted against time for a series of saccades towards the same downward target. The illustrated saccades were made before and after injection of mucimol into the INC region of a trained animal.

small contribution to saccade metrics. Any further undershoot could be caused by loss of a velocity signal from the burst component of INC neurons, but this would be difficult to distinguish from spread of muscimol to the nearby riMLF or motoneurons. Thus, the integrator, and INC in particular, does not appear to take part in local feedback.

More recent models of the local feedback loop have computed the current error signal by subtracting an estimate of current saccade displacement signal (produced by a separate, resettible integrator that receives input from burst neurons) from a desired displacement signal (Becker et al. 1981; Scudder 1988). The latter feedback loop would allow saccades to be accurate despite variations in burst neuron activity, as long as some burst neurons can drive the eye in the desired direction. Such a feedback loop should compensate for partial vertical burst neuron inactivation by increasing the duration of drive to the remaining neurons. Thus, these models predict that during partial riMLF inactivation animals would still produce large accurate saccades but with abnormally long durations. If the burst neurons are not in the local feedback loop, saccades should be vertically hypometric with normal durations.

As predicted by both models, the ratio between vertical saccade amplitudes and their durations dropped. However, the distribution of saccade amplitudes suggested that the burst neurons were not in the local feedback loop. Figure 64 illustrates that as inactivation of the riMLF progressed, the vertical component of saccades became smaller and smaller. The animals reached visual targets by a series of hypometric saccades. This was examined more rigorously in the two trained animals, MAR and BAR. Since a local feedback mechanism could not be effective if all of the burst neurons for a particular saccade direction have been inactivated, we concentrated on data from the initial milder stages of unilateral inactivation and oblique saccade directions that were less impaired (see Chapter 4). In these conditions, animals made saccades that had normal duration and nearly normal horizontal size, but were vertically hypometric (Fig.

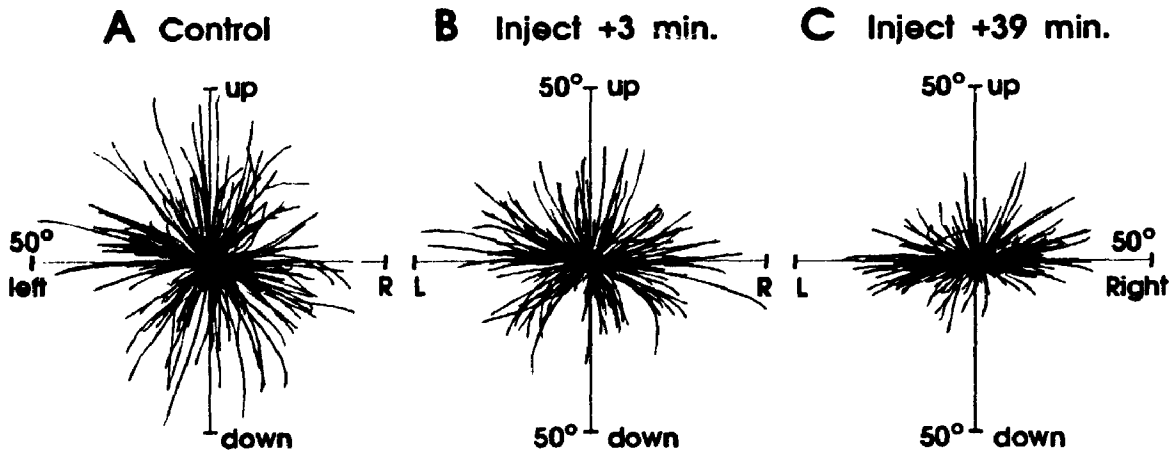

FIGURE 64. Reduction in vertical saccade magnitude during unilateral riMLF inactivation. Change in gaze direction is plotted (A) before, (B) 3 minutes after, and (C) 39 minutes after unilateral muscimol injection. Gaze directions (not quaternions) are shown, but the starting point of each saccade has been shifted to the origin. In each case, visual targets were presented so as to encourage large vertical and oblique saccades.

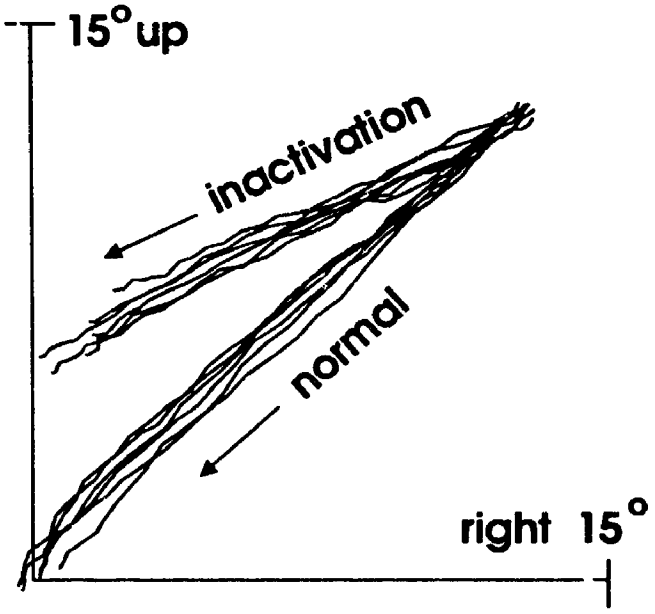

FIGURE 65. Accuracy of goal directed saccades following unilateral riMLF inactivation. Gaze directions (not quaternions) are shown for multiple saccades from a target placed 20° obliquely (up and right) towards centre, before muscimol injection and following muscimol injection to the right riMLF. Saccade duration before injection was 34.3 ± 3.4 ms (mean ± SD) and 33.5 ± 5.9 ms after injection. Cell recordings and stimulations indicated that there were no motoneurons near the site of injection.

65). These observations are not consistent with participation of riMLF burst neurons in a local feedback loop.

When the burst deficit was more advanced, particularly in the more impaired oblique directions, hypometric saccades were often followed by a second slower movement (duration 30 - 60 ms, peak speed < 200° per second) that caused gaze to curve slightly towards the target. These small movements were sometimes continuous with the saccade and sometimes separate within a series of consecutive trials. In addition, they appeared to be dependent on state of motivation, being more prominent in goal directed saccades performed for a reward than in random saccades. This variability is not consistent with the predicted actions of a local feedback loop, which would operate in a machine-like fashion to guide and accurately terminate every saccade. However, it is possible that they were triggered by the longer feedback loop. The main point for the purpose of this thesis is that these saccades were to slow and small to significantly affect the post-inactivation axis measurements in Chapter 4.

The participation of burst neurons in local feedback was also evaluated in MAR and BAR by microstimulating the riMLF (20-50 uA, 500-100 Hz, 10-20 ms) during goal directed saccades. In this case, local feedback models predict that the stimulus-evoked perturbation will be corrected almost instantaneously, causing the eye to reach an accurate final position. The results of intrasaccadic microstimulation are illustrated in figure 66 A. This figure shows that riMLF stimulation perturbed the saccade in two ways. First, there was a torsional deviation of the eyes as described above. Superimposed on this effect was a pause of variable magnitude in the preprogrammed vertical and horizontal components of the saccade. Since vertical burst neurons are not known to inhibit horizontal neurons and the pause only occurred with high stimulation frequencies and intensities, this effect may have been due to antidromic activation of burst neuron inputs, most likely omnipause neurons. Following the pause, the saccade

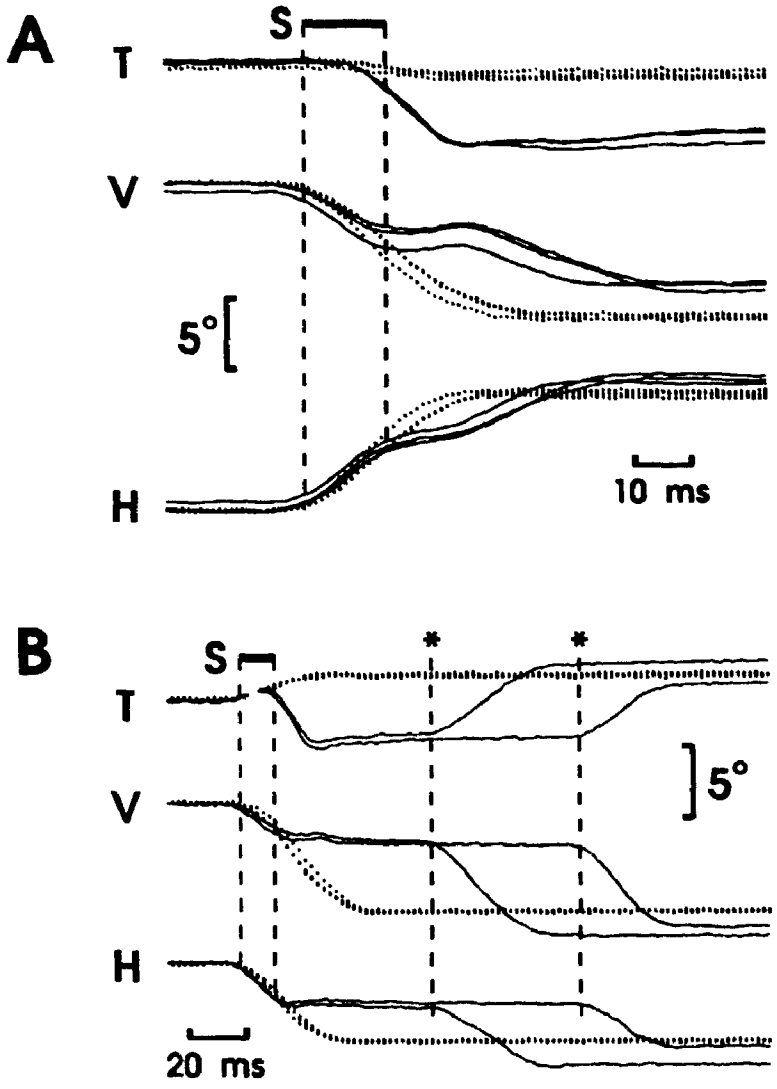

FIGURE 66. Perturbation of goal directed saccades by brief unilateral riMLF stimulation. Position quaternion components (T, H, V: torsional, horizontal, vertical) are plotted against time, in Listing's coordinates. The duration of stimulation (fifteen 0.5 ms pulses, 60μA, 1000 Hz) is indicated by the bars (S). **A**: Three normal downward-leftward saccades (dotted lines) superimposed with three perturbed saccades (solid lines) that paused and then continued without correcting the stimulus-evoked torsion. **B**: Three normal downward-rightward saccades (dotted lines) superimposed with two perturbed saccades (solid lines) that came to a complete halt, and were then followed by corrective saccades (*) at low latencies that eliminated the stimulus-evoked torsion.

resumed and horizontal eye position did not undershoot the target position. This result is similar to the effect of intrasaccadic pause neuron stimulation (Becker et al. 1981) and suggests that the unknown part of the saccade generator that is being inhibited (possibly upstream from riMLF neurons) is within a local feedback loop. In contrast, the direct effect of stimulating riMLF burst neurons, a large CCW deflection with a small upward component, was not corrected when the saccade resumed. Both monkeys failed to correct these primarily torsional stimulus-induced perturbations during 20° saccades in all directions. This strongly suggests that the riMLF burst neurons themselves were not within the local feedback loop.

Is there any way to determine the latency of the longer feedback loop that generates initial motor error? Depending on stimulus intensity and saccade direction, the pause effect seen in figure 14(a) was often strong enough to terminate the saccade completely. When this occurred, a second discrete saccade usually occurred (Fig 66 B, *) at a very short latency (< 100 ms) that brought gaze onto target and also always corrected the torsional deviation. The lowest latency observed for such correction was 30 ms. Similarly, when brief riMLF microstimulation was delivered just before a saccade, the resulting torsion was corrected at latencies as low as 30 ms. This is a relatively rapid correction, but still not fast enough to guide and terminate saccades. For example, a 30 ms overshoot could almost double the size of a saccade.

Thus, the riMLF burst neurons appeared to be within the longer 3-D feedback loop required to compute initial motor error. This loop apparently operates at latencies that are too long for moment-to-moment saccade guidance, but much shorter than the normal intersaccadic interval. However, the evidence pointed against participation of either the INC or riMLF in a local feedback loop that produces the current motor error signal for guiding and terminating saccades. Thus, our assumption that the INC and riMLF operated in feed-forward fashion during saccades appears to be justified. This suggests

that our interpretations based on kinematics of saccades during riMLF / INC inactivation were not obscured by feedback effects.

APPENDIX III. ANATOMIC LOCATIONS OF MUSCIMOL INJECTIONS

Based on our functional identifcation (Section 2.2.5), the vertical-torsional oculomotor integrator circuits appeared to be centered at stereotaxic coordinates anterior 7 mm, lateral 1.5 mm, and dorsal 5 mm, corresponding to the location of the interstitial nucleus of Cajal (Shantha et al. 1968). Figure 67 shows reconstructed muscimol injection sites in coronal sections (anterior 7) from all five animals. This shows that injections directly into the above-mentioned area (●) produced an immediate deficit in holding eye position, whereas the deficit developed more gradually after injections just outside this area (•). Injections 2 mm anterior or posterior to the illustrated sites did not produce immediate position-holding deficits.

FIGURE 67. Anatomic locations of muscimol injection sites. One coronal section (anterior 7) through th midbrain is shown for each of animals BAR (A), LAR (B), ART (C), MAR (D), and CAS (E). Inection sites are reconstructed from sterotaxic coordinates used during injection and the histologically observed locations of marker lesions. (●): sites which produced immediate ocular drift. (•): sites where ocular drift appeared within 30 minutes. (○): sites where drift did not appear within 30 minutes of injection. Anatomic structures are drawn and labeled according to the stereotaxic atlas of Shantha et al. (1968). Antatomic abbreviations: INC: interstitial nucleus of Cajal. III: third ventricle. FRTM: formatio reticularis tegmenti mesencephali. NOC: nucleus centralis n. oculomotorii. NOD: nucleus n. oculomotorii, pars dorsalis. NOV nucleus n. oculomotorii, pars ventralis. NR: nucleus ruber. DBC: decussatio brachii conjuntivi.

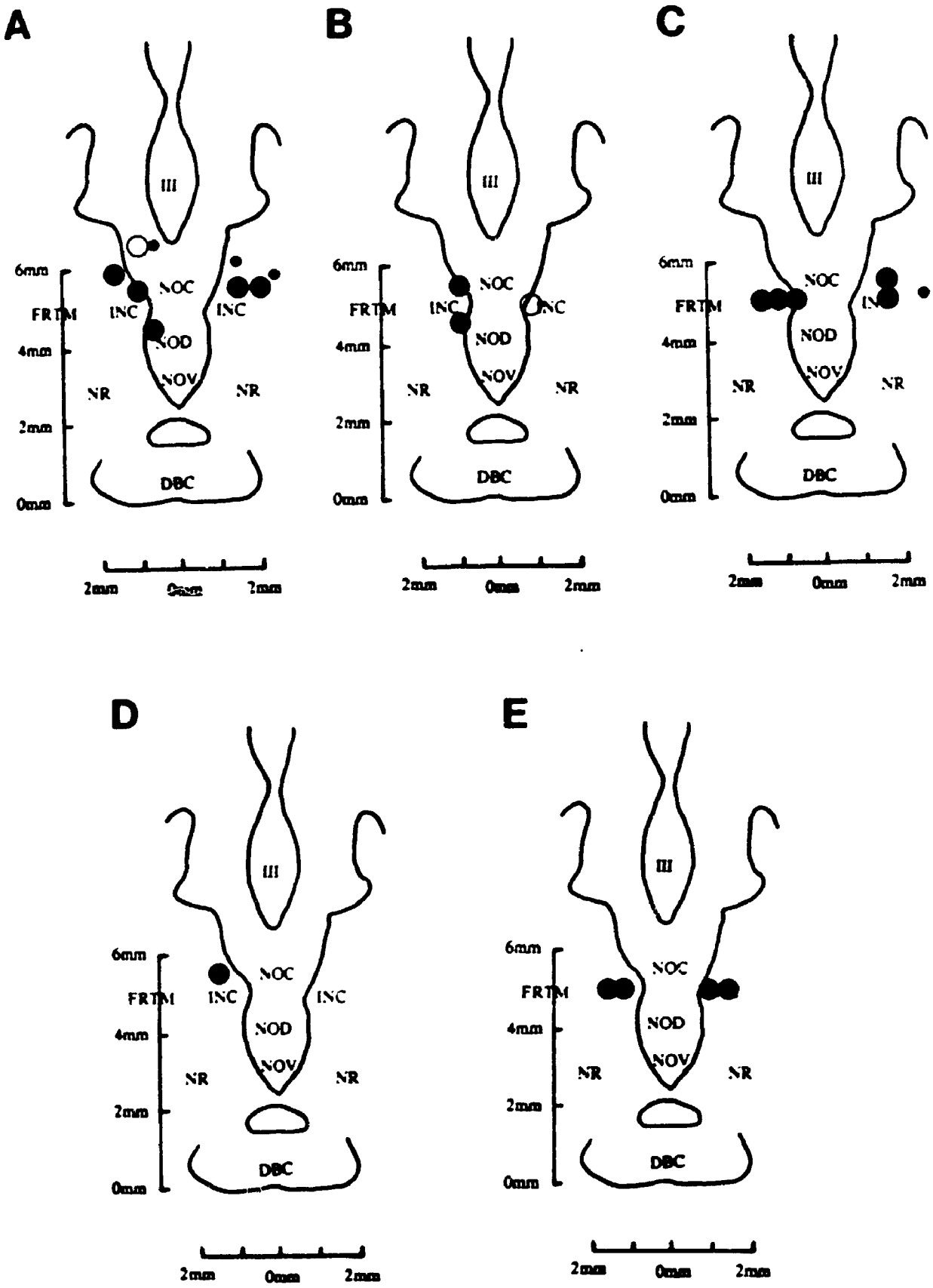
A
B
C
D
E
III
6mm
FRTM
4mm
2mm
0mm
NOC
INC
NOD
NOV
NR
DBC
2mm
0mm
2mm

REFERENCES

ABEL, L.A., DELL'OSSO, L.F. and DAROFF, R.B. Analog model for gaze-evoked ystagmus. *IEEE Trans. Biomed. Eng.* 25: 71-75, 1978.

ANASTASIO, T.J. Neural network models of velocity storage in the horizontal vestibulo-ocular reflex. *Biol-Cybern* 64: 187-196, 1991.

ANASTASIO, T. J. and ROBINSON, D. A. Distributed parallel processing in the vertical vestibulo-ocular reflex: learning networks compared to tensor theory. *Biol. Cybern.* 63: 161-167, 1990.

ANASTASIO, T.J. and ROBINSON, D.A. Failure of the oculomotor neural integrator from a discrete midline lesion between the abducens nuclei in the monkey. *Neurosci. Lett.* 127: 82-86, 1991.

ANDERSON, J. H. Ocular torsion in the cat after lesions of the interstitial nucleus of Cajal. *Ann. N.Y. Acad. Sci.* 374: 865-871, 1981.

ANDERSON, J.H., PRECHT, W. and PAPAS, C. Changes in the vertical vestibuloocular reflex due to kainic acid lesions of the interstitial nucleus of Cajal. *Neurosci. Lett.* 14: 259-264, 1979.

ANDERSON, R. A., ESSIK, G. K. and ZIPSER, D. Encoding of spatial location by posterior parietal neurons. *Science* 230: 456-458, 1985.

BAKER, J., GOLDGERG, J., HERMANN, G. and PETERSON, B. Optimal response planes and canal convergence in secondary neurons in vestibular nuclei of alert cats. *Brain Res.* 294: 133-137, 1984.

BARR, C. C., SCHULTHEIS, L. W. and ROBINSON, D. A. Voluntary, non-visual control of the human vestibulo-ocular reflex. *Acta. Otolaryngol.* 81: 365-375, 1976.

BECKER, W., KING, W. M. FUCHS, A. F., JÜRGENS, R., JOHANSON, G. and

KORNHUBER, H. H. Accuracy of goal directed saccades and mechanisms of error correction. In: *Progress in Oculomotor Research*, edited by A. F. Fuchs and W. Becker. New York: Elsevier North Holland, 1981, p. 29-37.

BERTHOZ, A., MELVILL JONES, G. and BEGUE, A. E. Differential visual adaptation of vertical canal-dependent vestibulo-ocular reflexes. *Exp. Brain. Res.*, 44: 19-26, 1984.

BEVINGTON, P.R. *Data Reduction and Error Analysis for the Physical Sciences.* McGraw-Hill: New York, 1969, p. 198-200.

BLANKS, R. H. I., CURTHOYS, I. S., BENNET, M. L. and MARKHAM, C. H. Planar relationships of the semicircular canals in rhesus and squirrel monkeys. *Brain Res.* 340: 315-324, 1985.

BONDAR, R.L., SHARPE, J.A. and LEWIS, A.J. Rebound nystagmus in olivocerebellar: A clinicopathological correlation. *Ann. Neurol.* 15: 474-477, 1984.

BÜTTNER, U., BÜTTNER-ENNEVER, J. A., and HENN, V. Vertical eye unit related activity in the rostral mesencephalic reticular formation of the alert monkey. *Brain Res. 130*: 239-252, 1977.

BÜTTNER-ENNEVER, J. A. and BÜTTNER, U. A cell group associated with vertical eye movements in the rostral mesencephalic reticular formation of the monkey. *Brain Res.* 151: 31-47, 1978.

BÜTTNER-ENNEVER, J. A. and BÜTTNER, U. The reticular formation. In: *Neuroanatomy of the Oculomotor System*, edited by J. A. Büttner-Ennever. Amsterdam: Elsevier, 1988, p. 135-138, 148-150.

CANNON S. C. and ROBINSON, D.A. An improved neural-network model for the neural integrator of the oculomotor system: More realistic neuron behavior. *Biol. Cybern.* 53: 93-108, 1985.

CANNON, S. C. and ROBINSON, D.A. Loss of the neural integrator of the oculomotor system from brainstem lesions in the monkey. *J. Neurophysiol.* 57, 1383-1409, 1987.

CANNON, S. C., ROBINSON, D.A., and SHAMMA, S. A proposed neural network for the integrator of the oculomotor system. *Biol. Cybern.* 49: 127-136, 1983.

CARPENTER, R. H. S. Cerebellectomy and the transfer function of the vestibulo-ocular reflex in the decerebrate cat. *Proc. R. Soc. London Ser. B* 181: 353-374, 1972.

CARPENTER, R. H. S. *Movements of the eyes (second edition).* Pion: London, 1988, p 68.

CHERRON, G. and GODAUX, G. Disabling of the oculomotor integrator by kainic acid injections in the prepositus-vestibular complex of the cat. *J. Physiol. (London)* 394: 267-290, 1987.

CHUN, K.-S. and ROBINSON, D. A. A model of quick phase generation in the vestibuloocular reflex. *Biol. Cybern.* 28: 209-221, 1978.

COHEN, B, KOMATSUZAKI, A, and BENDER, M. B. Electrooculographic syndrome in monkeys after pontine reticular formation lesions. *Arch. Neurol.* 18: 78-92, 1968.

COHEN, B. and KOMATSUZAKI, A. Eye movements induced by stimulation of the pontine reticular formation: evidence for integration in oculomotor pathways. *Exp. Neurol.* 36: 101-117, 1972.

COLLEWIJN, H., VAN DER STEEN, J., FERMAN, L. and JANSEN, T. C. Human ocular counterroll: assessment of static and dynamic properties from electromagnetic scleral coil recordings. *Exp. Brain Res.* 59: 185-196, 1985.

CRAWFORD, D., CADERA, W. and VILIS, T. The oculomotor velocity to position transformation involves the nucleus of Cajal. *Soc. Neurosci. Abstr.* 14, 386.8, 1988.

CRAWFORD, J.D and VILIS, T. Evidence for distributed parallel integration in the

interstitial nucleus of Cajal. *Soc. Neurosci. Abstr.* 18: 102.10, 1992.

CRICK, F. The recent excitement about neural networks. *Nature* 337: 129-132, 1989.

EIZENMAN, M., CHENG,P., SHARPE, J.A. and FRECKER, R.C. End-point nystagmus and ocular drift: an experimental and theoretical study. *Vision Res.* 30: 863-877, 1990.

EZURE, K. and GRAF, W. A quantitative analysis of the spatial organization of the vestibulo-ocular reflexes in lateral- and frontal-eyed animals-I. Orientation of the semicircular canals and extraocular muscles. *Neuroscience* 12: 85-93, 1984.

FERMAN, L., COLLEWIJN, H., JANSEN, T. C. and VEN DEN BERG, A. V. Human gaze stability in the horizontal, vertical and torsional directions during voluntary head movements, evaluated with a three-dimensional scleral induction coil technique. *Vision Res.* 27: 811-828, 1987a.

FERMAN, L., COLLEWIJN, H. and VAN DEN BERG, A. V. A direct test of Listing's law. I. Human ocular torsion measured in static tertiary positions. *Vision Res.* 27: 929-938, 1987b.

FERMAN, L., COLLEWIJN, H. and VAN DEN BERG, A. V. A direct test of Listing's law. II. Human ocular torsion measured under dynamic conditions. *Vision Res.* 27: 939-951, 1987c.

FERNANDEZ, C. and GOLDGERG, J. M. Physiology of peripheral neurons innervating semicircular canals of the squirrel monkey. I. Resting discharge and response to constant angular accelerations. *J. Neurophysiol.* 34: 635-660, 1971a.

FERNANDEZ, C. and GOLDGERG, J. M. Physiology of peripheral neurons innervating semicircular canals of the squirrel monkey. II. Response to sinusoidal stimulation and dynamics of peripheral vestibular system. *J. Neurophysiol.* 34: 661-675, 1971b.

FETTER, M., HAIN, T. C. and ZEE, D. S. Influence of eye and head position on the vestibulo-ocular reflex. *Exp. Brain Res.* 64: 208-216, 1986.

FLANDERS, M., HELMS TILLERY, S.I. and SOECHTING, J.F. Early stages in a sensorimotor transformation. *Behav. Brain Sci.* 15: 309-362, 1992.

FUCHS, A. F., KANEKO, C. R. S., and SCUDDER, C. A. Brainstem control of saccadic eye movements. *Ann. Rev. Neurosci.* 8: 307-337, 1985.

FUKUSHIMA, K. The interstitial nucleus of Cajal and its role in control of movements of head and eyes. *Prog. Neurobiol.* 29: 107-192, 1987

FUKUSHIMA, K. and FUKUSHIMA, J. 1992. Involvement of the interstitial nucleus of Cajal in the midbrain reticular formation in the position-related tonic component of vertical eye movement and head posture. *The Head-Neck Sensory-Motor System*, edited by A. Berthoz, W. Graf and P. P. Vidal. New York: Oxford University Press, 1992, p. 330-344. (Wiley Symp. Ser.)

FUKUSHIMA, K., FUKUSHIMA, J., HARADA, C., OHASHI, T. and KASE, M. Neuronal activity related to vertical eye movement in the region of the interstitial nucleus of Cajal in alert cats. *Exp. Brain. Res.* 79: 43-64, 1990a.

FUKUSHIMA, K., FUKUSHIMA, J., OHASHI, T. and KASE, M. Possible downward burster-driving neurons related to the anterior semicircular canal in the region of the interstitial nucleus of Cajal in alert cats. *Neuroscience Research* 12: 536-544, 1991.

FUKUSHIMA, K., HARADA, C., FUKUSHIMA, J. and SUZUKI, Y. Spatial properties of vertical eye movement-related neurons in the region of the interstitial nucleus of Cajal. *Exp. Brain Res.* 79: 25-42, 1990b.

FUKUSHIMA, K., OHASHI, T., FUKUSHIMA, J. and KASE, M. Ocular torsion produced by unilateral chemical inactivation of the interstitial nucleus of Cajal in chronically labyrinthectomized cats. *Neurosci. Res.* 13: 301-305, 1992.

GALIANA, H.L., and OUTERBRIDGE, J.S. A bilateral model for central neural pathways in vestibuloocular reflex. *J. Neurophysiol.* 51: 210-241, 1984.

GLENN, B. and VILIS, T. Violations of Listing's law after large eye and head gaze shifts. *J. Neurophysiol.* 68: 309-317, 1992.

GOLDBERG, M.E. and BRUCE, C.J. Primate frontal eye fields III. Maintenance of a spatially accurate saccade signal. *J. Neurophysiol.* 64: 489-508, 1990.

GONSHOR, A. and MELVILL JONES, G. Short-term adaptive changes in the human vestibulo-ocular reflex arc. *J. Physiol. (Lond)* 256: 361-379, 1976.

GORDON, S.E., HAIN, T.C. and ZEE, D.S. Rebound nystagmus. *Soc. Neurosci. Abstr.* 12, 297.21, 1986.

HAIN, T. C. and BUETTNER, U. W. Static roll and the vestibulo-ocular reflex. *Exp. Brain Res.* 82: 463-471, 1990.

HASSLER, R. Supranuclear structures regulating binocular eye and head movements. In: *Cerebral Control of Eye Movements and Motion Perception, Bibl. Ophthal., Vol* 82, edited by J. Dichgans and E. Bizzi. Basel: Karger, 1972, p. 207-219.

HELMHOLTZ, H. VON. *Treatise on Physiological Optics (English Translation)*, translated by J. P. C. Southall, Rochester NY: Opt. Soc. Am., 1925, vol. 3, p. 44-51.

HENN, V., HEPP, K., and VILIS, T. Rapid eye movement generation in the primate: Physiology, pathophysiology, and clinical implications. *Rev. Neurol. (Paris)* 145: 540-545, 1989.

HENN, V., LANG, W., HEPP, K. and REISINE, H. Experimental gaze palsies in monkeys and their relation to human pathology. *Brain* 107: 619-636, 1984

HEPP, K. On Listing's law. *Comm. Math. Phys.* 132: 285-292, 1990

HEPP, K., VILIS, T. and HENN, V. On the generation of rapid eye movements in three dimensions. In: *Representation of Three-Dimensional Space in the Vestibular,*

Oculomotor and Visual Systems, edited by B. Cohen and V. Henn. New York: *Ann. N.Y. Acad. Sci.* vol 545, 1988, p. 140-153.

HOLLERBACH, J. M. and ATKESON, C.G. Deducing planning variables from experimental arm trajectories: pitfalls and possibilities. *Biol. Cybern.* 56: 279-292, 1987.

HORE, J., WATTS, S. and VILIS, T. Constraints on arm position when pointing in three dimensions: Donder's law and the Fick Gimbal Strategy. *J. Neurophysiol.* 68: 374-383, 1992.

HORE, J., WATTS, S. and TWEED, D. Throwing in three dimensions. *Soc. Neurosci. Abstr.* 18: 1055, 1992.

HUBEL, D.H. and WEISEL, T.N. Receptive fields of single neurones in the cat's striate cortex. *J. Physiol.* (Lond.) 148: 574-591, 1959.

JÜRGENS, R., BECKER, W. and KORNHUBER, H. H. Natural and drug induced variations of velocity and duration of human saccadic eye movements: evidence for a control of the neural pulse generator by local feedback. *Biol. Cybern.* 39: 87-96, 1981.

KAMATH, B.Y. and KELLER, E.L. A neurological integrator for the oculomotor control system. *Math Biosci.* 30: 341-352, 1976.

KANEKO, C.R.S and FUCHS, A.F. Saccadic eye movement deficits following ibotenic acid lesions of the nuclei raphe interpositus and prepositus hypoglossi in the monkey. *Acta. Otolaryngol. (Stochh.) Suppl.* 481: 213-215, 1991.

KELLER, E. L. Participation of medial pontine reticular formation in eye movement generation in monkey. *J. Neurphysiol.* 37: 316-332, 1974

KELLER, E. L. and ROBINSON, D. A. Absence of a stretch reflex in extraocular muscles in the monkey. *J. Neurophysiol.* 34: 908-919, 1971.

KING, W. M. Vertical eye movement dificits after unilateral kainic acid lesions in cat midbrain. *Invest. Ophthalmol.* (Suppl.) 22: 86, 1982.

KING, W. M. and FUCHS, A. F. Reticular control of vertical saccadic eye movements by mesencephalic burst neurons. *J. Neurophysiol.* 42: 861-876, 1979.

KING, W.M., FUCHS, A.F. and MAGNIN, M. Vertical eye movement-related responses of neurons in midbrain near intersitial nucleus of Cajal. *J. Neurophysiol.* 46: 549-562, 1981.

KING,W.M. and LEIGH, R.J. Physiology of vertical gaze. In: *Physiology of Vertical Gaze in Functional Basis of Ocular Motility Disorders*, edited by G. Lennerstrand, D.S. Zee, and E.L. Keller, Pergammon Press: Oxford, 1982, 267-276

KOMPF, D., PASIK, T., PASIK, P. and BENDER, M. B. Downward gaze in monkeys. Stimulation and lesion studies. *Brain.* 102: 527-558, 1979.

LAND, M. F. and FERNALD, R. D. The evolution of eyes. *Ann. Rev. Neurosci.* 15: 1-30, 1992.

LEIGH, R. J., MAAS, E. F., GROSSMAN, G. E. and ROBINSON, D. A. Visual cancelation of the torsional vestibulo-ocular reflex in humans. *Exp. Brain Res.* 75: 221-226, 1989.

LEIGH, R.J. and ZEE, D.S. *The Neurology of Eye Movements. Edition 2.* F.A. Davis: Philadelphia, 1991, p. 188-191 (Contemporary Neurology Series).

LE TAILLANTER, M. The interstitial nucleus of Cajal of the cat. I Neuron activity related to vertical eye movements. *Arch. Italien. Biol.* 129: 73-85, 1991a.

LE TAILLANTER, M. The interstitial nucleus of Cajal of the cat. II Effects of kainic acid lesion on vertical optokinetic nystagmus and after-nystagmus. *Arch. Italien. Biol.* 129: 87-96, 1991b.

LUSCHEI, E. S. and FUCHS, A. F. Activity of brain stem neurons during eye

movements of alert monkeys. *J. Neurophysiol.* 35: 445-461, 1972.

MASINO, T. & KNUDSON, E.I Horizontal and vertical components of head movement are controlled by distinct neural circuits in the barn owl. *Nature* 345: 434-437, 1990.

MAYS, L. E. and SPARKS, D. L. Saccades are spatially not retinocentrically encoded. *Science* 208: 1163-1165, 1980.

MCINTYRE, A. K. The quick component of nystagmus. *J. Physiol.* (Lond.) 97: 8-16, 1939.

MILES, F. A. and FULLER, J. H. Adaptive plasticity of the vestibulo-ocular responses of the rhesus monkey. *Brain Res.* 80: 512-516, 1974.

MILLER, J. M. and ROBINS, D. Extraocular muscle sideslip and orbital geometry in monkeys. *Vision Res.* 27: 381-392, 1987.

MORRIS, R.G.M. Computational neuroscience: modelling the brain. In: *Parallel Distributed Processing. Implications for Psychology and Neurobiology*, edited by R.G.M. Morris. Clarendon Press: Oxford, 1989, p. 203-213.

MORROW, M. J. and SHARPE, J. A. Torsional optokinetic nystagmus in upright and supine positions in humans. Invest. Ophthalmol. Vis. Sci. 30: 51, 1989.

MOSCHOVAKIS, A. K., SCUDDER, C. A. and HIGHSTEIN, S. M. Structure of the primate oculomotor burst generator I. Medium lead burst neurons with upward on-directions. *J. Neurophysiol.* 65: 203-217, 1991.

MOSCHOVAKIS, A. K., SCUDDER, C. A., HIGHSTEIN, S. M. and WARREN, J. D. Structure of the primate oculomotor burst generator II. Medium lead burst neurons with downward on-directions. *J. Neurophysiol.* 65: 218-229, 1991b.

MOUNTCLASTLE, V.B. Modality and topographic properties of single neurons of cat's somatic sensory cortex. *J. Neurophysiol.* 20: 408-434, 1957.

NAKAYAMA, K. Kinematics of normal and strabismic eyes. In: *Vergence Eye Movements: Basic and Clinical Aspects*, edited by C. M. Schor and K. J. Ciuffreda. Boston: Butterworths, 1983, p. 543-564.

NICHOLSON, W. K. *Elementary Linear Algebra With Applications*. Boston: Prindle, Weber and Schmidt, 1986, p. 191-229.

PELLIONISZ, A. Tensorial relationship found for structural & functional reference frames of brain function: saccade neurons in monkey utilize frames composed of the eigenvectors of the frame of oculomotor muscles. *Soc. Neurosci. Abst.* 12: 1186, 1986.

PELLSIONISZ, A.J., and GRAF, W. Tensor network model of the "three-neuron vestibulo-ocular reflex-arc" in cat. *J. Theoret. Neurobiol.* 5: 127-51, 1987.

PELLIONISZ, A. J. and PETERSON B. W. A tensorial model of neck motor activation. In: *Control of Head Movement*, edited by B. W. Peterson and F. J. Richmond. New York: Oxford Univ. Press, 1988, p. 178-186.

PETERSON, B. W. and BAKER, J. F. Spatial transformations in vestibular reflex systems. In: *Motor Control: Concepts and Issues (Dahlem Workshop Reports)*, edited by D. R. Humphrey and H. -J. Freund. New York: John Wiley and Sons, 1991, p. 121-135.

PURVES, D., RIDDLE, D.R. and LAMANTIA, A-S. Iterated patterns of brain circuitry (or how the cortex gets its spots). *Trends in Neurosci.* 15: 362-368, 1992.

RAPHAN, T. and COHEN, B. Multidimensional organization of the vestibulo-ocular reflex (VOR). In: *Adaptive Processes in Visual and Oculomotor Systems*, edited by E. L. Keller and D. S. Zee. Oxford: Pergamon Press, 1986, p. 285-292.

RAYBOURN, M. S. and KELLER, E. L. Colliculoreticular organization in primate oculomotor system. *J. Neurophysiol.* 40: 861-878, 1977.

ROBINSON, D. A. A method of measuring eye movement using a scleral search coil in a magnetic field. *IEEE Trans. Bio. Med. Elect.* BME-10: 137-145, 1963.

ROBINSON, D. A. The mechanics of human saccadic eye movements. *J. Physiol. (Lond.)* 174: 245-264, 1964.

ROBINSON, D. A. Eye movement control in primates. *Science.* 161: 1219-24, 1968.

ROBINSON, D. A. Oculomotor unit behavior in the monkey. *J. Neurophysiol.* 33: 393-404, 1970.

ROBINSON, D.A. The effect of cerebellectomy of the cats vestibulo-ocular integrator. *Brain Res.* 71: 195-207, 1974.

ROBINSON, D. A. Oculomotor control signals. In: *Basic Mechanisms of Ocular Motility and Their Clinical Implications*, edited by P. Bach-y-Rita and G. Lennerstrand. Oxford UK: pergamon, 1975, p. 337-374. (Wenner-Gren Cent. Int. Symp. Ser.)

ROBINSON, D. A. Use of matrices in analyzing the three-dimensional behaviour of the vestibulo-ocular reflex. *Biol. Cybern.* 46: 53-66, 1982.

ROBINSON, D. A. The coordinates of neurons in the vestibulo-ocular reflex. In: *Adaptive Mechanisms in Gaze Control. Facts and Theories*, edited by A. Berthoz and G. Melvill Jones. Amsterdam: Elsevier, 1985, p. 297-311.

ROBINSON, D. A. Integrating with neurons. *Ann. Rev. Neurosci.* 12: 33-45, 1989.

ROBINSON, D. A. and KELLER, E. L. The behavior of eye movement motoneurons in the alert monkey. *Bibl. Ophthal.* 82: 7-16, 1972.

ROBINSON, D. A. and ZEE, D. S. Theoretical considerations of the function and circuitry of various rapid eye movements. In: *Progress in Oculomotor Research, Dev. Neurosci. Vol. 12*, edited by A. F. Fuchs and W. Becker. New York: Elsevier / North-Holland, 1981, p. 3-9.

RON, S., ROBINSON, D. A. and SKAVENSKI, A. Saccades and the quick phase of Nystagmus. *Vision Res.* 12: 2015-2022, 1972.

ROSEN, M.J. A theoretical neural integrator. *IEEE Trans. Biomed. Eng.* 19: 362-367, 1972.

ROSS, L. E. and ROSS, S. M. Saccade latency and warning signals: stimulus onset, offset and change as warning events. *Percep. Psychophys.* 27: 251-257, 1980.

ROVAINEN, C.M. Vestibulo-ocular reflex in adult sea lampreys. J. Comp. Physiol. 112: 159-164, 1976

SCHLAG-REY, M., SCHLAG, J. and SHOOK, B. Interactions between natural and electrically evoked saccades. I. Differences between sites carrying retinal error and motor error signals in monkey superior colliculus. *Exp. Brain. Res.* 76: 537-547, 1989.

SEJNOWSKI, T.E., KOCH, C. and CHURCHLAND, P. Computational Neuroscience. *Science* 241: 1299-306, 1988.

SCHULTHEIS, L. W. and ROBINSON, D. A. Directional plasticity of the vestibulo-ocular reflex in the cat. In: *Vestibular and Oculomotor Physiology*, edited by B. Cohen. New York: New York Academy of Sciences, 1981, p. 504-512.

SCUDDER, C. A., FUCHS, A. F., and LANGER, T. P. Characteristics and functional identification of saccadic inhibitory burst neurons in the alert monkey. *J. Neurophysiol.* 59: 1430-1454, 1988.

SEIDMAN, S. H. and LEIGH, R. The human torsional vestibulo-ocular reflex during rotation about an earth-vertical axis. *Brain Res.* 504: 264-268, 1989.

SHANTHA, T. R., MANOCHA, S. L. and BOURNE, G. H. *A Stereotaxic Atlas of The Java Monkey Brain.* New York: S. Karger, 1968, p. 32.

SHATZ, C. J. The developing brain. *Scientific American* 267: 60-67, 1992.

SIMPSON, J. I. Transformations of coordinates intrinsic to the vestibulo-ocular reflex. *Soc. Neurosci. Abstr.* 9, 95.4, 1983.

SIMPSON, J. I. and GRAF, W. The selection of reference frames by nature and its investigators. In: *Adaptive Mechanisms in Gaze Control. Facts and Theories*, edited by A. Berthoz and G. Melvill Jones. Amsterdam: Elsevier, 1985, p. 3-16.

SIMPSON, J. I., RUDINGER, D., REISINE, H. and HENN, V. Geometry of extraocular muscles of the rhesus monkey. *Soc. Neurosci. Abst.* 12: 1186, 1986.

SIMPSON, J. I., VAN DER STEEN, J., TAN, J., GRAF, W. and LEONARD C. S. Representations of ocular rotations in the cerebellar flocculus of the rabbit. *Prog. Brain. Res.* 80: 213-223, 1989.

SKAVENSKI, A. A. and ROBINSON, D. A. Role of abducens nucleus in vestibuloocular reflex. *J. Neurophysiol.* 36: 724-738, 1973.

SKAVENSKI, A. A., HANSEN, R. M., STEINMAN, R. M. and WINTERSON, B. J. Quality of retinal image stabilization during small natural and artificial body rotations in man. *Vision Res.* 19: 675-683, 1979.

SNYDER, L. H. and KING, W. M. Vertical vestibuloocular reflex in the cat: asymmetry and adaptation. *J. Neurophysiol.* 59: 279-298, 1988.

SYNDER, L. H. and KING, W. M. Effect of viewing distance and location of the axis of head rotation on the monkey's vestibuloocular reflex. I Eye movement responses. *J. Neurophysiol.* 67: 861-874, 1992a.

SYNDER, L. H. and KING, W. M. Changes in vestibulo-ocular reflex (VOR) anticipate changes in vergence angle in monkey. *Vision Res.* 32: 569-575, 1992b.

SOECHTING, J. F. and FLANDERS, M. Deducing central algorithms of arm movement control from kinematics. In: *Motor Control: Concepts and Issues (Dahlem Workshop Reports)*, edited by D. R. Humphrey and H. -J. Freund. New York: John

Wiley and Sons, 1991, p. 293-306.

SOECHTING, J. F. and FLANDERS, M. Moving in three-dimensional space: frames of reference, vectors, and coordinate systems. *Ann. Rev. Neurosci.* 15:167-192, 1992.

SPARKS, D. L. and MAYS, L. E. Signal transformations required for the generation of saccadic eye movements. *Annu. Rev. Neurosci.* 13: 309-336, 1990.

STRASSMAN, A., HIGHSTEIN, S. M. and MCCREA, R. A. Anatomy and physiology of saccadic burst neurons in the alert squirrel monkey: I. Excitatory burst neurons. *J. Comp. Neurol.* 249: 337-357, 1986a.

STRASSMAN, A., HIGHSTEIN, S. M. and MCCREA, R. A. Anatomy and physiology of saccadic burst neurons in the alert squirrel monkey: I. Inhibitory burst neurons. *J. Comp. Neurol.* 249: 358-380, 1986b.

STRAUBE, A., KURZAN, R. and BÜTTNER, U. Differential effects of Biccuculline and muscimol microinjections into the vestibular nuclei on simean eye movements. *Exp. Brain. Res.* 86: 347-358, 1991

STRAUMANN, D., HASLWANTER, T., HEPP-REYMOND, M.C. and HEPP, K. Listing's law for the eye, head and arm movements and their synergistic control. *Exp. Brain. Res.* 86: 209-215, 1991.

TOMLINSON, R.D. and ROBINSON, D.A. Signals in vestibular nucleus mediating vertical eye movements in the monkey. *J. Neurophysiol.* 51: 1121-1136, 1984.

TWEED, D., CADERA, W. and VILIS, T. Computing three dimensional eye position quaternions and eye velocity from search coil signals. *Vision Res.* 30: 97-110, 1990

TWEED, D., FETTER, M., ANDREADAKI, S., KOENIG, E. and DICHGANS, J. Three-dimensional properties of human pursuit eye movements. *Vision Res.* 32: 1225-1238, 1992.

TWEED, D. AND VILIS, T. Implications of rotational kinematics for the oculomotor

system in three dimensions. *J. Neurophysiol.* 58: 832-849, 1987.

TWEED, D. and VILIS, T. Geometric relations of eye position and velocity vectors during saccades. *Vision Res.* 30: 111-127, 1990a.

TWEED, D. and VILIS, T. The superior colliculus and spatiotemporal translation in the saccadic system. *Neural Networks.* 3: 75-86, 1990b.

TWEED, D. and VILIS, T. Listing's law for gaze-directing head movements. In: *The Head-Neck Sensory-Motor System*, edited by A. Berthoz, W. Graf and P. P. Vidal. New York: Oxford University Press, 1992, p. 387-391. (Wiley Symp. Ser.)

VAN GISBERGEN, J. A. M., ROBINSON, D. A. and GIELEN, S. A quantitative analysis of generation of saccadic eye movements by burst neurons. *J. Neurophysiol.* 45: 417-442, 1981.

VAN LEEUWEN, J.L. Neural network simulations of the nervous system. *Eur. J. Morphol.* 28: 139-147, 1990.

VAN OPSTAL, A. J., HEPP, K., HESS, B.J.M., STRAUMANN, D. and HENN, V. Two-rather than three-dimensional representation of saccades in monkey superior colliculus. *Science* 252: 1313-1315, 1991.

VIIRE, E., TWEED, D., MILNER, K. and VILIS, T. A reexamination of the gain of the vestibulo-ocular reflex. *J. Neurophysiol.* 56: 439-449, 1986.

VILIS, T., HEPP, K., SCHWARZ, U. and HENN, V. On the generation of vertical and torsional rapid eye movements in the monkey. *Exp. Brain Res.* 77: 1-11, 1989.

VILIS, T. and TWEED, D. B. A matrix analysis for a conjugate vestibulo-ocular reflex. *Biol. Cybern.* 59: 237-245, 1988.

WAITZMAN, D.M., MA, T.P., OPTICAN, L.M. and WURTZ, R.H. Superior colliculus neurons mediate the dynamic characteristics of saccades. *Journal of Neurophysiology* 66: 1716-1737, 1991.

WANG, S.-F. and SPENCER, R.F. Spatial organization and neurotransmitter utilization of premotor neurones related to vertical saccadic eye movements in the cat. *Soc. Neurosci. Abstr.* 18, 19.7, 1992.

WESTHEIMER, G. Kinematics of the eye. *J. Opt. Soc. Am.* 47: 967-974, 1957.

WESTHEIMER, G. and BLAIR, S. M. Mapping the Visual sensory onto the visual motor system. *Invest. Ophthalmol.* 11: 490-496, 1972.

WESTHEIMER, G. and BLAIR, S. M. The ocular tilt reaction - a brainstem oculomotor routine. *Invest. Ophthalmol.* 14: 833-839, 1975.

YASUI, S. and YOUNG, L. R. On the predictive control of foveal eye tracking and slow phases of optokinetic and vestibular nystagmus. *J. Physiol.* (Lond.) 347: 17-33.

YOKOTA, J., REISINE, H. and COHEN, B. Loss of integrator function after injection of GABAergic substances into the prepositus hypoglossi nuclei (PPH). *Soc. Neurosci. Abst.* 18: 509, 1992.

ZIPSER, D. and ANDERSON, R.A. A back-propogation programmed network that simulates response properties of a subset of posterior parietal neurons. *Nature* 331: 679-684, 1988.